UNIVERSITY OF MINHO
Department of Mechanical Engineering

Tribological Properties of CVD Diamond Coated Ceramic Surfaces

by

Cristiano Simões de Abreu

A Thesis submitted in partial fulfillment
of the requirements for the degree of

Doctor in Mechanical Engineering (Tribology)

September 2008

The Thesis of
Cristiano Simões de Abreu is approved:

Committee Chairperson

2008

Tribological Properties of CVD Diamond Coated Ceramic Surfaces

by

Cristiano Simões de Abreu

<csa@isep.ipp.pt>

This document was prepared with LaTeX using the following programs and templates:

- Text editor: GNU Emacs 21.4.1 (i686-pc-Linux-gnu, Motif Version 2.2.3)
- Typesetting system: TeX, Version 3.14159 (Web2C 7.4.5) (format=latex 2005.11.22)
- TeXdistribution: teTeX 2.0.2-r5
- Macro package: LaTeX 2ε
- Bibliography: BibTeX, Version 0.99c (Web2C 7.4.5)
- Hypertext links for LaTeX: hyperref 2003/01/22 v6.73n
- TeX DVI to PDF translator: dvipdfmx-20040411
- Platform: Linux 2.6.13-gentoo i686
- Base document class: ucthesis 2004/06/17, v3.0

I dedicate this thesis to my beloved wife and daughter, Teresa and Francisca.
Their unconditional love, utmost patience and understanding were most valuable and essential for me to accomplish this task.

Acknowledgements

First of all I would like to express my utmost gratitude to both my supervisors, Professor José Gomes and Professor Rui Silva, who introduced me to the wonderful subject of tribology and, in consequence, made possible this thesis. Praise be also given to their permanent support, encouragement, patience and friendship, starting from the first moment I had the privilege to work with both.

I would like also to express my gratitude to the following excellent researchers from whom I've learned so much, had many helpful discussions and became such good friend: Doctor Filipe Oliveira from CICECO - University of Aveiro, for helping me in the interpretation of experimental data, SEM characterization of samples and taught me the basics in order to do the AFM measurements, as well as helpful discussion and revision of the publications; Doctor Margarida Amaral also from CICECO, who helped in the preparation of samples, AFM characterization and discussion of the publications; Dr. António Fernandes, from the Department of Physics - University of Aveiro, for revision and fruitful discussion of the publications, film production and μ-Raman measurements; Doctor Manuel Belmonte, CSIC - Madrid, Spain, for sample preparation and characterization, and fruitful discussions as well as motivation for embracing this area; Doctor Mercedes Vila from CICECO - University of Aveiro, for helpful discussions on the production techniques of super-hard coatings and MSc. Ermelinda Salgueiredo, also from CICECO, for substrate preparation and kind words of support during more difficult moments. I'm also thankful to the lab technician Eng. Sergio Carvalho, working at the LOMT laboratory - Department of Mechanical Engineering, University of Minho, for his assistance during the calibration and, sometimes, followup of the tribological experiments when I was forced to be elsewhere.

I'm also indebted to the PRODEP program and Fundação para a Ciência e Tecnologia (FCT) foundation for their financial support, which made possible this work and allowed me to participate in several international conferences, which proven to be prolific in the dissemination of my findings and contact other research teams.

Finally, I would like also to express a word of gratitude toward my colleagues at the Physics Department of Porto Superior Engineering Institute (ISEP), for their extra-work in order to alleviate me from my teaching obligations while I was working in this PhD thesis.

Cristiano Simões de Abreu
<csa@isep.ipp.pt>

Abstract

Tribological Properties of CVD Diamond Coated Ceramic Surfaces

Recent developments in chemical vapour deposited (CVD) diamond coatings have attracted considerable interest and a host of new applications, each more challenging than the others. This increased attention results from the fact that CVD diamond films retain to a large extent the outstanding physical and chemical properties of natural single crystal diamond such as extreme hardness, chemical inertness and high corrosion resistance, optical transparency and high thermal conductivity. Diamond features also surprisingly low friction and high wear resistance in unlubricated sliding contacts. Moreover, as opposed to natural diamond where the friction and wear behaviour is highly dependent on crystal orientation, polycrystalline CVD diamond films supersede the monocrystalline variety due to isotropic tribological properties and possibility of coating complex shapes.

Several materials have been tested and more or less successfully used as substrates for CVD diamond coatings. Nonetheless, satisfactory adherence of diamond coatings films is often only attainable by the use of interlayers, in order to compensate for the large interfacial thermal expansion mismatch between the coating and substrate, which represent an additional processing step and added costs. A promising route will consist in using substrate materials with a low thermal expansion mismatch relative to that of diamond and, therefore, enhanced film adhesion. Among these, the ceramic silicon nitride (Si_3N_4) arises as a serious candidate.

As a general rule, available literature regarding the tribological performance of CVD diamond coated Si_3N_4 films is scarce, and the few available tribological data only deals with low applied loads. That being said, the correct tribological assessment of CVD diamond coated Si_3N_4 films under more realistic sliding conditions, reproducing the stresses found in applications fields such as the fluid handling and metalworking industry, as well as in emerging biotribological areas, is on the agenda.

In the present work, homologous tribological tests involving two distinct crystalline-scale diamond coatings, namely microcrystalline diamond (MCD) and nanocrystalline diamond (NCD) coatings, were performed under unlubricated and water lubricated sliding conditions.

The friction and wear behaviour of each diamond system was assessed using a reciprocating motion type geometry under moderated to high applied normal loads, reaching maximum values as high as 160 N in the case of lubricated MCD films. Influence of grain size effects and surface pre-treatments of the substrate on the tribological performance of MCD and NCD coatings, respectively, has also been undertaken.

Several complementary characterisation techniques, including scanning electron microscopy, atomic force microscopy and micro-Raman studies, were used in order to assess the diamond quality, stress state, topography evolution of worn surfaces, wear resistance and prevailing wear mechanisms. The distinct friction regimes occurring for diamond-on-diamond dry sliding tests and condition for the delamination of the coating were also studied by the means of acoustic emission measurements.

The friction performance of the MCD coatings under dry sliding were characterised by very low steady-state friction coefficient values in the range $0.03 - 0.04$, regardless of the applied load. Such exceptional atrituous behaviour under unlubricated conditions was accompanied by a high resistance to wear damage, with wear rates characteristic of mild to very mild wear regimes ($10^{-8} - 10^{-7}$ $mm^3N^{-1}m^{-1}$). The MCD water lubricated systems revealed even lower friction resistance ($0.01 - 0.03$), as well as a two-fold increase on the threshold load (150 N) prior to film delamination under tribological stress.

The inherent lower surface roughness of the NCD films was responsible for a marginally lower steady-state friction response ($0.02 - 0.03$) in relation to the MCD coatings, and showed to be independent of the finishing condition and substrate surface pre-treatments. Moreover, the moderate initial friction response occurring during the running-in period of accommodation between opposing MCD surfaces was greatly suppressed by the much lower starting surface roughness found in the NCD coatings. Similarly to what was observed in water lubricated MCD coatings, homologous pairs of NCD films sliding in distilled water displayed an improved tribological performance characterised by a high resistance to wear damage (10^{-8} $mm^3N^{-1}m^{-1}$) and higher threshold loads under tribological action, making them promising candidates for highly demanding tribological applications, namely in biotribology where their clinical use e.g. in total arthroplasty is a possibility.

Resumo

Propriedades Tribológicas de Superfícies Cerâmicas Recobertas a Diamante CVD

Desenvolvimentos recentes na produção de revestimentos de diamante fazendo uso do processo de deposição química em fase de vapor (CVD), têm atraído um considerável interesse e dado corpo a um conjunto de novas aplicações, cada qual mais inovadora do que a anterior. Este crescente interesse resulta do facto do diamante CVD reter em larga medida as notáveis propriedades físicas e químicas do diamante natural, tais como: dureza extrema, elevada inércia química e resistência à corrosão, transparência óptica e uma elevada condutividade térmica. O diamante é ainda caracterizado por gerar níveis surpreendemente baixos para o atrito e possuir uma elevada resistência ao desgaste, em situações de contacto não-lubrificado. Acresce o facto de que, contrariamente ao verificado no diamante natural em que as propriedades de atrito e desgaste dependem consideravelmente da orientação cristalográfica, os filmes policristalinos de diamante CVD suplantam a variedade monocristalina dada a isotropia das suas propriedades tribológicas e vantagem no revestimento de formas complexas.

Diferentes materiais têm vindo a ser testados e usados com algum sucesso como substratos na deposição de diamante CVD. Contudo, níveis de adesão satisfatórios são geralmente alcançados apenas com o recurso a inter-camadas, com o propósito de minimizar as diferenças consideráveis entre os coeficientes de expansão térmica linear do substrato e revestimento. Representando, contudo, a utilização de inter-camadas um custo acrescido e etapas adicionais durante o processamento dos materiais. Um caminho alternativo e promissor passa pela utilização de substratos com propriedades de expansão térmica próximas da do diamante, aumentando assim consideravelmente os níveis de adesão. De entre potenciais escolhas, o nitreto de silício (Si_3N_4) assume-se como um forte candidato.

Regra geral, a literatura disponível sobre o desempenho tribológico de revestimentos de diamante CVD depositados em substratos de Si_3N_4 é escassa, acrescendo-se o facto de as poucas referências encontradas envolverem pressões de contacto baixas. Assim sendo, uma adequada avaliação do desempenho tribológico de substratos Si_3N_4 revestidos a diamante CVD, sob condições de deslizamento envolvendo pressões de contacto presentes em diversas aplicações

tais como a indústria metalomecânica e transporte de fluídos, ou em áreas emergentes no campo da biotribologia, revela-se de grande importância.

No presente trabalho foram efectuados ensaios tribológicos envolvendo pares homólogos de dois tipos distintos de revestimentos de diamante, nomeadamente o diamante microcristalino (MCD) e diamante nanocristalino (NCD), tendo o deslizamento ocorrido em regime não lubrificado e lubrificado com água.

As propriedades de atrito e comportamento ao desgaste de ambos os tipos de diamante foram investigadas com recurso a ensaios tribológicos de movimento linear alternativo. Foram empregues valores moderados a elevados para a carga normal aplicada, atingindo-se um máximo de 160 N para os ensaios envolvendo MCD em meio lubrificado. A influência do tamanho de grão de diamante e pré-tratamentos superficiais do substrato cerâmico no comportamento tribológico dos revestimentos de MCD e NCD, respectivamente, foram também investigados.

Diversas técnicas complementares de caracterização, incluindo microscopia electrónica de varrimento, microscopia de força atómica e espectroscopia de μ-Raman, foram empregues no estudo da qualidade do diamante, estado de tensão e evolução da topografia das superfícies desgastadas, resistência ao desgaste e mecanismos de desgaste predominantes. Os diferentes regimes de atrito presentes durante o deslizamento a seco de diamante-sobre-diamante e cargas críticas conducentes à delaminação dos revestimentos, foram também estudados com recurso à técnica de emissão acústica.

As propriedades de atrito a seco dos revestimentos de MCD foram caracterizados por valores muito baixos para o coeficiente de atrito, situando-se no intervalo $0.03 - 0.04$ independentemente da carga aplicada. Este comportamento ao atrito excepcional na ausência de lubrificação foi acompanhado por uma elevada resistência ao desgaste, com taxas de desgaste características de regimes suave a muito suave ($10^{-8} - 10^{-7}$ mm^{3}N^{-1}m^{-1}). Os sistemas MCD lubrificados em água revelaram uma resistência ao atrito ainda mais baixa, com coeficientes de atrito no intervalo $0.01 - 0.03$, bem como um acréscimo para o dobro na carga crítica (150 N) de delaminação sob acção tribológica.

A menor rugosidade superfícial, intrínsica dos filmes de NCD, foi responsável por uma resposta ao atrito estacionário ligeiramente inferior ($0.02 - 0.03$) ao verificado nos revestimentos de MCD. Mostrou ainda ser independente do acabamento superfícial e pré-tratamentos de

superfície dos substratos. Acresce o facto de que o atrito moderado, observado durante o período inicial de acomodação de superfícies oponentes de MCD, revelou-se fortemente atenuado no caso do NCD, em resultado das muito mais suaves superfícies de partida destes últimos. De igual modo ao observado nos filmes de MCD lubrificados, os pares próprios de NCD lubrificados em água destilada denotaram uma melhoria do desempenho tribológico, sendo caracterizados por uma elevada resistência ao desgaste (10^{-8} $mm^3N^{-1}m^{-1}$) e cargas críticas mais altas. Estes resultados fazem deles candidatos com elevado potencial para aplicações tribológicas exigentes, nomeadamente em biotribologia onde o seu uso clínico em por ex. atroplastia total torna-se uma possibilidade.

Contents

List of Figures

List of Tables

Nomenclature

AA Arithmetic Average, in surface roughness

ADC Analogue-to-digital converter

AE Acoustic emission

AFM Atomic Force Microscopy

AM Amplitude modulated

AM-AFM Amplitude modulated AFM

BBS Ball-bearing steel

BOD Ball-on-disc tribo-experiments

BOF Ball-on-flat tribo-experiments

BOR Block-on-ring tribo-experiments

CC Cemented Carbid

CH_3^* Methyl radical

CLA Center-line average, in surface roughness

CVD Chemical Vapour Deposition

DLC Diamond-like carbon

FFM Friction force microscopy

FL Flat-lapped Si_3N_4 subtrate

FM Frequency modulated

FM-AFM Frequency modulated AFM

FWHM Peak full width at half-maximum

HDD Hard-disc drive

HFCVD Hot-Filament CVD

HPHT High-Pressure High-Temperature diamond

IBAD Ion beam assisted deposition

IR Infra-red radiation

k Specific wear rate (dimensional wear coefficient)

LIBAD X-ray low incident beam angle diffraction

MCD Microcrystalline Diamond Coating

MEMS Microelectromechanical Systems

MMA Moving Mechanical Assemblies, in MEMS and NEMS

μ_{max} (dynamic) initial friction coefficient peak

μ_{st} (dynamic) steady-state friction coefficient

MWPACVD (or MPCVD) Microwave Plasma-Assisted CVD

NCD Nanocrystalline Diamond Coating

NEMS Nanoelectromechanical systems

NSOM Near-field scanning optical microscopy

OM Optical microscopy

P Polished Si_3N_4 susbtrate

POD Pin-on-disc tribo-experiments

PP Pre-polished Si_3N_4 subtrate

PTFE Polytetrafluoroethylene

PVD Physical Vapour Deposition

PZT Lead zirconate titanate

$\mathbf{R}_a$ Surface roughness average (CLA)

$\mathbf{R}_q$ Root mean square (rms) surface roughness

R_t Maximum peak-to-valley height surface roughness

R_z Ten-point height surface roughness

RBS Rutherford back-scattering

r.f. PECVD Radio-frequency plasma-enhanced CVD

R.H. Relative Humidity

ROR Ring-on-ring tribo-experiments

SAM Scanning Auger Microscopy

SAW Surface acoustic wave devices

SEM Scanning Electron Microscopy

SFGD Smooth fine-grained diamond

Si_3N_4 Silicon nitride

σ Biaxial stress

sp^1 Only two electron forming strong covalent bonds

sp^2 Three of four valence electrons assigned to a trigonally directed sp^2 hybridization state

sp^3 The four valence electrons of carbon assigned to a tetrahedrally directed sp^3 hybridization state

SPM Scanning probe microscopy

SS Stainless steel

STM Scanning tunneling microscopy

TM-AFM Tapping mode AFM

UHV Ultra-high vacuum

UNCD Ultra-nanocrystalline diamond

v Sliding linear velocity

W Applied normal load

x Sliding distance

XRD X-ray diffraction

List of publications

This thesis dissertation consists of a summary of main results and eight publications:

Publication I (Ch.4.2) C.S. Abreu, F.J. Oliveira, M. Belmonte, A.J.S Fernandes, R.F. Silva, J.R. Gomes. *Grain size effect on self-mated CVD diamond dry tribosystems.* Wear 259 (2005) 771-778.

Publication II (Ch.4.3) C.S. Abreu, F.J. Oliveira, M. Belmonte, A.J.S. Fernandes, J.R. Gomes, R.F. Silva. *CVD diamond coated silicon nitride self-mated systems: tribological behaviour under high loads.* Tribology Letters, 21, 2 (2006) 141-151.

Publication III (Ch.4.4) C.S. Abreu, F.J. Oliveira, J.R. Gomes, M. Belmonte, A.J.S. Fernandes, R.F. Silva. *In-situ Friction Monitoring of Self-mated CVD Diamond Coatings using Acoustic Emission.* Materials Science Forum, 514-516 (2006), 749-753.

Publication IV (Ch.4.5) C.S. Abreu, E. Salgueiredo, F.J. Oliveira, A.J.S Fernandes, R.F. Silva, J.R. Gomes. *CVD diamond water lubricated tribosystems for high load planar sliding.* Wear 265 (2008) 1023-1028.

Publication V (Ch.5.2) C.S. Abreu, M.S. Amaral, F.J. Oliveira, A. Tallaire, F. Bénédic, O. Syll, G. Cicala, J.R. Gomes, R.F. Silva. *Tribological testing of self-mated nanocrystalline diamond coatings on Si_3N_4 ceramics.* Surface and Coatings Technology, 200, 22-23 (2006) 6235-6239.

Publication VI (Ch.5.3) C.S. Abreu, M. Amaral, A.J.S. Fernandes, F.J. Oliveira, R.F. Silva, J.R. Gomes. *Friction and wear performance of HFCVD nanocrystalline diamond coated silicon nitride ceramics.* Diamond and Related Materials, 15, 4-8 (2006) Pages 739-744.

Publication VII (Ch.5.4) C.S. Abreu, M. Amaral, F.J. Oliveira, A.J.S. Fernandes, J.R. Gomes, R.F. Silva. *Enhanced performance of HFCVD nanocrystalline diamond self-mated tribosystems by plasma pretreatments on silicon nitride substrates.* Diamond and Related Materials, 15, 11-12 (2006) 2024-2028.

Publication VIII (Ch.5.5) C.S. Abreu, M. Amaral, F.J. Oliveira, J.R. Gomes, R.F. Silva. *HF-CVD nanocrystalline diamond coatings for tribo-applications in the presence of water.* Accepted for publication in the international journal Diamond & Related Materials.

Chapter 1

Introduction

Carbon is one of the most intriguing elements in the Periodic Table. It forms many allotropes, some known from ancient times (diamond and graphite), some discovered 10-20 years ago (fullerenes and nanotubes) and very recently its two dimensional form (graphene). Indeed, carbon plays a unique role in nature and the capability of carbon atoms to form complex structures is fundamental to organic chemistry and the cradle for life's own existence, at least in its known forms [1]. Carbon-based materials play also a major role in today's science and technology. In recent years, there have been continuous and important advances in the science of carbon such as chemical vapour deposition of diamond, the growth of diamond nanostructures and aforementioned allotropes, as well as new developments in the field of disordered carbon, which altogether form the broad group of so called *new carbon materials*. Such breakthroughs in material science, has lead to a large number of applications ranging from coatings for magnetic storage devices, wear-protective coatings for tribological tools, engine parts, biomedical implants and microelectromechanical systems (MEMS), to cite but a few [2, 3].

From the various allotropes belonging to the carbon family, this thesis will focus solely in the microcrystalline and nanocrystalline varieties of chemically vapour deposited diamond, as a result of their unique properties for tribological applications. In fact, diamond constitutes one of the most exceptional naturally occurring materials, endowed with a number of extreme physical properties that enable a broad range of applications, particularly when these properties are combined [4]. The strong directional sp^3 bonding with a cubic lattice struc-

ture gives diamond many singular properties such as an extremely high hardness, a very high Young modulus, very good thermal conductivity and a very low thermal expansion coefficient [5, p. 282–324]. Diamond is in fact the hardest material known to man, with an indentation hardness of $\sim 1 \times 10^{11}$ N·m^{-2}, closely followed by cubic boron nitride with a hardness of $\sim 0.75 \times 10^{11}$ N·m^{-2}. In diamond, every carbon atom is surrounded by four nearest-neighbour carbon atoms, located at tetrahedral sites relative to the carbon atom at the origin. The C-C bond is formed by the overlapping of sp^3-hybridized atomic orbitals, which point towards the nearby carbon atoms. This result in strong binding in all three spatial directions, which is necessary for a high yield strength and indentation hardness [6, p. 92].

It is common thinking that the low dissipation of energy observed during sliding of diamond is probably not due to appreciable anisotropy of physical properties. The frictional behaviour of diamond as well as its strength and other physical properties do depend on the crystallographic plane exposed to the rubbing process, however the coupling is weak [7]. It as also become evident from experiments involving the rubbing of diamond surfaces against other solids, in ambient atmosphere, that the adhesion is generally small. In fact, fundamental tribological studies tend to show that such behaviour is not an intrinsic property of the material but rather due to adsorbed surface films [8, p. 339] [9].

While naturally occurring diamond exhibits outstanding physical and mechanical properties, they are rarely all found in the same crystal. Such variability and scarcity creates hindrances for natural diamond to have any practical commercial potential in many fields, including semiconductor and optical devices, as well as in tribological applications. Diamond synthesis using high-pressure, high-temperature (HPHT) processes and chemical vapour deposition (CVD) has been responsible for diamond's commercial use in many engineering areas. These synthesis routes have enabled the tailoring and reproducibility of specific material properties crucial for each application. CVD diamond synthesis technique and variants had become of particular importance for the development of the more 'high-tech' engineering applications [4]. Moreover, despite its polycrystalline nature CVD diamond films retain most of the outstanding properties of single-crystal natural diamond, without the anisotropy of properties of the later.

It is widely accepted that diamond is a "low friction and wear resistant material", but this is not always the case. The friction response not only is influenced by the nature of the opposing surfaces, but will depend on numerous factors. For instance, the surrounding environment plays a major role on the friction and wear behaviour of diamond. Thus, it is paramount to understand the factors limiting its performance and the way they affect the tribological behaviour. From the viewpoint of academic and technological applications, it is therefore desirable to understand the mechanisms governing the friction and wear behaviour of ultra-hard diamond coatings. Moreover, the determination of the threshold load or maximum sustainable load prior to film delamination under tribological stress, becomes of great importance in order to establish limits of applicability of the different CVD diamond varieties when submitted to severe sliding conditions.

This thesis is mainly composed by sets of scientific articles published in international journals. The articles are gathered into two chapters (Chap.4 and Chap.5), with the first section of each chapter corresponding to a short introduction into the field.

In the second chapter a comprehensive review of the state-of-the-art of self-mated diamond coated systems is presented. This same chapter begins with a short overview of the tribological properties of single-crystal natural diamond, due to their relevance in the comprehension of friction and wear mechanisms of diamond coatings. Emphasis has been put on the description of tribological data available on the open literature hitherto, regarding homologous pairs of microcrystalline and nanocrystalline varieties of CVD diamond coatings under diverse operating environments. The chapter ends with an overview of some of the major applications of diamond-coated systems nowadays, as well as an account of potential applications where diamond films could excel or are already under scrutiny.

The third chapter is dedicated to the description of the main characterisation techniques and experimental procedures employed in this thesis. Following a short overview regarding the preparation of the Si_3N_4 substrates and their treatment prior to diamond deposition, the different CVD based coating derivatives used in the present work and respective operating parameters are described more thoroughly. Two CVD methods have been used in the deposition

of the diamond films, namely the micro-wave plasma assisted CVD (MWPACVD) technique in the cases of MCD and some NCD coatings, and an hot-filament CVD (HFCVD) apparatus for the remaining NCD films. This latter technique was employed with the purpose of assessing the possibility of producing NCD-coated Si_3N_4 ceramics with equivalent or improved tribological properties as those found in MWPACVD based films, using a less complex and more cost-effective procedure.

The chapter continues with a description of the various techniques used in the characterisation of as-deposited and worn diamond-coated Si_3N_4 systems. First, a comprehensive description of the various equipments and arrangements used for tribological evaluation are presented, followed by a detailed account on the tribometer, geometry of contact and operating variables used in this thesis. The various tribological quantities used throughout this thesis are subsequently defined.

Standard techniques widely used in the characterisation of tribological coatings, like scanning electron microscopy (SEM), are described briefly. Despite Raman spectroscopy constitutes a standard method in the evaluation of the quality of deposited diamond films, an historical overview of its significance in the area is presented and, more importantly, to give an account for its use as an assessment tool in the evaluation of the final stress states of the coatings, induced by the tribological interactions. Methods believed to be original in the context of the macro-tribological characterisation of diamond coatings are addressed more in depth, as is the case of atomic force microscopy (AFM) and acoustic emission (AE).

The fourth chapter comprises four scientific papers (Publications I-IV) reporting on the tribological behaviour of self-mated MCD-coated Si_3N_4 systems. In those, experimental data concerning the friction and wear properties of this tribosystem are analysed and correlated with distinct grain size of the diamond crystallites, the operating environment in which the sliding occurred, i.e. ambient atmosphere or water lubricated, and level of applied normal load.

Based on the analysis of the morphological features and topography of the worn surfaces, the prevailing friction and wear mechanisms are described and related to published tribological information involving relevant diamond tribosystems or less severe sliding conditions. Detailed discussions regarding the distinct occurring friction regimes, as well as their explanation based on existing theories of friction for diamond coatings, are also addressed on various papers.

The article of Sec. 4.4 (Publication III) is dedicated to the analysis of experimental data regarding the establishing of a correlation between distinct friction regimes and AE events, occurring during the tribological interaction of MCD coatings.
Publication IV (Sec. 4.5) reports on the tribological evaluation of self-mated MCD coatings under water lubricated sliding conditions. Aside the description of the friction regimes and wear processes involved, a relationship between wear debris particles recovered from the lubricant and the morphology of diamond asperities is established.

In the fifth chapter, studies concerning the tribological characterisation of self-mated NCD-coated Si_3N_4 systems are gathered into four scientific articles (Publications V-VIII). Like in the works reported on the previous chapter, tribo-testing occurred under dry sliding, in open air, and water lubricated conditions. The first article is dedicated to the friction and wear behaviour of MWPACVD-based diamond coatings, whereas the remaining articles refer to HFCVD-synthesised diamond films.
The influence of three different surface finish conditions for the ceramic substrates, by means of mechanical procedures, thereby affecting the degree of interfacial adhesion between the coating and substrate, as well as the starting surface roughness of the NCD films, and concomitantly their tribological performance is explored in Publication VI (Sec. 5.3).
The influence of plasma treatments performed on Si_3N_4 substrates as a means to improve further the adhesional levels of smooth HFCVD-based NCD coatings and, concomitantly, the threshold loads under tribological actions is addressed in Publication VII (Sec. 5.4).
The last article, Publication VIII (Sec. 5.5), is dedicated to the tribological assessment of self-mated NCD coatings under water lubricated sliding conditions. There, the predominant wear processes and mechanisms are described, based on the morphology of worn surfaces and wear debris, and the influence of the lubricant accounted for the observed increase in maximum sustainable load under sliding contact.

Finally, the last chapter (Chap. 6) presents the main conclusions of this thesis and proposed future work, with the purpose of further assess the potential of MCD- and NCD-coated Si_3N_4 tribological coatings for highly demanding tribo-mechanical applications, or in leading edge applications where these coatings could represent an added value.

Chapter 2

State-of-the-art in self-mated diamond tribosystems

Diamond constitutes an excellent tribomaterial as a result of its corrosion resistance, light weight, extreme hardness and intrinsically low friction. Friction coefficients in the range $0.04 - 0.20$ have been reported for diamond-on-diamond atmospheric sliding experiments, without the necessity for additional lubrication, making self-mated diamond bearings an attractive proposition [9]. Furthermore, unlubricated diamond surfaces sliding on themselves result in extremely small surface damage. When metals slide on diamond the friction coefficient presents values of the same order, and the amount of metallic transfer is again very small. Therefore, diamond cutting-tools are very effective in the machining of hard metals. Moreover, since diamond possesses an extremely high melting-point and keeps its hardness to very high temperatures, it is very effective as a polishing powder [8, p. 163].

The truth is that diamond-on-diamond tribosystems are remarkable because the sliding friction is nearly the same with or without an organic lubrication fluid. Such behaviour finds its *raison d'être* in the high penetration hardness of diamond, which means that the local pressure in the contact areas is likely to be so high that the lubrication fluid is completely squeezed out. Moreover, diamond surfaces are usually passivated by hydrogen or oxygen, and are relatively inert [6, p. 145]. Not only does diamond reveals great potentialities as a replacement material in many existing tribo-applications, but it can also be used to reduce friction in chemically harsh environments where conventional lubrication is impractical [9].

2.1 Natural single-crystal diamond systems

Natural diamond is valued as a tribological material due to its extreme hardness and very low friction coefficient values, either sliding against itself or in dissimilar pairs. A study by Hayward et al. [9] showed that typical friction coefficients for diamond styluses sliding against single-crystal (100) diamond vary in the leeway $0.04 - 0.08$. The low friction of diamond is probably not related to the appreciable anisotropy of its physical properties. The strength properties do vary somewhat according to the crystallographic orientation, but the effect is small. A similar behaviour occurs for the friction, where only a small variation of friction with the crystal face exposed is observed. Experiments have showed that when surfaces slide on diamond the adhesion is small, but whether this is a property of the material *per se* or whether it is due to adsorbed layers is yet to be fully comprehended [8, p. 163]. However, more recent tribological experiments have shown that when the surface layers are removed from diamond by outgassing in vacuum conditions, the friction of diamond sliding on diamond can reach values as high as $\mu \sim 1.0$ [10, p. 46].

Figure 2.1 shows the schematic representation of typical diamond crystallographic planes for different diamond shapes. As is well known, singe crystal diamond is anisotropic in its physical and mechanical properties and, therefore, wear resistance and frictional behaviour will vary not only with different crystallographic planes but also within the same plane [7, 11].

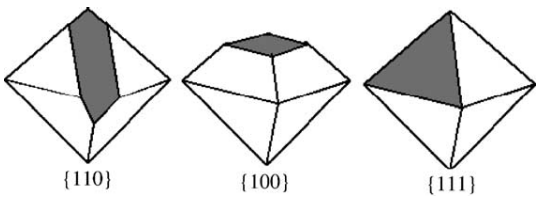

Figure 2.1: Schematic of different diamond crystallographic plane orientations [7].

With single-crystal diamond the friction is increased from about 0.05 in ambient atmosphere to about 0.40, after outgassing. The coefficient of friction falls off with increasing load and the behaviour is consistent with a contact primarily of the elastic type. Calculations of the real area of contact, using Hertz's equations of elastic deformation, have showed that the effective shear strength of the contact region is comparable to that of bulk diamond. Therefore,

such observations seem to point out that the friction of self-mated clean diamond surfaces result, as with metals, from strong bonds formed by adhesion at the interface. However, in contrast with metals, the absence of gross seizure may be due to the very small or non-existing ductility of diamond [8, p. 339].
Indeed, diamond constitutes a good example of a material where surface films can have a marked effect on the friction properties. Homologous pairs of diamond sliding in vacuum can reach friction levels of ~ 1.0 after cleaning or repeated sliding. Yet in air, much lower friction values in the range $0.05 - 0.15$ are measured and the surface modification responsible for those is more likely to be due to adsorption of gaseous species. The particularly low friction of diamond-on-diamond in air is due to the very low adhesive force between the surfaces in the presence of the adsorbed contamination, together with a small contribution from other dissipative processes, probably plastic deformation at the asperity contacts on a very fine scale [10, p. 46].

An article by Hayward et al. [9], citing several studies, report that the wear resistance of natural diamonds whilst rubbing with a variety of materials was characterized by specific wear rates of the order of 10^{-4} $mm^3N^{-1}m^{-1}$. These severe wear regimes could be explained by probable phase transformations arising from the high flash temperatures associated to high sliding speeds, where the rapid wear of diamond if used in machining or grinding steel is caused by local transformation of the diamond into graphite [10, p. 121]. The friction coefficient values for natural diamonds sliding on natural diamonds was observed to be in the range $0.04 - 0.20$. The friction coefficient for the diamond coatings tested in Hayward et al.'s work gave values from 0.03 up to values considerably higher (0.50). These higher values were explained as being a direct consequence of the higher surface roughness of the coatings sliding against a single-crystal diamond stylus.

Several models have been developed by tribologists to account for variations of the friction coefficient with surface roughness. As a general rule, the various models consider normally the abrasion or ploughing of softer materials by harder ones. Accordingly, ploughing, i.e. plastic deformation of the material and subsequent fracture of the generated ridges, is unlikely to be the prevailing mechanism for diamond coatings due to their extreme hardness. Tabor,

cited by Field [5, p. 325–350], proposed a combined adhesion/asperity-climbing mechanism based on a triangular model for asperities. This model predicts large increases in measured friction if the slope angles are large and could account for the high values of the friction coefficient, normally observed during the first cycles on tribo-tests with diamond coating surfaces with steep sided features, like those found in rougher microcrystalline diamond films with a micro-pyramidal morphology. For those, slope angles could reach values up to 70-80° and it is more than likely that interlocking summits of the asperities need to ascend and descend slopes with similar angles [9]. Another implication of the Tabor model is as wear damage evolves, the protruding asperities become progressively flattened and, concomitantly, friction interaction intensities are lowered in response to the resulting smoother surfaces and, therefore, major prevalence of smaller slope angles. Such behaviour is consistent with numerous works, where friction coefficient values for mechanically and chemically polished surfaces remained relatively unchanged throughout the full length of the tribo-experiments [9, 12, 13]. Another assumption in Hayward et al.'s work [9], was that chemical polishing produced smoother summits than the ones from mechanical processes or diamond sliding, which could explain the lower steady-state friction values observed by the authors, considering comparable starting surface roughnesses.

A different model of diamond friction has been proposed by Samuels and Wilks [14], which attributed the frictional behaviour to a combination of a ratchet (Coulomb) mechanism [15], elastic deformation and release of asperities, as well as fracture of asperities. Another approach in describing diamond's frictional behaviour consist in the so-called roughness theory [16], which hypothesises that the friction arises from the mechanical interaction between contacting asperities, implying that the energy dissipation occurs either by irreversible impact (generation of phonons) at low loads or by vibration of the asperities at high loads [17]. Considering the several existing mechanisms of friction until then, and the experimental evidence that organic lubricants do not reduce the friction coefficient from its value in air, many authors had come to imply that the surface roughness alone would be responsible for diamond's friction in air; since if adhesion had a role to play, then a lubricant would reduce or eliminate this contribution to the mechanism of friction. However, more recent studies have showed the effect of water in reducing the friction coefficient of diamond and, therefore, that an adhesion

component should also be considered to explain its frictional behaviour in open air [18, 19]. A comprehensive study of the friction properties of natural diamond, as well as the various proposed mechanisms of friction, can be found in the paper by Field and Pickles [11].

In conclusion, the frictional and wear properties of diamond are of considerable scientific and technological interest. As discussed earlier, natural diamond can exhibit very low friction coefficient values. However, the occurring values will depend on the crystallographic orientation, the direction of sliding and the number of traversals. Moreover, conventional lubricants have none to little effects in reducing the friction, but moisture can reduce its value under certain circumstances. Polycrystalline and CVD diamond possess more anisotropic properties which make them technologically more desirable [11].

2.2 Tribosystems involving polycrystalline CVD diamond coatings

According to the definition from Holmberg and Matthews [20, p. 1–6], tribological coatings are those which are sufficiently thin that the substrate plays a role in determining the friction and wear performance. Therefore, coatings which are so thick that there is little or no substrate influence on the tribological behaviour are excluded from the definition. In fact, thick films behave like bulk material in what concerns the tribological properties. That said, tribologically important properties required by the coating and respective substrate involve material strength and thermal attributes, which will be determined by their composition and microstructure as well as the porosity and homogeneity of the material. Thus, at the substrate/coating interface the adhesion and shear strength of the junction will play a major role, and at the coating surface, the chemical reactivity and surface roughness must be taken into account in addition to the shear strength.

Tribological requirements on a contact with coated surfaces normally comply with the following design guidelines [20, p. 1–6]:

1. The initial friction coefficient, the steady state friction coefficient and the friction instability should not exceed certain design values;
2. Wear material loss of the coated surface and that of the counterface should not exceed certain design values;
3. The lifetime performance of the tribosystem should, with a specified probability, be longer than the required lifetime. The coating lifetime limit can be defined as happening when one or both of the former conditions is no longer fulfilled.

In order to satisfy these tribological requirements, the coated surfaces must have a suitable combination of properties in terms of hardness, shear strength, adhesion to the substrate, fracture toughness, thermal expansion and elasticity. Therefore, improved coatings properties and selection procedures will lead to the achievement of extended and predictable service lives, and ideally, non-catastrophic failure modes.

Diamond coatings are increasingly attractive for many applications because they maintain the outstanding physical and chemical properties of natural diamond, such as an extreme hardness and chemical inertness. Diamond films can be grown on a variety of substrates by, e.g., chemical vapor deposition (CVD). Depending on the deposition techniques and processing parameters used, the films will have different physical properties. Coatings with higher surface roughness will generate a large wear if a softer body is slid on the film surface. Moreover, in contrast to most other engineering surfaces, the friction coefficient depends on the surface roughness of the films [21, 22], with the smoother ones approaching the reported value for natural diamond. Rough diamond films present high initial friction values when sliding against softer counterparts and are probably due to ploughing of the sharp protruding diamond asperities onto the softer material, and thus causing severe abrasion. After repeated traversals, the sharp asperities are progressively rounded and the valleys between asperities become filled with blanket and wear debris. This will eventually lead to reduced friction levels [6, p. 92].

CVD diamond coatings have wear properties similar to those of natural single-crystal diamond, as well as similar friction coefficients, once corrections are taken into account for the higher surface roughnesses of the former [9].
For polycrystalline diamond coatings a fracture of the tip asperity and/or an asperity climbing mechanism seem to be dominant for the first instants of the relative motion. According to several authors referred in a article by Barros et al. [23], more energy is spent in the sliding of rough surfaces, due to the fact that the asperities have to fracture or to overcome each other [8, ch. 1]. This gives rise to high initial friction levels, especially true for the various microcrystalline diamond morphologies which are substantially rougher than the nanocrystalline diamond surfaces.
Moreover, apart from the surface roughness factor, surface chemistry and tribo-induced adhesive interactions can also arise and will assume a major role in the friction and wear behaviour of all diamond films [24].

2.2.1 Microcrystalline diamond variety

Relatively recent developments in deposition techniques have made it possible to deposit a new class of hard carbon coatings. Various studies involving X-ray diffraction, transmission electron microscopy and μ-Raman spectroscopy have demonstrated that under specific deposition conditions the majority of the carbon produced is in the diamond phase. These diamond coatings differ from the natural single-crystal diamond due to their polycrystalline nature and higher intrinsic surface roughness [9].

Several tribological studies done in recent past have been reported for polycrystalline diamond coatings [25, 26]. The counterface materials have spanned metals [27, 28], ceramics [12, 13, 29] and even biocompatible polymers [30], as well as a few involved single-crystal diamond [9, 15, 19, 31] or diamond coatings [32, 33]. As a rule, extensive transfer of material to the diamond coating was observed for non-diamond sliding counterpairs and, as such, the friction and wear behaviour was in fact dominated by the softer materials.

The few tribological studies available on polycrystalline diamond coatings matted against mono-crystals or diamond coatings normally concentrate on the frictional properties

at high temperature and/or vacuum conditions. In a relevant work by Hayward et al. [9], the behaviour of single-crystal diamond sliding on polycrystalline diamond coatings in air, with special focus on the influence of the coating's surface roughness on the frictional behaviour, is addressed. In addition to results for as-deposited coatings, friction coefficients measured on mechanically and chemically polished diamond films are also presented. Moreover, the observed frictional behaviour was related by him to existing theories of diamond friction. Coatings used in his studies were obtained from a variety of techniques: CVD, microwave, d.c. plasma or hot-filament excitation. The coatings were deposited on single-crystal silicon substrates, with the surfaces exhibiting roughness values quoted as R_a in the range 7 nm to above 300 nm for d.c. plasma and hot-filament, respectively.

The friction experiments were conducted on a reciprocating sliding tribometer, with short stroke lengths of 1.2 mm and small applied loads of 2 N. The low sliding speed used, 0.3 mms^{-1}, resulted in that the bulk heating on the specimens could be considered negligible, as well as the possible occurrence of phase transformations from diamond to graphite due to high flash temperatures.

Wear tracks generated on the various diamond coatings by repeated traversals of the diamond stylus presented itself as shiny areas, easily observed by optical microscopy. Very small amounts of wear debris were reported at the edges and the ends of the tracks. Close examination of coatings by SEM showed the presence of smooth patches covering portions of the wear tracks, with the higher magnifications revealing what appears to be smeared wear debris [9]. These debris patches adhered strongly to the coating, since ultrasonic cleaning in acetone was enable to dislodge them from the film.

Scanning Auger Microscopy (SAM) was used to show that the wear debris patches were constituted by carbonaceous material, whereas the lack of a Si peak confirmed that no wear-through into the substrate occurred. Furthermore, the presence of abrasion grooves on the stylus tip were observable for the tests conducted with rougher coatings, whereas smoother ones produced relatively featureless flat surfaces on the tip.

The development of plateaus on natural diamond styluses caused by wear in contact with CVD diamond, demonstrates that polycrystalline coatings can significantly wear natural diamond. The observed grooving in the contact region of the tip, after the use of rougher coatings, also point out an abrasive wear mode, where the material causing abrasion is of comparable hardness

or harder than the material being abraded, i.e. natural diamond. Furthermore, no evidence of an incubation period was detected in the studies of Hayward et al. [9], such as occurs when a soft material wears diamond, which suggested that CVD diamond coatings have a comparable hardness to natural diamond.

Results of fundamental research on the tribological properties of self-mated CVD diamond were published in 1999 by Miyoshi et al. [34]. Their work encompassed a comparative study of the tribological performance of as-deposited, fine grain diamond, and surface-modified coarse grain diamond films by means of mechanical polishing and nitrogen ion implantation. Surface roughnesses of the tested films spanned values in the range 6-37 nm (rms) and were deposited on silicon, silicon nitride and silicon carbide substrates. The tribo-experiments were conducted at room temperature on a unidirectional, rotating apparatus (sliding velocities in the range 31 to 107 mms^{-1}), using various atmospheres (humid air, dry nitrogen and ultra-high vacuum), as well as distilled water.
In those testes, CVD diamond and surface-modified CVD diamond were made to slide against CVD diamond pins (radius, 1.6 mm), under an applied load of 0.49 N, which represented a mean Hertzian pressure of approximately 2 GPa. Selected results of such experiments are presented in the graphs of Fig. 2.2. There, the steady-state friction coefficient and wear rate of fine-grain and polished coarse-grain CVD diamond films are plotted for all tested environments. As can be seen, the as-deposited and polished films showed low values for the friction coefficient (< 0.10) and mild wear regimes (of the order of 10^{-6} $mm^3N^{-1}m^{-1}$) in three environments: humid air, dry nitrogen and water. It was only in ultra-high vacuum conditions that these films showed limitations, due to inappropriate friction coefficients (about 0.30) and severe wear rates (order of 10^{-4} $mm^3N^{-1}m^{-1}$), values which are clearly unacceptable for solid-film lubricating applications [35] or to be used has a tribological coating under such atmosphere [36]. Another conclusion of their study, was that polished coarse-grain CVD diamond films sliding in distilled water exhibited the lowest assessed wear rates, with extremely low values (far less than 10^{-10} $mm^3N^{-1}m^{-1}$), characteristic of ultra-mild wear regimes.

Dry sliding experiments employing self-mated textured diamond films, grown by HFCVD onto solid sintered silicon carbide, were carried out in a vertical ring-on-ring test rig

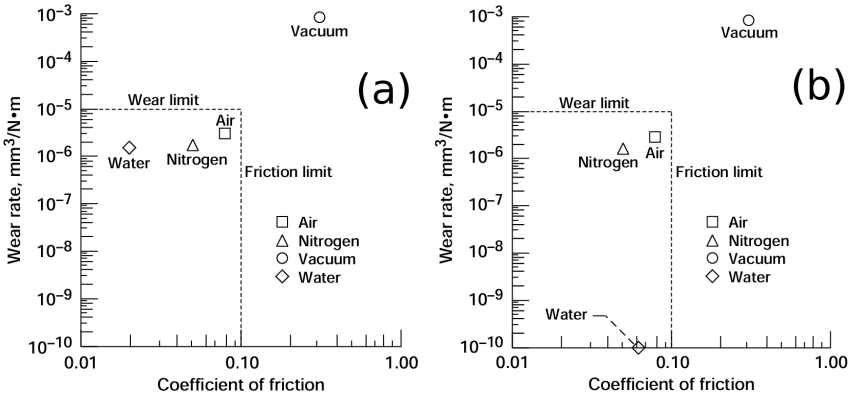

Figure 2.2: Coefficient of friction and wear rate, in different environments, of a: (a) fine-grain CVD diamond film sliding against CVD diamond pins and (b) polished coarse-grain CVD diamond film against CVD diamond pins [34].

by Schade et al. [37]. The main objective of their study was to investigate the influence of $\langle 100 \rangle$ and $\langle 111 \rangle$ fiber textured diamond coatings on the tribological performance. The choice for textured diamond coatings arose from the knowledge that the so-called grinding hardness, i.e. the resistance of a diamond facet to abrasion, is much greater for $\langle 111 \rangle$ diamond faces than for $\langle 100 \rangle$ diamond ones. The tribological experiments were conducted with an applied normal load of 70 N (representing a pressure of 0.4 MPa) and a fast mean sliding speed of 2.0 ms^{-1}. Their results revealed mean values for the friction coefficient in the range $0.24 - 0.37$ and a linear wear between $0.56 - 1.06$ μm. The wear loss of the $\langle 100 \rangle$ textured diamond films exhibited the same magnitude as the $\langle 111 \rangle$ films, on average. Therefore, they concluded that a higher wear resistance of the later could not be confirmed. After a sliding distance of 10 km, both textured films exhibited smoothly polished diamond faces without visible surface failures, i.e. film detachment. Sporadically, $\{100\}$ diamond faces counteracting against $\langle 111 \rangle$ textured films showed the presence of Hertzian cone cracks and a preferential propagation of such cracks along $\{111\}$ easy cleavage planes, in the substrate direction. The $\{111\}$ diamond faces of $\langle 111 \rangle$ textured grain also exhibited some large surface cracks, although no propagation towards the substrate was indicated. Such features can be observed in the SEM micrographs of Figs. 2.3(a) and (b), for $\langle 100 \rangle$ and $\langle 111 \rangle$ textured diamond grain films, respectively.

Despite of this crack formation, hardly any coating failure like film detachment was observed by them, which strengthens the idea of the high adhesion and abrasion resistance associated to HFCVD diamond films grown on ceramic substrates.

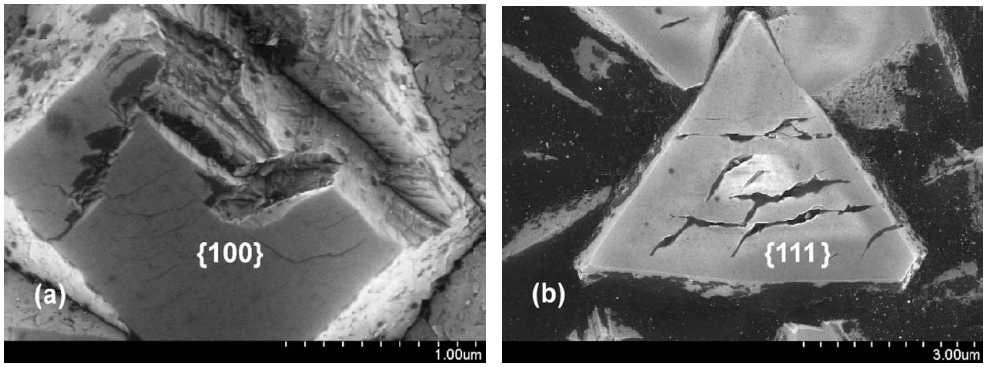

Figure 2.3: SEM micrographs of worn diamond crystallites after 10 km dry sliding against $\langle 111 \rangle$ textured diamond films: (a) $\langle 100 \rangle$ textured grain revealing the presence of Hertzian cone cracks; (b) $\langle 111 \rangle$ textured grain showing the presence of large surface cracks [37].

A compelling explanation for such high resistance to delamination can be inferred from Gunnars and Alahelisten's model of abrasive wear of brittle coatings [38], like diamond under high biaxial stresses. In this model, the stress state of diamond films is assumably dominated by high biaxial compressive stresses parallel to the interface, mainly as a result of the thermal expansion mismatch between the film and ceramic substrate at ambient temperature. Therefore, because of the relaxation-enabling inherent to the geometry of protruding grains, residual compressive stresses are low at those sites. This results in cracks nucleated in protruding grains to propagate preferentially along $\{111\}$ easy cleavage planes. However, when cracks happen to propagate deeper into the coating, the higher compressive residual stresses found there will deflect the cracks, forcing them to align parallel to the surface instead of going through easy cleavage planes.

In relation to the wear mechanisms, Schade et al. [37] concluded that the wear of homologous pairs of diamond coatings originally takes place at the protruding pyramidal tips of the as-deposited micro-rough surface. After all asperity tips are chipped off by abrasion, the prolongation of wear damage leads predominantly to smoothly polished diamond surfaces. They also observed the presence of minute diamond fragments, likely originating from the truncation of pyramidal tips. Such wear debris are subsequently crushed into progressively smaller fragments when entrapped in the contact surface. According to them, this crushing process could explain the large fluctuations observed for the friction coefficient, which happened at the earlier

stages of the sliding experiments. Moreover, μ-Raman studies conducted by the same authors have showed the generation of sp^2 hybridised ultra-fine grained amorphous and graphitic carbon debris, as a result of the high shear stresses and temperatures arising in the contact region. In addition, the valleys existing in between the abraded diamond crystallites were observed to serve as depots for such debris.

The tribological performance of polycrystalline diamond coatings deposited on top of titanium alloys has been addressed in a paper by Vandenbulcke and De Barros [39]. In addition, the surface roughness and diamond purity of the deposited films were analyzed as a function of the diamond growth conditions, which were shown to influence the hardness, residual stresses and other intrinsic mechanical properties of the coatings and, ultimately, their tribological behaviour. Tribo-testing was accomplished using a pin-on-disc tribometer in ambient air (40-60% R.H.) and a static applied normal load of 13 N. Diamond-coated Ti-6Al-4V hemispherical pins with a diameter of 6 mm were made to slide, at a linear velocity of 0.1 ms^{-1}, against diamond-coated Ti-alloy discs.
The diamond-on-diamond experiments showed different results as a function of the surface roughness, varying in the leeway $0.10 - 0.20$. However, these relatively high values were explained by the authors by the possibility that some titanium alloy became exposed at the contact region. The prevailing wear mechanisms was self-polishing, evidenced by the smooth resulting surfaces with final surface roughness values of 8 nm (rms). However, no experimental data was presented in regard to the wear rate of self-mated polycrystalline diamond pairs.
SEM studies conducted by the authors showed also the presence of possible deformations, resulting from the high shear stresses induced by friction at the tip of polycrystalline diamond grains. Such morphology, however, was not patent for the polycrystalline coatings submitted to sufficient low loads.

More recent experiments (2006), concerning the dry running of self-mated diamond-coated α-silicon carbide (α-SiC) were performed by Perle et al. [40]. Diamond deposition was conducted in an industrial HFCVD apparatus, which produced coating thicknesses with ~ 4 μm and an average crystal size of 3 μm. Tribological testing was carried out using a ring-on-ring tribometer with an applied normal load of 70 N, corresponding to a maximum contact pressure

of 0.4 MPa. The linear sliding speed was set to 2 ms^{-1} and the sliding distance of each test was 2 km. Moreover, the tribo-experiments were performed under various atmospheres, namely oxygen, argon, nitrogen and ambient air.
Friction evolution curves from Perl et al.'s work, under different atmospheres, are presented in Fig. 2.4. For the experiments performed in ambient air, three distinct friction regimes can be observed. The initial scope or regime (I), featured by the existence of a sharp peak, result from the interlocking of sharp asperities characteristic of the as-deposited micro-rough polycrystalline diamond coatings. Values for the friction coefficient of about 0.14 are indicated for this first regime and correspond to the first few revolutions. After this initial peak, a regime (II) with increasingly higher friction follows. Typical values of about 0.35 for the friction coefficient were observed in this second regime. Following this running-in period, which takes place up to a distance of 750 m, a steady response of the tribological system sets in and the friction coefficient exhibit small oscillations with an average value of $\mu \sim 0.30$.

Close examination of the worn surfaces after completion of the tribotests exhibited abraded diamond crystals, with the presence of minute wear debris. Further, Raman spectroscopy data showed that the quality of worn coatings were comparable to the as-deposited ones, with no detectable change in the residual stress of the diamond layer (0.6 GPa), intrinsic of the thermal expansion mismatch with the substrate. As can be seen from the curves, the frictional response under an oxygen atmosphere is comparable to the one under ambient air, apart the region (II) where some breaking out parts lead to instabilities in the running-in phase. No visible wear debris were observed by close examination of the worn surfaces and, like what happened during dry running in ambient air, the prevailing wear process was abrasion of the diamond crystals.

In the presence of nitrogen and argon inert gases, the coefficient of friction followed a similar initial trend as in ambient air. The main difference arose after a sliding distance of 1 km, where the slowly increasing slope gave place to an unstable regime in the leeway $0.20 - 0.40$. An examination of the abraded wear surfaces revealed the presence of localized thin films formed by agglomerates of wear particles (Fig. 2.5(a)). Using Raman spectroscopy, such agglomerates were identified as sp^2 hybridised carbon, therefore, revealing high contents of non-diamond phases without the characteristic diamond peak (1332 cm^{-1}) of pure sp^3 carbon

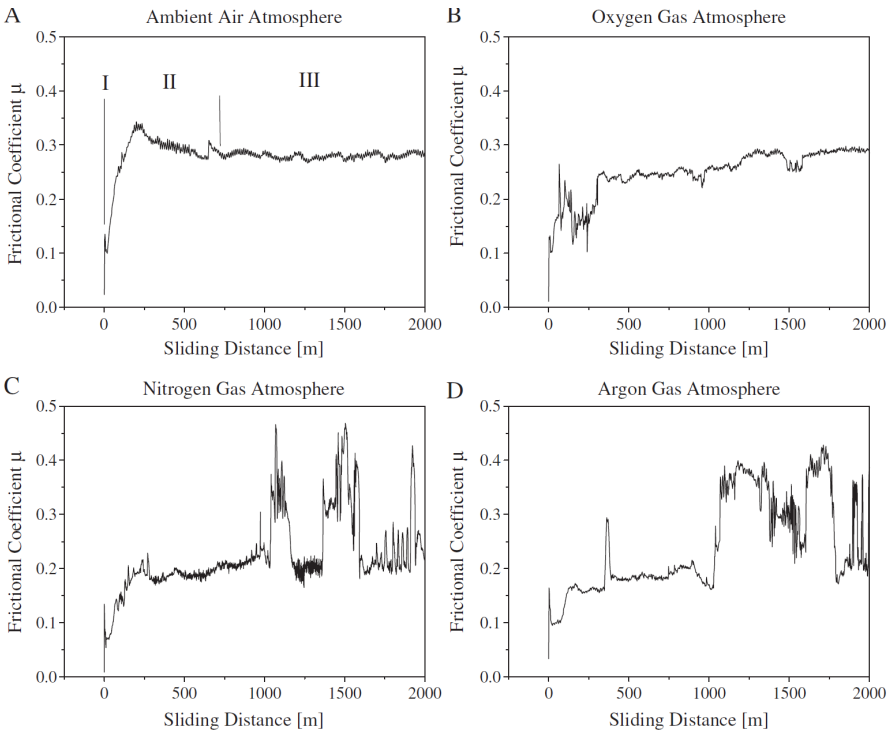

Figure 2.4: Friction evolution curves for self-mated polycrystalline diamond-coated SiC bearing surfaces subjected to dry running ring-on-ring tests, under various atmospheres (W = 70 N; v = 2 ms^{-1}) [40].

species. Since the as-deposited diamond coatings showed a content of 98% sp^3 carbon, Perl et al. [40] concluded that under the conditions of their study tribological stresses were responsible for turning sp^3 diamond into sp^2 hybridised carbon. Evidences of such transformation can be inferred from the Raman spectrum depicted in Fig. 2.5(b), taken from examined wear debris and which consisted of both species of carbon.

In the same article by Perl et al. [40], a thorough discussion taking into account basic wear models for crystalline diamond and the friction behaviour of carbon species under different atmospheres is presented to support their findings. Their proposed wear model for unlubricated self-mated diamond bearing surfaces is discussed in the following. According to Gardos [32] and Hollman [41], diamond in the as-deposited state is hydrogen saturated due to the reaction gases present during deposition and, therefore, hydrogen makes the surface hydrofilic and in-

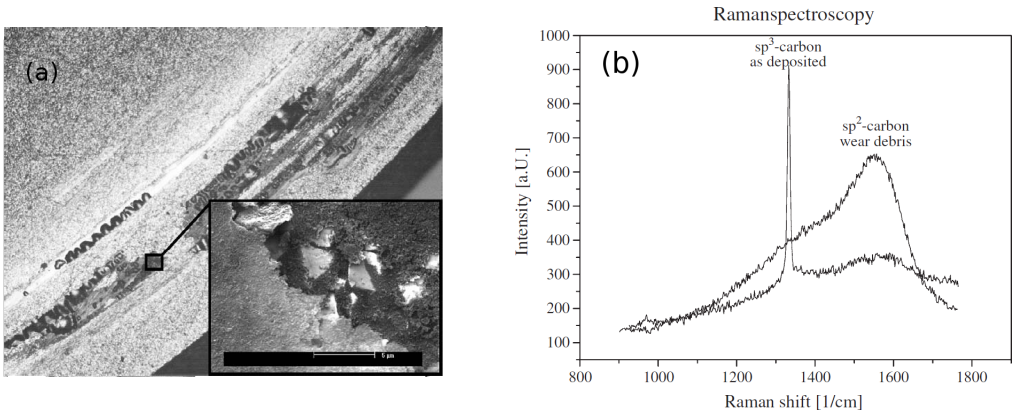

Figure 2.5: Tribological testing of polycrystalline diamond-coated homologous pairs: (a) SEM micrograph of wear debris produced in a inert atmosphere; (b) Raman spectra of wear debris and as-deposited coating, exhibiting the characteristic sp^3 diamond peak at 1332 cm^{-1}. The diagram evidences that sp^3 hybridised diamond transforms into the non-diamond sp^2 phase due to the tribological interaction [40].

hibits adhesion between mating surfaces due to the saturation of so-called dangling bonds.
At the beginning of all tribological experiments the interlocking of micro-roughness has to be conquered. A peak of the coefficient of friction indicates the necessary force to overcome this interlocking. The amplitude for such peak generally span the range 0.15-0.30, depending on the starting roughness of matting surfaces. Increasing the roughness invariably leads to higher peak values [40]. Moreover, during this initial breakage the mean contact pressure is responsible for stress peaks as a result of the small contact area of the micro-rough polycrystalline surfaces. As such, the applied load is inhomogeneously distributed and the real contact pressure becomes a multiple of the mean surface pressure. During the first cycles of motion, the real area of contact increases, therefore reducing the extreme surface pressure.

As wear progresses the hydrogen saturated surface is progressively removed and new species, such as oxygen or air humidity molecules, recreate bounds with the exposed surface. In the case of oxygen saturation, the replacement of hydrogen result in a change of surfaces' nature from hydrophobic to hydrophilic. Additionally non saturated dangling bonds can reconstruct with other dangling bonds. A reaction with a dangling bond of the mating surface increases adhesion and, therefore, an input of energy into the system is necessary to disrupt the bound [40].

Unsaturated bonds which react with the opposing surface increase the adhesional component of friction. This effect has been observed under vacuum conditions [42].

As can be seen in the friction curve of Fig. 2.4 (a), after the initial break-in phase (I and II) the rough disruption of diamond crystals decreases and constant friction and wear regimes sets in (III). For all the reported atmospheres, high temperatures and shear stresses occur between the opposing surfaces as a result of the frictional energy. Under high loads and high temperatures, phase transformations from sp^3 to sp^2 C-C bonding will normally occur [43]. In Perl et al. [40] work, measured bulk temperatures reached up to 200 °C and estimated flash temperatures more than 500 °C. Moreover, the generated wear debris were said to be very smooth which is in agreement with the presence of sp^2 graphitic carbon.

Despite that a consistent explanation of the graphitization process of diamond is lacking to date, many factors are associated to it, namely testing environment, temperature, pressure, diamond type (natural or man-made) and diamond particle size [43]. In general, the graphitization of diamond happens at appreciable rates only at high temperatures ($T > 2000$ K) in vacuum. However, such transformation occurs at relatively low temperatures ($T < 970$ K) when diamond is heated under a low pressure of oxygen [44]. This transformation is influenced by the desorption of hydrogen and oxygen from the surface. After decomposition the surface carbon atoms become more mobile, becoming what is normally referred to as free dangling bonds. At a latter stage, the dangling bonds can rearrange themselves into more thermodynamically favored structures, i.e. sp^2 graphite as this material constitutes the stable phase of carbon at atmospheric pressure, contrary to diamond which is unstable over the entire temperature range up to the melting point [44].

In the presence of air or pure oxygen both hybridization states (sp^3 and sp^2) react with oxygen at high temperatures forming CO_2, or CO in low levels of oxygen. Relatively to the combustion of carbon, the grain size of the wear particles becomes important. With decreasing size the combustion temperature gets lower, i.e. the amount of oxygen between interacting surfaces accelerates the combustion of diamond. As such, sliding in pure oxygen atmospheres will result in higher wear rates for diamond coatings [40]. Accordingly, this combustion is

inhibited by reducing the oxygen content in the testing environment and applying inert gases (nitrogen or argon) instead.

The generated wear debris cannot combust in very low oxygenated atmospheres and, as such, will accumulate forming agglomerates between the opposing surfaces. According to Perl et al.'s work [40], the agglomerated wear debris consist of small fractured particles of diamond as well as sp^2 hybridised carbon species. The dual nature of the debris will lead to unsteady values for the friction coefficient, as well as an increase of the wear rate due to surface disruption. Therefore, the wear rate will be dependent on the quantity of debris which remains between the mating surfaces, and a larger amount of diamond fragments will inevitably lead to higher damage of the coating. As such, the friction response will become unstable. Furthermore, Perl et al. have reported an increase in friction for sliding distance up to 50 km. Their explanation for such behaviour lays in the fact that the progressive polishing of the diamond surfaces and, therefore, decrease in the surface roughness inhibits atmosphere gases to reach the contact region. As a result, dangling bonds cannot be passivated because of the lack of oxygen and, concomitantly, the number of bonds reacting with the opposing surface rises. Such phenomenon causes friction coefficient values to approach magnitudes expected for vacuum conditions without delamination of the diamond film. However, it must be said that such straightforward explanation is supposedly only valid as a result of the type of configuration involved in Perl et al.'s work, i.e. ring-on-ring permanent contact, since for intermittent contact geometries - like ball-on-flat, for example - the passivation/de-passivation rates in relation to the oscillating frequency must also be considered into the equation.

2.2.2 Fine Grained and Nanocrystalline diamond variety

When a smooth planar surface is brought into contact with a smooth spherical surface of the same material, the deformation component (ploughing) of friction can be neglected. In this situation, smooth diamond surfaces constitute some of the slipperiest materials with a performance similar to polytetrafluoroethylene (PTFE) in ambient atmosphere. Friction coefficient values in the range $0.01 - 0.05$ are normally observed under unlubricated sliding conditions [45].

According to the classical model of Bowden and Tabor [8, p. 90–94], in its simplest form, the amount of friction resulting from a sliding contact is the sum of two contributing sources: mechanical deformation (ploughing) and/or fracture, and physical/chemical attraction or adhesion [26]. Intrinsically rougher microcrystalline diamond films were shown to produce ploughing, especially when MCD sharp asperity tips can apparently penetrate the softer counterfaces, hence giving rise to higher friction coefficient values. Moreover, these increased friction was also accompanied by wear intensification. However, for smooth and polished diamond coatings or cleaved natural diamonds, the ploughing component of friction is thought to be minimal, and friction is then largely controlled by the extent of adhesion between opposing surfaces [46].

In a study conducted by Miyoshi [45], fine grained (20 to 100 nm) diamond films were brought into contact with a natural diamond pin in reciprocating sliding motion in air. As a result of his work, he observed that the friction coefficient varied as the pin oscillated back and forth retracing its tracks against the coating, and that in humid air (40% R.H.) abrasion (ploughing) occurred and dominated the friction and wear behaviour. Another observation in Miyoshi's study, was that the single crystal diamond pin tends to penetrate into the flat surface of the diamond films, producing a wear track (groove). Moreover, SEM observations of the worn diamond coated (100)Si films revealed the presence of small fragments chipped off from the coating surface. Miyoshi also concluded that abrasive interactions between the diamond pin and the protruding asperities present in the relatively rough starting surface roughness (R_q = 15 nm) of the fine grained films, were responsible for friction coefficient values of about 0.13. The morphology and topography of these fine-grain CVD diamond films deposited onto (100)Si substrates can be seen in Fig. 2.6. From the AFM analysis, we observe that the surface is characterized by a granulated or spherulitic morphology, i.e. contains spherical asperities of different sizes.

As sliding progressed and the pin reciprocated over the same track, the friction coefficient was appreciably influenced by the wear damage on the fine-grain films. In fact, the repeated sliding produced a smooth wear track, where blunted and leveled-off asperities gave place to a low steady-state friction coefficient of about 0.03.

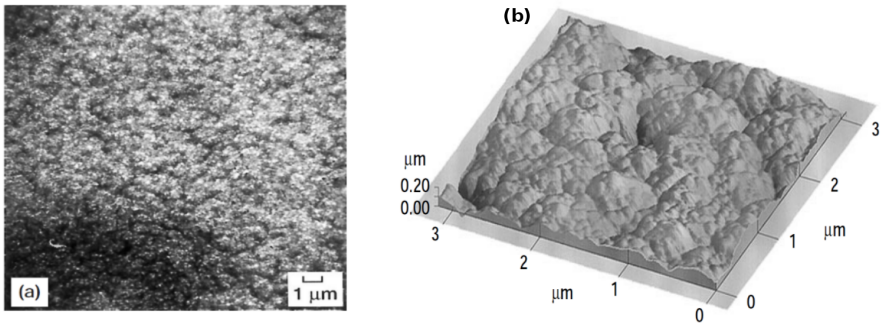

Figure 2.6: Fine-grain ($20 - 100$ nm) diamond films on (100)Si [45]: (a) SEM micrograph; (b) AFM image.

In another work, Miyoshi and Wu [26] addressed the influence of the environment on the tribological performance of fine-grain diamond films. The reason supporting such study, comes from the evidence that the environment to which CVD diamond films are exposed can markedly affect their friction and wear resistance. Once more, natural diamond pins were made to reciprocate against fine-grain diamond films in humid air, dry nitrogen and ultra-high vacuum (UHV) environments. Sliding in dry nitrogen was characterized by a similar trend in friction evolution as the one observed for humid air (40% R.H.), and previously described [45]. Nonetheless, the initial friction coefficient in dry nitrogen was slightly higher (~ 0.15) than in air (~ 0.13). Since the starting surface roughness of the diamond coatings can have a large influence on their initial friction, environment effects cannot account solely for this difference. Moreover, the equilibrium or steady-state friction coefficient ($0.03 - 0.04$) was observed to be independent of the initial surface roughness of the films and essentially the same for both environments, as well as abrasion occurred and dominated the friction and wear behaviour.

In UHV, the friction coefficient values were high (> 1.0) and increased with the number of passes, contrarily to what was observed for humid air and dry nitrogen. Furthermore, the starting surface roughness of the diamond films had no influence on friction. The friction behaviour observed by Miyoshi and Wu [26] is consistent with the results of other researchers, cited in the article, where self-mated single-crystal diamond and CVD diamond films in vacuum showed high friction values. A forwarded explanation was that as sliding continued, wear dulled the asperity tips and the gaps between asperities were filled by wear debris which lead to an increase

of the real area of contact (A_r), thereby causing the friction to rise. Moreover, continuous rubbing in vacuum conditions may also result in the removal of adsorbed contaminants from the surfaces, which represent a stronger interfacial adhesion between the diamond pin and the diamond films. In fact, the atoms exposed at the free surfaces possibly have a dangling bond, thus increasing adhesion and, concomitantly, friction. Therefore, those two effects conjugated would outdo the corresponding decrease in abrasion and friction that resulted from blunting the surface asperities. Experimental data supported such claim, since the equilibrium friction coefficient (1.70) was higher than the initial value (1.20) for fine-grain diamond films. Another observation from Miyoshi et al.'s study was that the wear rate of the diamond films in UHV depends on the initial surface roughness, generally increasing with it. Importantly, they were also found to be considerably higher ($\sim 10^{-4}$ $mm^3N^{-1}m^{-1}$) in UHV than in humid air ($\sim 10^{-8}$ $mm^3N^{-1}m^{-1}$) or dry nitrogen ($\sim 2 \times 10^{-8}$ $mm^3N^{-1}m^{-1}$). Once more, the adhesion between the opposing surfaces in UHV could account for such severe wear damage.

In a earlier article also by Miyoshi [33], the mechanisms of friction of fine-grain diamond films sliding against a polished natural diamond pin are addressed with some depth. The effects of carbon ion-implantation on the tribological behaviour of fine-grain diamond films were also analyzed, and their performance compared with as-deposited fine-grain films on the different environments studied. The carbon ion-implantation process (accelerating energy of 60 keV and dose of $1.2x10^{17}$ ions·cm^{-2}) causes a change in the surface chemistry of the films and structural damage to the diamond lattice. As a result, a thin layer (< 0.1 μm) of amorphous, non-diamond carbon is produced in the near surface region of the fine-grain diamond films. However, no appreciable change in surface roughness and morphology was observed by the author.

Since the surface of fine-grain diamond films was characterized by round shaped asperities and exhibited a smooth topography (rms, 15 to 50 nm), the ploughing term of friction can be neglected and, therefore, the friction coefficient arising between the film and the polished diamond pin is as follow [8, p. 98]:

$$\mu = \frac{A_r \times s}{W} \tag{2.1}$$

where, s, represents the shear strength of junctions, A_r, the real area of contact, and, W, the normal contact load. In humid air and dry nitrogen, the atmosphere provides a strongly bonded contaminant layer with a low s [33]. However, because the contaminant layer is thin (~ 2 nm), the load is largely supported by the hard diamond asperities and, consequently, A_r becomes small. Therefore, it results from Eq. 2.1 that the friction should be low in both environments, which has been confirmed by the experimental results [26]. In the case of the carbon ion-implanted fine-grain diamond films, and because both the amorphous carbon and contaminant layers have a low s, friction coefficient values must also be low (< 0.10) in these atmospheres. Miyoshi's experiments confirmed such theoretical predictions, where the tribotests showed equilibrium friction coefficients of 0.08 and 0.05 in humid air and dry nitrogen, respectively. Those values are slightly higher than those encountered for the as-deposited fine-grain films ($0.03 - 0.04$), however, the most beneficial effect of ion-implantation occurs for the sliding in UHV as will be discussed on the following. As said before, the sliding friction in UHV is high (> 1.0) for the as-deposited films [26], due to primarily from the adhesion between the opposing surfaces. In fact, the high elastic modulus and high hardness of the as-deposited diamond film will result in a small A_r, but s is correspondingly high. Moreover, the presence of dangling bonds - resulting from the deconstruction of surface bonds by the outgassing of adsorbed oxygen and water vapour in UHV [32] - and the "cleaning" of the contaminants (with low s) from the surface by rubbing in vacuum may play a significant role in the high shear strength of the junctions. These all contribute for the observed high friction values of diamond films in UHV.

After ion-implantation, the thin non-diamond carbon acts as a benign layer (i.e. friction lowering) since a combination of low s and small A_r, resulting from the high elastic modulus of the underlying diamond, produces low friction coefficients (< 0.10), even under UHV conditions. Thus, the non-diamond layer provides lubrication for the fine-grain diamond films in UHV.

In terms of wear performance, carbon ion-implanted fine-grain diamond films were characterized by wear rates on the order of 10^{-7} $mm^3N^{-1}m^{-1}$ in humid air and dry nitrogen, which indicates one order of magnitude above those measured for as-deposited films. Nonetheless, they represent an acceptable level of wear resistance for tribological applications. In UHV, a decrease in the wear rate was also observed for ion-implanted films (10^{-6} $mm^3N^{-1}m^{-1}$), in

comparison to the impractical values of as-deposited films in vacuum which are 30 to 60 times bigger.

Self-mated experiments involving nano-smooth fine-grained diamond (SFGD) coatings deposited onto Ti-6Al-4V titanium alloy, were performed by Met et al. [47] in different environments to approach the *in vivo* wear conditions. The coatings presented surface roughness values, measured by AFM, in the range $R_q = 14 - 33$ nm, and the gathered experimental data regarding the friction coefficient evolution, wear resistance and morphology of worn surfaces of SFGD-coated Ti-6Al-4V was used to assess their potential for biomechanical applications. Hemispherical pins (diameter of 6 mm and radius of curvature of ~ 10 mm) fabricated from diamond-coated Ti-6Al-4V were pressed onto diamond-coated Ti-6Al-4V discs (diameter of 34 mm and 5 mm thickness) with a normal load of 13 N, and tested on a rotating pin-on-disc (POD) tribometer at room temperature. A two-step process, each involving a different gas mixture (CH_4-H_2 and CH_4-CO_2), was used in diamond coating both triboelements on a MW-PACVD tubular reactor. The friction and wear tests were conducted at a sliding velocity of 0.1 ms^{-1} in ambient air ($40 - 60$ % R.H.), Ringer's solution and synthetic serum (Plasmion) containing 25 gl^{-1} of proteins.

Friction coefficient evolution curves concerning the diamond-on-diamond tribotests performed in all environments screened by Met et al. [47], are depicted in Fig. 2.7(a). As can be seen, all the curves reveal low values for the friction coefficient (< 0.10) up to the full length of the tests (8 km). According to the authors, the tribosystem characterized in ambient air revealed low levels of friction (mean value of ~ 0.06) even with the occurrence of some wearing-through of the SFGD coating at the pin tip and, subsequent, exposure of the Ti-6Al-4V substrate. The friction coefficient measured in Ringer's solution was about 0.03, while it was slightly higher in the presence of synthetic serum where the self-mated pairs exhibited a mean value of about 0.08. No explanation for this difference was given by the authors which, nonetheless, could be related to a series of factors likely related to the degradation (denaturation) of the proteins for such lengthy test [48] - since nothing is said in the original article regarding the regular substitution of the lubricants - or a protein attachment effect [49] which modifies the chemical nature and morphology of the bearing surfaces and, accordingly, causes a different friction

response. The gradual increase of the friction coefficient for the first kilometer or so of sliding distance, seem to point in that direction.

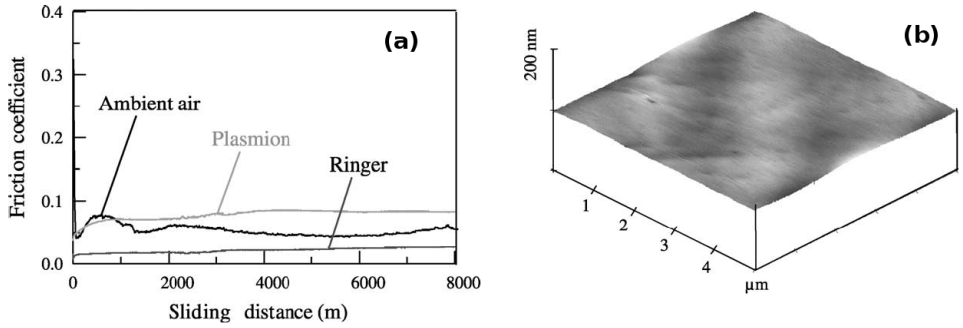

Figure 2.7: SFGD-coated Ti-6Al-4V self-mated experiments (W = 13 N) [47]: (a) friction coefficient evolution in different environments; (b) AFM 3D image of the disc wear track.

According to Met et al.'s [47] calculations, the initial Hertzian mean contact pressure, obtained by neglecting the influence of the thin diamond coating and the surface roughness, was ~ 460 MPa in all cases. Depending on the pin's wear scar, the final contact pressures oscillated in the leeway $60-200$ MPa. In turns, residual stress calculations using Raman spectroscopy of worn SFGD coatings, have revealed compressive stress values ranging from -3.2 ± 0.4 to -5.3 ± 0.4 GPa.

In terms of wear loss, the self-mated SFGD coatings were characterized by very low wear rates in all environments, with the worn surfaces revealing themselves unmeasurable in the case of the flat triboelements, using the cross-sectional profiles of the wear tracks or weight loss. In relation to the pins, estimated wear volumes using the diameter of the near-circular wear scars, resulted in a wear rate as low as 4×10^{-9} mm^{3}N^{-1}m^{-1} in ambient air. A very smooth ($R_q = 3$ nm) diamond surface was observed on the wear track region at the end of the test, as showed in Fig. 2.7(b). Such highly polished surface finishing was associated to a self-polishing mechanism, and was observed also during the relative motion of two diamond-coated discs. However, the authors clearly state that in this case the phenomenon has a rather short lifespan due to the fact that a substantial reduction of the local contact pressure happens after the diamond asperities are worn down.

In the Ringer's solution and synthetic serum, the pin surfaces exhibited even lower wear damage with the final wear rates ranging from $\sim 1 \times 10^{-10}$ to a few 10^{-10} mm^{3}N^{-1}m^{-1}, respectively. In

both lubricants, the SFGD coatings were still preserved in the two elements of the tribosystem after 8 km of sliding distance. Taking into consideration the excellent tribological performance evidenced by the SFGD-coated Ti alloy in physiological medium, the authors of the study concluded that self-mated nano-smooth diamond-coated surfaces could be materials of choice for various biomechanical applications.

The tribological behaviour of SFGD coatings deposited on titanium alloys has also been addressed in a paper by Vandenbulcke and De Barros [39]. Tribological experiments were performed using a pin-on-disc apparatus, in ambient atmosphere (R.H. 40-60%) and an applied load of 13 N. Diamond coatings deposited onto Ti-6Al-4V hemispherical pins (diameter of 6 mm) were made to slide, with a linear velocity of 0.1 ms^{-1}, against diamond-coated Ti-alloy discs.
The diamond-on-diamond sliding experiments were characterized by different behaviors, as a function of the diamond microstructure and surface roughness. A representative friction coefficient evolution for the SFGD coatings can be observed on Fig. 2.8(a). As can be seen, the friction coefficient, after a sharp peak of magnitude about 0.33, rapidly stabilizes at a value of approximately 0.06, until completion of the total sliding distance of 8 km. Moreover, the inherent smoother nature of the SFGD coatings were characterized by a better self-polishing of the counterfaces, with the worn surfaces exhibiting values of 3 nm (rms) for the surface roughness, instead of 8 nm like was the case of polycrystalline diamond coatings, also analyzed in their study. A value of 4×10^{-9} $mm^3N^{-1}m^{-1}$) was indicated for the final wear rate of SFGD self-mated tests, which represent a very-mild wear regime.

Another inherent advantage of SFGD over polycrystalline diamond coatings referred by the authors, comes from the difference in the initial local contact pressures ($\sim$ 2 GPa for a load of 13 N) which depend on surface roughness. In fact, the SEM studies conducted by the authors showed the presence of possible deformations resulting from the high shear stresses induced by friction at the tip of polycrystalline diamond grains. This morphology is depicted on Fig. 2.8(b) and was not evidenced in the case of polycrystalline diamond coatings subjected to sufficient low loads, as well as for the SFGD under 13 N. A plausible explanation for the latter situation would result from the intrinsic smoothness and lower modulus of SFGD coatings.

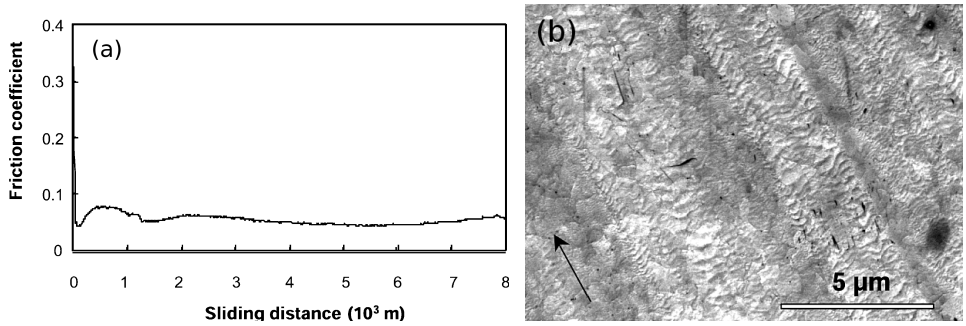

Figure 2.8: Self-mated diamond-coated Ti-alloy under an applied load of 13 N, in ambient air [39]: (a) friction coefficient evolution as a function of the sliding distance for SFGD homologous pairs; (b) secondary electron images of polycrystalline diamond-coated contact region, showing evidences of deformations associated to high shear stresses induced by friction.

As far as it is known, experimental data concerning the macrotribology of self-mated nanocrystalline diamond systems is non-existent or unavailable in the open literature hitherto. Therefore, it was not until the findings of the present thesis work got published, that data for NCD homologous tribosystems was made available to the community. Moreover, a similar outcome resulted regarding the micro- and/or nanotribological information of self-mated NCD films. Nonetheless, several studies have been published by tribologists interested on the comprehension of the friction and wear properties of tribosystems involving NCD coatings, as one of the counterparts. Antagonist materials have spanned metals, ceramics and polymers. A selection of the most relevant results of some of these studies, due to their pertinence to the present thesis work, are discussed in what follows.

Results concerning the friction properties of smooth nanocrystalline diamond coatings sliding against various metals, in dry and lubricated (water and polyalfaolefin oil) conditions, have been reported in a article by Hollman et al [41]. The NCD coatings were deposited onto cemented carbide (CC) substrates using a biased hot flame equipment and tested against CC, ball-bearing steel (BBS), stainless steel (SS), Ti and Al counterparts. Tribotesting was carried out in a ball-on-disc (BOD) tribometer with constant experimental parameters (W = 2 N, x = 120 m, v = 0.1 ms^{-1}). The as-deposited coatings presented an average grain size of 8 nm and surface roughness $R_a \sim 30$ nm, and were characterized by steady-state friction coefficient values

in the range $0.06 - 0.08$ against CC, BBS and SS in all three environments. The lowest friction was obtained with water lubrication and a very mild wear regime (1.9×10^{-10} $mm^3N^{-1}m^{-1}$) was reported during the dry sliding of NCD against SS. This investigation showed that smooth NCD coatings display exceptionally low friction and high wear resistance against metallic materials in dry and water lubricated sliding, thus opening new areas of tribological opportunities.

In a paper by Zuiker et al. [21], tribological data relative to BOD experiments of Si_3N_4 balls sliding against NCD films is presented. The diamond films were grown in a MWPACVD reactor on top of single crystal Si wafers and exhibited surface roughness values varying in the range $30 - 125$ nm (rms), depending on the deposition parameters. The tribotests were conducted in dry N_2 environments under a constant applied load of 2 N, and for a sliding distance of 200 m and rotational speeds varying in the range $50 - 150$ r.p.m ($v = 25 - 40$ mms^{-1}). The smoothest Ar-grown NCD films showed friction coefficient values in the leeway $0.04 - 0.06$, whereas large fluctuations in the friction traces and very high initial friction coefficient values (up to 0.70) were observed for the roughest films. The authors attributed those initial features to the ploughing and interlocking of asperities across the sliding surface. Thus, severe abrasion and ploughing on the softer Si_3N_4 counterpart is caused by the hard and sharp asperity tips of diamond crystals, prevailing on the rough films. With increasing sliding distance, the sharp asperity tips are progressively blunted and worn down, and the valleys existing across the asperities filled with a blanket of wear debris. Therefore, the combination of these two physical phenomena leads to a relatively smooth surface finishing of the rough diamond films, resulting, eventually, in lower friction levels (~ 0.20). In the case of the much smoother NCD films, continuous sliding produced contact surfaces with exceedingly smooth appearance and little to no wear of the diamond films could be assessed with surface profilometry. Thus, frictional losses for the tribosystem NCD/Si_3N_4 remain low, especially after the breaking-in regime. Wear rates of about 0.2×10^{-10} $mm^3N^{-1}m^{-1}$ were reported by the authors.

In two other works involving the ceramic Si_3N_4 as an antagonist, Erdemir et al. [13, 24] reports on the tribological properties of NCD-coated Si_3N_4 films grown by a novel method in Ar-C_{60} and Ar-CH_4 microwave plasmas. Laser polished NCD films were also evaluated and their tribological performance compared with the as-deposited ones. Grain sizes of the films produced by the novel method exhibited very small sizes ($10 - 30$ nm) and lead to

much smoother surfaces (R_q = 20 − 40 nm) than those obtained by conventional H_2-CH_4 MW-PACVD deposition. The tribotests were run under an applied load of 2 N in ambient atmosphere (30-40% R.H.) and dry N_2. Friction curves acquired during the sliding of a smooth NCD film (R_q = 30 nm) against a Si_3N_4 ball counterpart in open air and for MCD versus Si_3N_4, for comparison purposes, are shown in Fig. 2.9(a). As is clear, after an initial running-in period characterized by relatively high friction coefficient values, the friction steadily decreases to ∼ 0.10, whereas the MCD film exhibits high and unsteady friction values. Thus, sliding friction tests results demonstrated that smooth NCD films can provide low friction levels when in relative motion against Si_3N_4, without lubrication.

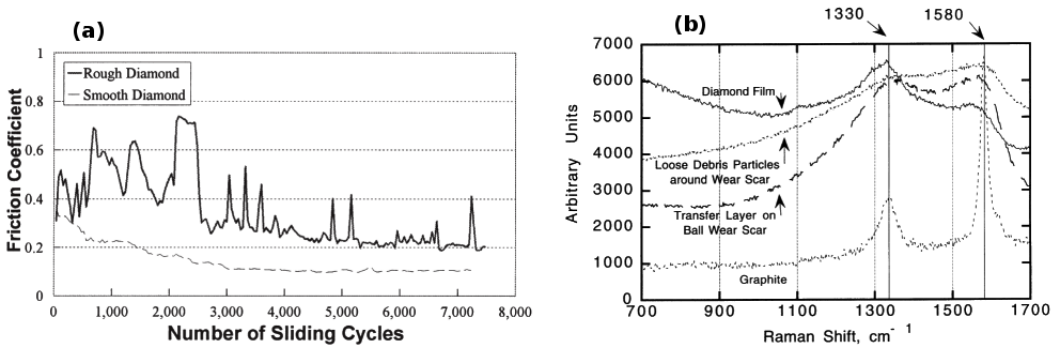

Figure 2.9: Tribological testing of NCD films against Si_3N_4 balls (W = 13 N, v = 0.05 ms^{-1}) [24]: (a) friction coefficient evolution in open air and comparison with MCD coatings (rough diamond); (b) Raman analysis of wear debris and transfer layers formed on an Si_3N_4 ball, in dry N_2.

A comprehensive explanation to why smooth NCD films exhibit such low-friction can be find in both Erdemir et al.'s papers [13, 24]. In short, mechanistically, the low-friction nature of smooth diamond surfaces has been widely attributed to the highly passivated nature of their surfaces. In fact, it has been postulated that gaseous adsorbates, existing in the surrounding atmosphere (preferably hydrogen, but also oxygen or water vapour), could effectively passivate the surface dangling bonds, and subsequently reduce drastically the adhesion between antagonist surfaces. Moreover, the ploughing component of friction becomes insignificant in the case of smooth NCD films. Another possibility taken into account by the authors to explain the low friction, is the likely occurrence of phase transformations due to extreme contact pressures and high frictional heating at local asperities (flash temperatures).

The logic behind such a transformation is that under the combined influence of highly concentrated normal and shear forces and frictional heating during sliding, the summits of the diamond asperities may undergo a gradual phase transformation or graphitization. Diamond, which is thermodynamically unstable, could, therefore, transform into a more stable form of carbon, like graphite. The occurrence of graphitization has also been reported on another study by Pimenov et al. [50], dealing with NCD films rubbing against a ruby counterpart. As sliding progresses, the transformation continues and the graphitic debris accumulate at the sliding interface. Evidences of such graphitization of the entrapped wear debris and transfer layers formed on the ceramic balls, can be inferred from the Raman spectra of Fig. 2.9(b). Specifically, two broad Raman features (centered at 1330 and 1580 cm^{-1}) match the D- and G-bands of crystalline graphite [51] (see also Sec. 3.4.3), suggesting that the debris particles are in fact sp^2 coordinated.

In terms of wear performance, average specific wear rates of the order of 5×10^{-7} $mm^3N^{-1}m^{-1}$, have been reported for the Si_3N_4 ceramic balls. It is also noteworthy to stress the fact that the amounts of wear loss on smooth NCD films were unmeasurable [13], once more confirming the exceptional wear resistance of NCD films in open air.

2.3 Applications of diamond-coated systems

Recent advances in diamond film technology has the potential to revolutionize products, industrial and consumer applications, particularly in the field of tribology. Diamond coatings offer a wider tribological potential than do natural and high-pressure high-temperature (HPHT) synthetic diamond, due to the fact that considerations like size, geometry and cost will not be as restrictive [34].

In fact, diamond coatings can improve many of the surface properties of engineering substrate materials, including wear resistance, hardness, friction reduction, erosion and corrosion resistance. Nowadays, applications of CVD diamond in the field of tribology, particularly those involving areas such as cutting and forming tools, automotive and aeronautics wear parts and mechanical face seals, constitute an industrial fact. Moreover, the excellent resistance of diamond against any chemical attack makes this coating material highly desirable for the chemical and pharmaceutical industry, as well in nuclear power plants [34, 52].

More so, recent advances in CVD technologies have pioneered the development of nano–structured diamond, which provide extreme properties ranging from super-hardness to super-lubricity; characteristics which are very desirable for use in micro-systems and seal applications [53]. As such, diamond will probably become one of the most versatile coating materials in the near future, once the deposition temperatures can be lowered to more moderate ones and its toughness further enhanced [36].

Due to the fact that diamond has an extremely high melting-point and sustains its hardness to very high temperatures, traditional applications involve cutting tools, wire drawing, machining and sawing, as abrasives for grinding wheels and lapping suspensions, polishing powder and other intensive tribological applications [8, 11, 54]. The advantages of diamond-coated tools are versatile tool geometry, higher cutting speed, extended tool life and lower cutting force, which minimizes the probability of structural damage on the materials and, also, lower power consumption [34].
As wear parts and in the fluid handling industry, diamond coatings have been successfully applied to bearing surfaces, extrusion and drawing dies, transport guides, indenters, abrasion-resistant decorative coatings (for example in watch parts), engine parts (valves and rotors), high pressure nozzles and, in general, as self-lubricating, anti-wear chemical barriers for moving mechanical assemblies [34, 55]. Moreover, the use of diamond coatings in styluses, nano-indentation hardness measurement and scratch tips, and conductive AFM tips has become widely disseminated, nowadays [56, 57].

Diamond is also unique among infrared optical material, in that it can provide a combination of high strength and durability with transparency in the ultraviolet, visible and infrared (IR) regions of the light spectrum [58]. Thus, a combination of strength, high thermal conductivity and chemical inertness make CVD diamond a far IR “window” material of choice in extreme environments, like those found in very high power CO_2 laser exit windows and in high temperature resistant aircraft windows [11, 58]. CVD diamond coatings are also excellent materials for electron field emitters due to their low or negative affinity, combined with excellent mechanical and chemical properties, and capacity to withstand ion bombardment. These all make diamond field emitters potentially advantageous in vacuum electronics [59].

In microelectronics assembly technology, diamond films have been used to coat the contact surface of tools, ex. in push pins, bonding tools, tubes, etc..., with the purpose of providing wear resistant chemical barriers.

Researchers are also spending a considerable amount of effort to develop novel applications, such as moving mechanical assemblies (MMA) to be used in microelectromechanical systems (MEMS) like microengines, micro-bearings, micromachines or other devices requiring the production of torque [46]. Diamond, in its nanocrystalline form, is also being sought as a potential material for MEMS with the electrical properties more in evidence, like in heater elements for water microjet used in inkjets [60]. Other potential applications include diamond-coated ball and roller ceramic bearings, as well as scratch-resistant coatings to be used in computer hard-disc drives [34]. Environmentally durable barriers, like e.g. chemical and mechanical barrier for Space Shuttle's check valves, constitute another case of potential application of CVD diamond coatings [26].

Presently, most of the MEMS devices explored and designed are primarily based on silicon (Si), because of the technological know-how accumulated on this particular semiconductor at the micro-scale and available surface machining technology [61]. However, a major problem with Si-based MEMS technology derive from the poor mechanical and tribological properties exhibited by this material. As such, practical MEMS devices are currently limited mainly to applications dealing with bending and flexural motion, like cantilever accelerometers and vibration sensors. Moreover, the dynamic range of such devices is also very limited as a result of the poor mechanical properties of Si. Therefore, novel MEMS applications involving significant rolling or sliding contact will necessarily require the use of new materials with enhanced mechanical and tribological behaviour [62].
Due to its ability to perform well in harsh environments, a brittle fracture strength 23 times that of Si and a projected wear life for MEMS MMAs 10^4 times greater than that of Si-based MMAs, diamond becomes a material of choice for such critical applications. Conventional MCD films are generally ill-suited for MEMS MMA applications due to their large grain size and rough surfaces. However, recent advances in the synthesis of phase-pure ultrananocrystalline diamond (UNCD) coatings with morphological and mechanical properties ideally suited

for MEMS in general, and MMA devices in particular, grants this variety of diamond a huge potential in the development of state-of-the-art MEMS components [62].

Potential technological and industrial applications of diamond films have also reached the biomedical field, where they have been submitted to scrutiny for their use in biomedical equipment and devices, like surgical tools, diamond shafts and bearings for blood or heart pumps [34, 63]. Other studies involve the use of CVD diamond as X-ray micro-dosimeters [64], as detectors of DNA [65] or micro-systems for biochemistry [66].
In addition, based on the excellent tribological properties demonstrated by self-mated water lubricated NCD coatings in the present thesis work (see Sec. 5.5), and more particularly from biotribological studies conducted on NCD films by our group [67, 68], the collected data seem to put in evidence the great potential of applicability of NCD for clinical use, like in total joint arthroplasty.

Chapter 3

Experimental techniques

A combination of advanced characterization techniques already consolidated in the area of materials science and state-of-the-art diamond deposition techniques, producing highly adherent coatings with exceptional tribological performance, were used in the present thesis work. Those techniques will be presented in the following sections.

3.1 Silicon nitride substrate material

The spontaneous nucleation of chemical vapour deposition (CVD) diamond on a foreign substrate has a low probability, with e.g. nucleation densities on the order of 10^4 nuclei·cm^{-2} for silicon substrates. As such, the achievement of much higher nucleation densities becomes imperative in order to produce thin continuous diamond films or conformal coatings deposited onto surfaces with intricate shape. This increased growth will be accomplished by placing diamond seeds on the substrate before or during the deposition. For nucleation densities in the range $10^8 - 10^{10}$ nuclei·cm^{-2}, grains of 0.1-1.0 μm in size are typically observed on the substrate, which evolve into columnar crystallites with their size gradually increasing in proportion with film thickness. Moreover, the surface relief of the nucleation side of a free-standing diamond film will become a replica of the substrate's relief, with the quality of the reproduction improving with increased nucleation density [51].

Therefore, and since the surface processing of diamond, in particular polishing, is a difficult and time consuming procedure, it is of great advantage that the nucleation side of the film can

be made smooth enough by using polished substrates, in order for the as-deposited coatings to be used in applications where low surface roughness values are paramount.

Owing to its high strength, low density, excellent oxidation resistance and low elastic modulus, silicon nitride (Si_3N_4) is one of the strongest structural ceramics [69]. A very good thermal shock resistance constitutes also one of its assets, which result from a low thermal expansion coefficient and aforementioned properties. Furthermore, Si_3N_4 is emerging as a serious candidate in many tribological applications [70, 71].
In order to obviate the large thermal expansion coefficient mismatch existing between the diamond coating and substrate material, the traditional route has consisted in using intermediate interlayers, mainly for metallic substrates. However, diamond films deposited on intermediate layers frequently show lower adhesion levels as compared to optimized direct deposition on adequate substrate material, like ceramic substrates [72]. Among those, Si_3N_4 reveals a great potential in the production of stress-free highly adherent diamond coatings for demanding tribo-applications, because of its low thermal expansion coefficient mismatch with diamond and carburizing nature [73].

A number of seeding procedures are at disposal to strongly enhance diamond nucleation and, henceforth, film homogeneity and conformity to intricate substrates. A simple mechanical abrasion of the substrate, for example, using a diamond grit promotes nucleation. However, if the surface damage becomes too high as a result of increasing defects and abrasion scratches, the procedure may not held adequate results [51]. Therefore, a very popular procedure consists in seeding by ultrasonic treatment in a suspension of diamond powder in an appropriate liquid (acetone, alcohol, etc.), which enables the coating of intricate shapes and minimizes surface damage. Moreover, nanoscale seeds can penetrate with the liquid into surface porosity, allowing the diamond deposition inside.

In the present thesis work, Si_3N_4 flat specimens were produced by pressureless sintering at 1750 °C for 2 h, under a nitrogen atmosphere, in order to obtain dense substrate material for diamond deposition. Complementary details regarding the powder preparation and processing route of Si_3N_4 flat substrates are described in Publication I (see Sec. 4.2). Commercially

available (Kema Nord) Si_3N_4 balls (5 mm of diameter) were also used as the counterbody substrate material.

Several procedures were employed to enhance the adhesion levels of the various diamond coating varieties studied, prior to deposition. In relation to the microcrystalline diamond (MCD) variety, the flat substrates were submitted to the following finishing pre-treatments, in order: grinding with a 46 μm grit size diamond wheel, diamond polishing (15 μm) and manual scratching with $0.5 - 1$ μm sized diamond powder on a silk cloth. As a mean to remove loose diamond particles, the flat specimens were initially rinsed for 10 min in an ultrasonic bath containing acetone, and afterwards in an ethanol bath with the same duration.
Owing to the intrinsic high surface roughness of the Si_3N_4 ball substrates, those were subjected to a gradual polishing with 15, 6 and 1 μm sized diamond powder in order to reduce the surface roughness. All spherical specimens were subsequently subjected to microflawing by ultrasonic agitation with a diamond suspension ($0.5 - 1.0$ μm) in hexane to promote diamond nucleation and adhesion.

Regarding the preparation of Si_3N_4 substrate material for the deposition of nanocrystalline diamond films, similar processing routes were followed as the ones described for the MCD coatings. Nonetheless, different pre-treatments were employed in order to cope for the specificities presented by the NCD coatings. Figure 3.1 shows a SEM image revealing the typical aspect of the Si_3N_4 substrate in a ball specimen and corresponding NCD coating. It is noteworthy to refer to the micro-porosity observed on the substrate surface, resulting from plasma etching, which warrants improved adhesion levels and a more effective diamond seeding.

Concerning the microwave plasma-assisted chemical vapour deposited (MWPACVD) NCD films (see page 45), both substrate geometries were submitted to an appropriate ultrasonic pre-treatment in a 40 μm sized diamond powder suspension before the plasma treatment, as a mean to enhance diamond nucleation.
In relation to the NCD coatings synthesized using the hot-filament CVD technique, the flat Si_3N_4 substrates were ground and submitted to three different surface finish conditions, in order

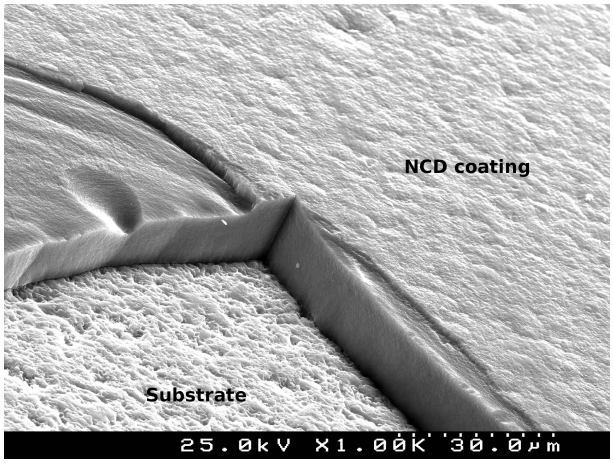

Figure 3.1: SEM image detail showing the typical aspect of a nanocrystalline diamond-coated Si_3N_4 ball specimen, where the coating has been fractured in order to expose the ceramic substrate.

to procure the best condition characterized by an increased adhesion and lowest possible surface roughness. As such, the three mechanical pre-treatments were (i) flat lapping with 15 μm diamond slurry; (ii) hard cloth polishing with 15 μm diamond slurry; and (iii) polishing to a mirror-like finish with colloidal silica (0.25 μm). The substrates were subsequently scratched for 1 h, in an ultrasonic suspension with 1 μm diamond powder in n-hexane (1 g/100 ml).
In order to further enhance the ceramic surface for improved NCD adhesion, both substrate geometries were chemically etched by hydrogen plasma for 30 min in another study (see Publication VII, Sec. 5.4).

3.2 Diamond deposition

The relevance and rapid development experienced by tribological coatings in recent years result largely on the availability of novel and efficient deposition techniques, which are capable of providing the level of control of properties that were unattainable not so long ago. Such properties include the morphology, composition, structure and enhanced adhesion to the substrate. Considering the various deposition techniques pertinent today, plasma and ion-based methods are among the ones that concentrate the most attention and give growing impetus to the field of tribological coatings [20, p. 7].

According to Rickerby and Matthews' general classification system for the deposition processes, cited in Holmberg and Matthews [20, p. 8], these can be divided into four generic groups, as follow:

- ▷ gaseous state processes;
- ▷ solution state processes;
- ▷ molten and semi-molten state processes;
- ▷ solid state processes.

Owing to the relevance of gaseous state processes in the present thesis work, they will be addressed in the following. In general terms, this group of processes cover engineering techniques in which the coating or surface treatment material passes through a gaseous or vapour phase prior to deposition or surface modification. Gaseous state processes can be further sub-divided into three main sub-groups, namely chemical vapour deposition (CVD), physical vapour deposition (PVD) and ion beam assisted deposition (IBAD). The CVD technique makes use of gaseous reagents delivered into the reaction chamber, that will act as the source of coating species, whereas in PVD one or more species are evaporated or otherwise atomized from the solid phase, inside the reaction chamber [20, p. 11].
Two derivates of the CVD technique were used in the deposition of MCD and NCD coated Si_3N_4 systems studied in the the present thesis work and, therefore, will be discussed in more detail in the following sections.

The strength of CVD technique result from its ability to produce well adhered, uniform and dense surface layers. The grain orientation and size, coating composition and properties can be tailored by selecting adequate processing parameters. It can be employed to deposit successfully a vast range of wear resistant coatings, such as borides, carbides, nitrides, oxides, carbo-nitrides and oxy-nitrides of almost all the transition metals [20, p. 14].
There exists many derivatives of the CVD process, which emerged in response to certain desirable characteristics for the deposited coatings and/or ability to coat a wide range of substrate materials. Examples of such requisites are lower deposition temperatures, epitaxial growth of films, improved coating adhesion and controllable deposition rates. Moreover, several means

of assisting the CVD process have been developed, such as through the use of laser or electron beams, or by ion bombardment of the growing films [20, p. 13].
A preferred route to reduce the deposition temperature consists in using the plasma-assisted variants of the CVD technique, where an electrical discharge in a low-pressure gas is used to accelerate the kinetic of the CVD process [10, p. 236].

The Chemical Vapour Deposition (CVD) technique

The chemical vapour deposition (CVD) technique is characterized by thermally–induced chemical reactions at the surface of a heated substrate, with the reagents supplied as gaseous species. The substrate material itself may be involved in these reactions, but rarely do so. Typical deposition temperatures of CVD processes usually cover the range $600 - 1100\,^{\circ}C$, although efforts are being pursued to develop new processes that will operate at lower temperatures. At these temperatures significant thermal effects may occur on the substrate, which makes the use of CVD impractical for materials with low fusion temperatures. The simplest form of CVD involves the pyrolytic decomposition of a gaseous compound on the substrate, therefore providing a coating of a solid reaction product [10, p. 234].
The high process temperatures involved in CVD will be responsible for various solid-state reactions, such as phase transformations, precipitation, recrystallization and grain growth. Moreover, it will also be responsible for appreciable interdiffusion between the coating and substrate material [20, p. 15]. This generally means higher adhesion levels but, nonetheless, could also lead to the formation of intermediate phases or brittle intermetallic compounds at the interface of some systems. These occurrences impair the mechanical properties and the effective adhesion of CVD coatings. Possible solutions consist in the use of diffusion barriers interlayers or adequate substrate material [10, p. 235].

The equipment involved in CVD technique is normally constituted of a heated reaction chamber and associated gas-handling equipment. The substrate is usually heated by convection and radiation within the reaction chamber, and the whole CVD process is controlled by varying the temperature of the substrate and the composition, mass or volume ratios and partial pressures of the gaseous species involved. Optimum deposition rates generally occur at pressures bellow atmospheric.

The deposition rate depends strongly on the processing parameters, but values in the range 0.1 to 10 μm·min^{-1} are typical. In terms of microstructure, CVD coatings usually exhibit a columnar growth, although the initial deposit is sometimes equiaxed. The microstructure and grain size will, once more, depend largely on the processing conditions and are generally self-excluding, i.e. a compromise must be established between high deposition rates, attractive for economical reasons, and a fine-grained microstructure normally showing the best tribological performance [10, p. 235].

Diamond coatings are deposited by CVD processes at high substrate temperatures (on the order of 800 °C). The best adhesion levels are achieved on silicon or silicon-based substrates, requiring an interlayer for other substrates to adjust thermal expansion mismatch at the interface. Growth of the diamond phase on a non-diamond substrate is triggered by nucleation either at randomly seeded sites or at thermally favored sites, as a result of the statistical thermal fluctuations occurring at the substrate surface.
Depending on deposition temperature and pressure conditions, favored crystal orientations dominate the competitive growth process. Typically, the deposited diamond coatings exhibit a polycrystalline nature with relatively large grain sizes (> 1 μm), as well as rough surfaces with values of R_q in the range of a few tenth of micron to tens of micron [54].

In order to produce diamond thin films, several CVD methods have been developed that require a volatile hydrocarbon precursor, an energy source, and an abundant source of atomic hydrogen. The growth species is the methyl radical (CH_3^*) and is typically produced by CH_4-containing plasma. For the plasma chemistry, atomic hydrogen plays essentially two major roles: the first consists in the preparation of CH_3^* adsorption sites by depleting hydrogen atoms from the hydrogen-passivated diamond surface, and secondly it removes afterwards hydrogen atoms from the adsorbed CH_3^*, thus allowing carbon atoms to move into the position corresponding to an extension of the diamond lattice, i.e. contributing to diamond growth. In addition, atomic hydrogen preferentially regasifies the graphitic phase, which is thermodynamically more stable than bulk diamond, therefore hindering the formation of non-diamond sp^2 phases.
Growth of diamond films that are largely free of non-diamond secondary phases is possible by

using plasmas extremely rich in H_2 ($98-99\%$). However, atomic hydrogen is also responsible for etching the diamond phase, therefore resulting in the formation of intergranular voids and a columnar morphology [62].

Microcrystalline diamond variety

Conventional microcrystalline diamond (MCD) films are synthesized in hydrocarbon-hydrogen gas mixtures consisting typically of 1% CH_4 in 99% H_2. The role played by hydrogen in the plasma chemistry has been considered of crucial importance in the various diamond CVD processes developed over the years, especially in the absence of oxygen and perhaps halogens. Typically, atomic hydrogen is produced either by collision-induced processes or by thermal decomposition in the plasma, and constitutes an essential component from which diamond CVD films are grown [46] (see previous Section).
Increasing the CH_4/H_2 ratio in the plasma will have the effect of decreasing the grain size of MCD coatings, with values as low as $50-100$ nm, which implies a corresponding reduction of the surface roughness. However, such effect will also contribute to the introduction of intergranular non-diamond carbon phases, thereby degrading the coatings' mechanical properties by limiting the brittle fracture strength [62].

The microwave plasma-assisted CVD (MWPACVD) technique constitutes a derivative of the basic non-enhanced CVD process and is commonly used for MCD synthesis [74]. A schematic of a MWPACVD apparatus is depicted in Fig.3.2. It mainly consists of a low-pressure chamber placed inside a resonant microwave cavity, where the gas mixture is activated by a microwave power supply. The substrate is heated by the plasma and by an additional heating source, thereby providing a means to control the substrate temperature independently of other growth parameters [75].
Likewise, the deposition of MCD films using the MWPACVD variant consists on the decomposition of gaseous species containing a carbon precursor, in the presence of hydrogen and, sometimes, oxygen. The gas composition and processing parameters will strongly influence the film properties and deposition rate [10, p. 236].

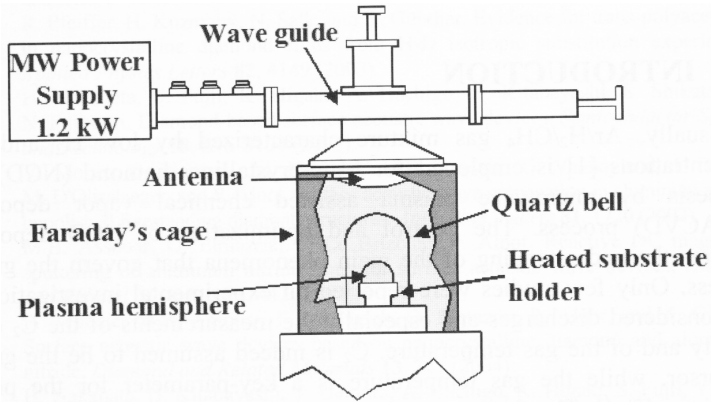

Figure 3.2: Schematic of a MWPACVD apparatus [75].

In the present thesis work, MCD coatings were synthesized onto flat and ball-shaped Si_3N_4 substrates using a MWPACVD apparatus (ASTeX PDS18, Seocal and Seki Technotron Corp.), and where the process parameters have been adjusted to achieve similar thicknesses in both geometries, as follow: microwave power, ~ 3 kW; total gas pressure, 1.2×10^4 Pa; H_2/CH_4 gas flow, 400/25 sccm and 400/16 sccm for the flat and ball specimens, respectively; deposition time, 2.5 h. These conditions were responsible for coating thickness and diamond grain size values of $12 - 14$ μm and 2.5 μm, respectively. Representative SEM micrographs of the as-deposited MCD coatings are showed in Fig. 4.8 of Publication II (see Sec. 4.3), for example.

Nanocrystalline diamond variety

As was discussed previously, CVD diamond constitutes an important route in the production of this singular material. Beginning from the first successful CVD diamond depositions, efforts were generally done with the main objective of maximizing the crystalline quality of the synthesized films. However, it was found that diamond grown under non-optimum conditions, such at lower temperatures or higher carbon activity in the plasma, produces films with small crystallite sizes. This material is commonly referred to as nanocrystalline diamond (NCD), even if the grain size exhibit values in the leeway $5 - 100$ nm [76]. Following its discovery, many research works in the area of diamond coatings aim the production of the NCD variety under specific conditions, since smaller grain sizes imply according to the well-know Hall-Petch

relation improved mechanical and physical properties [36], as well as a greater potential for low friction, due to the inherent reduction in surface roughness [76].

Like was referred before, in conventional CVD diamond growth process involving the CH_3^* precursor, large concentrations of atomic hydrogen are needed due to the low probability of CH_3^* to enter a diamond lattice site, i.e. as a consequence of the hindering effect of the sterile hydrogen-terminated diamond surface. However, aside the high cost and danger hydrogen represents during manipulation, such a high concentration of atomic hydrogen will generate film morphologies and surface roughnesses which are inadequate for many tribological applications. Consequently, fresh methods have been developed which make use of MWPACVD variant, and involve a new C_{60} or CH_4/Ar chemistry [62]. In these processes, the diamond-growth species are now gaseous carbon dimers (C_2), resulting either from the fragmentation, induced by collisions, of gas phase C_{60} in a Ar plasma or from CH_4 in H_2 poor atmospheres, via the following reactions:

$$\begin{aligned} 2CH_4 &\rightarrow C_2H_2 + 3H_2 \\ C_2H_2 &\rightarrow C_2 + H_2 \end{aligned}$$

Several studies have showed that the diamond film morphologies are essentially independent of the carbon dimer precursor species. Moreover, as a result of the limited amount of atomic hydrogen in the plasma, very high renucleation rates are sustained ($\sim 10^{11}$ nuclei$\cdot$cm^{-2}s^{-1}) and grain coarsening is hindered. The resulting diamond films consists of equiaxed grains with sizes as low as a few nanometer, depending on the process parameters. Furthermore, the scarcity of atomic hydrogen will also minimize the regasification of these very small grains, thus leading to relatively high linear growth rates and the deposition of continuous films, even at very low thicknesses [62].

Due to the very small grain sizes, diamond becomes also the thermodynamically most stable phase of carbon, thereby avoiding the need to suppress the formation of sp^2 non-diamond phases [62]. Nonetheless, in the followup of several studies in which hydrogen had been totally replaced by a noble gas, such as Ar, it has been shown that the presence of C_2 in microwave plasma, inevitably results in films largely composed of amorphous or short-range order non-diamond phases, like graphite. The carbon dimer is highly reactive and is one of the carbon

species resulting from the sublimation of graphite. In microwave plasmas, it is generated from hydrocarbon molecules under highly unstable conditions, resulting in super-saturated carbon vapour [46]. In turn, the Ar concentration influences secondary formation of nuclei [77].
Gas mixtures composed of $Ar/H_2/CH_4$ and characterized by low H_2 and CH_4 concentrations, are commonly employed in the synthesis of NCD thin films using MWPACVD [75]. However, the easy production of large quantities of the fullerenes, has provided an opportunity to rethink the whole synthesis of diamond films from noble gas plasmas, using very low contents of hydrogen and C_{60} as a precursor molecule instead of CH_4 [46].

Two factors become preponderant in the synthesis of NCD films. One consists in increasing the nucleation density to $10^9 - 10^{10}$ nuclei·cm^{-2} during the initial stages, the second implies to control the crystal grain growth to achieve nanometer-scaled sizes. In fact, the content of hydrogen and hydrocarbon, for e.g. C_2, CH_3, CH, etc., in the reaction chamber will have a profound influence in the size and structure of the diamond grains. On one side, a high content of hydrogen promotes the nucleation and growth of diamond grains, therefore accelerating the coating growth rate. On the other hand, the grain growth is restrained by the increase of the ratio of secondary nuclei formation, due to the reduction of hydrocarbon content, and vice-versa [77]. Moreover, the gas temperature constitutes a key parameter in the plasma chemistry [46].

In the present thesis work, NCD-coated Si_3N_4 substrates were produced by runs in MWPACVD and hot-filament (HFCVD) apparatuses. For the first technique, NCD deposition occurred in continuous wave (CW) and pulsed wave (PW) mode for the flat and ball specimens, respectively, under $Ar/H_2/CH_4$ microwave discharges. The same gaseous species were also used in the second deposition method. The main process parameters used in both techniques are summarized in Tab. 3.1.

For the case of MWPACVD deposition, operated in PW mode, the pulse repetition rate used was 1000 Hz, with a duty cycle of 50% for a maximum input microwave power of 800 W. A deposition time of 3 h was employed, which resulted in film thicknesses of about 12 μm. Relatively to the HFCVD films, the aforementioned parameters produced growth rates of 1.6 μmh^{-1} and 2.2 μmh^{-1} for the flat and ball specimens, respectively. Deposition times of 12 h and 24 h lead to the formation of NCD crystallites with an average grain size of 28 nm.

Table 3.1: Process parameters used in the NCD deposition (P, total pressure; T_{sub}, substrate temperature; T_W, filament temperature; sccm, standard cubic centimeter per minute).

Technique	Gas mixture	Gas flow	P	Power	T_{sub} (°C)
MWPACVD	$Ar/H_2/CH_4$	250 sccm	200 mbar	600 W	825; 925
	96%:3%:1%			800 W	925

Technique	Gas mixture	Gas flow	P	T_W (°C)	T_{sub} (°C)
HFCVD	$Ar/H_2/CH_4$	50 ml·min^{-1}	50 mbar	2300	750
	Ar/H_2 = 0.1 CH_4/H_2 = 0.04				

The morphology and topography of as-deposited NCD coatings synthesized by MWPACVD and HFCVD techniques can be seen in Publication V (Sec. 5.2), and Publication VI (Sec. 5.3) and VII (Sec. 5.4), respectively.

3.3 Tribo-testing and definition of quantities

Tribological testing, or tribo-testing, involves the study of friction, wear and lubrication. According to Uetz et al., cited by Zum Gahr [78, p. 116], although a very large variety of equipment and arrangements have been in use for tribo-testing, these can be broadly classified into the following six categories: field test, bench test, subsystem, component test, simplified component test and model test. Moreover, tribological data accumulated from tribo-testing can be extrapolated into service to a degree that decreases from the field test - the closest to the practical situation - to the less complex model test - the furthest away from the practical situation - as a result of the simplifications of environment and operating variables. Usually, the highest level of simplification, i.e. the model test, is characterized by a relatively short test duration and increased loading or sliding velocity, in order to assess the tribological behaviour of the materials under more extreme conditions, than those normally occurring during service. Henceforth, such experiments will sometimes be designated as accelerated tribo-tests.
The duration of the tests is frequently shortened by increasing the real area of contact between the elements of the tribosystem, i.e by increasing the surface pressure (applied load) or by starved lubrication. However, an increase in loading or change of lubrication regime in the model test to reduce the duration of the experiments could make the extrapolation into service more difficult, and sometimes even unpredictable. In fact, in the scope of the model test not only very different wear rate values could be observed, but also several wear mechanisms could arise during the duration of the tribo-test. It's therefore mindful to ensure, by measurement of friction and by close inspection of the worn surfaces and wear debris particles after the test, that the dominant mechanisms of wear are the same in the model test as in the practical application [10, p. 82]. The same loading conditions and the same structure should also be satisfied [78, p. 117]. Only then can the tribological data be extrapolated with confidence to a real application.

Model tests are particularly advantageous in the study of friction and wear phenomena due to the much lower expenditure incurred, as compared to field tests for example, and because of the greater control they provide in adjusting, sustaining and changing the operating parameters, i.e. to analyse their influence on the tribological behaviour. Therefore, the high

reproducibility of operating variables and hence repeatability of test results constitutes a great asset of model tests, and an important factor to take into consideration in the scientific investigation of tribological phenomena. Moreover, model tests can also be used for materials screening and selection, and the capability of simulating otherwise complex systems using relatively simple arrangements is of particular relevance in the study of basic mechanisms of friction, wear and lubrication [78, p. 118].

Model tests characterized by many different experimental arrangements or configurations have been used to study sliding wear. The main objectives of these laboratory investigations have consisted mainly in the assessment of the mechanisms by which wear occurs, or to simulate practical applications with the purpose of recording experimental data regarding wear and friction performance of tribo-materials. Moreover, careful control and measurement of all the variables which may influence wear and friction is essential, since an apparently small modification in experimental conditions can lead to abrupt changes in the prevailing mechanisms and associated wear and friction values [10, p. 78–79].

Some of the most common geometrical arrangements found in tribo-testing apparatuses are depicted in Fig. 3.3. The word tribometer, first coined in 1774 for an instrument intended to measure friction, is now widely used to refer to the tribo-testing rig, and more recently the name tribotester has become part of the tribologist's lexicon. Virtually all types of tribometers can be used either unlubricated ("dry" sliding) or lubricated. In the later case, the lubricant can be supplied to the contact region in different manners, e.g. by recirculating the lubricant fed from a reservoir or using a pool type configuration. The purpose of producing friction and wear data with any tribometer will be aimed at predicting the tribological performance of materials eventually shaped in some sort of moving mechanical assembly or transfer device [79].
Despite the multiplicity of geometries in use today, Hutchings [10, p. 78–79] divides them into two groups:

- *Symmetrical arrangements*, in which the sliding surfaces are symmetrically disposed and where identical materials should experience similar wear loss. The ring-on-ring (or two

discs) apparatus, where the triboelements are in contact either along a line or face to face constitutes an example of such arrangement;

- *Asymmetrical arrangements*, in which the two sliding elements, even if made of the same material, will almost certainly experience different rates of wear as a result of the inherent asymmetrical design. In this type of arrangement, the most widely used for tribological characterization, one component of the mating pair, usually the pin or block, is usually treated as the specimen to analyse in terms of wear loss, while the other, often the disc or plate, is called the counterface. Pin-on-disc (POD), block-on-ring (BOR) or ball-on-flat (BOF) geometries are all examples of asymmetrical design.

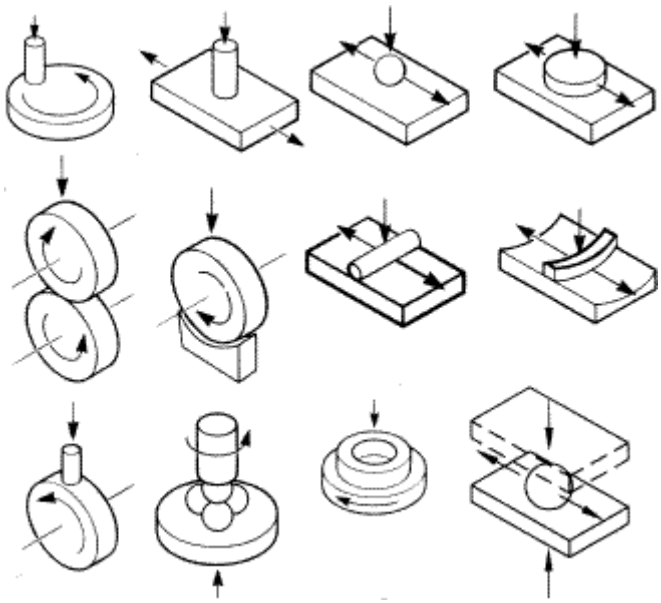

Figure 3.3: Schematics of some of the geometries employed in sliding tribo-tests (from PLINT Tribology products, www.phoenix-tribology.com).

Additionally, the geometry of contact can be further classified in conformal and counterformal (sometimes referred as concentrated or non-conformal), where the first is characterized initially by an extended nominal contact area between conforming triboelements (e.g. a flat-ended pin against a flat disc) and the latter by contact only at a point or line (e.g. a hemispherical pin on a disc).

In the present thesis work, a BOF counterformal asymmetrical design has been chosen for all tribo-tests because of its overall combination of appropriate attributes, namely the reciprocating motion, i.e. to be a model test having the type of motion similar to the ones generally found in biotribological assessment using simple low cost designs [80, p. 186–191], as well as having the advantage that modest loads give high surface pressures, useful in tribo-testing aimed at highly demanding tribological applications (like cutting tools); the possibility of using small samples, for easiness of production and to enable their characterization using state-of-the-art SEM and AFM techniques; obviate alignment problems between triboelements often found in conformal geometries like POD (which could result in different wear rates for different samples), and more importantly to enable the estimate of wear rate values for at least one of the specimens (from the near-circular wear scar imprinted on the ball, see Eq. 3.3), since the diamond coatings were characterized by very low wear, immeasurable by conventional weight-loss or profilometry techniques.

A somewhat broader but coherent classification with Hutchings' division is presented by Zum Gahr [78, p. 120–121], where the multitude of existing apparatuses for tribo-testing are grouped as follow:

- *"Closed" system tribometers*, where the tribological behaviour of all the triboelements is investigated and of relevance;
- *"Open" system tribometers*, where the tribological behaviour of only the solid body is of interest.

Examples of closed systems would be the POD, BOF and ring-on-ring (ROR) tribometers. In general, tribometers for the study of adhesive, tribo-chemical and surface fatigue wear belong predominantly into this group. On the other side, tribometers used exclusively for the study of abrasive wear constitute usually good examples of open systems, like micro-abrasion testers where a suspension of abrasive particles recirculates into the contact region, as do apparatuses used in blast wear test for erosive wear assessment.

Bennewitz [81], describes the friction phenomenon as "... the result of the collective and quite possibly interdependent mechanical behaviour of a multitude of small contacts be-

tween shearing surfaces, which are constantly being formed, deformed and ruptured. The time scales for these local transformations range from the lifetime of individual microscopic contacts over the periods of mechanical resonances in the sliding bodies ...". It is this collective effect or macroscopic friction that will be recorded by the standard tribometer.

In normal conditions, the macroscopic friction will be continuously monitored and recorded during tribo-testing. The acquisition of the friction force is usually carried out by measuring the tangential force signal applied on the specimen by means of a load cell, or by the generated torque on a rotating counterface. Therefore, continuous monitoring of the friction force will provide experimental values for the friction coefficient, μ, according to Coulomb's friction law [6, p. 13]:

$$\mu = \frac{F}{W} \tag{3.1}$$

where, F, represents the tangential friction force and, W, the normal force. The constant recording of F will also allow to follow the evolution of μ with the distance slid and, therefore, detect changes in the sliding behaviour, which often result from modifications in the surface nature or topography of the materials, or in the prevailing wear and friction mechanisms [10, p. 81]. Such monitoring capability is important for example in the analysis of running-in regimes, lubrication failure or in the detection of delamination of protective coatings. This follow-up capacity has been explored in the present thesis work, as a mean to detect diamond coating failure by film delamination or exposure of the Si_3N_4 substrate by progressive wear through.

Sliding wear will be dependent on the sliding distance, x, but also to some degree on both the sliding velocity, v, and the duration of the tribo-test, independently. This happens because v affects the rate of dissipation of the frictional energy, and hence the interface temperature. Therefore, radical changes in predominant wear mechanisms and wear rate values can in fact occur as v is modified [10, p. 81]. Moreover, lengthier tribo-tests could put in evidence new wear modes (e.g. wear by surface fatigue) which will not appear in shorter experiments.

Wear will also depend on the nominal contact pressure between antagonist surfaces, where a transition between different wear regimes can occur as a result of the variations in contact pressure.

Apart the main operating variables in tribo-testing, i.e. normal load, contact area, sliding ve-

locity and test duration, several other factors should be taken into account and properly monitored. For example, the environment temperature could influence the mechanical properties of the materials under screening or induce thermally activated processes, although these are mainly dominated by frictionally-generated temperature rises. In lubricated tests it could affect the lubricant viscosity, therefore changing its performance. The testing atmosphere is of utmost importance as well, since the presence of certain gaseous species like water vapour and oxygen could strongly influence the friction and wear behaviour of the materials. This is the case with diamond, where the friction behaviour is radically distinct if sliding occurs in humid air or vacuum conditions, as discussed previously in Section 2.1. The relative orientation or layout of the triboelements can also influence wear, since e.g. an inverted POD[1] configuration would mean that the wear debris particles could depart easily from the contact region, by the action of gravity, instead of accumulating in the wear track like what happens in standard POD [10, p. 81].

As mentioned by Zum Gahr [78, p. 119], other relevant experimental variables must be considered in tribo-testing also, i.e. the loading conditions (static or cyclic loading), sample geometry and surface finishing. Moreover, in addition to the tribological characteristics, some physical and chemical properties of the materials have often to enter the equation, namely their strength, toughness, thermal conductivity, endurance to fatigue or corrosion resistance.

Definition of wear and contact stress quantities

Wear is usually assessed either by removing the specimen from the tribometer at intervals and weighing it (weight-loss method) or measuring its dimensions, or by continuously monitoring its position using a transducer and deduce afterwards the wear loss from its change in dimensions [10, p. 80]. In the cases involving counterformal geometries, wear causes the apparent area of contact to increase and, therefore, wear rate values can be estimated by measuring the dimensions of the wear scar on the specimen.

Such procedure of estimating wear rate values has been used in the present thesis work for the ball specimens, since the conventional weight-loss technique and standard profilometry were both inadequate to account for the observed very low wear losses.

[1] POD configuration in which the pin becomes the lower specimen

The general expression for calculating the wear volume (W_V^{ball}) from wear scars imprinted on the ball specimens is [82]:

$$W_V^{ball} \approx \frac{\pi d_\perp^2 d_\parallel^2}{64r} \tag{3.2}$$

where, $d_\perp$, and, $d_\parallel$, represent the dimension of the wear scar perpendicular to and parallel to the sliding direction, respectively, and, r, the radius of the ball. Nonetheless, considering the occurrence of near-circular wear scars of diameter, d, on the pole of the ball [83], the same expression can be simplified to:

$$W_V^{ball} \approx \frac{\pi d^4}{64r} \tag{3.3}$$

Considering the contact between a sphere of an elastic material pressed against a plane under a normal load, W, the Hertzian pressure is hemispherically distributed on a plane with the contact radius, a, defined as follow [10, p. 15]:

$$a = \left(\frac{3Wr}{4E}\right)^{1/3} \tag{3.4}$$

where, E, is an elastic modulus which depends on Young's moduli, E_1 and E_2, and the Poisson's ratios, ν_1 and ν_2, for the materials constituting the sphere and the plane in the following way [78, p. 52]:

$$E = \frac{E_1 E_2}{E_2(1-\nu_1^2) + E_1(1-\nu_2^2)} \tag{3.5}$$

Therefore, the contact between a ball loaded elastically against a flat specimen, as is the case in the present study in first approximation, will occur over a circular area where the mean Hertzian pressure (normal stress), P_{mean}, is given by [10, p. 15]:

$$P_{mean} = \frac{W}{\pi a^2} \approx 0.386\left(\frac{WE^2}{r^2}\right)^{1/3} \tag{3.6}$$

Thus P_{mean} varies as $W^{1/3}$. However, this stress is not uniformly distributed over the circular area of contact, but reaches a maximum at the center and falls to zero at the edge. Hence, the maximum contact pressure, which has a value of 3/2 times the P_{mean} [10, p. 16], will become:

$$P_{max} \approx 0.579 \left(\frac{WE^2}{r^2} \right)^{1/3} \tag{3.7}$$

Moreover, considering the same material for both the ball and flat specimens ($E_1 = E_2$ and $\nu_1 = \nu_2 = 0.3$), the maximum shear stress, τ_{max}, occurs at a depth, z_m, beneath the contact surface [78, p. 54]:

$$\tau_{max} \approx 0.31 P_{max} \tag{3.8}$$

$$z_m \approx 0.47a \tag{3.9}$$

For the sake of an example, lets consider a self-mated diamond-coated Si_3N_4 tribosystem under dry sliding conditions, where $W = 40$ N and $r = 2.5$ mm. Supposing a contact radius $a = 0.2$ mm and, therefore, that the highest stresses occur at a depth below the diamond coating (having just a few tens of μm of thickness), as suggested by Eq. 3.9, the elastic modulus E (see Eq. 3.5) will then be calculated considering solely the substrate contribution. Hence, using a typical value of 300 GPa for the Young modulus of Si_3N_4 [84], we have that $E \approx 165$ GPa and the various contact pressures: $P_{mean} \approx 2.2$ GPa, $P_{max} \approx 3.2$ GPa and $\tau_{max} \approx 1.0$ GPa.

According to the Archard wear equation, the wear rate, Q, i.e. the volume worn per unit of sliding distance, is written as follow [10, p. 83]:

$$Q = \frac{KW}{H} \tag{3.10}$$

where, W, is the applied normal load, H, the hardness of the softer surface and, K, a dimensionless constant less than unity, usually termed the wear coefficient. This later constant is of fundamental importance, and provides a valuable means of comparing the severity of wear in different tribosystems. Moreover, the consequences of Eq. 3.10 are that Q should be constant in the case of K being constant for a given tribosystem, and if W changes then Q should vary proportionally.

However, for practical purposes the ratio K/H is often more useful and is called the dimensional wear coefficient, k [10, p. 84]. Thus, Eq. 3.10 can be rewrite in terms of k as:

$$k = \frac{Q}{W} \tag{3.11}$$

with k normally expressed using the units $mm^3m^{-1}N^{-1}$ and, therefore, representing the volume of material removed by wear (mm^3), per unit distance slid (m), per unit normal load (N). The measure of wear given by k will be particularly useful when comparing wear rates in different classes of material.

According to Hutchings [10, p. 84], experiments involving many systems have showed that the wear loss is proportional to the sliding distance, as well as to the sliding velocity. Thus, a simple model for wear would suggest that the amount of material removed from a sliding body, W_v, would depend on the sliding distance, x, and on the normal load, W. From the meaning of Q, the dimensional wear coefficient (or specific wear rate) will hence be given by:

$$k = \frac{W_V}{W \cdot x} \tag{3.12}$$

In the present thesis work, BOF tribo-tests were carried out in a PLINT TE/67R tribometer, adapted for reciprocating motion. The accelerated friction and wear experiments were performed over a wide range of applied loads ($10 - 180$ N) depending on the system studied, i.e. self-mated MCD or NCD coatings, as well as on the testing environment, i.e. in ambient atmosphere dry sliding or water lubricated. The main reason behind the variation of the applied normal load and, therefore, initial normal stress, while keeping unchanged the stroke length (6 mm) and oscillating frequency (1 Hz) for all experiments, was to assess the threshold load of the various types of diamond coatings, i.e. to determine the load supporting capability prior to film failure by delamination under tribological stress. Moreover, such a wide gamut of applied loads, would also allow the analysis of the tribological behaviour of the diamond films as a function of the contact stresses and identify the occurring friction and wear mechanisms.

Figure 3.4 shows photographs of the experimental setup used for tribo-testing in the present thesis work. The upper ball diamond-coated specimen is fixed on the sample holder arm, which is in contact with a load cell used to measure the tangential force. The flat diamond-coated specimen is fixed on the lower oscillating table, to reproduce the reciprocating motion. The tribo-tests were carried out over two different length scales, namely the standard ones with a duration of 2 h, which represent a sliding distance of ~ 86 m, and the endurance tests, corresponding to a distance slid of ~ 690 m. The shorter standard tests were used to study in more detail the running-in regime, using higher acquisition rates to more accurately record variations on the friction signal, and also for screening the different diamond films with respect to their threshold

loads under distinct sliding conditions and applied loads. The lengthier endurance tests were used to study in more detail the steady-state regime, fatigue effects, possible occurrence of coating failure due to progressive wear through to the substrate, measure the steady-state friction coefficient and more accurately assess the wear rates of the diamond coatings (reducing the contribution of the running-in more intense surface interactions).

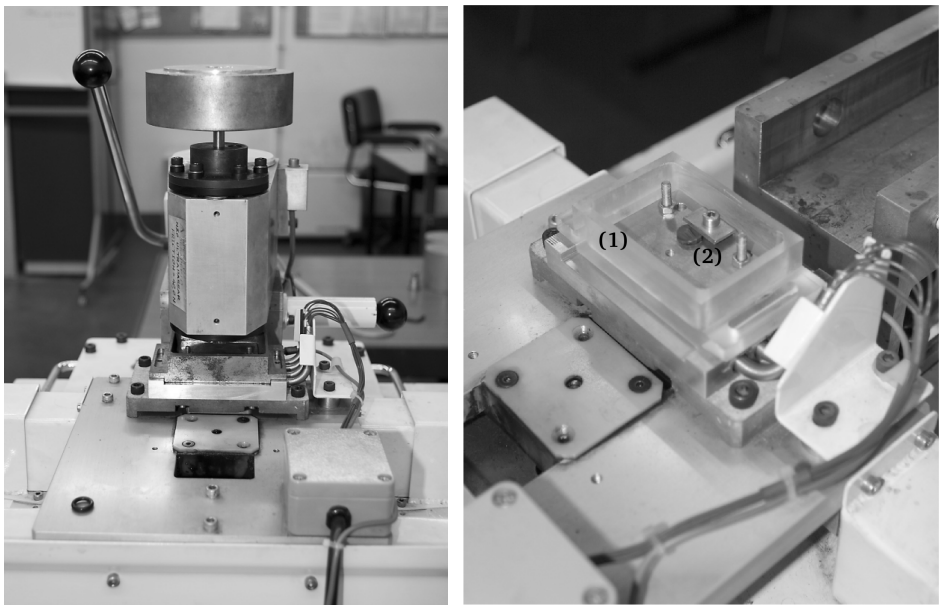

Figure 3.4: Photographs of the setup used for tribo-testing: (a) general view of the tribometer's upper arm and static applied loads; (b) close-up view of the lower sample holder for lubricated tests and positioned flat diamond coated specimen. Legend: (1) sample holder for lubricated tests; (2) flat diamond-coated specimen.

At the end of the experiments, both samples are removed from the tribometer and cleaned in a ultrasonic bath prior to wear assessment, to dislodge non-adherent wear debris particles. Due to the high wear resistance exhibited by the diamond coatings, wear volumes were estimated from the dimensions, measured by SEM, of near-circular wear scars imprinted on the balls specimens. Where considered appropriate, the wear volume of flat specimens was also assessed using AFM-based techniques and novel approaches developed for the present thesis work, as described in Publication II (Sec. 4.3) and Publication VIII (Sec. 5.5).

3.4 Other characterization techniques

Several non-destructive characterization techniques commonly used in the area of materials science were employed to analyse the as-deposited CVD diamond coatings, as well as in studying relevant properties and morphologies of these coatings when subjected to tribological damage. In the following sections, such techniques will be presented and their relevance to the area of the tribology of CVD diamond coatings emphasized.

3.4.1 Scanning Electron Microscopy (SEM) of diamond films

Due to its very large depth of field as compared with optical microscopy, its wide range of magnifications of the same surface features and its relative ease of application in the study of surfaces, scanning electron microscopy (SEM) has become a standard technique for surface analysis and microstructural evaluation. Moreover, the use of SEM has become almost mandatory in any tribological study [85, p. 61, 217]. The wide range of magnifications available at any given part of the sample surface, make SEM a very polyvalent technique with the possibility of low magnifications (approximately $\times 10$) up to very large magnifications ($\times 10^3$ or more). Therefore, the analysis using low magnification images of the morphology of wear tracks or scars, in search of features typical of specific wear modes (like the presence of abrasion grooves e.g.); the possibility to analyse with great detail very small areas of the contact region using high magnifications, and to characterize the size and morphology of wear debris particles would give insightful information for describing the predominant friction and wear mechanisms.

The SEM instrument essentially produces a narrow beam of primary electrons, which are scanned across the sample to analyses in a similar fashion as a television type raster. The secondary electrons generated from the interaction between the scanning beam and matter are then used to form an image of the sample surface. This imaging process is accomplished by collecting the secondary electrons in a charged collector and subsequently amplifying the incident current. The magnification is controlled by varying the area of scan on the sample using a lens system. A conventional electron gun is used as the source for primary electrons, which are

then accelerated through a potential reaching up to several tens of kV in relation to the grounded frame of the microscope [85, p. 61–62].
A lens system is used to control the size of the beam by collimating it, so that the smallest possible "spot" is obtained for scanning the sample. The size of this spot will determine the lateral resolution of the SEM instrument. Resolutions of a several tens of Å have been reached using specially built lens systems [85, p. 61–62].

The contrast existing on a SEM micrograph is the result of differences in atomic number between the various elements present in the analyzed surface, as well as its topography. In the case of a single-element specimen, the relative slopes of the roughnesses are responsible for the contrast or distinction between surface features, instead of the surface heights. The use of SEM equipments in analyzing the surfaces of tribosystems has been more of a qualitative nature, due to their great depth of field, which hinders any measurement of relative surface heights by selective focus on the lowest and highest z-position of the surface features being observed. However, more recent advances in SEM technology have enabled the use of back-scattered primary electrons to resolve surface profiles, i.e. using Rutherford back-scattering (RBS) [85, p. 62–63].

SEM *ex-situ* analytical technique, in combination with energy dispersive spectroscopy (EDS), has become one of the most useful tool for researchers who need not only morphological and topographical information about surfaces, but also information regarding the composition of near-surface regions of the analyzed material. Although diamond is an insulator, its analysis can be carried out using low primary electron beam voltages ($\leq$ 5 keV) which, nonetheless, brings implications in terms of loss in image resolution. However, if the diamond surfaces are coated with a thin conducting film (10 to 20 nm of thickness), such as carbon or gold, it will be possible to study the coatings with a image resolution of 1-50 nm [45].
Moreover, SEM's high sensitivity in spectroscopic modes and the ever evolving technology associated to it, have enabled the microstructural characterization of diamond thin films with a spatial resolution reaching $\sim$ 0.2 nm or better [46].

Representative SEM photomicrographs of worn diamond-coated Si_3N_4 films are shown in Fig. 3.5. Two different range of magnifications have been used consistently throughout the present thesis work, in order to analyse as-deposited and worn coatings. Low magnification (normally $\times 100$ or $\times 150$) images were used to analyse the microstructure and topography of the as-deposited films, to measure the dimensions of the near-circular wear scar imprinted on ball specimens, as well as that of the wear tracks on flat samples with the purpose of estimating wear rate values for the diamond coatings on both tribo-elements (see Eqs. 3.3, 3.12). Moreover, these were also used to identify features particular to wear modes and mechanisms, like e.g. wear grooves or ultra-smooth surfaces (thus denoting abrasion or self-polishing), as well as to see if the substrate was exposed after wear testing.

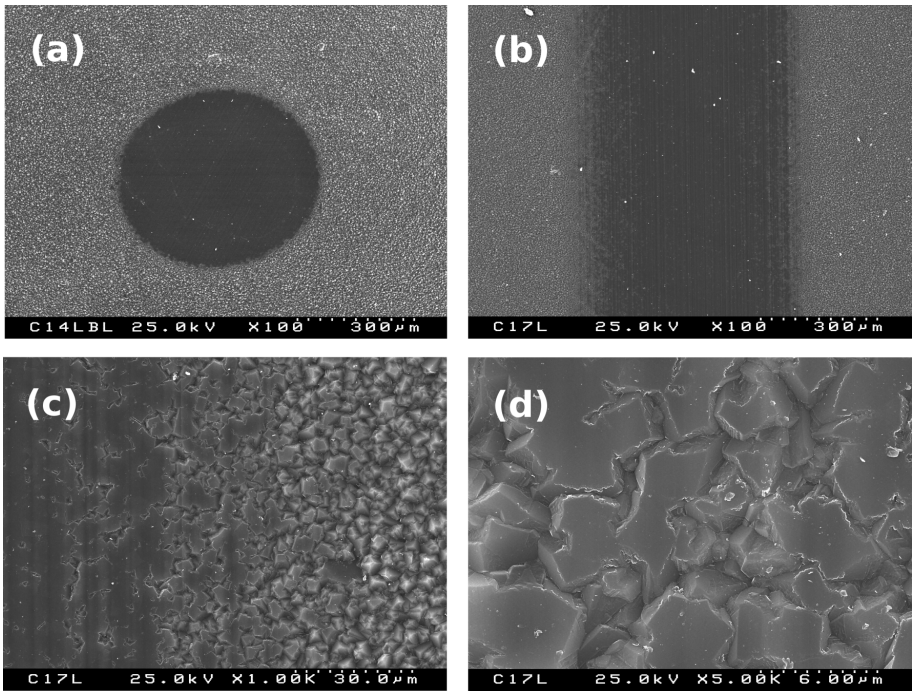

Figure 3.5: Representative SEM micrographs of worn MCD-coated Si_3N_4 tribo-elements: (a) low magnification ($\times 100$) image of a wear scar on a ball specimen; (b) low magnification ($\times 100$) image of a wear track on a flat specimen; (c) high magnification ($\times 1$ k) detail at the wear track border; (d) high magnification ($\times 5$ k) detail in the wear track region.

High magnification images (normally in the range $\times$1k to $\times$5k) were mainly used to study the morphology and topography of worn surfaces, identify prevailing wear modes and mechanisms, and observe the morphology and size of wear debris particles. One of the advantages of analyzing wear debris is since wear debris could result from different wear mechanisms, they have distinct characteristics which can then be associated with the specific wear mechanisms. Moreover, worn surfaces and wear debris may provide insightful information regarding the validity of a wear test used for a particular application. In addition, high magnification images were also used to assess the grain size and thickness of the coatings.

Thus, SEM characterization technique constituted an essential tool in the study of worn diamond coatings, being done after ultrasonic cleaning (10 min in alcohol) of the tribotested samples to dislodge loosen wear debris and posteriorly to other employed techniques, i.e. atomic force microscopy and Raman spectroscopy. This is so because all diamond films were coated with a thin layer of carbon to render the samples electrically conducting for adequate imaging.

3.4.2 Atomic Force Microscopy (AFM) of diamond films

Scanning probe microscopy (SPM) makes feasible nanometer-scale mapping of numerous sample properties, in essentially any environment. In fact, this singular combination of high spatial resolution and polyvalence has lead to the application of SPM to numerous fields of science and technological areas, especially those involved in the study of materials' structure and properties at the nanometer scale [86, p. 117].

SPM's images are created by raster scanning a sharp probe tip over the sample and measuring some highly localized tip-sample interaction as a function of position. The SPM working principles are based on various types of interactions, the major ones including scanning tunneling microscopy (STM) which measures an electronic tunneling current; atomic force microscopy (AFM), which measures force interactions; and near-field scanning optical microscopy (NSOM), which measures local optical properties by exploiting near-field effects. These surface techniques allow the characterization of many properties (structural, mechanical, electronic, optical) on essentially any material and virtually all environments (vacuum, liquid,

or ambient air) [86, p. 117].

Several technological breakthroughs have been developed for SPM, or borrowed from other techniques. In AFM for example, optical deflection systems and micro-fabricated cantilevers can detect forces down to the picoNewton range. Environmental control has been developed to allow SPM imaging in ultra-high vacuum (UHV), cryogenic conditions, at elevated temperatures, and in fluids. Microfabrication techniques have been developed for the mass production of probe tips, making SPMs widely available and which allowed the development of many new SPM modes and combination with other surface characterization techniques [86, p. 118].

AFM, invented and introduced in 1986, is the most widely used form of SPM, since it requires neither an electrically conductive sample, as in STM, nor an optically transparent sample or substrate, as happens in most NSOMs. Basic AFM modes measure the topography of a sample with the sole requisite being that the sample is deposited on a flat surface, rigid enough to withstand the scanning process. Moreover, because AFM can resolve a variety of interactions, like Van der Waals forces, electrostatic forces, magnetic forces, adhesion forces and friction forces, specialized modes of AFM can also be used to characterize the electrical, mechanical and chemical properties of materials [86, p. 117–119].

AFM can be viewed as a mechanical profiling technique that produces a three-dimensional mapping of the surface under analysis. A sharp probe attached to a microfabricated force-sensing cantilever scans the surface. The forces that act between the tip of the cantilever and the sample are used to control the vertical distance and, therefore, profile its surface [87].

In so-called AFM dynamic operation modes, as opposed to static or contact mode AFM, the cantilever is deliberately vibrated. There are two basic methods of dynamic operation: amplitude modulation (AM) and frequency modulation (FM) operation. In AM-AFM or so-called tapping mode (TM-AFM), the actuator is driven by a fixed amplitude at a constant frequency, close to the eigenfrequency of the cantilever. When the tip approaches the sample,

elastic and inelastic interactions cause variations in both the amplitude and the phase (relative to the driving signal) of the cantilever. These perturbations are then used as the feedback signal [88, p. 145]. The experimental advances that made high-resolution AFM possible began with the introduction of FM-AFM. In this dynamic mode, a cantilever with a high quality factor is driven to oscillate at its eigenfrequency by positive feedback with an electronic circuit that keeps the amplitude constant [87].

The AFM has been used for topographical measurements of surfaces of technological relevance on the nanoscale, as well as for adhesion and electrostatic force measurements. Subsequent modifications of the AFM led to the development of the friction force microscope (FFM), which as been used for atomic-scale and micro-scale studies of friction since it measures forces in the scanning direction. Moreover, AFM/FFMs are considered tools of the trade in the investigation of various tribological phenomena, including adhesion, scratching, micro- and nano-wear, indentation, detection of material transfer, and boundary lubrication. The AFM is also being used for micro/nano fabrication and machining by extending its micro-scale scratching capabilities [56, p. 316, 362, 383].

The working principle of an AFM relies on a scanning procedure to produce very high resolution, 3-D images of the sample surface. It resolves ultra-small forces (< 1 nN) existing between the AFM tip surface and the sample's surface. These small forces are determined by measuring the motion of a very flexible cantilever beam with an ultra-small mass by a variety of measurement techniques including optical deflection, optical interference, capacitance and tunneling current. In the operation of high resolution AFM, available for the measurement of small samples (generally no larger than 10x10 mm^2), it's the sample that is generally scanned, rather than the tip to avoid vibration induced by the cantilever motion. AFMs are also available for measurements of large samples, where the tip is scanned and the sample stays stationary [56, p. 318].

Surface roughness is routinely measured using the AFM. For the case of the laser deflection technique, a beam coming from a diode laser is directed by a prism onto the back of a cantilever near its free end, which is tilted downward (about 10°) with respect to the horizontal

plane. The reflected beam from the vertex of the cantilever is then directed through a mirror and focused on a quad photosensitive diode (split photodetector with four quadrants), which allows the measurement of vertical and torsional bending of the cantilever [89, p. 250]. Therefore, the AFM signal will result from the difference of signal intensities of top and bottom photodiodes, and represents a sensitive measure of the tip vertical deflection which in turns translates the topographic features. In AFM's height operating mode, used for topographic imaging, or any other mode where the applied normal force is to be kept unchanged, a feedback circuit is used to modulate the voltage applied to a piezoelectric crystal (usually, lead zirconate titanate or PZT) tube scanner to adjust its height. It's this variation in height that will represent a direct measure of the sample's surface roughness [56, p. 320].

The vast majority of todays AFMs can be operated in the intermittent contact or so-called tapping mode (TM-AFM), which constitutes one of the most commonly used modes in dynamic AFM operated in air, and even liquid. In TM-AFM, the cantilever/tip assembly is made to oscillate sinusoidally by a piezo mounted above it, and the vibrating tip briefly taps the surface at the resonant frequency ($70-400$ Hz) with a constant oscillating amplitude ($20-100$ nm) in the vertical direction. Therefore, oscillation amplitude and phase during approach of tip and sample serve as the experimental observation channels. During the scanning, the average normal force applied onto the surface is kept constant by a feedback loop [56, p. 320]. A schematic of a typical TM-AFM setup is depicted in Fig. 3.6. A laser beam is deflected by the back side of the cantilever, and the deflection detected with a split photodiode (detector). A lock-in amplifier analyses subsequently the oscillation amplitude and the phase (not shown in the diagram) of the incoming detector signal. This amplitude is then compared to the set-point, and the deviation or error signal is used as a feedback signal to adjust the z-piezo, i.e. the probe-to-sample distance. An external function generator supplies the modulated signal for the excitation piezo and, simultaneously, the oscillation signal is fed to the lock-in amplifier to serve as a reference [89, p. 253–255].

The tapping mode is used in topography measurements to minimize the effects of friction and other lateral force, as well as to measure the topography of soft surfaces, which would become impractical using static AFM. Moreover, the oscillating amplitude is kept high

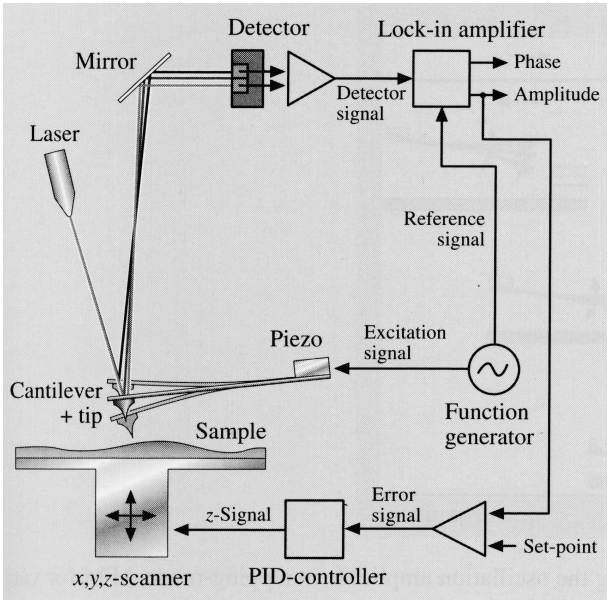

Figure 3.6: Schematic of a dynamic AFM operated in tapping mode [89, p. 255].

enough so that the tip does not adhere to the sample, as a consequence of adhesive forces. In the contact mode, topographic measurements are usually made with a sharp microfabricated square-pyramidal Si_3N_4 tip (radius of $30-50$ nm) on a triangular cantilever with normal stiffness of about 0.5 Nm^{-1} at a normal load around 10 nN. In TM-AFM, the probe is typically designed as a square-pyramidal shaped tip - with a smaller radius of $5-10$ nm - made of an etched single-crystal silicon (SiO_2), which is physically attached to a stiff (50 Nm^{-1}) rectangular SiO_2 cantilever of high resonant frequency. The trajectory of the tip follows a triangular pattern as the sample (or the tip) is scanned in two dimensions, with data being recorded solely during tip traversal along the fast scan direction. The scanning speed (or scanning rate) in the directions of slow and fast scan will depend on the scan area and scan frequency. Typical values found for the scanning frequency are less than 0.5 Hz to 122 Hz, and scanning areas range from less than 1×1 nm^2 to 125×125 μm^2. Due to physical limitations, higher scan rates are only possible with smaller scan lengths [56, p. 320–322].

A number of parameters have been developed to characterize surface topography. The most commonly used surface descriptors are the statistical surface parameters. At least

two parameters are needed to adequately characterize the surface, one related to the variation in height (i.e. height parameter), the second describing how height varies in the plane of the surface (i.e. spatial parameter) [90, p. 452]. The deviation of a surface from its mean plane is assumed to be a random process, which can be described by a number of statistical surface roughness parameters. The most commonly quoted quantity is the *average roughness*, R_a, also known as *center-line average* (CLA) or *arithmetic average* (AA):

$$R_a = \frac{1}{L}\int_0^L |z|dx \tag{3.13}$$

R_a is defined as the arithmetic mean deviation of the surface height, z (at a distance x from the origin), from the mean line over the sampling length, L. In turn, the mean line is defined such as equal areas of the profile lie above and below it [10, p. 8]. Since the R_a is directly related to the area enclosed by the surface profile about the mean line, any redistribution of material has no effect on it, i.e. it can give identical values for surfaces with totally different characteristics. This averaging effect can be rectified using the *rms roughness*, R_q, which is more sensitive than R_a to deviations from the mean line, since it is weighted by the square of the heights [90, p. 452]. Therefore, R_q, will be defined as the root mean square deviation of the profile from the mean line, as follow:

$$R_q = \sqrt{\frac{1}{L}\int_0^L z^2 dx} \tag{3.14}$$

Two other surface roughness parameters are indicated on the following. The maximum peak-to-valley height, R_t, represents the largest single peak-to-valley height in five adjoining sample lengths,

$$R_t = \frac{1}{5}\sum_{i=1}^{5} R_{max_i} \tag{3.15}$$

The ten-point height, R_z, represents the average separation of the five highest peaks (p_i) and the five lowest valleys (v_i) within the sampling length:

$$R_z = \frac{p_1 + \cdots + p_5 + v_1 + \cdots + v_5}{5} \tag{3.16}$$

In addition to the determination of the aforementioned statistical parameters, any technique for measuring surface roughness characteristics (i.e. short wavelength irregularities) should also be capable of measuring the *waviness*, i.e. long wavelength deviations from the intended surface, and *form error*, i.e. a measure of the departure from the intended surface or ideal shape [10, p. 8] [85, p. 60], in order to acquire further information regarding the surface topography. A thorough discussion on spatial parameters and multi-scale characterization methods of surface topography can be found in Stachowiak and Batchelor [90, p. 452–460].

In Fig. 3.7 are depicted AFM 3D gray-scale images of as-deposited (100)-textured and worn (111)-textured polycrystalline diamond coatings, from a study by Fu et al. [91]. The diamond coatings were deposited by MW-PACVD on pure titanium substrates, and tribologically tested against Al_2O_3 balls. As can be seen in Fig. 3.7(a), AFM analysis shows that the (100) crystals are nearly parallel to the coating surface. The as-deposited coating exhibited a surface roughness of about $R_a = 0.245 \pm 0.09$ μm, indicating a smoother surface topography in relation to (111)-textured diamond coatings ($R_a = 0.387 \pm 0.12$ μm) with a micro-pyramidal morphology. After removal by ultrasonic cleaning of the wear debris loosely accumulated in the valleys, the AFM image of the worn (111)-textured coating (Fig. 3.7(b)) reveals the typical traces of brittle fracture and cleavage of diamond crystals, i.e. the evidence that diamond asperities were fractured by tribological interaction.

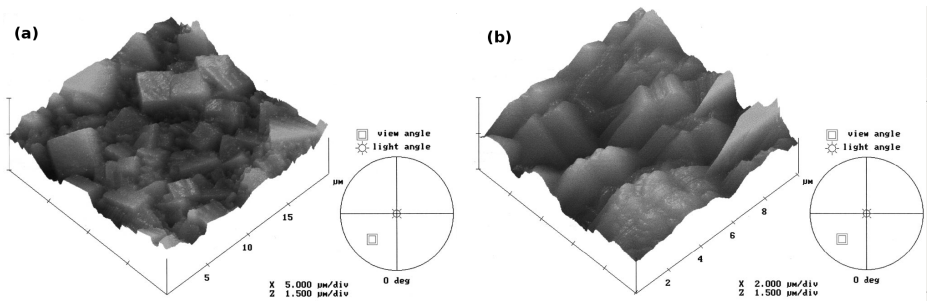

Figure 3.7: AFM 3D images of MCD films [91]: (a) as-deposited (100)-textured coating; (b) worn (111)-textured coating.

For the purpose of comparing their surface topography, AFM 3D gray-scale images of distinct varieties of diamond coatings from several studies [62, 92] are presented in Fig. 3.8.

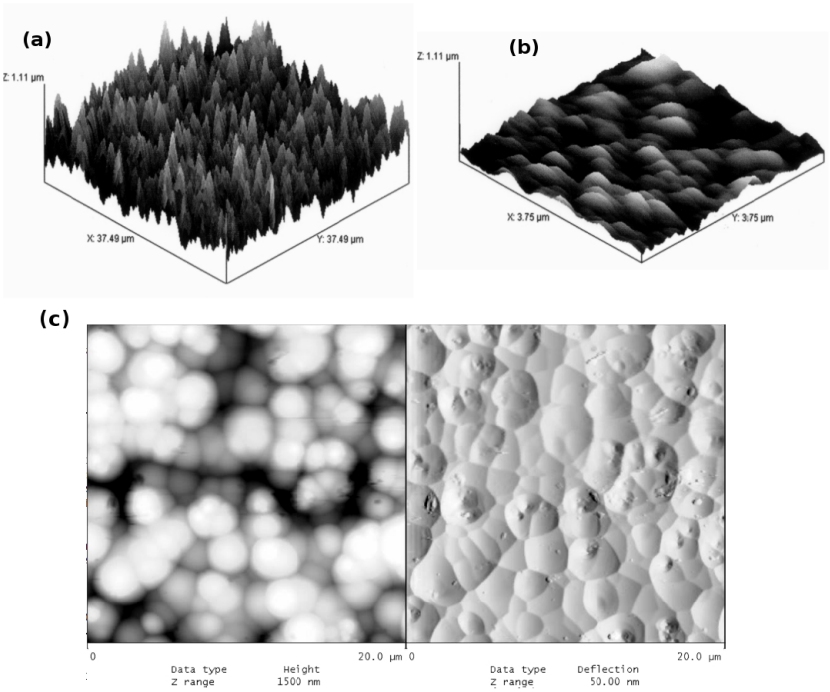

Figure 3.8: AFM comparison of the surfaces of diamond coatings with different microstructures: (a) MCD and (b) UNCD [62]; (c) NCD coated Si_3N_4 [92].

A conventional CVD-grown (99% of H_2 and 1% of CH_4) MCD film with its sharp topographic features is depicted in Fig. 3.8(a), while Fig. 3.8(b) exhibits the smoother surface of a ultra-nanocrystalline diamond (UNCD) film grown in an atmosphere composed of: 98% of Ar, 2% of H_2 and C_{60}. It can be readily seen from these images that the nature of a sliding contact involving such surfaces will be very different for these two varieties of coatings. Moreover, the displayed topographies are in perfect harmony with the microstructures characterized by micro-sized columnar grains ($\sim 0.5-10\,\mu$m) and randomly oriented nanometer-sized equiaxed grains ($2-5$ nm) of MCD and UNCD, respectively. RMS surface roughness values were in the range 400 nm to 1 μm and $20-40$ nm, respectively, for the MCD and UNCD films. An AFM 2D image of a NCD coated Si_3N_4 surface is shown in Fig. 3.8(c) [92]. The examination of the $20\times 20\,\mu m^2$ scan produced surface roughness values of $R_a = 0.34\,\mu$m, $R_t = 3.01\,\mu$m and

$R_z = 2.57\ \mu$m, with the aforementioned height parameters defined like in Eqs. 3.13, 3.15, 3.16, respectively. In terms of surface topography, the NCD coating deposited by radio-frequency plasma-enhanced CVD (r.f. PECVD) exhibit clustered growth domains, often referred to as a "cauliflower-like" structure.

3.4.3 Raman spectroscopy of diamond films

The origin of Raman spectroscopy dates back to the early 20^{th} century. Theoretical studies postulated that photons should inelastically scatter from molecules in a similar fashion to the Compton scattering of X-rays. In other words, Raman spectra result from the inelastic scattering of optical photons by lattice vibration phonons [45]. The first experimental evidence for such scattering events was provided by Raman, hence the name, and Krishnan, in 1928. With the invention of the laser, the last 40 years have witnessed the transformation of Raman spectroscopy into a sophisticated technique [93].

Raman spectroscopy has become a very popular technique for diamond film characterization, for which no special requirements regarding sample preparation are needed. Indeed, because Raman scattering is about 50 times more sensitive to π-bonded amorphous carbon and graphite than to the phonon band of crystalline diamond, it constitutes a method of choice for assessing the quality of CVD diamond films [46]. This results from its ability to give a fingerprint of a material, with enough resolving power to discriminate between the distinct carbon phases present. Moreover, for diamond films with very small (less than tens of nanometer) defect-free regions, the size of those coherent scattering sites can be inferred from Raman data and, concomitantly, dimensions (thicknesses) of distinct phase domains estimated [94].

Highly oriented pyrolytic graphite shows a strong E_{2g} mode at 1580 cm^{-1} (G-band). If graphite is reduced to small crystallites, say by mechanical grinding, additional modes associated to disordered graphite appear approximately at 1360 cm^{-1} (D-band) and 1620 cm^{-1} (D'-band) [43]. In contrast, tetrahedrally coordinated (sp^3) pure diamond crystals exhibit a very narrow F_{2g} peak centered at 1332 cm^{-1}, which is frequently used as a signature of high crystalline nature [76]. A downshift and asymmetric broadening of the Raman line occurs for

nanodiamond as a result of the phonon confinement effect. Furthermore, using the intensity ratio I_G/I_d, i.e. the ratio of the graphite G-band peak intensity in relation to the diamond peak intensity, makes possible the assessment of the relative distribution of graphite on the diamond surface over the sampled area, as well as estimate phase domain sizes [43].

Under specific conditions, instead of the appearance of a sharp diamond peak, the triple degeneracy of the first-order Raman line may be partially or completely lifted as a result of the distortion of the cubic symmetry under biaxial or uniaxial stresses. According to Windischmann and Gray [95], this phenomenon, which depends on the direction of the stress relative to the crystallographic direction, will show its signature on the Raman spectrum by the appearance of split peaks relative to the singlet and doublet lines. Another possible explanation for the multiplicity of peaks was suggested by the same authors, where it is said that the effect originates from a highly heterogeneous strain field occurring over micrometer length scales, with possible sources for the strain field coming from dominant planar structural defects observed in diamond, i.e. twining and stacking faults.

Figure 3.9(a) displays the Raman spectrum of a diamond coating produced by MW-PACVD technique, where the main feature is the presence of a sharp peak clearly identifying the tetrahedrally coordinated (sp^3) diamond [54]. The diamond peak is centered at a frequency of 1333 cm^{-1}, i.e. very close to that of natural diamond (1332 cm^{-1}), with a line width of 7.9 cm^{-1}. This close vicinity to the diamond natural frequency is an indication that the coating is not under stress. Moreover, the large line width compared with that of natural diamond (2 cm^{-1}) points out that the microcrystallites likely have a high concentration of defects.

Selected results from a study conducted by Nistor et al. [94], regarding the Raman characterization of diamond films grown at different CH_4/H_2 ratios (3, 30 and 100 %), are represented in Fig. 3.9(b). The coatings, deposited on Si substrates in a d.c. discharge reactor, were of polycrystalline (3 % ratio) and nanocrystalline nature (30 and 100 % ratios). Readily, it can be seen that the methane content appears to affect preferentially the shape of the fundamental diamond mode, with the rest of the spectrum more or less unchanged for all films investigated. Using computer deconvolution and subtraction of the photoluminescence background,

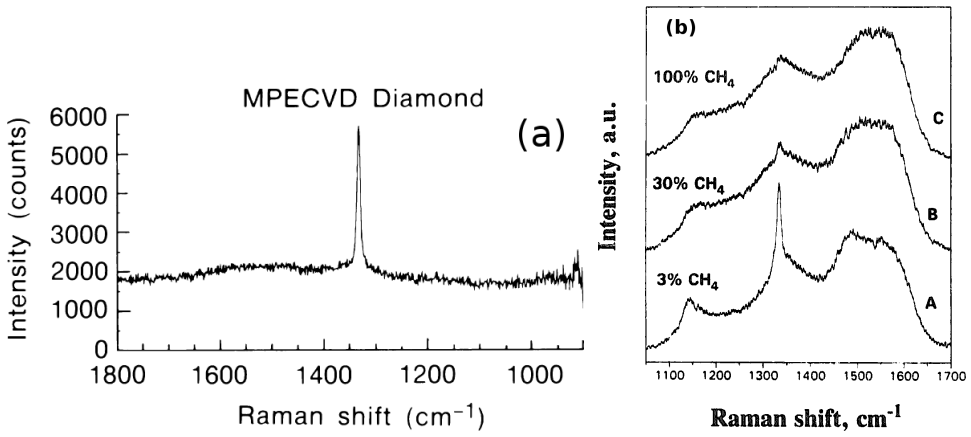

Figure 3.9: Raman spectra of diamond films: (a) produced by MWPACVD [54]; (b) grown at different methane contents [94].

six spectral components of Gaussian shape were identified for spectrum A, i.e. corresponding to the polycrystalline diamond coating. Each component was classified as follows: disordered sp^3 carbon at peak position 1140 cm^{-1}, C-N vibrations (1195 cm^{-1}), diamond (1334 cm^{-1}), disordered graphite or D-band (1349 cm^{-1}), distorted sp^3 carbon (1488 cm^{-1}) and graphite (1579 cm^{-1}). Nonetheless, it should be noted that the origin of the band at approximately 1150 cm^{-1} and the prolonged shoulder near 1480 cm^{-1} still constitute a source of intense debate [46, 76, 94]. In fact, the very existence of a 1150 cm^{-1} Raman peak is widely used by many researchers as a simple signature for the presence of NCD while others advocate that no relation exists with any diamond frequency. In a recent study (2001) by Ferrari and Robertson [76], it is argued that the 1150 cm^{-1} line cannot originate from a nanodiamond or related sp^3-bonded phase, but instead arise from a coexisting sp^2 phase hypothesized as being transpolyacetylene. Therefore, Raman spectra are useful in following the transition from microdiamond to nanodiamond, but one must be cautious in attempting to resolve C-C bonding information.

Besides the application of Raman spectroscopy to characterize the chemical bonding and microstructure, its use as a stress measurement tool for CVD diamond films was first reported by Knight and White [96] as far back as 1989. Since then, the straightforward model of stress-induced linear shift in the peak position to assess stress states in diamond films has been widely used. However, this simple model doesn't take into consideration several effects which

will contribute as sources of error in the final stress calculations. In fact, temperature changes, domain size effects, non-hydrostatic stress leading to lifting of the triple degeneracy of the sp^3 line and variations in the stress sensitivity of the peak due to crystallographic orientation, can all produce a measurable peak shift [95].

The diamond Raman peak suffers a downshift with increasing temperature. In a work by Herchen et al. [97], a peak translation of -0.2 cm^{-1} per 10 °C temperature rise was reported, which can account for an error of 80 MPa in the estimative of stress levels in diamond coatings. Almost ten years before Knight and White's work [96], Richter et al. [98] had developed the phonon confinement (domain size) model to explain the observed peak shift in microcrystalline silicon, associated to the lack of wave vector momentum conservation. Thus, accurate calculations for stress levels in diamond films must also take into consideration domain size corrections, depending on the grain size. Measurement of the diamond Raman peak full width at half-maximum (FWHM) will give the domain size correction [95].

For single-crystal diamond, a mean stress gauge factor of 2.58 cm^{-1} per GPa of compressive stress has been evaluated based on results concerning the shift in Raman frequency as a function of hydrostatic stress [99]. However, this hydrostatic stress factor cannot be used when considering films deposited on substrates, since those are in a biaxial stress state. Considering the specific case of biaxial plane stress, generally the stress tensor can be expressed as a superposition of an hydrostatic and shear stress component. In such conditions, the hydrostatic component represents only 2/3 of the biaxial stress. Therefore, the hydrostatic stress gauge factor must be multiplied by 3/2 in order to estimate the biaxial stress. Applying this correction factor to a measured Raman peak shift around 3.57 cm^{-1} (stress value of 1385 MPa), for the case of a 70 μm diamond film deposited onto a 3 mm thick molybdenum substrate, Windischmann and Gray [95] reported a value around 2.10 GPa for the film's biaxial stress. Moreover, they also refer an agreement with stress values calculated from substrate curvature measurements, which validates the approach.

As said earlier, the stress-induced dependence of both shift and splitting of the diamond peak will vary with crystallographic orientation. In fact, a single Raman line is observed under

inexistent or hydrostatic stress states. For the case of CVD diamond, Ager and Drory [99] have derived residual biaxial stress gauge factors for polycrystalline films. A more thorough discussion regarding biaxial stress calculations using Ager and Drory's model and micro-Raman spectroscopy data of CVD diamond coatings, relevant to the present thesis work, is presented in Publication II (Sec. 4.3). There, experimental data from μ-Raman studies of worn CVD coatings were used in order to assess the tribologically-induced biaxial stresses of damaged diamond films, as well as their implications in terms of maximum sustainable load for the deposited coatings under sliding.

3.4.4 Acoustic Emission (AE)

The real-time non-destructive acoustic emission (AE) technique was originally developed for testing and monitoring the integrity of static structures. However, over the years its field of application has been broadened to include the monitoring of rotating machines and rolling bearings, and to investigate the macroscopic response of materials to strain fields. The AE phenomenon originates from the rapid release of strain energy caused by a deformation or damage within or on the surface of a material, where part of it radiates from the source in the form of transient high frequency elastic waves (50 kHz to 2 MHz) [100, 101]. Regarding tribological phenomena, AE can be defined as the transient elastic waves generated by the interaction of two surfaces in relative motion [102].
Possible sources for these elastic waves would include crystal defects and dislocations, grain boundary movements, initiation and propagation of cracks and fractures and compression of voids or inclusions, among others [100]. The formation of subsurface cracks owing to the Hertzian cyclic contact stress in rolling or sliding tribosystems will also constitute a source for AE activity [102].

After the realization that sliding friction and wear constitute phenomena involving in general deformation and/or fracture and, therefore, could be processes triggering AE activity, several issues arose. The most pertinent questions left to answer related to the amount of AE energy emitted from sliding counterparts and how such quantity could be correlated to parameters ruling the behaviour of tribosystems [100]. Accordingly, several studies have been carried out to investigate such relationship, if it existed, with some of a more practical nature deal-

ing with the application of AE technique to diagnose specific tribosystems, like rolling contact bearings [102, 103], tool wear evaluation [104, 105] or head/disc interface wear in hard-disc drives (HDD) [106]. In another work involving HDD, Matsuoka et al. [107] made use of the AE technique to study the contact conditions between the slider and disc, with the purpose of assessing the minute wear which affects the performance of HDD. In their study, an expression relating the AE signal (rms voltage) and wear coefficient, which depends on two experimental constants previously determined by different sets of measured wear volume and observed AE activity, is presented. Therefore, once these experimental parameters are determined, the *in-situ* wear of HDD's head/disc components could be evaluated by recording the AE signal [107].

In a more fundamental research work, Lingard and Ng [100] conducted several experiments with the objective of measuring the AE in severe sliding of metallic specimens, so as to determine a possible correlation between AE signal and wear-friction parameters. The authors found that AE is readily observed in dry sliding and that emissions rates vary systematically with the applied load, sliding speed and material combination. A correlation was also observed between the cumulative AE count and the total frictional work done. Nonetheless, no consistent relationship between the AE activity and absolute wear rate could be established by the authors. In a work by Hisakado and Warashina [108], AE event counting was investigated as a mean to estimate the wear rate and surface damage resulting from the sliding of metal surfaces under various lubricated conditions. A general conclusion drawn by the authors was that an increase of the mean AE event counting rate was readily observed with increasing values of the mean friction coefficient and specific wear rates of the tribo-elements. Moreover, the AE event counting rates were seen to increase with the mean depth of micro-grooves resulting from wear.

A comprehensive review of some of the most relevant research works existing previously on AE applied to tribological phenomena, is presented in a paper by Jiaa and Dornfeld [101]. As a common denominator, the sensitivity of the AE signal to friction and wear phenomena was clearly demonstrated on the various cited works. Among those, the study conducted by Diei [109], incorporating AE measurements during pin-on-disc (POD) tribo-tests, have suggested a close relationship between AE and friction work generated from the sliding contact. Moreover, Diei also found that a distinction between "running-in" (self-accommodation)

and "steady-state" friction regimes could be identified by looking at the level of AE voltage (rms). An increase in the rate of AE with the length of apparent area of contact was observed as well. Besides, it's noteworthy that Diei's experimental findings also lead him to propose a power function relation between AE rms signal and the rate of frictional energy dissipation.
Jiaa and Dornfeld's own experimental results have drawn the authors to divide the entire sliding process into three distinct regions (running-in, steady-state and self-accelerating), based on AE rms voltage and measured wear rate generated from the sliding contact of metallic pairs on a POD apparatus. The influence of process variables such as the loading conditions, sliding speed and distances, on the AE activity was also verified. Results showed that, under a steady-state regime, the AE rms voltage increases with increasing applied load and sliding speed, and the mechanical properties of the materials will also influence the AE rms signal. Other important conclusions of their study were: the analysis of the raw AE signal in the frequency domain enabled the detection of stick-slip phenomena in sliding contact, and the transition from running-in to steady-state regime could be monitored using the rms level of AE signals. Therefore, the effectiveness of AE techniques in detecting changes in the tribological characteristics of the sliding surfaces was clearly demonstrated by them.

The usual measured parameters in AE technique for diagnostic or monitoring purposes are the maximum amplitude of the signal (in Volt), rms voltage (a measure of signal intensity), energy (Vs), pulse count and events. In counts operating mode, the number of times the amplitude of the AE signal exceeds a preset threshold level (i.e. voltage) in a given time is accounted for, while an AE event represents a group of counts which implies a transient elastic wave [102]. Some of the most common methods of AE measurements are depicted in Fig. 3.10, to better comprehend their meaning.
During sliding contact, the optimal use of AE technique could be sometimes compromised due to the fact that many wear mechanisms could occur simultaneously. This could pose difficulties during acquisition, when e.g. using the pulse count mode. Nonetheless, these limitations can be greatly lessen with the use of the rms amplitude measurement principle instead, where the AE rms voltage represents the energy of the AE activity [110].

Based on the aforementioned works, positive remarks can be drawn regarding the use of AE technique in monitoring the friction and wear behaviour of sliding materials, therefore

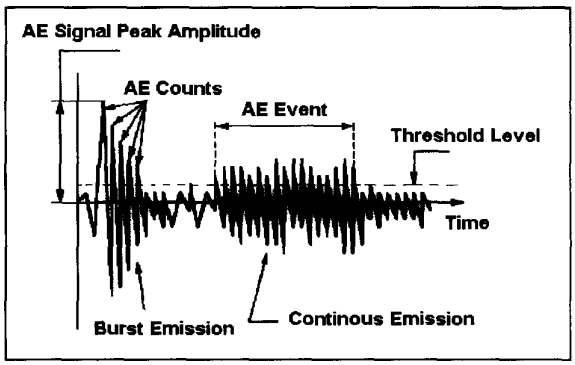

Figure 3.10: Some of the most common measuring principles for AE technique [111].

demonstrating the validity of this real-time non-destructive technique in the study of the tribological performance of hard coatings. Moreover, one of the main advantage of AE, especially for tool wear monitoring, is that the frequency range of AE signals is much higher than that of the environmental noise or tribosystem vibrations, thus eliminating the risks of overlapping interference [105]. The possibility of detecting in the early stage singular events like film seizure by delamination or other forms of severe damage to the coatings constitutes another asset of the AE technique.

However, several factors that affect the propagation of AE waves should be taken into consideration, namely the materials microstructure, inhomogeneities, geometrical arrangement of free surfaces, loading conditions, relative velocity or rotational speed of antagonist surfaces, and the number of component interfaces. Moreover, It has been shown that the nature of the lubricant could also influence the AE signal [102]. Besides, the type and positioning of the AE transducer relative to the contact surface needs also a careful thought.

An AE acquisition system is normally composed of a AE transducer or sensor, one or more amplification and filtering stages, analogue-to-digital converter (ADC) and data acquisition board to record the experimental data into a personal computer. The most commonly used vibration transducers are of the piezoelectric and resonance accelerometers types, which should be conveniently coupled to the source of elastic waves.

In the present dissertation work a “broad band” AE transducer of the piezoelectric-type (Bruël & Kjaer) was attached directly on the flank of the flat specimens sample holder, in close proximity to the contact region, in an attempt to correlate AE information and the tribological interaction of self-mated MCD coatings. Further details regarding the experimental setup and results of the investigation are presented in Publication III (see Sec. 4.4).

Chapter 4

Microcrystalline CVD diamond tribosystems

4.1 Introduction

This chapter gathers four scientific articles (Publications I-IV), reporting on the tribological characterisation of self-mated MCD-coated Si_3N_4 tribosystems conducted in this thesis. Tribo-testing for all studies was carried out in an adapted ball-on-flat (BOF) tribometer (PLINT TE/67R), with linear reciprocating motion. The oscillating frequency (1 Hz) and amplitude (3 mm) was kept constant in all studies, whereas the applied normal load and operating environment constituted the experimental variables. Moreover, two durations were used in tribo-testing, namely 2 h for the standard tests and 16 h for the endurance tests, which correspond to approximate sliding distances of 86 m and 690 m, respectively.

The ceramic Si_3N_4 was used as the substrate material, where the flat specimens were produced by pressureless sintering (1750 °C for 2 h), while the ball specimens were from commercial origin (Kema Nord). Diamond deposition was carried out in a microwave plasma-assisted CVD reactor, for the production of all samples used in these studies and where data relative to the diamond grain size, film thickness and other processing parameters can be found in the experimental procedure section of each article.
As a general procedure, the as-deposited and worn coatings were studied by several characterisation techniques, namely scanning electron microscopy (SEM), atomic force microscopy (AFM), optical microscopy (OM) and micro-Raman, with the purpose of assessing the diamond quality and morphology of the coatings, their topography and prevailing wear mechanisms. Moreover, the two tribological parameters, friction coefficient and specific wear rate (or dimensional wear coefficient), were determined for all tribosystems and experimental conditions.

Publication I (Sec. 4.2) is dedicated to the study of the influence of diamond deposition time and, therefore grain size, on the tribological performance of self-mated MCD coatings. Three deposition times (1 h, 2.5 h and 10 h) were analysed in order to assess which MCD coatings bear the most adequate tribological performance and, therefore, to be selected for subsequent studies involving microcrystalline diamond-on-diamond tribosystems.
For such purpose, reciprocating unlubricated sliding experiments were performed in ambient atmosphere, at room temperature, with applied normal load values in the leeway $10-105$ N.

Moreover, this wide range of applied contact loads enabled the determination of the threshold load of the MCD coatings under tribological stress, prior to film failure by delamination.
In this study, micro-Raman spectroscopy was also used to assess the diamond film quality of the as-deposited coatings and to gather information concerning the residual stress state of worn coatings, based on the diamond line shift.

In Publication II (Sec. 4.3), a comprehensive study of the tribological behaviour of MCD-coated Si_3N_4 systems is presented, with particular emphasis on the various friction regimes occurring and their explanation in terms of existing friction theories of diamond; the identification of prevailing wear processes and mechanisms, as well as other surface damage mechanisms leading to the degradation of the coatings' surface roughness.
Additionally, a novel method is presented to estimate the specific wear rate of MCD flat specimens, using AFM and OM characterisation techniques, which bears excellent results, in agreement with those expected from the measurement of near-circular wear scars imprinted in round specimens.

Publication III (Sec. 4.4) reports on the findings of a study concerning the application of the acoustic emission (AE) technique to monitor the friction behaviour during the sliding contact of MCD coatings. In particular, it aims to establish a correlation between the AE signal and the frictional behaviour. For this purpose, the AE signal was recorded by a piezoelectric transducer (Brüel & Kjaer), firmly secured to the lower sample holder in a perpendicular position relative to the sliding direction. An amplification/filtering stage (Brüel & Kjaer), with a frequency window of 50 kHz-2 MHz, was employed in the conversion of the AE pressure intensity into a measurable voltage at adequate acquisition rates.
Besides the use of AE, this work was complemented by other characterisation techniques, namely SEM, AFM and μ-Raman studies in order to analyse the as-deposited and worn features of the MCD coatings.

The fourth article (Publication IV, Sec. 4.5) in this chapter is dedicated to the analysis of the friction and wear behaviour of self-mated MCD-coated Si_3N_4 films, when subjected to water lubrication. In this last work, intense contact stress conditions were experimented during

sliding by imposing high loads ($70-160$ N), in order to evaluate the potential of MCD-coated Si_3N_4 films in, e.g., metalworking and fluid handling applications.
A comprehensive study using AFM's three-dimensional resolving power, of wear-induced surface features and topography resulting from the application of such high contact loads is equally presented in the article.
Moreover, a relationship between the diamond surface asperities and morphology of the generated wear particle debris, entrapped in the aqueous media, is also established, which corroborates the description of the predominant wear mechanisms for MCD coatings.

(A) UNLUBRICATED TESTS

4.2 Grain size effect on self-mated CVD diamond dry tribosystems [Publication I]

C.S. Abreu, F.J. Oliveira, M. Belmonte, A.J.S. Fernandes, R.F. Silva, J.R. Gomes
Wear, 259 (2006) 771-778

Abstract

Chemical vapour deposited (CVD) diamond coatings are important for tribological applications due to their unique combination of properties. Previous work demonstrated that silicon nitride (Si_3N_4) excels as a substrate for diamond coatings due to its low thermal expansion coefficient mismatch relative to diamond films resulting in a significant adhesion improvement. In this study, dense Si_3N_4 substrates were fabricated by pressureless sintering and diamond coated by microwave plasma chemical vapour deposition (MPCVD). The deposition time varied between 1 and 10 h in order to investigate the effect of the diamond grain size and film thickness on the tribological behaviour of self-mated CVD diamond coatings on Si_3N_4. Reciprocating dry sliding ball-on-flat wear tests were performed in air up to 16 h, at room temperature, with normal applied load ranging from 10 N to 105 N. The stroke and frequency of the sliding motion were kept constant with values of 6 mm and 1 Hz, respectively. Several characterisation techniques (SEM, AFM, micro-Raman) were used to identify the prevailing surface damage mechanisms. After a very short running-in regime, with high friction coefficients, a steady-state regime is reached, characterized by extremely low friction values ($\mu \sim 0.03$). A mild wear mode was achieved for the longer runs, with wear coefficient values around 10^{-8} $mm^3N^{-1}m^{-1}$. The larger grain sized and thicker coatings present smaller compressive residual stresses (below 1 GPa) due to a better in-depth accommodation of the contact pressure. This delays film delamination to much higher applied loads (105 N) than the thinner, small grain sized coatings, grown for 1 h that fail in sliding under 35 N of normal load.

Keywords: Wear, Friction, CVD diamond, Grain size

4.2.1 Introduction

Diamond coating films can improve many surface properties of engineering substrate materials, including erosion, corrosion, and wear resistance. Moreover, cleaved diamond surfaces exhibit one of the lowest friction coefficients of any known material, making them ideal for highly demanding tribological applications in open air [26, 32]. In particular, diamond films obtained by chemical vapour deposition (CVD) technique have demonstrated suitable behaviour that makes them appropriate for many technological applications where these characteristics are determinant. This technology has significantly lowered the cost of synthetic diamond comparing to that of the conventional high pressure-high temperature (HPHT) diamond. Thus, CVD diamonds films are used or being considered as coating material for machine cutting tools, mechanical face seals, protective coatings for aerospace components, hard disks and medical implants [33, 112, 113, 114].

Various metallic and nonmetallic substrate materials are employed for CVD diamond deposition [24]. Among them, silicon nitride (Si_3N_4) is gaining increasing importance due to the low thermal expansion coefficient mismatch between the diamond film and substrate. This minimises the interfacial residual stresses between the coating and substrate, leading to enhanced diamond/substrate adhesion. Further, Si_3N_4 possesses high hardness, high fracture toughness, an excellent thermal shock resistance, low coefficient of friction in open air and excellent wear resistance [52, 73].

Most diamond-on-diamond tribological studies have been performed using mainly natural single-crystal diamond as the counterpart material [9, 19, 26, 33]. Moreover, recent work on CVD diamond films were primarily oriented on the study of frictional properties of the coatings under vacuum conditions, under partial pressures of atmospheric gases or performed with small applied normal loads [47]. Gardos [32] performed scanning electron microscope (SEM) tribometry studies of self-mated diamond films in vacuum, or at partial pressures of hydrogen and oxygen, to examine the surface chemistry-induced friction and wear changes as a function of atmospheric environment and temperature. Miyoshi et al. [25] investigated the potential of CVD diamond-coated Si_3N_4 substrate for solid film lubrication, among other coatings,

under humid air, dry nitrogen and ultra-high vacuum conditions. Low coefficients of friction (< 0.1) and moderate wear rates ($\leq 10^{-6}$ mm^{3}N^{-1}m^{-1}) were reported for the unlubricated sliding of self-mated CVD diamond films in humid air. However, such tests were performed with an applied load of only 0.98 N. To such an extent, very limited information regarding the wear properties of self-mated CVD diamond-coated Si_3N_4, particularly for higher applied loads, is available in the open literature.

The objective of this study is to investigate the influence of diamond grain size on the tribological performance of self-mated CVD diamond-coated Si_3N_4 parts. Sliding tests were performed in open air using a reciprocal motion ball-on-flat (BOF) configuration in order to assess their friction and wear properties at several loads ($10-105$ N range). Further, the critical load prior to film delamination, originated by tribological action, was identified. SEM and AFM were used to characterize the morphology of the worn surfaces. Micro-Raman spectroscopy was used to study the quality of the deposited films and to investigate the residual stress induced by tribological action.

4.2.2 Experimental Procedure

Substrate material

Substrate material consisting of dense silicon nitride (Si_3N_4) was prepared from starting powders of α-Si_3N_4 (Starck grade M11), Y_2O_3 (Starck grade C) and Al_2O_3 (ALCOA CT-3000SG). Batch compositions with weight proportions of 89.3, 7.0 and 3.7%, respectively, were Si_3N_4 ball milled in isopropyl alcohol during 4 h. The obtained homogeneous suspension was then dried at 60 °C, sieved with an 115 μm mesh and burnt at 400 °C during 4 h. In order to achieve full densification of the Si_3N_4 substrates ($> 99\%$ of the theoretical density) the mixed powders were consolidated by uniaxial pressing at 30 MPa, followed by isostatic pressing at 200 MPa and then placed inside powder-bed Si_3N_4/BN protected graphite crucibles. Flat quadrangular samples with 10 mm sides and thickness of 3 mm were finally pressureless sintered at 1750 °C for 2 h, under nitrogen atmosphere. Dense commercial balls of Si_3N_4 with a diameter of 5 mm were also used as substrate material.

Prior to diamond deposition, all of the sintered flat samples were submitted to the following surface pre-treatment: grinding with 15 μm diamond paste and subsequently polishing to a specular finishing with colloidal silica (0.25 μm; type Syton). In the follow-up, the samples were manually abraded with $0.5-1$ μm sized diamond powder on a silk cloth and then rinsed in acetone/ethanol ultrasonic bath for 10 min, to remove loose diamond particles. The chosen procedure for the surface pre-treatments relies on a study showing superior results, concerning diamond nucleation density and film homogeneity, for the mechanically microflawed Si_3N_4 substrates [115]. Surface modification pre-treatments of the ball samples consisted in polishing with 0.25 μm sized colloidal silica, followed by microflawing by ultrasonic agitation of diamond powder ($0.5-1$ μm) suspension in *n*-hexane.

Deposition technique

Diamond deposition was carried out in a microwave plasma chemical vapour deposition (MPCVD) system (ASTeX PDS18, Seocal and Seki Technotron Corp., Japan). Different deposition conditions were used in order to achieve diamond films with distinct grain sizes and to adjust the deposition procedure to the distinct substrate geometries involved aiming similar film thicknesses in the flat and ball specimens. In the present study, three types of CVD diamond-coated Si_3N_4 materials were tested corresponding to depositions times of 1 h, 2.5 h and 10 h. The deposition parameters were as follows: microwave power = 2 kW; chamber total pressure = 1.2×10^4 Pa; H_2/CH_4 gas flow = 400/20 standard cubic centimetre per minute (sccm) and 400/16 sccm for the flat and ball specimens, respectively.

The diamond films in all the samples exhibited a fully adhered and continuous film aspect. A former study done by Belmonte et al. [73] in regard to the adhesion behaviour of CVD diamond-coated Si_3N_4 produced using the same setup and similar deposition conditions (deposition time = 2 h), demonstrated that the coatings did not delaminate up to an indentation load of $\sim$ 800 N. The chosen deposition conditions lead to a growth rate of approximately 3 μmh^{-1} [116].

Structural and tribological characterisations

In this study, a variety of experimental techniques were used in order to assess diamond film quality, surface morphology and tribological response of the CVD diamond-coated Si_3N_4 ceramics. The combination of measurements and diagnostic techniques was applied to correlate diamond grain size effect on the tribological performance of the diamond films. Ultrasonic cleaning of samples in ethanol was performed before each characterisation procedure.

Friction and wear testing of self-mated CVD diamond-coated Si_3N_4 samples were conducted using an oscillating BOF adapted tribometer (PLINT TE67) in order to investigate the influence of diamond grain size on the tribological behaviour of this tribosystem. The diamond-coated balls (upper specimen) were fixed in a sample holder arm and made to contact with a defined load onto the diamond-coated flat square specimens mounted on a reciprocating table. The tests were performed under a dry sliding arrangement in open air ($\sim 50-60\%$ RH) with a constant stroke and frequency of 6 mm and 1 Hz, respectively. The duration of the tribological experiments were chosen to be 2 h for the regular tests, which corresponded to a sliding distance of approximately 86 m. Endurance tests run for an uninterrupted period of time of 16 h (sliding distance, $x \sim 691$ m) were also performed for some selected contact forces. Static normal loads ranging from 10 to 105 N were applied directly over the ball specimens, by means of dead-weights. Assuming Hertzian theory for the elastic contact between a spherical/planar geometry, these conditions produced an initial contact pressure of approximately $5-11$ GPa, respectively [117]. The friction force was measured by a load cell, its signal amplified and processed by a personal computer. Prior to testing, the load cell was calibrated by applying two to three known dead weights in the range of the measured loads.

Micro-Raman spectroscopy was used to characterise the atomic bonding state and diamond film quality of the CVD coatings [25, 26]. Further, measurements of the Raman diamond peak shift of worn CVD diamond films permitted residual stress state evaluation induced by the tribological action [113, 118]. Micro-Raman measurements were carried out with a Jobin-Ybon spectrometer (Model T6400) using the 514.5 nm line of an argon-ion laser beam focused onto the film, with a spot size of 1 μm and a laser power of few tens of mW.

A Digital Instruments NanoScope IIIa atomic force microscope (AFM) was used to study the surface morphology of as-grown and worn CVD diamond films. Roughness values and surface features were calculated by inherent NanoScope III software. The surface microstructure, grain size and coating thickness of the studied CVD diamond films were observed by a Hitachi (model S-4100) scanning electron microscope (SEM). Furthermore, low amplification observations by SEM were also conducted with the purpose of measuring the radius of near circular wear scar of the ball specimens and thereby estimate the wear volume of this triboelement.

4.2.3 Results and Discussion

Morphology of as-grown and worn diamond films

The initial diamond grain size and morphology of the three distinct coatings in this work is shown in Fig. 4.1. The polycrystalline films are composed of sharp, well faceted microcrystallites with diamond grain sizes of 1.8 ± 0.8 μm, 2.4 ± 1.1 μm and 4.6 ± 1.7 μm, for the 1 h, 2.5 h and 10 h deposited coatings, respectively. The corresponding initial surface roughness (Ra) estimated from AFM characterization are 155, 170 and 396 nm (load = 0 N in Fig. 4.2). Triangular $\{111\}$ facets predominate in the larger grains. Such a surface morphology is characteristic of most conventional CVD-grown thin films [52, 118].

Selected AFM images of unworn and tribologically tested flat samples are presented in Fig. 4.3. Fig. 4.3(a) and (b) correspond to 1 h deposited specimens for the initial and the smoothest finishing condition, respectively. The latter one results from extensive self-polishing action against the coated sphere counterpart. A homologous pair but for the 2.5 h diamond-coated material is depicted in Fig. 4.3(d) and (e). The images set in Fig. 4.4 correspond to the topographic features as a function of applied normal loads for the 10 h diamond-coated plate. The pictures show enhanced smoothening of the surface with increasing load, the diamond asperities being truncated as a result of the sliding process, as quantitatively revealed in Fig. 4.2. One of the features evidenced in Fig. 4.2 is the surface degradation above a specific load where a minimum of roughness takes place, namely for 1 and 2.5 h curves. This behaviour is supported by the image in Fig. 4.3(c), where some evidence of what seems to be diamond pull-outs are

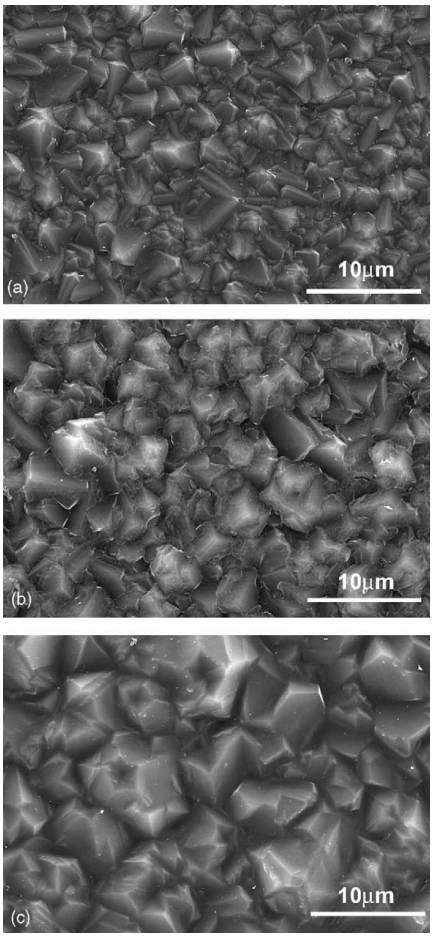

Figure 4.1: SEM micrographs of CVD diamond coatings on Si_3N_4 flat specimens: (a) 1 h of deposition time; (b) 2.5 h; (c) 10 h.

visible, i.e. micron-sized pits caused by localized removal of crystal aggregates. From Fig. 4.2, it is also clear that "endurance tests" of 16 h runs lead to similar finishing (very low R_a values of 8 nm) independently of the initial diamond grain size. Similar surface morphologies for worn CVD diamond films were reported by a number of other works [26, 32, 47, 52].

The plots for each coating growth time given in Fig. 4.2, which are directly proportional to film thickness, also depict the respective critical loads (35, 80 and 105 N) prior to gross film detachment by delamination, therefore, leading to coating failure under tribological action. However, it is worth noting that a complete coverage of the diamond film on Si_3N_4 substrate can

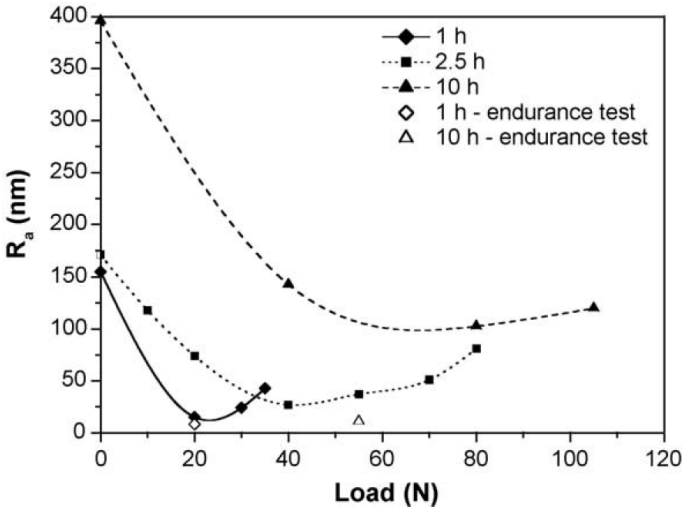

Figure 4.2: Roughness average values as a function of applied load used in ball-on-flat tribological experiments for distinct CVD deposition times (1, 2.5 and 10 h). "Endurance" tests refer to 16 h sliding whereas the remaining results represent 2 h test runs.

still be observed after 16 h of sliding contact, even under 55 N of normal load, which suggest a strongly adhered coating to the substrate. Similar intense mechanical solicitation is not found in literature for tribological performance comparison.

Bonding and stress state evolution induced by tribological action

Raman spectroscopy is a suitable optical technique for analysing carbon based materials, since it is able to give both chemical (non-diamond phases, dopants, impurities) and structural (strain) information [118]. The laser-optical Raman technique can differentiate with great precision the atomic bonding states of the carbon atoms (sp^3 for diamond and sp^2 for other non-diamond forms of carbon such as graphite) due to their different vibrational modes [26].

Representative expanded micro-Raman spectra for a given sample (10 h deposited) are shown in Fig. 4.5(a) as a function of BOF applied load. For reference purposes, the Raman spectrum of the as-deposited film (untested) is also represented. Also, the curves were vertically displaced for viewing purposes. These curves are enlarged around the diamond peak (1332 cm^{-1}) with the purpose of evidencing diamond peak shifts and associated residual stress

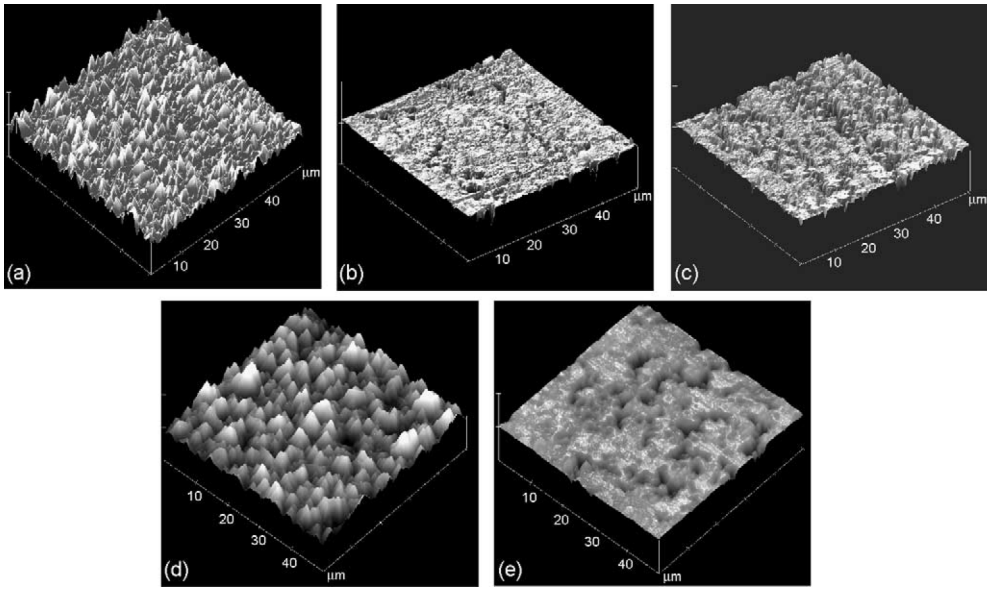

Figure 4.3: AFM images of selected CVD diamond-coated Si_3N_4 flat specimens: (a) 1 h deposited untested sample; (b) 1 h deposited and tested under 20 N; (c) 1 h deposited and tested under 35 N; (d) 2.5 h deposited untested sample; (e) 2.5 h deposited and tested under 40 N.

state of each film. The picture shows a positive shift of the diamond peak with increasing loads as well as FWHM broadening resulting from enhanced compressive state and anisotropic stress distribution resulting from the contact pressures arising during the sliding tests [118]. The same trend is observed for increasing sliding distances, at constant load, as depicted in Fig. 4.5(b). Full spectra do not show any signs of graphitic phases even after tribological action (see Fig. 4.5(c)).

Several groups have used Raman spectroscopy for stress measurements in diamond films. The dependence of the diamond Raman line shift on applied pressure can be estimated from the expression $\sigma \sim -0.34\ \Delta\nu$ GPa·cm^{-1}, where represents the shift of the diamond line [113]. An upward or downward shift will indicate a compressive or tensile stress state for the diamond film, respectively. Results from residual stress calculations are plotted in Fig. 4.5(d). All studied films have revealed a compressive nature, which is less accentuated for the thicker coatings grown for 10 h due to a better in-depth accommodation of the contact

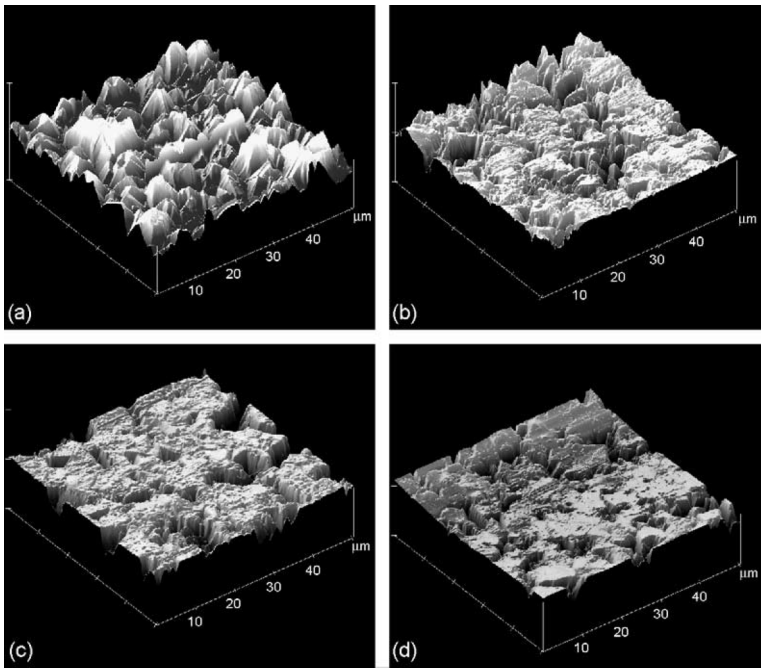

Figure 4.4: AFM pictures showing the variation of topographic features with applied loads for the 10 h grown CVD diamond coatings: as-deposited (a); after 40 N (b); 80 N (c); 105 N (d) sliding.

pressure. The increment of the peak shift with load already seen in Fig. 4.5(a) reflects itself in the positive slope of the compressive residual stress vs. load plot, Fig. 4.5(d).

Friction and wear properties of diamond films

Typical friction curves obtained for the sliding tests of the self-mated CVD diamond-coated Si_3N_4 materials are characterized by an initial ephemeral sharp peak followed by a gradual decay of the coefficient of friction to very low steady state values ($\mu \sim 0.03$). To illustrate the friction regimes occurring in the sliding tests, a detail of an overall instantaneous friction curve is shown in Fig. 4.6(a). Identified in each plot are three distinct regimes (labeled I, II and III) that correspond to a different behaviour for the friction coefficient. Regime I is the initial transient resulting from intense mechanical interactions between the sharp tips of diamond asperities of both the contacting surfaces. As sliding continued and the ball passed repeatedly over the same track, the coefficient of friction is significantly affected by the gradual blunting of

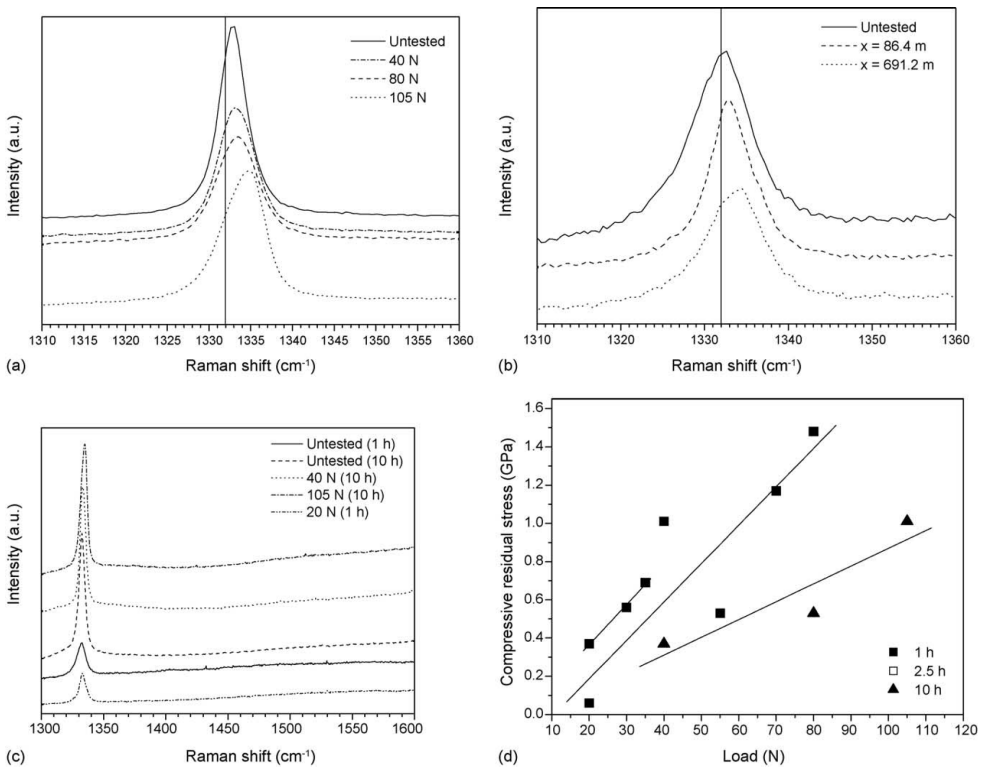

Figure 4.5: Micro-Raman spectra around the diamond peak (1332 cm^{-1}): (a) curves for untested and worn samples of the 10 h grown CVD diamond flat specimens for different applied normal loads; (b) curves for untested and worn samples of the 1 h grown CVD diamond flat specimens for different sliding distances under 20 N; (c) extended spectra including the graphite band region for untested and worn samples of 1 and 10 h grown CVD diamond flat specimens for different applied normal loads; (d) calculated compressive residual stresses induced by tribological action plotted as a function of applied load for different films.

asperities tips. Regime II corresponds to a relatively short transition stage and it is the result of the running-in effect of accommodation between counter-bodies and debris action. Afterwards, and for the rest of the duration of the tests, the coefficient of friction leveled off and tended stabilise (Regime III). Likewise, after the coefficient of friction has reached its steady state value it remained stable for the full duration of the tests, even for the endurance tests (sliding distance $x \sim 691$ m). This behaviour for the stationary friction coefficient is in accordance with data from other authors [26, 47] for the dry sliding of diamond films in humid air, being a consequence of the resulting smooth passivated contacting surfaces and low final Hertzian contact pressures.

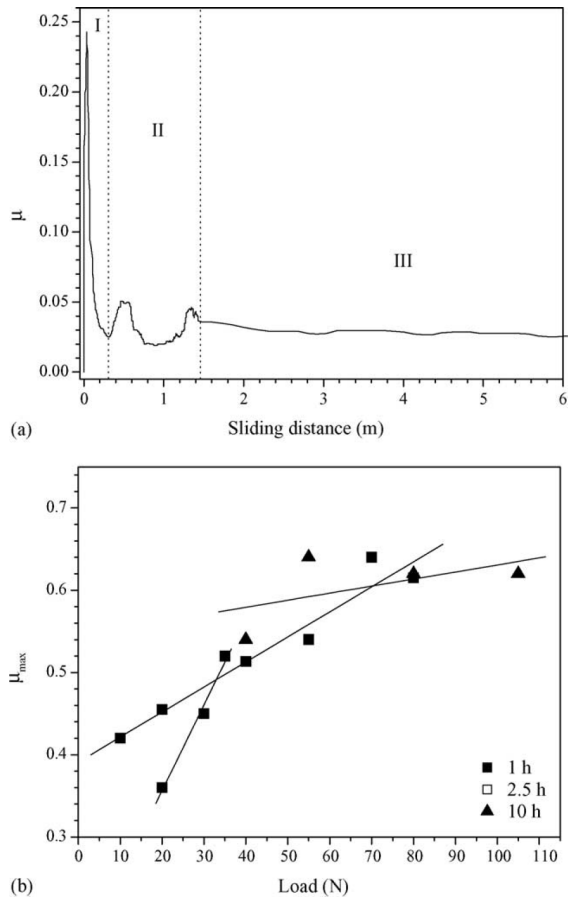

Figure 4.6: (a) Representative curve of the friction coefficient evolution showing distinct friction regimes (1 h deposited film tested under 20 N). (b) Variation of the initial friction coefficient (μ_{max}) with applied normal load for the three kind of CVD coatings.

The variation curves for the initial maximum friction coefficient (μ_{max}) with applied normal load are presented in Fig. 4.6(b). As expected, μ_{max} shows a growing tendency with increasing load as a result of the higher initial maximum contact pressures at stake that in turn gave rise to bigger friction forces. Likewise, a direct dependence of μ_{max} on the initial surface roughness of the film is observed [26].

The wear coefficient of the ball specimens (K_b) were calculated from the diameter of the near circular wear scars observed after completion of the tests. That is, in cases that wear can be neglected on the flat specimen, i.e. only wear of the ball is considered on a BOF tri-

bosystem, the volumetric wear (V) can be calculated from the diameter (d) of the scar and the radius (r) of the ball according to: $V = \pi d^4/64r$ [119]. Fig. 4.7 shows the calculated values of K_b for the distinct films after 2 h sliding tests. The wear coefficient values were calculated in accordance with Archard's law: $K_b = V/xW$, were x is the sliding distance, and W the applied load. Wear coefficients in the 10^{-7} $mm^3N^{-1}m^{-1}$ order of magnitude denote a mild wear mode for the self-mated CVD diamond films sliding in ambient air. It is noteworthy that the assessed values for the tests show values one order of magnitude smaller, i.e. in the ultra-mild wear mode range. As can be seen from Fig. 4.7, the wear coefficients are slightly dependent on grain size, or initial surface roughness, of the CVD diamond films.

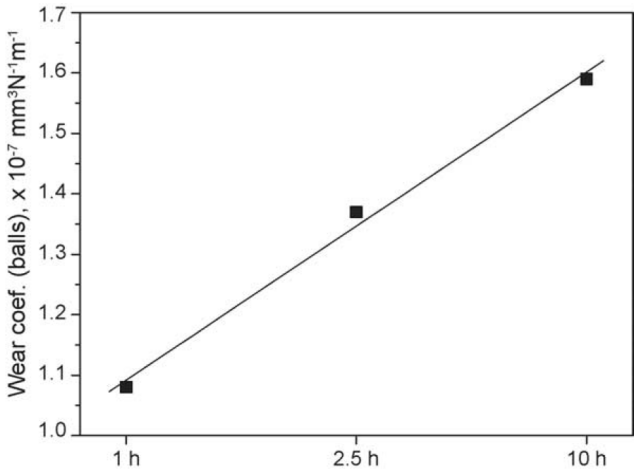

Figure 4.7: Average ball wear coefficient values for self-mated tribological tests with distinct deposition time CVD diamond films.

Miyoshi [33] found wear coefficients in the 1.0×10^{-7} to 1.2×10^{-7} $mm^3N^{-1}m^{-1}$ range for coarse grain (3.3 μm) diamond films, similar to the present ones. However, the tribosystem used consisted of a natural single-crystal diamond pin sliding over a CVD diamond-coated α-SiC substrate, in humid air (R.H. of 40%). In other work by Miyoshi et al. [25], observed wear rates in the 2×10^{-6} to 3×10^{-6} $mm^3N^{-1}m^{-1}$ range are reported for a CVD diamond pin sliding over a polished diamond film in humid air (R.H. of 40%) and an applied load of just 0.98 N. Considering the widely differing roughness and experimental geometries involved, the wear rates shown in the present study are consistent with those of the diamond

on diamond experiments previously referred, if not betters. Further, higher applied loads have been used in the present work. This suggests that CVD diamond-coated Si_3N_4 films have comparable wear resistances to single-crystal diamonds, despite their polycrystalline morphology and associated grain boundaries.

4.2.4 Conclusions

Continuous, well-adhered CVD diamond on silicon nitride flat and ball specimens were produced by microwave plasma technique. Self-mated ball-on-flat tribological dry tests reveal a self-polishing mechanism accomplished by diamond asperities truncation. This lead to very low surface roughness finishing of approximately 8 nm after 16 h sliding runs. Such extremely low values occur at a specific applied load above which some surface degradation takes place by diamond pull-outs. The finishing quality is improved for the lower grain sized coatings (1.8 μm) but these fail at much lower loads (35 N) than the larger grain sized (4.6 μm) and thicker ones that delaminate only at 105 N.

Micro-Raman characterisation of the tested samples did not reveal any signs of surface graphitic phase transformation. Spectra show increasingly diamond peak broadening and positive shift deviation with increasing loads, or increasing sliding distances, coming from higher compressive residual stresses and enhanced stress anisotropy imposed by the contact pressures, or working time. The compressive magnitude of the residual stresses is smaller for the thicker coatings grown for 10 h, with values below 1 GPa, due to a better in-depth accommodation of the contact pressure.

The friction evolution of the self-mated tests with the CVD diamond-coated Si_3N_4 materials start with a sharp peak arising from mechanical interlocking between the diamond asperities. A subsequent transition regime of running-in, corresponding to the accommodation between counter-bodies, leads to a final steady-state regime where very low friction values (~ 0.03) are attained. In this regime, the wear coefficient of the balls reached a value of the order of 10^{-8} $mm^3N^{-1}m^{-1}$, denoting a mild wear mode.

Acknowledgements

C.S. Abreu acknowledges PRODEP III funds supporting his PhD work. The financial funding from the FCT Project POCTI/CTM/45423/2002 is also gratefully acknowledged.

4.3 CVD diamond coated silicon nitride self-mated systems: tribological behaviour under high loads [Publication II]

C.S. Abreu, F.J. Oliveira, M. Belmonte, A.J.S. Fernandes, J.R. Gomes, R.F. Silva
Tribology Letters, 21, 2 (2006) 141-151

Abstract

Friction and wear behaviour of self-mated chemical vapour deposited (CVD) diamond films coating silicon nitride ceramics (Si_3N_4) were investigated in ambient atmosphere. The tribological tests were conducted in a reciprocal motion ball-on-flat type tribometer under applied normal loads up to 80 N ($\sim$ 10 GPa). Several characterisation techniques - including scanning electron microscopy (SEM), atomic force microscopy (AFM) and micro-Raman studies - were used in order to assess the quality, stress state and wear resistance of the coatings. In addition, a novel method is presented to estimate the wear coefficient of the diamond coated flat specimens from AFM and optical microscopy (OM) observations of the wear tracks.

Keywords: CVD diamond, Silicon nitride, Residual stresses

4.3.1 Introduction

Diamond films grown by chemical vapour deposition (CVD) technique keep most of the outstanding properties of natural diamond, including extreme hardness, high resistance to abrasion, very low coefficient of friction in ambient atmosphere, chemical inertness and high corrosion resistance. CVD diamond has already found applicability or constitutes a material with acknowledged potential for the aerospace, automotive, machining and fluid-handling industries [33, 114], and more recently in microelectromechanical systems (MEMS) and biomechanical applications [47, 62].

Tribological characterisation of dissimilar pairs involving diamond against ceramics or cemented carbide, generally shows that the counterbody suffers intense wear damage as opposed to diamond, that almost invariably stays unaltered [119, 120, 121, 122]. Thus, in order to

know the correct tribological performance of diamond under more realistic conditions, diamond on diamond sliding tests must be performed, particularly under high loads and without lubrication.

Earlier studies done by a number of researchers, concerning the tribological behaviour of natural diamond and diamond films, are summarised in the papers by Field et al. [11] and Habig [42]. For reciprocating sliding tests of diamond film discs in contact with natural diamond pins and under an applied load of 1 N, in humid air, the reported values for the friction coefficient range between $0.03 - 0.04$ with a wear coefficient of 2×10^{-7} $mm^3N^{-1}m^{-1}$ for the flat specimens. In another mentioned work, fretting studies of homologous pairs of diamond films produced by hot filament CVD report a decrease of the friction coefficient from initial values in the $0.2 - 0.3$ range to steady-state 0.05, in ambient atmosphere (R.H. 50-60%). However, the substrate material used for the deposition of the diamond coatings is not indicated.

Concerning the testing of self-mated systems of CVD diamond coatings, various metallic and non-metallic substrate materials have been used by a number of authors. Hollman et al. [123] investigated the performance of self-mated hot flame diamond coated cemented carbide as a face seal material. Unlubricated sliding tests in ambient air, under a nominal contact pressure of 0.5 MPa, showed an initial coefficient of friction of 0.05 which increased to a steady state value of 0.2. With respect to the wear behaviour of the coatings only a qualitative description is given by the authors and no values for the wear coefficient were reported. Kelly et al. [55] tested homologous pairs of polycrystalline diamond coatings deposited by microwave plasma CVD (MPCVD) onto SiC substrates. Friction coefficients in the range $0.05 - 0.07$ were recorded, under an applied pressure of ~ 0.5 MPa and marginal water lubrication. Once more, no wear coefficients for the diamond coated discs are presented.

In a study conducted by Gahlin et al. [124], the effects of high biaxial compressive stresses on the abrasive wear of diamond coatings were evaluated using the crater grinding method. Diamond coatings were deposited on cemented carbide substrates by the hot flame method and subjected to abrasion with diamond particles under an applied load of 0.3 N. An important conclusion of this study was that the coatings with residual compressive stresses

($\sim$ 2 GPa), showed lower values for the wear coefficient (10^{-7} $mm^3N^{-1}m^{-1}$) compared to that of free-standing stress-free films (2.2×10^{-6} $mm^3N^{-1}m^{-1}$), i.e. a reduction of an order of magnitude.

In more recent studies, long-term experiments with the purpose of assessing the tribological behaviour of diamond coated Ti-6Al-4V self-mated pairs were conducted by De Barros et al. [23], and Vandenbulcke and De Barros [39]. The tests were carried out with a moderate applied load (13 N) on a pin-on-disc apparatus in ambient air (R.H. $40-60\%$) and for sliding distances as high as 70 km. The polycrystalline diamond counterparts exhibited an evolution of the friction coefficient characterised by a rapid decrease down to ~ 0.05, after a sliding distance of 200 m, followed by an increase up to ~ 0.2 and thereon fluctuated in the $0.15-0.20$ range for the rest of the test. However, these relatively high final friction values for diamond coated counter-pairs, in ambient air, were explained by the arising of some of the Ti-alloy in the contact zone. A final wear coefficient of 1×10^{-9} $mm^3N^{-1}m^{-1}$ was reported for the pin specimen [23]. Such low value was mainly attributed to the decrease of the contact pressure and polishing of the diamond track on the disc. As it was too low to be properly measured, no wear coefficient for the disc specimen is indicated in both works. A recent case study by Met et al. [47] also reports on homologous pairs of smooth diamond coated Ti-6Al-4V substrates, in ambient air, using a pin-on-disk tribometer. The friction and wear tests were carried out under an applied load of 13 N and a sliding distance of 8 km. The reported friction coefficient and pin wear rate were 0.06 and 4×10^{-9} $mm^3N^{-1}m^{-1}$, respectively. Analogously, as it was too low to measure, the wear coefficient for the disc is not given.

Nonetheless, satisfactory adherence of diamond coating films to Ti-6Al-4V and other metallic substrates was only attainable by the use of interlayers, in order to compensate the large interfacial thermal expansion mismatch between the coating and substrate material. Furthermore, diamond coatings deposited on intermediate layers generally show worse adhesion compared to optimised direct deposition on adequate substrate material [72]. In order to cope with these constraints, research has been done using substrate materials exhibiting a low thermal expansion coefficient mismatch relative to that of diamond. A serious candidate to be used as a substrate material for diamond coatings is the technical ceramic Si_3N_4 [73]. Stud-

ies concerning the tribological characterisation of CVD diamond coated Si_3N_4, in different environments, were performed by Miyoshi et al. [25]. Hemispherical pins produced by brazing a free standing hot-filament CVD diamond film on a steel pin were made to slide against CVD diamond coated Si_3N_4 flat specimens, in ambient air (R.H. 40%). These self-mated tests were characterised by low friction coefficient values (~ 0.08) and moderate wear coefficients ($\sim 3 \times 10^{-6}$ mm^{3}N^{-1}m^{-1}). However, the relatively low Hertzian contact pressures (~ 2 GPa) used in such experiments cannot give a correct image regarding the performance of self-mated CVD diamond coating in more severe conditions. Further, no experimental values for the critical load of the coatings under tribological action are presented.

To conclude and as a general rule, available literature on the tribological performance of diamond-on-diamond tribosystem focuses mainly on the friction properties of single-crystal diamond or diamond coatings, and is normally conducted under relatively low applied loads. In addition, the wear coefficients for the flat counterparts specimens are generally not presented, mainly due to the inherent difficulty in assessing such low wear volumes for this specimen. Furthermore, there is no indication of the critical loads prior to film delamination, under tribological actions.

In the present study, the tribological performance of CVD diamond coated Si_3N_4 homologous pairs in ambient air is described. Sliding tests of diamond coatings were conducted using a reciprocal motion ball-on-flat geometry under moderate to high applied loads (10 N to 80 N range). The main criteria for coating performance evaluation in terms of tribological response were the friction coefficient, wear coefficient and critical load for delamination under reciprocal sliding interaction. The various friction regimes were identified and analysed based on friction models. Different analytical techniques - including micro-Raman spectroscopy, SEM and AFM - were used to assess the quality, surface morphology and topography of the as-deposited and worn CVD diamond films. Micro-Raman studies also permitted investigation of the residual stress state of the diamond films induced by tribological action. A novel method for assessing the wear coefficient of flat counterpart specimens is also presented.

4.3.2 Experimental setup and test procedure

Dense disc-shape Si_3N_4 substrates with a diameter of 10 mm and thickness of 3 mm were pressureless sintered at 1750 °C/2h for diamond deposition. Details of the processing conditions for the production of Si_3N_4 substrates are described elsewhere [115]. Commercial ball specimens (Kema Nord) of Si_3N_4 with a diameter of 5 mm were also used as substrates for diamond deposition, in order to act as counter-bodies in the tribological tests. The flat samples were submitted to the following finishing pre-treatments: grinding with a 46 μm grit size diamond wheel, 15 μm diamond polishing, and finally, manually scratching with 0.5-1 μm sized diamond powder on a silk cloth. To remove loose diamond particles, all the Si_3N_4 discs were firstly rinsed in an acetone ultrasonic bath for 10 min and subsequently in an ethanol bath for 10 min. Due to the high intrinsic roughness of the Si_3N_4 balls, a gradual polishing with 15, 6 and 1 μm sized diamond powder was done to reduce surface roughness, followed by microflawing by ultrasonic agitation with diamond suspension ($0.5 - 1$ μm) in hexane to promote adhesion.

Diamond deposition runs were performed in a Microwave Plasma Chemical Vapour Deposition (MPCVD) apparatus (ASTeX PDS18, Seocal and Seki Technotron Corp.). The deposition conditions were adjusted to achieve similar film thickness in both flat and ball samples as follows: microwave power, ~ 3 kW; total pressure, 1.2×10^4 Pa; H_2/CH_4 flow, 400/25 sccm and 400/16 sccm, respectively; deposition time, 2.5 h. The diamond films for both types of samples exhibited approximately a thickness and a diamond grain size of $12 - 14$ μm and 2.5 μm, respectively, without a preferential grain morphology. The average diamond grain size and film thickness of the coatings were obtained, respectively, from stereological and cross-sectional image analysis from higher magnification SEM (Model S-4100, Hitachi) micrographs.

Diamond coatings were characterised by a variety of techniques in order to assess diamond quality, surface morphology and tribological response of the film. Micro-Raman study of as-deposited and worn films was carried out with a Jobin-Ybon T6400 spectrometer, using a 514.5 nm Ar^+ incident laser beam, with a few tens of mW power at the sample and a spot size of ~ 1 μm. The instrument was calibrated using the strong Raman diamond peak line of a highly transparent geological type IIa gem. Micro-Raman spectra allowed the characterisation of the films in terms of diamond quality and purity.

Self-mated wear tests of CVD diamond coated Si_3N_4 were conducted on a ball-on-flat adapted tribometer (PLINT TE67) using an unlubricated reciprocating sliding arrangement. The coated balls (upper specimen) were fixed in a sample holder arm and pressed with a defined load onto diamond coated Si_3N_4 disc-shape flat specimens mounted on a reciprocating table. All the tests were performed in ambient air (R.H. $\sim 50-60\%$) at room temperature with constant stroke (6 mm) and frequency (1 Hz). The normal applied load varied in the range 10 to 80 N. Assuming elastic contact (Hertz theory) [117], these conditions produced initial maximum contact pressures (P_{max}) of ~ 5 to 10 GPa for 10 to 80 N, respectively. In order to assess the short and long term evolution of the tribological response of the diamond coatings, reciprocating sliding tests were conducted over sliding distances ranging from 3×10^{-2} m to 690 m (endurance tests). Normal tribological tests were completed for a sliding distance of 86 m.

The friction coefficient was continuously measured during tests with a load cell. Prior to testing, the load cell was calibrated by applying two known dead-weights in the range of the measured loads. The wear volume of the diamond coated ball specimens (W_v^{ball}) was calculated from SEM observation of the diameter (d) of near circular wear scars, as follows [119]:

$$W_v^{ball} = \frac{\pi \cdot d^4}{64 \cdot r} \tag{4.1}$$

where, r, represents the ball radius. According to Archard's law, the ball wear coefficient can then be calculated using the expression:

$$k_{ball} = \frac{W_v^{ball}}{P \cdot x} \tag{4.2}$$

where, P, is the applied load and, x, the sliding distance. Due to the difficulty in correctly measuring the wear volume of the flat specimens by the usual techniques (weight loss or conventional profilometry), a model for the estimation of the wear coefficient of the flats is proposed in the discussion.

After the sliding tests, the surface morphology of as-deposited films and wear tracks were observed by SEM. Topographical information and surface roughness parameters of as-deposited films and worn samples were assessed using atomic force microscopy (AFM, Model

NanoScope IIIa, Digital Instruments) operated in tapping mode, by acquiring three fields with a scan size of $50 \times 50\,\mu m^2$. Those parameters are defined as: R_a is the arithmetic average of the absolute values of the surface height deviations from the mean plane, R_z the average difference in height between the five highest peaks and five lowest valleys relative to the mean plane, and R_{max} the maximum vertical distance between the highest and lowest data points in the image.

Optical Microscopy (OM) observations were performed in order to measure the lateral width of the wear tracks on the flat specimens and to quantify the percentage of worn area. Furthermore, analysis of the diamond peak shift on ultrasonically cleaned worn samples by micro-Raman spectroscopy makes possible evaluating the stress state of diamond coatings induced by tribological action [118].

4.3.3 Results and discussion

Morphology of diamond films

Polycrystalline CVD diamond coated surfaces are characterised by crystallites having a triangular faceted morphology typical of diamond [26, 52]. In this study, all films deposited on Si_3N_4 substrates presented faceted diamond crystallites with preferential $\langle 100 \rangle$ crystallographic growth orientation, showing a similar surface morphology for both ball and flat specimens. A SEM micrography of an as-deposited CVD film is depicted in Fig. 4.8(a) which reveals prevailing octahedral asperities and a rough morphology. Surface roughness parameters of as-deposited flat specimens assessed by AFM measurements showed average values of $R_a \sim 170$ nm, $R_z \sim 1450$ nm and $R_{max} \sim 1480$ nm. Columnar growth of large diamond crystallites on top of Si_3N_4 substrate, resulting in rough surfaces, is also observed in Fig. 4.8(b). Micro-Raman studies of as-deposited films showed the presence of sharp peaks around the diamond frequency line of 1332 cm^{-1} and no evidence of graphitic bands (Fig. 4.9). These features, combined with excellent adhesion between studied CVD films and Si_3N_4 substrates, assessed elsewhere by acoustic emission studies [73], confirms the high purity and good quality of the tested films.

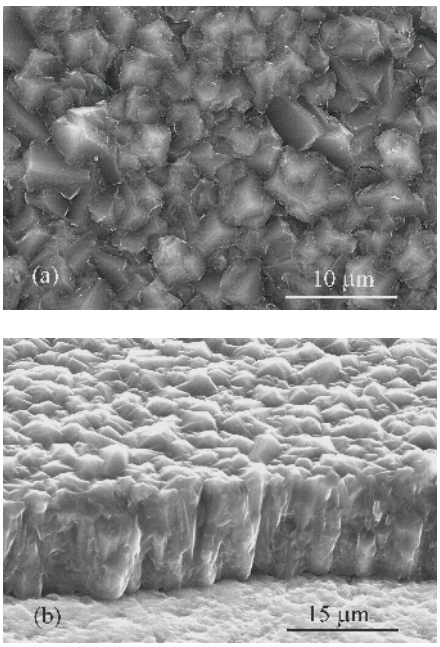

Figure 4.8: SEM micrographs of as-deposited CVD diamond coated Si_3N_4 ceramics: (a) Typical appearance of $\langle 100 \rangle$ oriented micropyramidal film; and (b) cross-sectional view showing columnar growth.

In Fig. 4.10 are depicted AFM images of samples subjected to tribological action, with the purpose of analysing the topographic evolution of worn surfaces for different applied normal loads (10, 20, 40, 55, 70 and 80 N). The pictures show a progressive smoothening of the surface for increasing load with asperity peaks having been truncated as a result of the sliding process. This feature is reported after a sliding distance of $\sim$ 86 m. Nonetheless, a phenomenon of surface degradation is observed for the higher load condition (80 N) where the presence of diamond pull-outs can be seen, i.e. micron-sized pits caused by localised removal of crystal aggregates.

Figs. 4.11(a) and 4.11(b) show SEM photomicrographs of flat CVD specimens after 86 m and 690 m of sliding distance, respectively, under an applied load of 55 N. The worn surfaces appear to be rather smooth, which is an indication of gradual wear of the diamond coating by abrasion. If the untouched valleys of the diamond films are discarded from the AFM surface roughness calculation, the polished zones exhibit very low roughness, $R_a \sim 16$ nm and ~ 13 nm, respectively. Furthermore, the endurance test (690 m) micrography (Fig. 4.11(b)) shows the

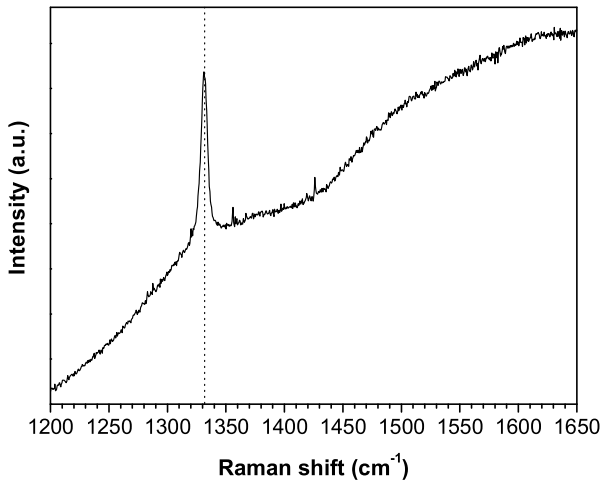

Figure 4.9: Typical micro-Raman spectrum of as-deposited CVD diamond films, showing a sharp peak centered at the diamond frequency line of 1332 cm^{-1}.

preservation of the complete coverage of the Si_3N_4 substrate by the diamond film after sliding interaction, without signs of delamination. Similar surface morphologies for worn CVD diamond films deposited on various substrates are reported in the literature [26, 32, 47, 52]. Although in a different experimental setup (abrasion wear tester) but similar applied load (50 N), Mallika et al. [52] suggested that such progressive wear is an indication that wear processes of diamond coatings are not related to microcracking and brittle fracture of the film but to attritious wear by abrasion. In the present study, a small amount of submicron wear debris was observed on the surfaces of the flat samples (Fig. 4.11(c)), mainly located in the voids between asperities plateaus, therefore, leaving the real areas of contact essentially free of wear debris.

The surface roughness parameter R_a for the tested CVD flat specimens is represented as a function of the applied normal load in the plot of Fig. 4.12(a). The plotted values result from AFM fields taken in two distinct locations on the wear track of the flat specimens, namely at the centre and near the boarder (labeled edge) of the track. The curve relative to the centre of the track shows an accentuated decrease in R_a ($\sim 80\%$) with increasing applied normal load until 40 N, as a result of the intensification of the self-polishing effect obtained with greater contact

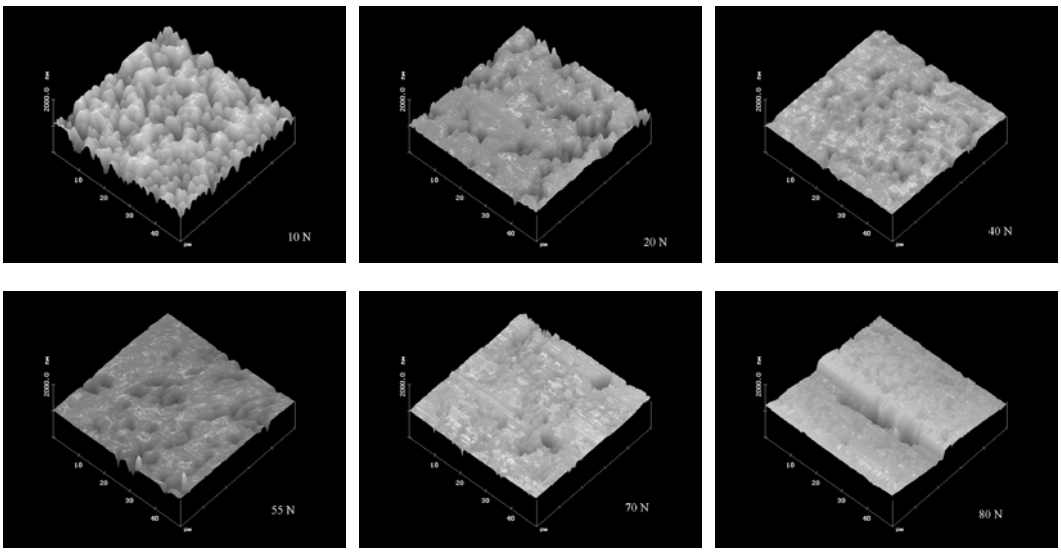

Figure 4.10: AFM images of worn diamond coated surfaces. Evolution of the surface topography of flat specimens wear tracks with different applied loads (10, 20, 40, 55, 70 and 80 N).

pressures. Higher values of applied load reflect themselves in an increase of R_a. Nonetheless, the variation of R_a is smaller than that observed for the 10 N to 40 N range. The minimum of R_a at 40 N is observed both at the centre and at the edge of the track. A similar behaviour is found for the surface parameter R_z (Fig. 4.12(b)) where a minimum also occurs for 40 N.

The greater values of R_a and R_z for high applied loads ($70-80$ N) can be explained by the degradation of the diamond surface, associated to the increasing importance of brittle microfracture of the coating in the overall wear mechanisms at stake, leading to diamond pull-outs. This trend is also visible on the results for R_{max} (Fig. 4.12(c)), where a very high value is observed for 80 N in the centre of the track rather than near the edge. This feature is consistent with AFM observations of worn films where pronounced grooves and depressions are visible for the highest applied load (Fig. 4.10, 80 N).

Bonding and structure of diamond films

Micro-Raman spectroscopy was used to characterise the structure of CVD diamond coated Si_3N_4 films. The Raman spectra of natural diamond exhibits a single sharp peak at

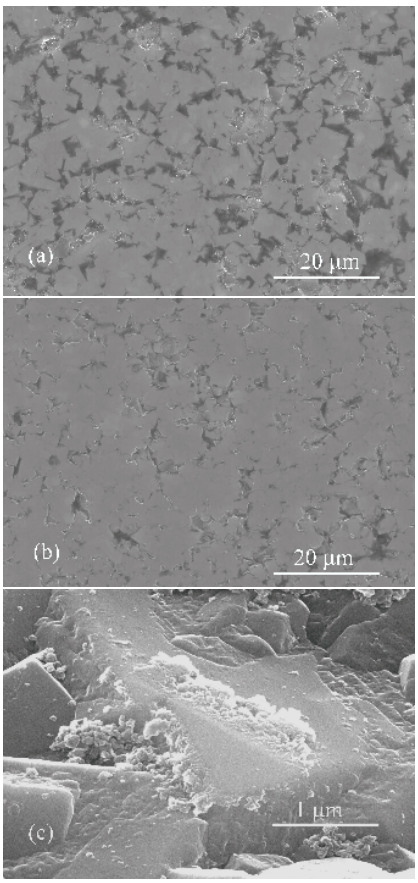

Figure 4.11: SEM micrographs of worn diamond coated flat specimens: (a) after a sliding distance of 86 m and with an applied load of 55 N; and (b) after 690 m and with an applied load of 55 N; (c) aspect of submicron wear debris, mainly located between the voids of truncated micropyramidal diamond crystals (applied load of 10 N and a sliding distance of 30 m).

1332 cm^{-1} (sp^3 C-C bonding), with a full width at half-maximum (FWHM) of ~ 2 cm^{-1}. For CVD diamond films the sharp line characteristic of natural diamond is normally shifted relative to the stress-free frequency due to internal residual stress, and a broadening of the peak occurs as a result of crystal defects or anisotropic stress distribution [118, 125]. Consequently, many authors have used this shift in order to assess the total residual stress in diamond films [126, 113]. The diamond peak shift changes linearly with residual stress, depending on the nature of the stress state (uniaxial or biaxial constraints). For polycrystalline diamond films the constraints are of the biaxial type and a proportionality factor of -0.384 GPa/cm^{-1} has been calculated by

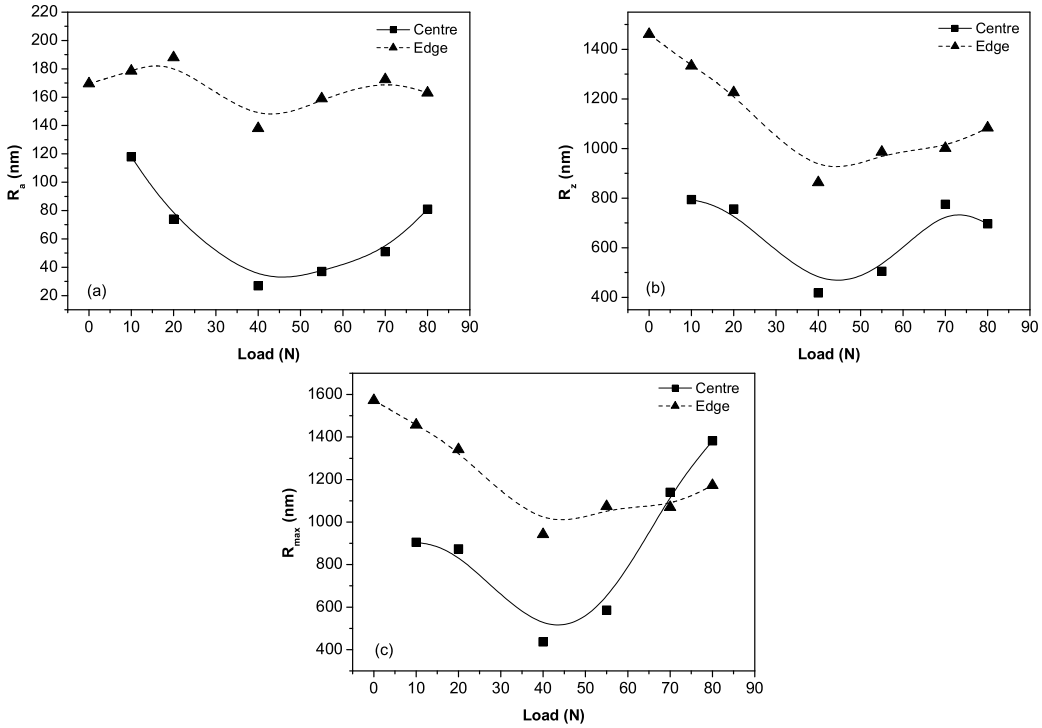

Figure 4.12: Variation of surface roughness parameters of the tested CVD diamond films as a function of the applied normal load – measured at the centre and edge of the wear tracks – calculated from AFM observations of flat specimens: (a) R_a; (b) R_z ; and (c) maximum peak-to-valley height (R_{max}). All results are relative to a sliding distance of 86 m.

Ager and Drory [99] for the doublet phonon, over all crystallite orientations. However, since the examination of Raman spectra of tested CVD films reveals a single diamond line (no observed splitting for singlet and doublet Raman components), values for the total biaxial residual stress (σ) of worn diamond flat specimens were calculated using a factor proposed by other authors [127, 128, 129] in cases of a single peak, as follows:

$$\sigma(\text{GPa}) \sim -0.488 \cdot \Delta_V(\text{cm}^{-1}) \tag{4.3}$$

where, Δ_V, represents the diamond peak shift. A positive (or negative) Δ_V corresponds to a compressive (or tensile) total residual stress state.

Micro-Raman spectra taken from wear tracks of worn diamond films are presented in Fig. 4.13(a). The vertical dotted line corresponds to the Raman frequency of stress-free diamond (1332 cm^{-1}) and the spectrum of an as-deposited film is depicted for comparative purposes. The two graphitic broad bands at $\sim$ 1360 cm^{-1} (D-band) and $\sim$ 1580 cm^{-1} (G-band) are not present, instead a sloped luminescence background appears mostly generated by the substrate. All depicted curves exhibit the characteristic diamond line and a pronounced peak located at $\sim$ 1331 cm^{-1} with a FWHM of $\sim$ 6 cm^{-1} was obtained for the as-deposited film, confirming that high quality unstressed diamond coatings were deposited on-top of Si_3N_4 substrates.

The plot of Fig. 4.13(b) shows the expanded micro-Raman spectra around the diamond peak of worn coatings, taken from the wear track region of flat specimens, altogether with a reference spectrum of the as-deposited CVD diamond film. The various spectra were vertically displaced for viewing purposes and correspond to a sliding distance of 86 m, and different applied loads. Frequency-shifted diamond peaks are indicative of residual stresses induced by tribological action. However, the presence of a single diamond peak represents weaker constraints as compared to spectra were the degeneracy is lifted [127]. Another revealed feature is the increasing positive Δ_ν relative to the stress-free frequency with load increment, which represents higher compressive constraints for the films. A broadening and decreasing of the diamond peak height relative to the as-deposited curve can also be observed for the worn films. This effect can be attributed to inhomogeneous distribution of stresses resulting from the contact pressures arising during the sliding tests.

Results for the residual biaxial stress of worn flat specimens and corresponding FWHM of the diamond line, as a function of the various loads used in the tribological tests, are represented in Fig. 4.13(c). The plotted values were calculated from Eq. 4.3 and correspond to a sliding distance of 86 m. The data for the as-deposited film, not subjected to wear stress (0 N), is also represented for comparing purposes. As can be seen from the figure, the as-deposited film reveals a slight tensile residual stress state of magnitude $\sim$ 0.4 GPa. Furthermore, tribological tests conducted under an applied load of 10 N were unable to change the nature of the film stress state. For higher loads ($\geq$ 20 N) the graph trend shows a shifting from tensile to a

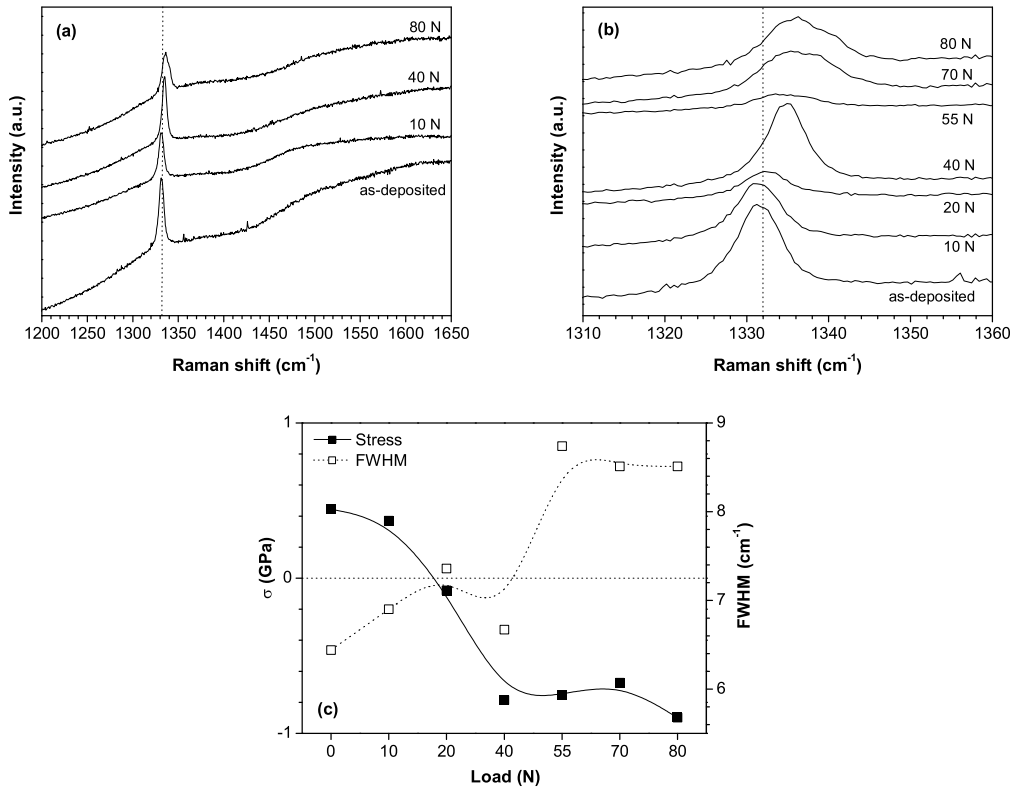

Figure 4.13: Micro-Raman spectra of studied CVD diamond films. The curves are vertically displaced for viewing purposes: (a) full spectra of worn samples (10, 40 and 80 N) and as-deposited diamond coating; (b) expanded view around the diamond peak for various applied loads; (c) residual biaxial stress and respective FWHM as a function of the applied load. All results correspond to a sliding distance of 86 m.

compressive stress state, with constraints of ~ 0.1 GPa and ~ 0.8 GPa for tests conducted under 20 N and 40 N, respectively. Further increase in the applied load resulted in small changes for the magnitude of the residual biaxial stress of worn coatings.

In what concerns the FWHM of the diamond peak, results shown in Fig. 4.13(c) reveal an increasing broadening with applied load up to ~ 9 cm^{-1} (under 55 N), which relates to an increase in anisotropy of the in-plane biaxial stress distribution. The existence of a plateau for loads ≥ 55 N could also indicate the freezing of stress anisotropy, until film delamination occurs (> 80 N). As a concluding remark, examination of Raman spectra of worn CVD films indicates

that compressive biaxial residual stresses of up to ~ 0.9 GPa can be accommodated in the film prior to delamination. This suggests a strongly adhered coating, resilient to film detachment provoked by tribological solicitation under high contact pressures (up to ~ 10 GPa).

Tribological parameters of diamond films

Fig. 4.14(a) presents the evolution curves of friction coefficients (μ) for three levels of applied normal load. As it can be seen from the plots, three distinct regimes (labeled I, II and III) mark out the general behaviour of the friction curves. Regime I is characterised by an ephemeral peak with a relatively high amplitude and is attributed essentially to the mechanical interlocking between sharp tips of diamond asperities, occurring during the relative motion of contacting surfaces. The measured values for the initial friction coefficient (μ_{max}) as a function of the applied load are represented in the plot of Fig. 4.14(b). It can be observed that $\mu_{\max}$ shows a growing tendency with increasing load, as a result of higher initial contact pressures. The highest measured value for μ_{max} during the sliding of self-mated diamond coatings in ambient air was 0.67. However, the naturally occurring surface roughness of as-deposited diamond films can also affect μ_{max} [26, 33]. Likewise, this helps to explain the dispersion found for the experimental data of μ_{max} under similar applied loads.

As sliding continued and repeated traversals on the same wear track occurred, the friction coefficient was appreciably affected by the progressive blunting of diamond surface asperities. Following the initial friction peak, a "running in" regime (II), associated to the accommodation of opposing counterfaces, sets in. As it can be seen from Fig. 4.14(a), this "running in" stage lasts for a short distance ($\lesssim 2$ m) and depends on the applied load. Afterwards, and for the remaining duration of the tests, the friction coefficient levels off and tends to stabilise (regime III). This regime is characterised by very low steady state friction coefficient ($\mu_{eq} \sim 0.03 - 0.04$) values, for unlubricated sliding in ambient air. Furthermore, μ_{eq} has proven to be independent of the initial roughness of the CVD diamond coatings. The endurance tests ($x = 690$ m) showed no modification in this friction behaviour, i.e. the initial surface roughness has influence in the initial μ_{max}, but not in the long term μ_{eq}. Such behaviour agrees with results found in the literature [26, 33, 47].

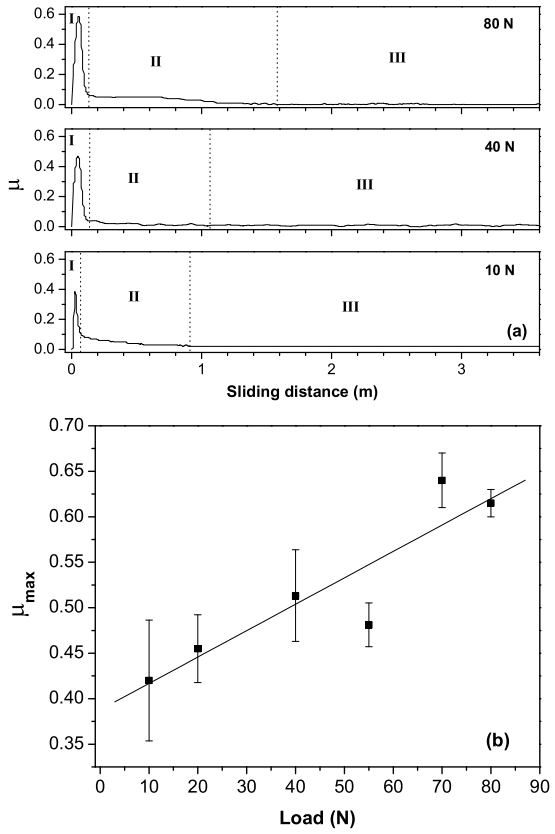

Figure 4.14: Friction coefficient of self-mated CVD diamond films in ambient air: (a) evolution under different applied loads with indication of the distinct friction regimes; (b) initial friction coefficient (μ_{max}) as a function of the applied load.

Directly related to the friction behaviour, the critical load for the tested CVD diamond films on Si_3N_4 substrates has been established as 80 N ($P_{max} \sim 10$ GPa). In other words, experimental results showed that diamond coating tribological failure by film delamination only occurred when the initial μ_{max} surpasses the threshold value of ~ 0.65 (attained with an applied load of 80 N), which corresponds to a maximum bearable tangential frictional force of ~ 52 N for these $12 - 14$ μm thick coatings.

The generally accepted mechanism of wear for diamond is that of small fragments chipping off the surface [33], which is characteristic of a self-polishing abrasive type of wear, as stated before. During the tests the ball produced a narrow wear track on the flat specimen, with both contacting surfaces showing a dark coloration at the end. This suggests the formation of flaky carbonaceous material in the contact region, since later ultrasonic cleaning with alcohol could dislodge it from the coatings. Direct OM observation of the wear tracks (flats) and scars (balls) revealed smooth polished surfaces, with both counterfaces still diamond coated (Fig. 4.11(b)).

The wear volume of the ball specimens, as a function of the applied load, is depicted in Fig. 4.15(a). As can be seen, W_v^{ball} increases linearly with load and reveals an approximate eight-fold variation when load changes from 10 N to 80 N. The ball wear coefficient values were characterised by a mild wear regime, i.e. values for k_{ball} - calculated with Eq. 4.2 and a sliding distance of 86 m - were of the order of magnitude of 10^{-7} $mm^3N^{-1}m^{-1}$. It is noteworthy that the endurance tests produced very mild wear (10^{-8} $mm^3N^{-1}m^{-1}$). A plausible explanation for this result is that, for low sliding distances (few tens of meters), the wear coefficients assessed using the wear scar diameter are out-weighted by the imposed initial damage to the surfaces, i.e. the truncating of diamond micro-pyramids as a result of the sliding process. Therefore, the contribution of this initial wear damage will become diluted for greater sliding distances, which correspond to the steady-state regime of self-polishing abrasion wear mechanism.

It is worth noting that it was not possible to assess the wear volume of the flat specimens (W_v^{flat}) by the usual techniques (weight loss method and conventional profilometry) since only smooth wear tracks were obtained. Nonetheless, using the results from AFM and OM observations, a model was developed to give an adequate estimation for W_v^{flat}. Thus, considering that the produced wear track has a rectangular-shaped cross section, its wear volume can be expressed as follows:

$$W_v^{flat} = \frac{1}{3} \cdot A_f \cdot a \cdot b \cdot \Delta_h \tag{4.4}$$

where, a, b, and, Δ_h, represents the length, width and depth of the wear track, respectively, and, A_f, the fraction of polished area on the wear track. The correction factor $\frac{1}{3}$ results from con-

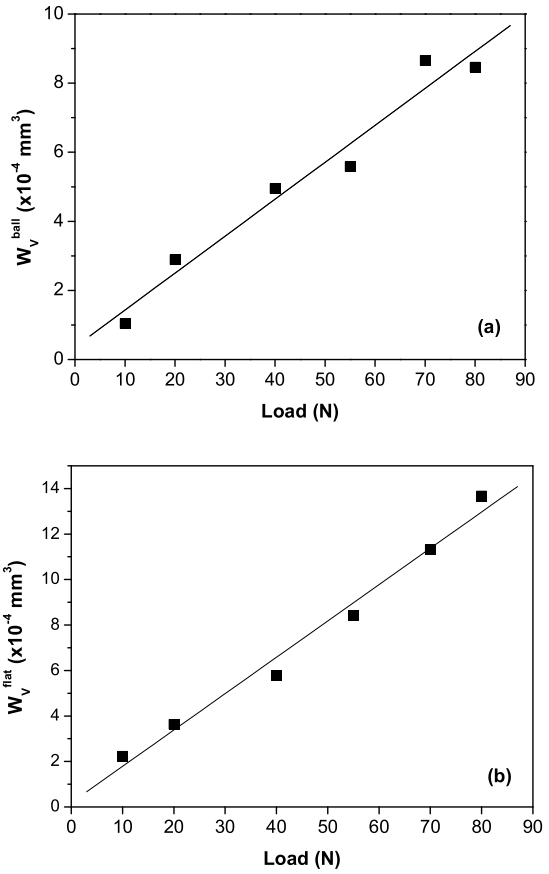

Figure 4.15: Wear volume of CVD diamond films as a function of the applied load (sliding distance of 86 m): (a) wear volume of ball specimens; (b) estimated wear volume of flat specimens.

sidering the volume of pyramidal diamond grains, with preferential $\langle 100 \rangle$ orientation, instead of prismatic grains. The wear track depth (Δ_h) can then be calculated from AFM results of the maximum peak-to-valley height (section 4.3.3), using the expression: $\Delta_h = R_{max} - R'_{max}$, where, R_{max}, and, R'_{max}, are the maximum peak-to-valley height of the as-deposited and worn coating, respectively.

However, an assumption must be implemented on the model in order to cope with the fact that AFM results show the occurrence of diamond pull-outs for the higher applied

loads, thus giving misleading R_{max} values. Therefore, it was established that for applied loads $P > 40$ N, R'_{max} will be extrapolated from the linear fit curve of the maximum peak-to-valley height AFM data (Fig. 4.12(c), track centre) – considering for the fit only the heights measured in the load range 10 N to 40 N – since for higher loads an inversion in the curve trend occurs.

Fig. 4.15(b) shows the track wear volume of flat samples, as a function of the applied load, calculated from Eq. 4.4. The plot reveals a linear increase of W_v^{flat} in relation to the applied load, with an approximate six-fold variation when load changes from 10 N to 80 N. This result is in accordance with the variation ($8\times$) observed for the ball specimens W_v^{ball}. Furthermore, the flat parts exhibit a larger absolute wear volume than their ball counterparts at all loads, Fig. 4.15(a) and 4.15(b), which is expected due to fatigue effects resulting from the intermittent contact.

A contributing factor for the variation of W_v^{flat} with the applied load comes from an increase in the polished area, A_f, since the track length is fixed and its lateral width suffered minimal changes especially for the higher loads. The fraction of polished area in the wear track was calculated based on image segmentation procedure of taken OM photomicrographs. As can be seen in Fig. 4.16(a), typical values of A_f fall in the range 0.50 (10 N) to 0.87 (80 N), for a sliding distance of 86 m. In addition, a plateau at ~ 0.65 exists in the range of applied loads $20-55$ N, which indicates a stall in the intensification of wear damage by progressive self-polishing. Only bigger contact pressures, i.e. higher applied loads, can further increase A_f.

Estimated values for the dimensional wear coefficient of flat specimens (k_{flat}) – calculated using Eq. 4.2 and the proposed model for W_v^{flat} (Eq. 4.4) – are depicted in Fig. 4.16(b). The presented values are relative to a sliding distance of 86 m and show a mild wear regime for this triboelement, i.e. magnitudes of the order of 10^{-7} mm^{3}N^{-1}m^{-1}. The curve trend reveals a minimum at 40 N for k_{flat}, which was linked to the aforementioned plateau in the fraction of polished area of the wear tracks (Fig. 4.16(a)). As a final remark, it is worth to note that the estimated values for k_{flat} are in good agreement with what would be expected from the results of the wear performance of the ball specimens.

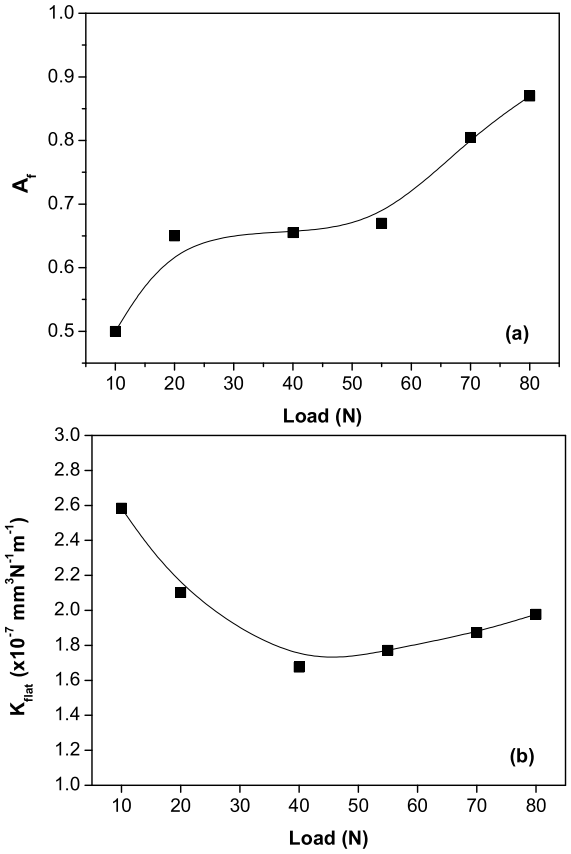

Figure 4.16: Tribological performance of CVD diamond coated Si_3N_4 ceramics flat specimens as a function of the applied load (sliding distance of 86 m): (a) fraction of polished area in the wear track; (b) estimated wear coefficient.

Tribological tests involving self-mated CVD diamond coatings in ambient atmosphere report mostly low values for the friction coefficient and wear coefficients of magnitude 10^{-7} to 10^{-6} $mm^3N^{-1}m^{-1}$ [25, 33, 124, 130]. However, those were performed under relatively low applied loads or Hertzian contact pressures and, in some cases, involved the use of polished coatings or interlayers to ensure adequate adhesion to the substrate. Therefore, considering the distinct material substrates, deposition techniques, surface morphology and test conditions found in the literature, the CVD diamond coated Si_3N_4 specimens tested in the present study showed a comparable friction and wear behaviour under more severe conditions, i.e. in terms

of applied load. Complementary, the observed adequate adhesion to the substrate is essential for the good tribological performance of CVD diamond coated Si_3N_4 substrates.

4.3.4 Conclusions

High quality unstressed, continuous and well-adhered diamond films were deposited on Si_3N_4 ceramic substrates using MPCVD technique. The friction behaviour of diamond-on-diamond sliding tests, in ambient atmosphere, was characterised by a short-life initial friction peak followed by a "running in" regime resulting from the accommodation between counter-bodies. Subsequently, the coefficient of friction leveled-off and reached low steady-state values $(0.03 - 0.04)$, regardless of the applied load.

Morphological and topographical analysis revealed a self-polishing abrasive wear mechanism accomplished by truncation and subsequent blunting of diamond asperities, leading to very smooth surface finishing. The wear coefficient for the ball specimens was of the order of 10^{-7} $mm^3N^{-1}m^{-1}$, characteristic of a mild wear regime. In addition, lower values by one order of magnitude were assessed for the longer endurance tests, denoting a very mild wear regime.

Micro-Raman spectra analysis of the diamond line peak shift showed an augmentation in the compressive stress state of worn coatings with increasing applied loads (maximum of ~ 0.9 GPa at 80 N). This tribologically activated stress state modification was not accompanied with surface phase transformations to non-diamond forms of carbon.

Surface-topographical information obtained from AFM observations revealed the occurrence of diamond pull-outs for applied loads higher than 40 N. The $12 - 13$ μm thick diamond coatings were unable to sustain stable operation under tribological stress when the applied normal load exceeded 80 N, due to gross film detachment by delamination.

A new method for estimating the wear coefficient of diamond coated flat specimens has been presented. Small wear damage, hardly measurable with conventional techniques, can then be quantified using AFM and OM observations of the wear track region. Application of the proposed model gave estimated wear coefficients for the flat specimens of the order of

10^{-7} $mm^3N^{-1}m^{-1}$, i.e. characteristic of a mild wear regime, which is in very good agreement with the measured wear for the counterbody specimen.

The present results suggest that CVD diamond coated Si_3N_4 ceramics constitute a viable solution where diamond-on-diamond tribological applications are required.

Acknowledgements

This work was supported by the project NANODIAM (FCT POCTI/CTM/59449/2004). C.S. Abreu also acknowledges PRODEP III funds supporting his PhD work, and M. Belmonte the financial support from the "Ramón y Cajal" program (MEC, Spain).

4.4 In-situ friction monitoring of self-mated CVD diamond coatings using acoustic emission [Publication III]

C.S. Abreu, F.J. Oliveira, J.R. Gomes, M. Belmonte, A.J.S. Fernandes, R.F. Silva
Mater. Sci. Forum, 514-516 (2006) 749-753

Abstract

In-situ measurements of acoustic emission (AE) in self-mated tribological pairs of CVD diamond coated silicon nitride (Si_3N_4) were made with the purpose of investigating the relationship between AE signal and friction events. A good correlation is found between the energy dissipation/emission processes, therefore enabling the possibility of monitoring the different friction regimes occurring during the sliding contact of microcrystalline diamond (MCD) coatings. Deposition of MCD on flat and ball-shaped Si_3N_4 samples was accomplished using microwave plasma assisted chemical vapour deposition (MPCVD) with H_2/CH_4 gas mixtures. The friction behaviour of self-mated MCD coatings was assessed using a reciprocating ball-on-flat geometry. The tests were run in ambient atmosphere without lubrication, the frequency (1 Hz) and stroke (6 mm) were kept constant while the applied normal load varied in the range $10 - 80$ N. The microstructure, surface topography and roughness of the MCD coatings were characterised by SEM and AFM techniques. The diamond quality was assessed from micro-Raman spectroscopy. The friction evolution was characterised by a short running-in period where the main feature is a sharp peak reaching values as high as approximately 0.6 followed by a steady-state regime with very low values in the range $0.03 - 0.04$.

Keywords: CVD diamond, Silicon nitride, Friction behaviour, Acoustic emission

4.4.1 Introduction

Acoustic emission (AE) is a phenomenon originating from a rapid relaxation of strain energy produced by deformation, part of which radiates as a short time stress wave that can be detected by an appropriate transducer, coupled to the source surface [110]. Research has been undertaken into the use of AE technology in monitoring the material response to tribological

strain, principally on how significant the emission from sliding pairs is and how it relates to parameters governing the behaviour of tribosystems [100]. A relationship was found between the acoustic phenomenon and the dissipation of mechanical energy that can be used to classify different friction contacts [104].

Homologous contacts of chemical vapour deposition (CVD) diamond coated films are characterised by a wide range of friction coefficient values, depending on the sliding conditions. Even in ambient atmosphere, which gives very low equilibrium friction values, a variation of more than one order of magnitude could be found between the steady-state value and the starting friction coefficient. This wide range makes difficult analysing the friction behaviour in terms of prevailing friction events or mechanisms, due to physical limitations in the measuring range of load cells. Thus, in-situ friction monitoring by AE could allow an easier detection of the distinct friction regimes or sliding events. The aim of this investigation was to study the use of AE for condition monitoring the sliding contact of self-mated microcrystalline diamond (MCD) coatings, submitted to high applied loads, in a dry sliding reciprocating arrangement.

4.4.2 Experimental setup and test procedure

Dense silicon nitride (Si_3N_4) substrates were prepared from powder mixtures of α-Si_3N_4 (Starck grade M11), Y_2O_3 (Starck grade C) and Al_2O_3 (ALCOA CT-3000SG) with, respectively, the following proportions (wt.%): 89.3/7.0/3.7. Following a procedure of homogenisation and sieving, the mixed powders were consolidated by uniaxial pressing (30 MPa), followed by isostatic pressing (200 MPa). Pressureless sintering in a conventional graphite furnace (1750 °C, 2 h), was used to produce fully dense ($>$ 99% of the theoretical density) disc-shaped Si_3N_4 substrates. All the sintered samples were ground in order to achieve the final dimensions of 10 mm of diameter and thickness of 3 mm. Commercial balls (Kema Nord) of Si_3N_4 with 5 mm diameter were also used as substrate material for the counter-bodies. In order to achieve adequate adhesion level and to enhance nucleation density, the flat specimens were submitted to surface pre-treatments with diamond paste polishing (15 μm), followed by manual scratching with $0.5 - 1$ μm sized diamond powder on a silk cloth. A more thorough description of the processing of Si_3N_4 substrates can be found elsewhere [73].

The deposition of MCD films was carried out in a microwave plasma chemical vapour de-

position (MPCVD) system (ASTeX PDS 18, Seki Technotron Corp.). The deposition parameters used for all tested samples were as follows: microwave power = 3 kW; chamber pressure = 1.2×10^4 Pa; H_2/CH_4 gas flow = 400/25 sccm; deposition time = 2.5 h.

The tribological response of the MCD coated Si_3N_4 films was assessed by a ball-on-flat tribometer (PLINT TE67/R). Self-mated sliding tests were conducted using a reciprocal dry sliding arrangement in ambient atmosphere ($\sim 50-60\%$ RH). The diamond coated flat specimens were fixed to an oscillating table and made to contact with diamond coated balls (upper specimen), firmly attached to a sample holder arm. All the tests were performed with a constant stroke (6 mm) and frequency (1 Hz), while static applied normal loads in the range 10 N to 80 N were applied directly over the ball specimens. Considering a Hertzian elastic contact model, these loads produced initial pressures of $5-10$ GPa [117].
The friction force was measured by means of a load cell, its signal amplified and acquired by a PC. Before each test, the load cell was calibrated by applying external dead-weights in the range of the measured loads. The sliding distance varied between 2×10^{-2} m and 86 m in order to have a systematic account of the friction phenomenon, focused at different phases of the sliding interaction.

The AE signal was recorded during the sliding tests by a piezoelectric transducer (Brüel & Kjaer) tightly fixed to the disc sample holder, in a position perpendicular to the sliding direction. An amplification/filtering (Brüel & Kjaer) stage, with a frequency window of 50 kHz-2 MHz, was used to convert the acoustic pressure intensity into a $0-10$ V DC signal, at adequate acquisition rates by means of an A/D conversion board (Keithley PCMCIA 12 AIH). The diamond quality of the deposited films was studied by ex-situ micro-Raman spectroscopy using a 514.5 nm Ar^+ incident laser beam, with a spot size of ~ 1 μm and few tens of mW power at the surface. Atomic force microscopy (AFM, Digital Instruments NanoScope IIIa) was used to study the surface topography and roughness of as-deposited and worn MCD coatings. Surface roughness values were assessed using inherent NanoScope III software, by acquiring three AFM fields with a scan size of 50×50 μm^2. The surface microstructure, diamond grain size and film thickness were analysed by a Hitachi (model S-4100) scanning electron microscope (SEM).

4.4.3 Results and Discussion

The most conventional morphology of CVD-grown diamond thin films corresponds to pyramidal micro-crystallites with well defined triangular (111) facets and a preferential ⟨100⟩ crystal growth orientation [52]. The SEM photomicrograph in Fig. 4.17 (a), taken from a diamond coated Si_3N_4 flat specimen, is a clear example of that morphology.

All the CVD diamond coated samples exhibited a fully adhered and continuous aspect. The average diamond grain size and film thickness of the MCD coatings, obtained from stereological and cross-sectional image analysis of higher magnifications SEM photomicrographs, showed values of 2.4 ± 1.1 μm and $\sim 12 - 14$ μm, respectively.

A representative AFM micrograph of an as-deposited MCD flat sample is presented in Fig. 4.17 (b). As it can be seen, the films present a hilly topography combined with the presence of some deep valleys. These rugged surfaces were characterised by surface roughness parameters of $R_a \sim 170$ nm, $R_z \sim 1450$ nm and maximum peak-to-valley height of ~ 1480 nm.

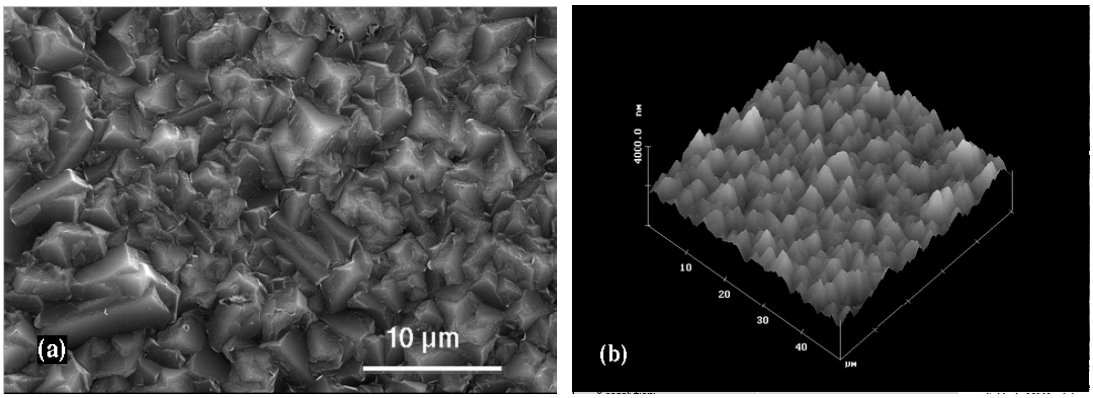

Figure 4.17: As-deposited diamond coated Si_3N_4 films: (a) SEM micrograph of representative C{111}-micro-pyramidal film on flat samples; (b) AFM image of typical flat specimens.

Fig. 4.18 (a) shows a micro-Raman spectrum of the diamond films deposited onto flat specimens. The presence of a sharp peak centred around the line of natural diamond (1332 cm^{-1}) and no evidence of broad graphitic bands (sp^2 C-C bonding), confirms the high quality and purity of the deposited films, while showing a stress-free state.

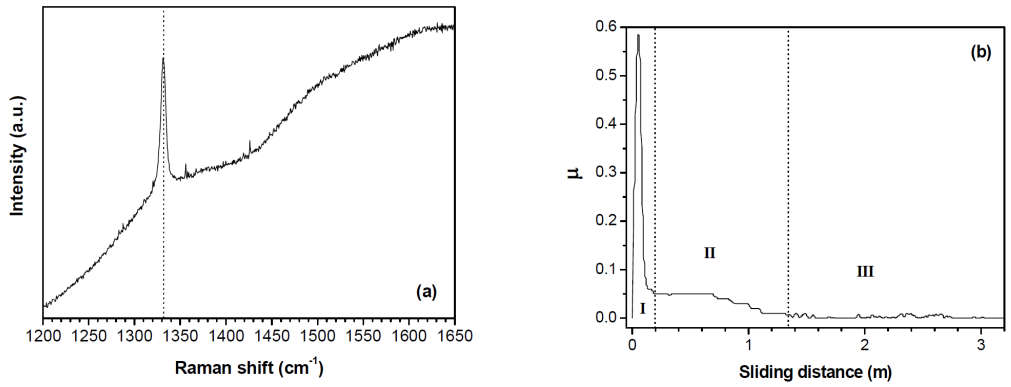

Figure 4.18: Characterisation of MCD coated Si_3N_4 films. (a) micro-Raman spectrum of as-deposited coatings, revealing a sharp peak centred at the diamond frequency line (1332 cm^{-1}); (b) representative friction curve evolution showing the different friction regimes (applied load of 80 N).

A typical friction coefficient evolution curve for self-mated MCD films is depicted in Fig. 4.18 (b). The plot reports to an applied load of 80 N and shows, as its main feature, a pronounced initial peak with a friction coefficient of ~ 0.60, followed by a gradual decay to very low friction coefficient values. These different behaviours for the friction coefficient are identified in the plot according to three distinct regimes (labeled I, II, III). Regime I results from the initial intense mechanical interaction between diamond asperities of contacting surfaces. Furthermore, it was observed that the magnitude of this sharp peak, for films with the same starting surface roughness, depends on the applied load, which corroborates a friction mechanism based on the interlocking of asperities. Such dependency is also found in the literature [33]. As sliding progressed the friction coefficient was significantly affected by the truncating and gradual blunting of diamond tip asperities. As such, regime II is related to a running-in effect associated to the accommodation of mating surfaces. The experimental results also showed that the length of this transition regime depended on the applied load. Afterwards, and for the remaining length of the sliding tests, the friction coefficient levels-off and enters into a steady-state phase (regime III), characterised by very low values ($\sim 0.03 - 0.04$), this time as a result of the interaction between flattened diamond asperities and the minor contribution of adhesion for the overall friction mechanism in ambient atmosphere [32]. Regime III is also characterized by

very low surface roughness values. AFM measurement yielded $R_a \sim 27$ nm after tribological tests run under an applied load of 40 N for 86 m.

The relation between the sliding distance run immediately after completion of regime I, taken from the friction curves, and the duration of the AE signal burst corresponding to the friction peak is represented in the graph of Fig. 4.19 (a), as a function of the applied load. The AE signal burst was considered extinct when its amplitude had fallen below the background noise threshold level. As can be seen, a good correlation exists between the two curves stating that a process of energy dissipation driven by friction mechanisms of asperity interlocking/truncating is intimately related to a process of acoustic emission. This was accompanied by the production of an intense strident sound that lasted for a few initial reciprocating cycles (< 20). In addition, the plotted curves reveal an almost linear variation of the sliding distance run after ending of regime I, with increasing applied load, until 55 N. Afterwards, and up to the critical load for film delamination (> 80 N), both curves suffer little changes.

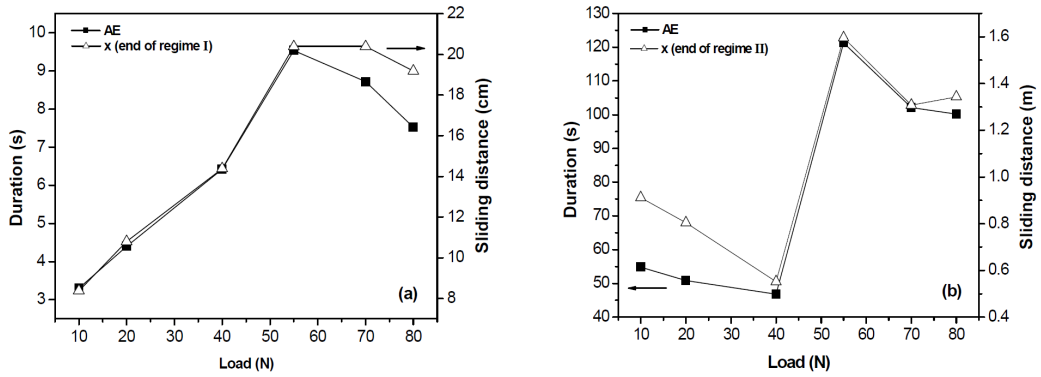

Figure 4.19: Correlation between the sliding distance run at the end of (a) regime I and (b) regime II and the duration of AE signal burst, for various applied loads.

Similarly, the relation between the sliding distance run at the end of regime II and the duration of the corresponding AE signal burst is depicted in Fig. 4.19 (b), for different applied loads. The correlation between the two curves is significant, which opens the possibility to clearly identify the distinct sliding regimes of MCD films by means of AE signal monitoring. Another feature shown in Fig. 4.19 (b), is that steady-state sliding condition is achieved sooner

for an intermediate applied load of 40 N, i.e. the accommodation between opposing surfaces ends after a shorter sliding distance. A possible explanation for this could be related to a competing effect between the contact pressure level and the subsequent rate of surface smoothening by the blunting of asperities – translated in a shorter or longer running-in regime – and some surface degradation by diamond pull-outs observed for the higher loads, which delays further the accommodation of mating surfaces.

4.4.4 Conclusions

The friction behaviour of MCD coated Si_3N_4 films revealed a characteristic running-in regime denoting an intense initial friction peak, followed by a short transition period, which in turns leads to very low equilibrium friction coefficients ($\sim 0.03 - 0.04$).

A correlation exists between the AE signal and the frictional behaviour of sliding contacts. The friction peak at beginning and its evolution is closely followed by the AE signal. A steady-state response is achieved sooner for an intermediate load (40 N). This relates to a competing effect between the rate of the blunting of asperities and surface degradation by diamond pull-outs. This confirms the possibility of monitoring the distinct friction regimes by AE techniques.

Acknowledgements

C.S. Abreu acknowledges PRODEP III funds supporting his PhD work. M. Belmonte acknowledges the financial support of the “Ramón y Cajal” program (MEC, Spain). The financial support of project POCTI/CTM/45423/2002 is gratefully acknowledged.

(B) WATER LUBRICATED TESTS

4.5 CVD diamond water lubricated tribosystems for high load planar sliding [Publication IV]

C.S. Abreu, E. Salgueiredo, F.J. Oliveira, A.J.S. Fernandes, R.F. Silva, J.R. Gomes
Wear, 265 (2008) 1023-1028

Abstract

Water lubricated tribological systems involving chemical vapour deposited (CVD) diamond coatings are appealing to many practical situations, namely in metalworking and fluid handling applications. The motivation behind the present study lies in insufficient knowledge on the behaviour of these water-based lubricated tribosystems especially under high loads. The microwave plasma chemical vapour deposition technique was used to coat dense Si_3N_4 substrates from CH_4-H_2 gas mixtures, setting adequate deposition parameters during 2.5 h, resulting in a film thickness around 15 μm. Self-mated planar reciprocating sliding ball-on-flat wear tests were performed up to 16 h (690 m of sliding distance) with normal applied load ranging from 70 N to 160 N. SEM and AFM characterisation techniques were used to identify the prevailing wear mechanisms. The worn surfaces exhibit a polished appearance resulting from diamond asperities abrasion on the counterface combined with the action of nanometric debris. Some longitudinal wear grooves along the sliding direction are the result of two-body abrasive action of larger debris spawn from the truncation of aggregates of crystals in the first steps of sliding. A steady-state sliding regime sets for almost the test full duration, with a very low friction coefficient in the range $0.04 - 0.05$ and a wear coefficient of about 10^{-8} $mm^3N^{-1}m^{-1}$. Partial film wear-out was found at a threshold load of 160 N, however without seriously affecting the tribosystem performance.

Keywords: Sliding wear, Diamond, CVD coatings, Water lubrication

4.5.1 Introduction

The study of water lubricated CVD diamond tribological systems is important in order to anticipate the frictional and wear response of such highly protective coatings in many practical situations. The intentional use of water-based lubricants is found in metalworking technologies, like wire drawing [131] and cutting or grinding operations [132]. Special applications in fluid handling industry, as in mechanical face seals [37, 133], undergo wet functioning after the initial dry running-in regime. Still, information involving CVD diamond-on-diamond water lubricated tribosystems is scarce and, therefore, comprehensive studies on the subject are in the agenda.

In a paper by Grillo and Field [15], a natural diamond stylus was made to slide against a (100) textured hot filament CVD polycrystalline diamond film deposited on Si_3N_4 ceramic substrates. The experiments were performed in water solutions of different pH at low speeds ($0.05 - 0.2$ mms^{-1}) and small applied loads ($0.5 - 2$ N). For the neutral de-ionized water solution, sliding speed of 0.2 mms^{-1} and applied load of 1 N, they observed a reduction of the friction coefficient from its value in air, around 0.1, to 0.07. This slight decrease was attributed to the passivation of surfaces originating from the chemisorption of hydride and hydroxyl groups on the surface. In line with earlier studies of diamond friction in water or moist air, the reduction in friction has been attributed to the formation of thin hydrocarbon waxy surface layers [9, 134]. A similar trend has also been observed for CVD diamond coatings by Enomoto et al. [134], who suggested the possible occurrence of a tribochemical wear mode on diamond surfaces reacting with water or moisture.
In the studies indicated above, tests were performed under small applied loads and, generally, constitute more fundamental works concentrated on the friction properties of diamond coatings. As such, a better understanding on both the friction and wear performance of CVD diamond submitted to high applied loads is needed to assess their tribological properties under more intense sliding conditions, better approximating practical use.

The present authors have previously characterized the unlubricated tribological behaviour of homologous pairs of CVD diamond coated Si_3N_4 [135]. The steady-state coefficient

of friction displayed values in the range $0.03 - 0.04$, regardless of the applied load ($10 - 80$ N). The wear coefficient values for both ball and plate specimens revealed a mild wear regime (10^{-8} $mm^3N^{-1}m^{-1}$). Above a threshold applied load of 80 N, it was observed gross film detachment induced by the tribological action. The present study now deals with the CVD diamond-on-diamond planar sliding water lubricated contact at moderate to high normal loads ($70 - 160$ N). The frictional behaviour is related to existing models of polycrystalline diamond friction and predominant wear mechanisms were identified. Results concerning the maximum sustainable load for CVD diamond coated Si_3N_4 ceramics submitted to tribological stress are also presented.

4.5.2 Experimental Procedure

Dense silicon nitride (Si_3N_4) ceramics were used as the substrate material for the deposition of CVD diamond. Details regarding substrate processing can be found in a previous work by the authors [135]. Geometries used in the present work were as follows: circular discs with 10 mm diameter and 3 mm of thickness, and 5 mm diameter balls. Before diamond deposition, the flat samples were subjected to the following surface pre-treatment: 46 μm grit size diamond wheel grinding, 15 μm diamond polishing on a metallic plate, and manual scratching with $0.5 - 1$ μm sized diamond powder on a silk cloth. Subsequently, the Si_3N_4 discs were rinsed in an acetone ultrasonic bath for 10 min and then in an ethanol bath for 10 min. Concerning the Si_3N_4 balls, these were gradually polished with 15, 6 and 1 μm sized diamond powder suspension followed by microflawing by ultrasonic agitation with diamond suspension ($0.5 - 1$ μm) in *n*-hexane to promote diamond nucleation.

A microwave plasma reactor was used for the production of CVD diamond coatings on both the flat and ball specimens. The deposition parameters of the MPCVD process were as follows: microwave power = 3 kW; chamber total pressure = 1.2×10^4 Pa; H_2/CH_4 gas flow = 400/25 standard cubic centimetre per minute (sccm) and 400/16 sccm for the flat and ball specimens, respectively. The selected growth conditions were previously reported to lead to similar film thicknesses for both geometries, around $12 - 14$ μm, after 2.5 h of deposition [135].

Planar sliding wear tests were performed in a ball-on-flat reciprocating configuration. Prior to each tribotest, both plate and ball specimens were cleaned with alcohol for 10 min in an ultrasonically agitated bath. The diamond coated balls were mounted as the upper sample and the disc shaped flat specimens were fixed to the oscillating table. The contact region remained immersed in a pool type container filled with distilled water. The tests were performed at constant stroke (6 mm) and a frequency of 1 Hz, corresponding to an average linear velocity of 9 mms^{-1}, during 16 h (690 m of sliding distance). The normal applied load varied in the range $70-160$ N. The friction coefficient was determined from measurements of the tangential force exerted on a load cell attached to the upper sample holder. The wear coefficient (k) of the ball specimens was estimated from the diameter (d) of near-circular wear scars, the ball radius (r), the applied normal load (W) and sliding distance (x) following Archard's law of wear [119]:

$$k = \frac{\pi d^4}{64 r W x} \tag{4.5}$$

The surface topography of the as-deposited and worn films was characterized by atomic force microscopy (AFM), using tapping mode. The surface roughness parameter R_q (RMS), as determined from AFM $50 \times 50\ \mu m^2$ scans, was used to quantify surface degradation. The coatings morphology of pristine and damaged specimens was observed by scanning electron microscopy (SEM), which also allowed direct measurements of the radius of the ball wear scars and wear debris.

4.5.3 Results

Tribotesting of CVD diamond coated Si_3N_4 ceramics was performed using two ranges of applied normal load magnitudes hereafter labeled as moderate and high. The first group of experiments involved applied load values in the range $70-90$ N and were selected based on experimental data from former studies using self-mated CVD diamond systems under dry sliding conditions [135]. To also assess the maximum sustainable load of deposited CVD diamond coatings under planar sliding, i.e. prior to delamination by gross film detachment or film wear-out, the second group of tests involved harsher conditions using heavier loads in the range $110-160$ N.

Moderate loads (70-90 N)

In Fig. 4.20, SEM micrographs of as-deposited and worn CVD diamond coated Si_3N_4 films are depicted. Fig. 4.20 (a) and (b) show that the surface morphologies of both the as-deposited plate and ball specimens are characterized by the presence of well faceted crystallites with preferential ⟨100⟩ crystallographic growth orientation. Aside the presence of prevailing octahedral diamond crystallites, ball specimens (Fig. 4.20 (a)) also exhibit some tilted grains whereas plate specimens do not (Fig. 4.20 (b)), however, both geometries show the occurrence of grain twining. Insets in each micrography reveal also larger crystallites in the case of films deposited on the balls. Therefore, plate specimens possess a more homogeneous surface morphology as well as smaller diamond grains.

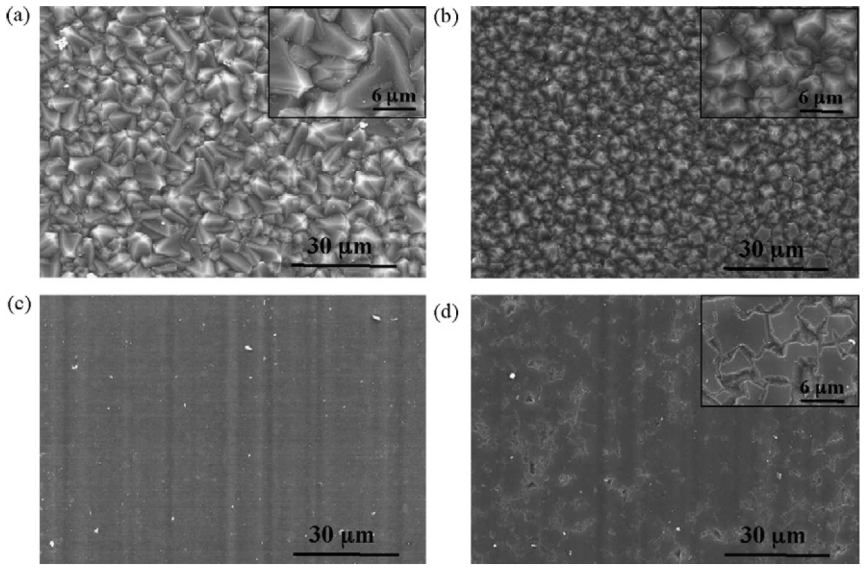

Figure 4.20: SEM micrographs of as-deposited CVD diamond coatings: (a) on the ball; (b) on the plate.Worn surfaces after self-mated testing under 70 N: (c) ball; (d) plate. High magnifications are shown on the insets.

Fig. 4.20 (c) and (d) show the general aspect of worn CVD diamond coatings submitted to a moderate load of 70 N. These figures illustrate that the octahedral protruding asperities were worn down and surfaces exhibit a polished appearance. From the inset of Fig. 4.20 (d), it

can also be observed that the polishing was performed to a lesser degree on the plate specimen, where voids corresponding to the valleys existing between pyramidal shaped asperities are still visible. These micro-pyramids were leveled off into plateaus of (100) diamond planes. Superimposed to the polished topography of worn CVD diamond films, parallel wear grooves along the sliding direction are observed on both specimens which, however, present a higher spatial density in the ball.

Representative AFM 3D scans of as-deposited and worn CVD diamond films are depicted in Fig. 4.21. The aspect of the pristine plate specimens is characterized by a hilly topography, where high sharp peaks corresponding to the octahedral asperities are surrounded by deep valleys (Fig. 4.21 (a)). AFM measured values for the R_q of as-deposited plate specimens varied in the range $330-418$ nm. The surface topography of a worn plate resulting from a sliding test under a load of 70 N is shown in Fig. 4.21 (b). The presence of longitudinal wear grooves, reported above in the SEM images of worn films, can be observed here with increased detail. However, evidence of the deepest valleys are still visible for this moderate load. The surface roughness suffered an approximately five-fold reduction, $R_q \sim 74$ nm, resulting from the substantially lower heights of the wear grooves as compared to the octahedral peaks. An AFM 3D scan and a 2D profile cut-out performed at the edge of the wear track are shown in Fig. 4.21 (c) and (d), respectively. The variation of the vertical characteristics of the surface topography can be observed with greater detail on the 2D profile of Fig. 4.21 (d), spanning 50 μm from the wear track border.

Typical friction coefficient evolution curves of water lubricated self-mated coatings are represented in Fig. 4.22. The friction behaviour under a moderate load of 70 N (Fig. 4.22 (a)) is characterized by an initial sharp peak attaining a value of about 0.38 (regime I), followed by a rapid transition (regime II) to a steady-state regime (regime III) in which the friction response is very low ($0.04-0.05$). As observed from the inset, the change from moderately high friction values (regime I) to a very low energy dissipation condition (regime III) occurs within only a few meters of sliding distance. Moreover, the naturally occurring friction noise remained relatively low throughout the entire steady-state regime, without evidencing pronounced spikes.

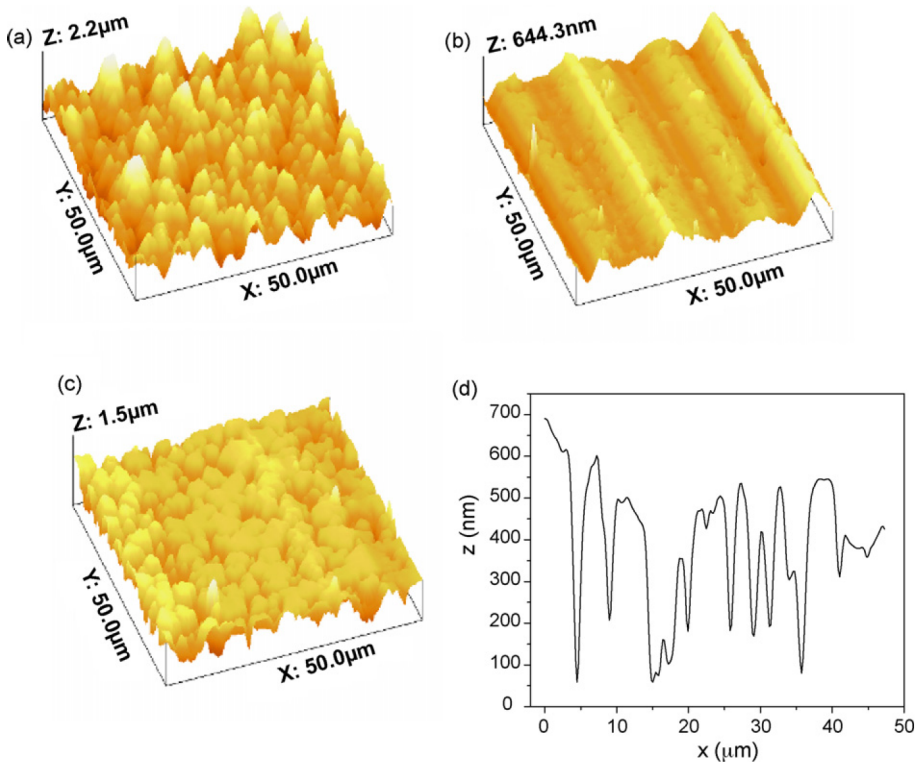

Figure 4.21: Tapping mode AFM scans of CVD diamond coatings on plate specimens. (a) As-deposited. (b)Worn surface inside the wear track after self-mated testing under 70 N. 3D image (c) and 2D profile cut (d) of the transition topography at the wear track border after self-mated testing under 70 N.

Fig. 4.22 (b) corresponds to the friction behaviour under high loads and it will be addressed in the next sub-section.

High loads (110-160 N)

SEM micrographs of worn CVD films under high loads are depicted in Fig. 4.23. A wear damaged ball and the mating plate specimen, submitted to a normal load of 110 N and sliding of 690 m, are shown in Fig. 4.23 (a) and (b), respectively. As can be readily observed, the resulting surfaces are much smoother than as-deposited ones and also present wear grooves parallel to the sliding direction. Moreover, as verified in the moderate loads tribotests, the ball specimens tend to show a higher number of grooves with respect to the CVD diamond coated

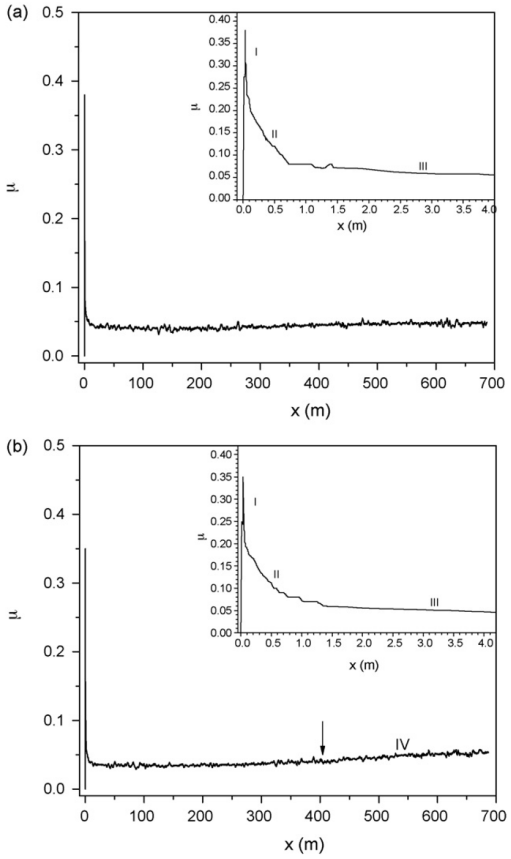

Figure 4.22: Friction curve evolution as a function of sliding distance under an applied load of 70 N (a) and 160 N (b). Details of the first 4 m of the tests are shown in the insets. Labels correspond to: I – initial friction peak; II – running-in period; III – steady-state regime; IV – partial contact with the substrate.

plates. For the highest load (160 N), the SEM micrography of the ball specimen (Fig. 4.23 (c)) shows a near-circular wear scar with a lighter area at the centre. This corresponds to the Si_3N_4 ceramic material being exposed and, therefore, it reveals partial wear-out of the coating. However, the regular contour of this lighter region indicates progressive wear damage instead of premature failure by gross film detachment, characterized by highly irregular borders as referred to in unlubricated tests [135]. The resulting counterbody plate surface is depicted in Fig. 4.23 (d) without disclosure of the planar substrate. A magnified image in the inset shows with higher detail, the resulting morphology of the worn surfaces closer to the wear track border

where CVD diamond micro-pyramids were truncated and progressively leveled to form extensive plateaus.

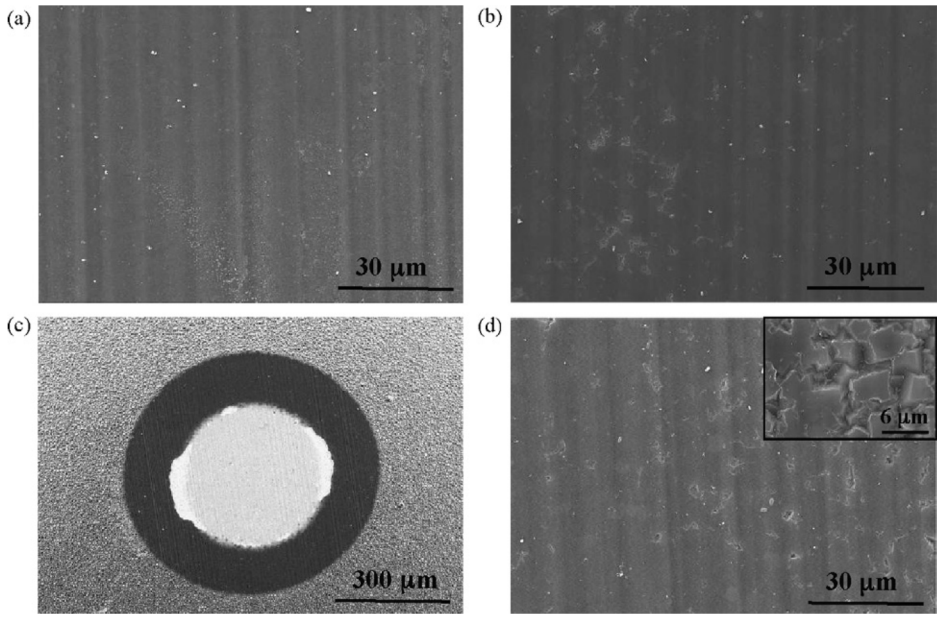

Figure 4.23: SEM micrographs of CVD diamond worn surfaces after self-mated testing under 110 N: (a) ball; (b) plate. Worn surfaces after self-mated testing under 160 N: (c) ball; (d) plate (inset: high magnification).

3D AFM images of a worn plate resulting from a tribotest with an applied load of 160 N are represented in Fig. 4.24 (a) and (b), inside the wear track region and border, respectively. As expected from such high stress conditions, the wear track topography reveals no traces of the original CVD diamond features and exhibits closely spaced wear grooves, indicative of abrasion wear processes.

The typical morphology of the wear debris collected from the lubricant is shown in Fig. 4.25. The low magnification on Fig. 4.25 (a) reveals the presence of large blunted particles with different shapes. Elongated particles prevail and a few show a peculiar doughnut-like shape. At the higher magnification of Fig. 4.25 (b), agglomerates of submicrometric debris particles are also discernible. These spread in between the large particles as well as are covering

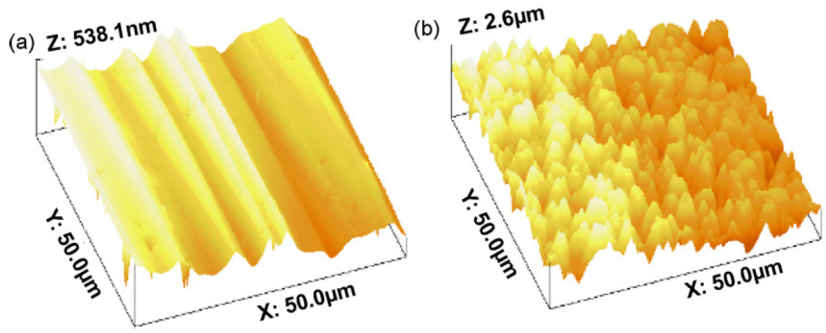

Figure 4.24: Tapping mode AFM scans of CVD diamond coatings on plate specimens. (a) Worn surface at the centre of the wear track after self-mated testing under 160 N. (b) 3D image of the transition topography at the wear track border after self-mated testing under 160 N.

them as a result of the SEM sample preparation. Fig. 4.22 (b) depicts the friction curve under an applied load of 160 N. The friction evolution as a function of sliding distance is similar to the one previously described for moderate loads (Fig. 4.22 (a)) from a new regime (IV) appearing after 400 m of sliding distance translated by a slight increase in slope.

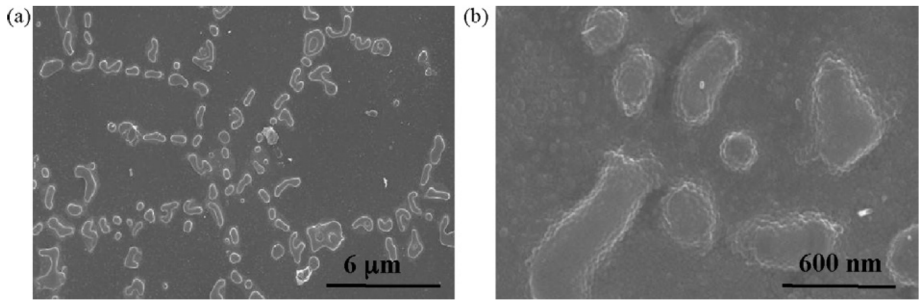

Figure 4.25: SEM images of the morphology of the wear debris. (a) Low magnification. (b) Detail of debris showing distinct sizes.

4.5.4 Discussion

The present water lubricated tests of homologous pairs of CVD coated materials revealed striking differences compared with the dry sliding behaviour of the same materials, pre-

viously reported [135]. First, to achieve destructive conditions leading to film removal, higher loads ($150-160$ N) were needed than those for film delamination (80 N) under unlubricated conditions. Secondly, results showed a different worn morphology, where the lubricated samples revealed a grooved surface (for example Fig. 4.21 (b)), in contrast to the more flattened surfaces tested in dry conditions, although the later denoted extensive occurrence of pull-outs of diamond crystal aggregates [135]. The enhanced load supporting capability of the tribosystem can be attributed to a different stress distribution promoted by the lubricant film, resulting in a substantial reduction of the Hertzian contact pressures, estimated to be around 4.5 GPa in dry conditions [135].

Water also constituted a diamond debris reservoir, as the lubricant is not renewed during the test. This way, a sort of abrasive suspension with a wide size distribution of diamond particles (Fig. 4.25) act on the contact region, promoting three-body abrasion and intense groove formation. On the contrary, in dry experiments, the largest debris particles are rapidly expelled from the contact region and the abrasive action takes place at a smaller length-scale leading to a more effective polishing [135].

A mechanical wear type governed the CVD diamond material loss in the presence of water. The revealed surface topography features in Fig. 4.21 (c) give clues on the different phases of wear damage, as well as point out some of the occurring wear mechanisms. A transition between near pristine sharp diamond crystallites, truncated peaks and progressively leveled-off and blunted asperities towards the centre of the wear track is observed. It is realistic to establish a correspondence between this spatial gradient and the sequence of events taking place during wear damage. This is corroborated by the images sequence in Fig. 4.26 that exemplifies the relationship between the as-deposited diamond film and generated debris morphologies entrapped in the aqueous media. The smallest fragments result from a single crystal vertex cut-off, while the larger ones outcome from truncation of aggregates of crystals. Both types of debris subsequently round-off and flattened under the sliding interaction of the mating surfaces, acting at the same time as abrasive particles, assisting on the self-polishing process, although allowing groove formation by the action of the larger particles.

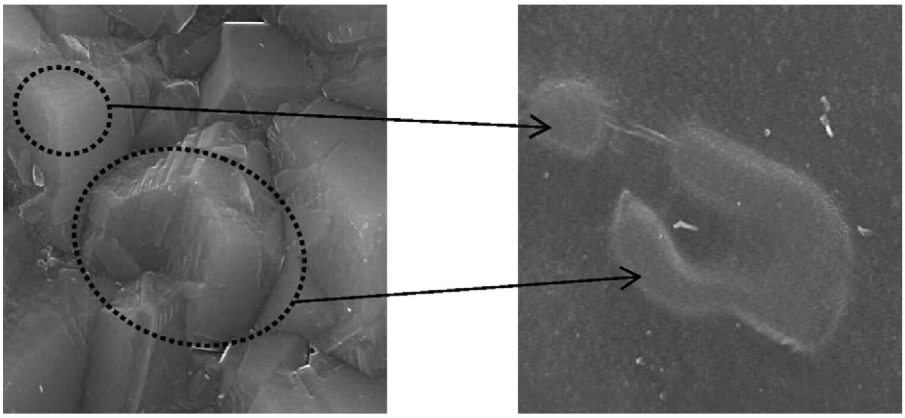

Figure 4.26: Schematics of the correspondence between protruding asperities of diamond crystals and wear debris particles, featuring two distinct morphologies corresponding to single and agglomerated crystals.

A possible explanation for the higher density of grooves observed on the balls (see for example Fig. 4.20 (c) and (d)) could result from the influence of the gravitational force on the wear debris, forcing them to stay attached statistically for longer periods of time to the lower flat specimen, and, therefore, abrading more aggressively the upper specimen (ball). In other words, the debris predominantly performs as a two-body abrasive agent on the ball, while they act as a three-body on the disc.

In contrast to most other engineering surfaces, the friction coefficient depends on the surface roughness of the diamond films [6, p. 92, 93] which explains the occurrence of three different regimes in the friction curves of the water lubricated self-mated CVD diamond tests (Fig. 4.22). In the beginning of the tribotest, the interlocking of rough diamond asperities produces a peak in the friction trace (regime I). This initial sharp peak corresponds to the maximum recorded values for the friction coefficient. After this initial phase, a range with rapidly decreasing friction coefficient values takes place (regime II). During successive sliding passes, the sharp asperity tips are blunted and the valleys between asperities are filled with wear debris particles. This corresponds to a running-in phase of accommodation between opposing surfaces and lasts up to about 2 m. Afterwards an equilibrium of very low frictional response sets in for the rest of the test when leveled diamond plateaus are in mating contact (regime III).

The described frictional response of the lubricated systems has no striking differences when compared to dry sliding conditions with the same coatings [135]. The main distinction is in the initial friction peak, with amplitudes as low as about 60% than those observed in the unlubricated case (maximum of ~ 0.60, for 80 N). The change in behaviour caused by the water lubricant is attributed to the reduction of two contributions: (i) adhesion component, by the passivation of the diamond surfaces by hydrogen and hydroxyl ions, which bind to the surface dangling bonds and lead to a reduction of the adhesion component of the friction [18]; (ii) mechanical component, due to the role of the lubricant in reducing the real area of contact and, therefore, the lowering of the incidence of contacts. Moreover, the absence of friction spikes and localized film detachments, and/or other catastrophic events below 160 N, constitutes an indication of progressive wear for the self-mated coatings. The small increase in slope in the friction coefficient starting at 400 m of sliding distance for the 160 N test (Fig. 4.22 (b)) is believed to be related to wear-through of the CVD diamond coating on the ball, exposing the ceramic. However, an outer circular diamond crown surrounding the exposed substrate (Fig. 4.22 (c)), is responsible for maintaining essentially a homologous diamond contact of relatively low friction, instead of a distinctive Si_3N_4/CVD diamond trace. Reports on water lubricated Si_3N_4/diamond systems were not found by the authors, however, these contacts under 60% of relative humidity showed a friction coefficient value around 0.1 [136].

The water lubricated diamond films exhibited an excellent wear resistance. Estimated wear coefficient values based on damage scars imprinted on the balls specimens revealed a very mild wear regime ($\sim 10^{-8}$ $mm^3N^{-1}m^{-1}$) for all tested loads. The assessed values showed a slight increase in wear damage from 2.3×10^{-8} $mm^3N^{-1}m^{-1}$ to 3.0×10^{-8} $mm^3N^{-1}m^{-1}$ when testing under moderate (70 N) and high loads (110 N), respectively.
Experimental data by Miyoshi et al. [34] show for the friction coefficient of water lubricated polished coarse-grain CVD diamond sliding against CVD diamond pins, values around 0.06 and an ultra-mild wear regime ($< 10^{-10}$ $mm^3N^{-1}m^{-1}$). The equilibrium friction values of the present study are slightly better, although exhibiting a lower wear resistance, since the wear coefficient values are two orders of magnitude higher. However, the much lower applied load (0.49 N) used in the work of Miyoshi et al. [34] accounts for the better wear performance, since it represents a less intense tribological interaction than the one here presented.

4.5.5 Conclusions

Ball-on-plate self-mated reciprocating tests of CVD diamond coated Si_3N_4 ceramics in the presence of water proved that these materials constitute an effective wear-resistant and low-friction alternative for demanding tribo-applications.

Under moderate loads, up to 90 N, the worn surfaces exhibit a polished appearance corresponding to a five-fold reduction of the RMS value in relation to the as-deposited films, after 16 h (690 m) of continuous sliding. The topography of the worn film also reveals some longitudinal wear grooves along the sliding direction. The sequence of the wear damage events is described as follows: truncation of protruding diamond asperities, blunting of exposed edges, grooving with large debris particles and self-polishing at microscale level by two-body and three-body abrasion. The steady-state sliding regime is reached after a few reciprocating traversals (~ 2 m) attaining a very low friction coefficient in the leeway $0.04 - 0.05$ and a wear coefficient as low as 2.3×10^{-8} $mm^3N^{-1}m^{-1}$.

For high-loading tribotests ($110 - 160$ N), the density of resultant grooves on the surface is higher and progressive wear damage is observed until the threshold load (160 N) to film partial wear-out in the balls. However, the very low friction behaviour is essentially kept due to the load supporting role of a peripheral diamond crown in the ball. The CVD diamond coatings keep a high wear resistance (3.0×10^{-8} $mm^3N^{-1}m^{-1}$) for loads below 160 N.

Acknowledgements

C.S. Abreu acknowledges PRODEP III funds supporting his PhD work. The financial funding from the FCT Project POCTI/CTM/45423/2002 is also gratefully acknowledged.

Chapter 5

Nanocrystalline CVD diamond tribosystems

5.1 Introduction

This chapter comprises four scientific articles, with the first three (Publications V-VII) already published in international journals and a fourth (Publication VIII, Sec. 5.5) accepted for publication in the international journal Diamond & Related Materials. All four papers report on particular aspects of the tribological characterization of homologous pairs of NCD-coated Si_3N_4 tribosystems conducted in this thesis.

The friction and wear behaviour of the NCD films was assessed in the same operating environments as those as the MCD coatings, i.e. unlubricated sliding in open air and water lubrication, both at ambient temperature. Tribo-testing in all studies was carried out in an adapted ball-on-flat (BOF) tribometer (PLINT TE/67R) with linear reciprocating motion, and where the frequency (1 Hz) and amplitude (3 mm) was kept unchanged. Thus, the experimental variables covered in the various studies were the applied normal load (contact pressure), NCD deposition technique, sliding environment and type of substrate surface pretreatment

As was the case for the MCD coatings, several non-destructive techniques were employed in the characterization of as-deposited and worn NCD films, namely SEM, AFM and μ-Raman. The first two techniques were mainly used to study the morphology and topography, as well as to obtain the surface roughness parameters of virgin and wear damaged diamond coatings. Information provided by those techniques was also used to identify the prevailing wear processes and mechanisms, and to estimate specific wear rates for the NCD films. Moreover, X-ray diffraction analysis was used exceptionally in Publication V (Sec. 5.2) for crystallographic studies and to estimate the diamond grain size.

The first article (Publication V, Sec. 5.2) appearing in this chapter is dedicated to the evaluation of the tribological properties of self-mated NCD-coated Si_3N_4 films, synthesized by the microwave plasma-assisted chemical vapour deposition (MWPACVD) technique. Diamond growth was achieved in a $Ar/H_2/CH_4$ gas mixture, using microwave discharges in continuous wave (CW) and pulsed wave (PW) mode for the flat and ball specimens, respectively. The self-mated diamond coatings were made to slide in ambient atmosphere, under applied normal loads spanning the range $10-40$ N, which correspond to severe sliding contact conditions.

Tribo-testing was performed over two different length-scales, i.e. shorter standard experiments,

corresponding to a sliding distance of approximately 43 m (1 h), and lengthier endurance experiments of about 690 m (16 h). The choice of two distinct sliding distances enabled a better representation of the evolution of the friction coefficient, where the shorter distance is more appropriate to analyse the initial friction peak and running-in regime, as well as in screening the threshold load under sliding, whereas the endurance tests become important for assessing the steady-state friction coefficient, resistance to fatigue wear and more accurately estimate specific wear rate values for the NCD coatings (because the tribosystem reaches a stable regime, where the predominant wear mechanisms remain unchanged).

Publication VI (Sec. 5.3) reports on the tribological properties of self-mated NCD-coated Si_3N_4 films, this time using the hot-filament CVD (HFCVD) variant because of its lower complexity, greater versatility and lower costs involved as compared with MWPACVD.
Prior to diamond deposition, the flat substrates were submitted to three different surface finish conditions, namely flat lapping, pre-polishing and polishing to a specular surface condition. The mechanical processes used to achieve these surface finish conditions are found in the experimental section of this second paper.
In order to compare the tribological performance of MWPACVD and HFCVD nanocrystalline diamond coatings, tribo-testing in this second study was performed under the same operating conditions, i.e. at ambient temperature without lubrication and using applied normal loads of the same order ($10-40$ N). Once more, two different sliding distances resulting from test durations of 2 h ($x \sim 86$ m) and 16 h ($x \sim 690$ m) were used to better analyse the various occurring friction regimes.
Complementary to the objective of assessing the tribological potential of the more cost-effective HFCVD-based NCD films, this paper reports also on the influence of the mechanical surface pretreatments applied to the Si_3N_4 substrates in terms of the friction and wear performance of NCD coatings. This will make possible to choose an adequate pretreatment for subsequent studies.

In the third article (Publication VII, Sec. 5.4), the influence of plasma pretreatments on Si_3N_4 substrates and their effect on the tribological performance of self-mated HFCVD-based NCD coatings is addressed. The main objective of this study consisted in further im-

proving on the adhesion levels demonstrated by the smoothest NCD coatings, described in the preceding work (Publication VI, Sec. 5.3), i.e. those obtained by polishing the substrate to a mirror-like finish. As referred in Publication VI (Sec. 5.3), these were characterized by the lowest friction resistance, which make them serious candidates for biotribological applications. Nonetheless, they were also characterized by the least resistance to delamination under intensive tribological stress and, therefore, needed to be more thoroughly studied to enhance their potential of applicability.
For the purpose of analyzing the tribological potential of plasma pretreated NCD coatings, the substrates were etched by an hydrogen plasma inside a MWPACVD reactor for 30 min, and the dry sliding experiments performed under normal loads in the leeway $10-90$ N, in open air.

Finally, the last article (Publication VIII, Sec. 5.5) is dedicated to the tribological evaluation of NCD-coated Si_3N_4 tribosystems under water lubrication. Likewise, the Si_3N_4 substrates were mechanically polished to a specular finish to obtain the smoothest and lowest friction coatings, which bear an higher potential for biotribological applications, such as in total arthroplasty. Moreover, as a result of the beneficial effect observed in plasma pretreated coatings (see Publication VII, Sec. 5.4), the ceramic substrates were also subjected to a tetrafluoromethane (CF_4) plasma etching for 1 h (Emitech, K 1050X), in order to enhance film adhesion. The tribo-tests were carried out by maintaining the contact region permanently immersed in a water pool type reservoir, attached to the lower oscillating table, and under applied normal load values ranging from 10 to 90 N.
The morphology of as-deposited and worn NCD films, as well as of the wear debris particles, were studied by SEM to conclude on the prevailing wear processes and mechanisms. The topographic features and surface roughness parameters of the NCD coatings were also obtained from AFM measurements operated in non-contact tapping mode. Moreover, when considered useful, a comparison is given between the tribological performance of HFCVD-based plasma pretreated NCD coatings in the presence of water and dry sliding conditions.

(A) UNLUBRICATED TESTS

5.2 Tribological testing of self-mated nanocrystalline diamond coatings on Si_3N_4 ceramics [Publication V]

C.S. Abreu, M.S. Amaral, F.J. Oliveira, A. Tallaire, F. Bénédic, O. Syll, G. Cicala
J.R. Gomes, R.F. Silva
Surf. Coat. Tech., 200 (2006) 6235-6239

Abstract

Due to their much lower surface roughness compared to that of microcrystalline diamond, nanocrystalline diamond (NCD) films are promising candidates for tribological applications, in particular when deposited on hard ceramic materials such as silicon nitride (Si_3N_4). In the present work, microwave plasma-assisted chemical vapour deposition of NCD is achieved using $Ar/H_2/CH_4$ gas mixtures on plates and ball-shaped Si_3N_4 specimens either by a conventional continuous mode or by a recently developed pulsed regime. The microstructure, morphology, topography and purity of the deposited films show typical NCD features for the two kinds of substrate shapes. Besides, tribological characterization of the NCD/Si_3N_4 samples is carried out using self-mated pairs without lubrication in order to assess their friction and wear response. Worn surfaces were studied by SEM and AFM topography measurements in order to identify the prevalent wear mechanisms. Friction values reached a steady-state minimum of approximately 0.02 following a short running-in period where the main feature is a sharp peak which attained a maximum around 0.44. Up to the critical load of 35 N, corresponding to film delamination, the equilibrium friction values are similar, irrespective of the applied load. The calculated wear coefficient values denoted a very mild regime ($K \sim 1 \times 10^{-8}$ $mm^3N^{-1}m^{-1}$) for the self-mated NCD coatings. The predominant wear mechanism was identified as self-polishing by micro-abrasion.

Keywords: Nanocrystalline diamond; Silicon nitride; Tribological characterization

5.2.1 Introduction

In the past few years, an increasing interest has been focused on the synthesis of nanocrystalline diamond films (NCD) due to their extreme hardness and their nanometre-scale grain size which ensures a very low surface roughness [137, 138]. However, the mechanical and tribological applications of such coatings are mainly limited by the weak properties of the substrates used since depositions are usually performed on silicon. Recently the possibility to use silicon nitride (Si_3N_4) ceramics as substrates has been pointed out [139, 140]. Indeed Si_3N_4 is a tough and hard material that ensures load-bearing capability for mechanical purposes and an adequate affinity and adhesion with diamond. NCD films deposited on silicon nitride substrates could find applications in numerous fields such as biomaterials, mechanical face seals, bearings or cutting tools. Diamond films have a very low friction and high wear resistance under a wide range of sliding contact conditions [24] whose performance may be improved if ultra-smooth NCD films are used. Values of the friction coefficient in the range of $0.03 - 0.06$ were obtained in self-mated fine grain microcrystalline diamond coatings [39]. Also, high values were measured in the early phases of wear tests of microcrystalline diamond films [41, 141]. It is then of great interest to further assessing the tribological properties of NCD coated Si_3N_4 substrates in what matters their friction and wear behaviour.

High quality homogeneous NCD films can be deposited on Si_3N_4 substrates with typical growth rates of a few micrometers per hour using microwave plasma assisted chemical vapour deposition (MPACVD) process working in a conventional continuous mode [140]. Controlling the deposition temperature is, however, quite difficult when depositing on complex-shape substrates since the dielectric sample may deeply penetrate the discharge which leads to a pronounced edge effect and to a subsequent graphitisation of the film [142]. This phenomenon is particularly important for Si_3N_4 material due to its low thermal conductivity, but can be successfully overcome by the use of an appropriate pulsed microwave discharge [142].

In this work, the tribological properties of Si_3N_4 ceramic substrates coated with a NCD thin layer are investigated. The diamond depositions were performed under $Ar/H_2/CH_4$ microwave discharges both on silicon nitride plates and on ball-shaped substrates in continuous

wave (CW) and pulsed wave (PW) mode, respectively. Tribological characterization of such NCD films is achieved using self-mated pairs (ball and plate) without lubrication in order to assess their friction coefficient values and wear behaviour when subjected to such extreme surface contacts.

5.2.2 Experimental details

Dense Si_3N_4 plates ($10 \times 10 \times 3$ mm^3) and balls (5 mm diameter) were used as substrates for diamond deposition. The mirror polished plates were produced by pressureless sintering at 1750 °C/2 h under nitrogen atmosphere, followed by cutting, grinding, lapping and finally polishing with colloidal silica. The balls, commercially available (Kema Nord), were polished down to 1 μm with diamond slurry before scratching for NCD growth. NCD deposition was carried out using previously optimised growth conditions in a bell-jar type reactor [140, 142]. Prior to the plasma treatment, all the samples (plates and balls) were submitted to an appropriate ultrasonic pre-treatment in a 40 μm grain size diamond powder suspension in order to enhance diamond nucleation on the substrate surface [143]. Two ceramic plates, referred as P1 and P2, were successively recovered by a thin NCD layer ($\sim$ 12 μm) using the conventional CW mode. The feed gas was an $Ar/H_2/CH_4$ mixture (96%:3%:1%) with a total flow rate of 250 sccm. The pressure in the chamber was set to 200 mbar while the injected microwave power was maintained constant at 600 W. The surface temperature monitored with a bichromatic infrared pyrometer was controlled using an additional heating system located in the substrate holder and set at 925 and 825 °C for samples P1 and P2, respectively. In order to avoid the edge effect induced by the shape of the substrates, the two Si_3N_4 balls, labeled B1 and B2, were coated under PW discharges. The gas mixture and flow rate were the same than those described above, but in this case the input power was modulated with a pulse repetition rate of 1000 Hz and a duty cycle of for a maximum input microwave power of 800 W. The balls were carefully placed in a circular hole made in the molybdenum substrate holder, the depth of which was approximately half their diameter. The surface temperature was estimated for both samples at 925 °C. The growth duration imposed for each sample was 3 h to give a final thicknesses of approximately 12 μm for the flat substrates.

The microstructure, morphology, topography and purity of NCD films deposited on Si_3N_4 ceramic plates and ball-shaped substrates in the conditions described above were discussed in previous papers [140, 142]. The main features are briefly summarized in the next section where observations by scanning electron microscopy (SEM) (Hitachi S4100), atomic force microscopy (AFM) (Digital Instrument Multimode IIIa) and micro-Raman spectroscopy (high-resolution confocal spectrometer Jobin-Yvon HR800) are also reported.

The tribological characterization of the NCD films was achieved using a ball-on-flat reciprocating tribometer (PLINT TE67/R). Unlubricated self-mated tests were performed in ambient atmosphere (RH of $50-60\%$) at room temperature, with constant stroke (6 mm) and frequency (1 Hz). The NCD-coated balls (upper specimen) were mounted in the sample holder arm and made to contact with a defined applied load onto the counter surface. The oscillatory relative motion between the opposing surfaces was obtained by clamping NCD-coated square plate counterbodies (lower specimen) on a reciprocating table. The applied normal load varied in the range of 10 to 40 N. Considering a Hertzian elastic contact for a sphere pressed by a determined load into a flat specimen, the applied loads used in this study produced initial peak pressures under the ball in the range of $5-8$ GPa [62, 117]. All tribological experiments were conducted over a sliding distance (x) of 43 m, for the normal tests, and 690 m for the endurance tests.

Friction scans were completed during the sliding tests by means of a load cell, previously calibrated by applying known dead-weights in the range of the measured loads. The wear coefficient (k) of the NCD-coated balls was assessed from the volumetric wear (V) of this triboelement determined from SEM observations of the near circular wear scars produced in the contact zone [141].
After completion of the sliding tests, the worn surfaces were examined by SEM and AFM (Digital Instrument NanoScope IIIa) with the purpose of ascertain the morphological and topographical characteristics of the films subjected to damage stress, and correlate the results with the friction and wear mechanisms of NCD films in ambient atmosphere.

5.2.3 Results and Discussion

Characterization of the NCD films

All the NCD films synthesized either under CW or PW discharges exhibit smooth granular surfaces where no faceted crystallites can be noticed. Typical SEM and AFM images obtained on sample P2 are presented in Fig. 5.1 as an illustration. The SEM micrograph (Fig. 5.1 (a)) emphasises the full recovering and uniformity of the NCD films, whereas the AFM image (Fig. 5.1 (b)) points out their surface smoothness, with typical surface roughness values (R_a) in the range between 20 and 40 nm. For the ball-shaped samples B1 and B2, the deposit consisted in a hemispherical NCD film recovering homogeneously the upper part of the balls since only a portion of the substrates was exposed to the plasma due to their position on the substrate holder.

Raman spectroscopy of the samples was performed using the 488 nm line of an Ar^+ laser as the excitation wavelength (Fig. 5.2). Typical NCD features are observed for both plates and ball-shaped substrates, in particular the trans-polyacetylene bands at 1150 and 1480 cm^{-1}, the graphite D and G bands around 1350 and 1580 cm^{-1}, respectively, and a weak broad diamond peak at 1332 cm^{-1} [76, 144]. Note that, in the spectrum of sample P1, the trans-polyacetylene bands and the diamond peak have a weaker intensity with regard to sample P2. This may be due to the higher deposition temperature imposed for sample P1 since an increase of the surface temperature was shown to provoke a transition towards more graphite-like NCD layers [145]. The XRD analysis done in the NCD films deposited on Si_3N_4 plates give evidence a good crystallinity through the observation of the characteristic $\langle 111 \rangle$ and $\langle 311 \rangle$ diffraction peaks. The grain size was estimated around 12 nm from the broadening of the $\langle 111 \rangle$ peak [142]. By measuring the thickness of the films on cross-section SEM images, the growth rate of the NCD layers on the ceramic plates was estimated to be about 4 μmh^{-1}.

Tribological behaviour

A first set of ball-on-flat reciprocal tests was carried out to determine the maximum critical load the NCD films could withstand. The NCD coatings sustained stable operation, without film breakage, under tribological action for applied loads up to 35 N that corresponds

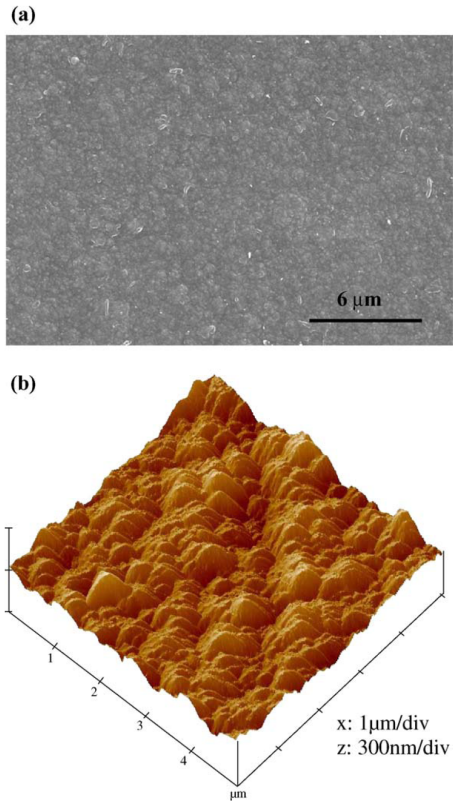

Figure 5.1: Typical morphology and topography of the deposited NCD films as observed for sample P2 by: (a) scanning electron microscopy; (b) atomic force microscopy on a 5×5 μm^2 surface.

to a maximum contact pressure of ~ 6.8 GPa.

Fig. 5.3 shows typical friction scans of self-mated NCD coatings on Si_3N_4 ceramics as a function of the sliding distance. The represented curves reveal a running-in effect with a pronounced peak as its main feature, followed by a stationary phase with extremely low friction coefficients. The initial friction coefficient of examined NCD coatings is in the range from 0.13 to 0.44 and denoted a significant dependence on the starting surface roughness of as-deposited films. This behaviour exists in spite of the nano-scale nature of the surface roughness of the NCD thin films, and has been referred in some studies involving fine-grained ($20-100$ nm) polycrystalline self-mated CVD diamond coatings [33]. This same feature was observed for

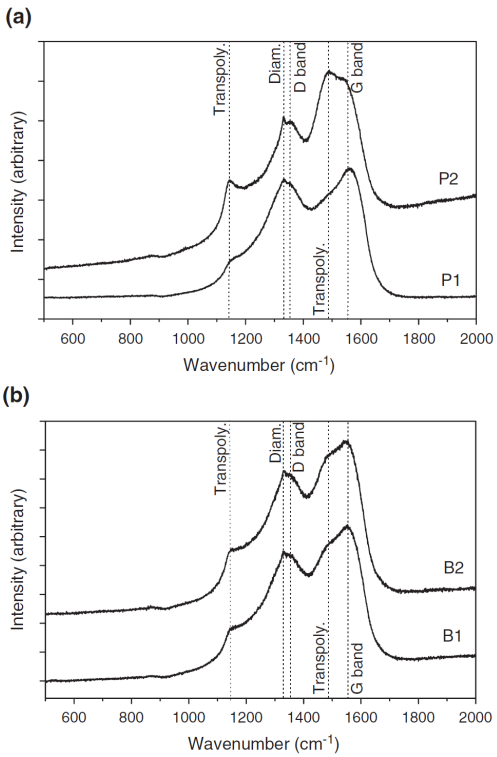

Figure 5.2: Raman spectra of the NCD films deposited on the silicon nitride substrates: (a) P1 and P2 plates; (b) B1 and B2 balls. The excitation line was 488 nm and the main bands are indexed on the spectra.

larger grain sized MPACVD diamond films ($1.8-4.6\ \mu$m) in experiments similar to those of the present work [141]. This suggests that the initial friction regime is predominantly by a strong interaction between surface asperities, i.e. by a mechanism of fragmentation and deformation of contacting asperities. This process can be observed in the SEM micrograph of Fig. 5.4 (a), where a change from the nominal NCD topography (Fig. 5.1 (a)) to more flattened surfaces took place. In this case, there is not a large degree of polishing due to the low load (10 N) and short sliding distance (43 m). For longer distances, the surface becomes fully flattened, revealing extensive polishing. The micrograph in Fig. 5.4 (b) was taken from the border of the wear track of a test conducted for 690 m under 10 N. In the centre of the track, the NCD film is fully flat (lack of topographic contrast under SEM), with surface roughness values of about 2 nm (rms) determined by AFM, while laterally it still contains unpolished zones.

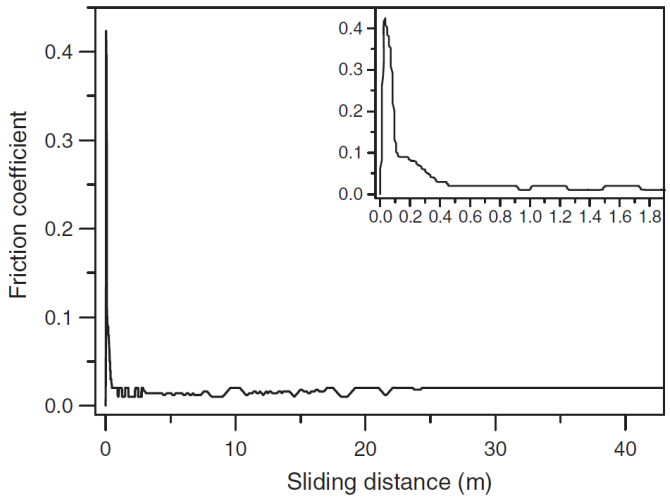

Figure 5.3: Representative evolution of the friction curve, for unlubricated self-mated NCD films in ambient atmosphere, as a function of the sliding distance on a sample tested for $x = 43$ m under $W = 30$ N.

As sliding continues, an equilibrium track is reached with the nano-asperities worn down. The relevance of the interlocking mechanism gradually looses its importance in the overall friction phenomena thus giving very low steady-state friction values ($0.02 - 0.04$). This idea is reinforced by the well known fact that the adhesive component of friction is highly reduced during the sliding of smooth passivated diamond surfaces in ambient atmosphere, following saturation of the dangling carbon bonds by adsorbed species [19]. Another feature observed in this study was that the steady-state friction values remained the same, irrespective of the starting surface roughness of as-deposited NCD films and applied load. Miyoshi [33] reports a similar behaviour in terms of the starting surface roughness influence in the final equilibrium friction of self-mated fine-grained polycrystalline diamond. In addition, as can be seen from the inset of the friction curve of Fig. 5.3, the leveling of the friction coefficient is readily achieved after a few decimeters of sliding distance, thus indicating a short running-in regime for homologous pairs of NCD in open air.

The AFM micrographs shown in Fig. 5.5 reveal the differences between the centre and sides of wear tracks produced at short (Fig. 5.5 (a)) and long (Fig. 5.5 (b)) running distances

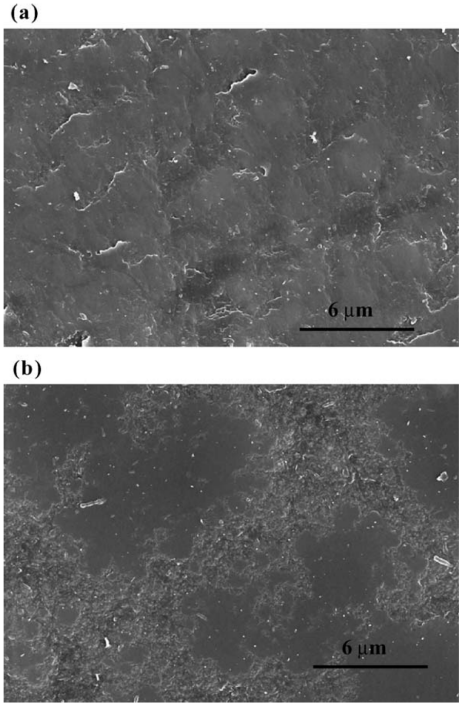

Figure 5.4: SEM micrographs of NCD films revealing the smooth morphology of worn disc specimens: (a) $x = 43$ m, $W = 10$ N at the centre of the wear track; (b) $x = 690$ m, $W = 10$ N near the border of the track, showing ultra-smooth plateaus.

under 35 N and 30 N loads, respectively. Even for the 43 m experiment, the centre of the track is already very smooth (rms ~ 7 nm), unlike the case of the 10 N test (Fig. 5.4 (a)). For longer distances, the surfaces become even smoother as the AFM micrograph of Fig. 5.5 (b) clearly evidences. Surface roughness values in the range of ~ 2 nm (rms) are achieved. The observed morphology and this extremely flattened topography are characteristic of a self-polishing wear mechanism by micro-abrasion.

The wear coefficient values of balls sliding against NCD plate specimens varied in the range of $1.0 - 1.4 \times 10^{-8}$ mm^{3}N^{-1}m^{-1}, indicating a very mild wear regime in ambient atmosphere for the long duration tests (690 m). It is worth noting that the wear of the NCD plate specimens was not measurable by standard techniques (weight loss and conventional profilometry) although the NCD film becomes smoothened as described above (Figs. 5.4 (b) and 5.5 (b)).

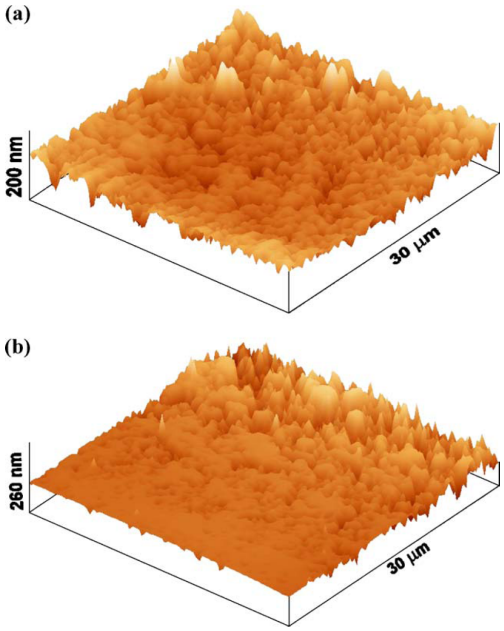

Figure 5.5: AFM scans of worn NCD coatings taken from the borders of wear tracks on disc specimens using tapping mode: (a) $x = 43$ m, $W = 35$ N; (b) $x = 690$ m, $W = 30$ N.

Although the deposited NCD diamond films contain some non-diamond phases (Fig. 5.2), there is no apparent effect of their presence on the friction coefficients or wear resistance. The main differences relatively to wear tests conducted with self-mated microcrystalline diamond are the lower starting friction coefficient peaks and shorter running-in periods. These can be accounted for entirely by the much smaller starting surface roughness of NCD films relatively to polycrystalline diamond ones. Thus, the role of graphitic phases on the wear behaviour of these NCD-coated Si_3N_4 ceramics is yet to be fully understood.

5.2.4 Conclusions

NCD films were successfully deposited by MPACVD method from $Ar/H_2/CH_4$ gas mixtures on Si_3N_4 ceramic plates and balls, using CW and PW modes, respectively.

Ball-on-flat tribological experiments allowed the estimation of a critical load of 35 N (~ 6.8 GPa) for film delamination.

Friction curves show a pronounced friction peak attributed to the mechanical interlocking of sur-

face diamond asperities, quickly followed by very low steady-state friction coefficients ($0.02 - 0.04$) caused by the decrease of surface roughness through extensive polishing mechanism. Final surface roughness reached values of the order of 2 nm (rms) after long running distances (690 m). Such low wear damage of the coated plates hindered a weight loss sufficient enough to be measured by usual techniques. In the balls, the calculated wear coefficient is typical of a very mild wear regime, in the range of $1.0 - 1.4 \times 10^{-8}$ $mm^3N^{-1}m^{-1}$.

The very low friction, high wear resistance and enhanced adhesion of the NCD coatings deposited on Si_3N_4 substrates make this tribosystem an excellent choice for dry tribological applications involving high contact stresses, such as cutting tools or mechanical seals.

Acknowledgements

C.S. Abreu and M. Amaral acknowledge PRODEP III funds and FCT for the grant SFRH/BD/9272/2002, respectively, in support of their PhD works. FCT is acknowledged for funding this work under project POCTI/CTM/45423/2002. This work was also supported by the CNRS/GRICES project no. 14153 and a bilateral agreement between CNR and CNRS.

5.3 Friction and wear performance of HFCVD nanocrystalline diamond coated silicon nitride ceramics [Publication VI]

C.S. Abreu, M.S. Amaral, A.J.S. Fernandes, F.J. Oliveira, R.F. Silva, J.R. Gomes
Diam. Relat. Mater., 15 (2006) 739-744

Abstract

Silicon nitride (Si_3N_4) ceramics were selected as substrates due to their thermal and chemical compatibility to diamond that ensure the adequate NCD adhesion for mechanical purposes. NCD deposition was performed by hot-filament chemical vapour method (HFCVD) using $Ar/H_2/CH_4$ gas mixtures. The tribological assessment of homologous pairs of NCD films was accomplished using reciprocating ball-on-flat tests using NCD coated Si_3N_4 plates and balls. The friction evolution is characterized by an initial running-in regime with a sharp peak up to 0.7, shortly followed by a steady-state regime identified by very low friction coefficient values ($0.02 - 0.03$). The threshold load prior to delamination depends on the starting surface roughness of the substrates and attains a value of ~ 40 N. In terms of wear performance, the NCD films reveal a mild wear regime ($K \sim 10^{-7}$ $mm^3N^{-1}m^{-1}$) for self-mated dry sliding conditions.

Keywords: Nanocrystalline; Hot-filament CVD; Tribology

5.3.1 Introduction

Nanocrystalline diamond coatings (NCD) are gaining increasing interest as serious candidate materials for high performance engineering surfaces in mechanical and tribological applications, due to their intrinsic smoothness combined with most of the outstanding properties of natural single-crystal diamond [24]. Highly demanding tribological applications where NCD coatings are already in use or thought of vary from the fluid handling and cutting tools industries to, more recently, micro-electromechanical systems (MEMS) and biomedical applications [62, 92, 146].

The wear performance and, more extensively, the friction properties of NCD coatings sliding against metallic or ceramic dissimilar counterpairs have been studied [21, 41]. However,

to our knowledge, no reports are found in the literature concerning the tribological performance of unlubricated homologous pairs of NCD films under high applied stresses.

Silicon nitride (Si_3N_4) ceramics constitute a novel and prospective substrate material for the deposition of NCD films due to their chemical compatibility and low thermal mismatch with diamond, which translates as an improved adhesion [73, 141]. Being one of the toughest ceramic materials, it possesses an advantageous combination of intrinsic mechanical, thermal and chemical properties, as well as good wear resistance, imperative for demanding tribomechanical applications.
The hot-filament chemical vapour deposition (HFCVD) technique is one of the most common available methods of producing polycrystalline diamond films and, more recently, NCD films. This versatile CVD based deposition technique allows the diamond deposition in a simple and cost-effective way, overcoming some of the limitations of other more sophisticated CVD techniques such as microwave plasma CVD (MPCVD), namely in the ability of coating complex geometries.

Reciprocating ball-on-flat experiments were undertaken to assess the tribological behaviour of NCD homologous pairs. Three different surface finishing states were employed on the Si_3N_4 substrates. The applied load threshold at which delamination of the films occurs under tribological stress was determined for all tested conditions. Different characterization techniques were used in order to examine the quality, morphology and topography of the deposited and worn NCD films, respectively, μ-Raman spectroscopy, scanning electron microscopy (SEM) and atomic force microscopy (AFM).

5.3.2 Experimental details

Details on powder preparation and sintering of Si_3N_4 substrates can be found elsewhere [147]. Square substrates ($10 \times 10 \times 3$ mm^3) were cut from dense ceramics, ground and submitted to three different surface finish conditions: (i) flat lapping with 15 μm diamond slurry (FL samples); (ii) hard cloth polishing with 15 μm diamond slurry (PP); and (iii) polishing to a mirror-like finish with colloidal silica (P). Commercial silicon nitride balls (Ø 5 mm, Kema Nord) were also used for diamond deposition, in order to act as counterbodies in the sliding

experiments. Silicon nitride substrates were then scratched for 1 h in an ultrasonic suspension with 1 μm diamond powder in *n*-hexane (1 g/100 ml). Nanocrystalline diamond films were grown by the HFCVD technique using an $Ar/CH_4/H_2$ gas mixture where the Ar/H_2 and CH_4/H_2 ratios were fixed at 0.1 and 0.04, respectively. The other deposition conditions were the following: W filament temperature – 2300 °C, total gas flow – 50 ml·min^{-1}, total pressure – 50 mbar, substrate temperature – 750 °C. The nanodiamond growth rates were, respectively, 1.6 μm·h^{-1} on the plates and 2.2 μm·h^{-1} on the balls.

All the substrates were characterized by AFM (Digital Instruments, IIIa, USA) before and after deposition in order to distinguish their topographic features. The morphology and thickness of the NCD films were assessed using SEM (Hitachi S4100, J). The NCD quality of the as-deposited films was characterized by a μ-Raman spectrometer (Jobin Yvon T64000, F) with the 514.5 nm line.

The tribological testing of self-mated NCD films was performed on a ball-on-flat reciprocating sliding tribometer (PLINT TE67/R, UK). Tests were conducted in ambient atmosphere ($\sim 50-60\%$ RH), under unlubricated conditions, with a constant stroke of 6 mm and frequency of 1 Hz. Sliding distances were chosen to be of $\sim$ 86 m (regular tests) and for the lengthier ones $\sim$ 690 m (endurance tests), which correspond to 2 h and 16 h of in-interrupt sliding, respectively. Normal loads in the range of 10 to 40 N were applied by means of weights and were kept constant for each run. Considering a purely elastic contact of the sphere/plane surface, these conditions represent a mean Hertzian pressure (normal stress) in the range of $4.4-7.1$ GPa [10, 148].
Following the sliding tests, the worn NCD surfaces were examined by SEM and AFM techniques. The wear coefficient of the balls was assessed by measuring the corresponding wear scar diameter in SEM.

5.3.3 Results and Discussion

Morphology of substrates and as-grown NCD films

The morphology of the as-deposited NCD films on silicon nitride substrates reveals a good uniformity, as shown in Fig. 5.6 (a), for a $\sim 25\ \mu$m thick film grown on a ball. The included inset exhibits the presence of a pattern of smooth round elevations on the top of which the nano-sized diamond grains are perceptible. Fig. 5.6 (b) depicts a representative μ-Raman spectrum of an as-deposited NCD film, containing the diamond characteristic peak at $\sim 1332\ \text{cm}^{-1}$ and the features usually assigned to transpolyacetylene (at 1140 and 1480 cm^{-1}), typical of NCD films [76, 149]. The D and G bands (at 1350 cm^{-1} and 1580 cm^{-1}, respectively) associated with the sp^2 coordinated material are also present.

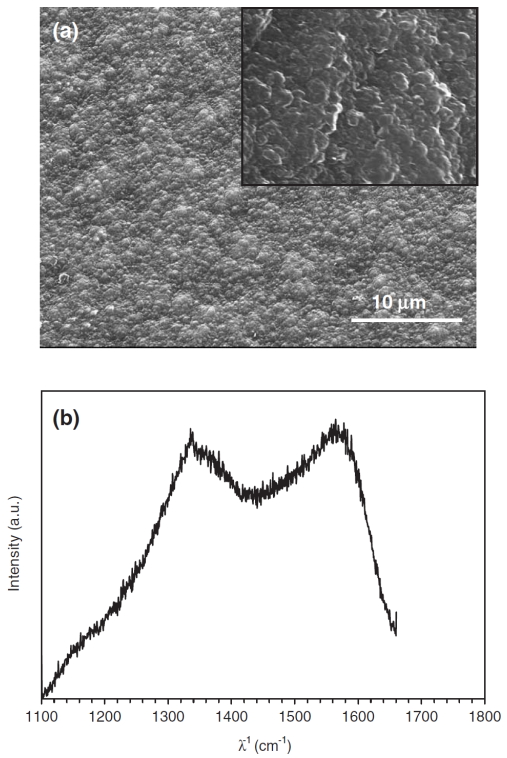

Figure 5.6: (a) Morphology of a representative NCD film on a Si_3N_4 ball substrate. The inset shows a detail five times magnified relative to the main micrograph; (b) Raman spectrum of a typical as-deposited NCD film.

AFM scans of the Si_3N_4 substrates with the distinct surface finishing conditions analyzed in the present study, along-side with the corresponding deposited NCD films, are presented in Fig. 5.7. Each 3D plot is accompanied by its respective surface roughness value, R_q (rms). The different uncoated substrate surface finishing quality is clearly evidenced: for the FL sample, deep grooves are visible as a result of the roughing operation; for the PP sample, a somewhat irregular surface topography is still patent, however without the presence of grooves; finally, for the P sample, a high smoothness was achieved. The above described surface distinct conditions are corroborated by their relative R_q values, in the range of 169 nm for the roughest and of 15 nm for the smoothest one. After coating, the roughness rank is kept. However, particular phenomena must be taken into account. In fact, for deposition time used, the film tends to magnify the roughness for rougher starting surfaces, such as in the case of FL (Fig. 5.7 (a), (d)). As it can be seen, the NCD film growth follows the grooves of this sample, while prominent conglomerates formed in the vicinity of local asperities, resulting on increased R_q up to 206 nm. On the other hand, since the PP sample presents lower starting roughness, the magnifying effect does not take place, a smoothing occurs instead (Fig. 5.7 (b), (e)). For this sample, the NCD smooth deposit actually improves the surface finish, whose initial roughness was not enough to promote the above described magnifying effect. The intrinsic smoothness of the NCD deposits is put in evidence for the case of the P sample, whose starting R_q roughness of 15 nm augmented to only 41 nm for a ~ 20 μm thick film. Concerning the NCD coated a nominal roughness of 87 nm was obtained.

Morphology of worn NCD films and tribological behaviour

As can be seen from the low magnification SEM micrograph of the FL wear track (Fig. 5.8 (a)), material loss by polishing takes place under an applied load of 20 N for shorter runs ($\sim$ 86 m), without completely masking the deep scratches inherent to this surface finish condition. In the PP wear track, a similar morphology of the worn surface indicates identical phenomena, although a more evenly distribution of polished sites can be observed due to the lower initial roughness associated to this surface finish condition.

At high magnification (Fig. 5.8 (c)), depressions can be observed alongside with plateaus formed by a self-polishing (micro-abrasion) mechanism, which lead to the truncating of NCD conglomerates and subsequent flattening. The depressions between the plateaus correspond to undamaged NCD regions.

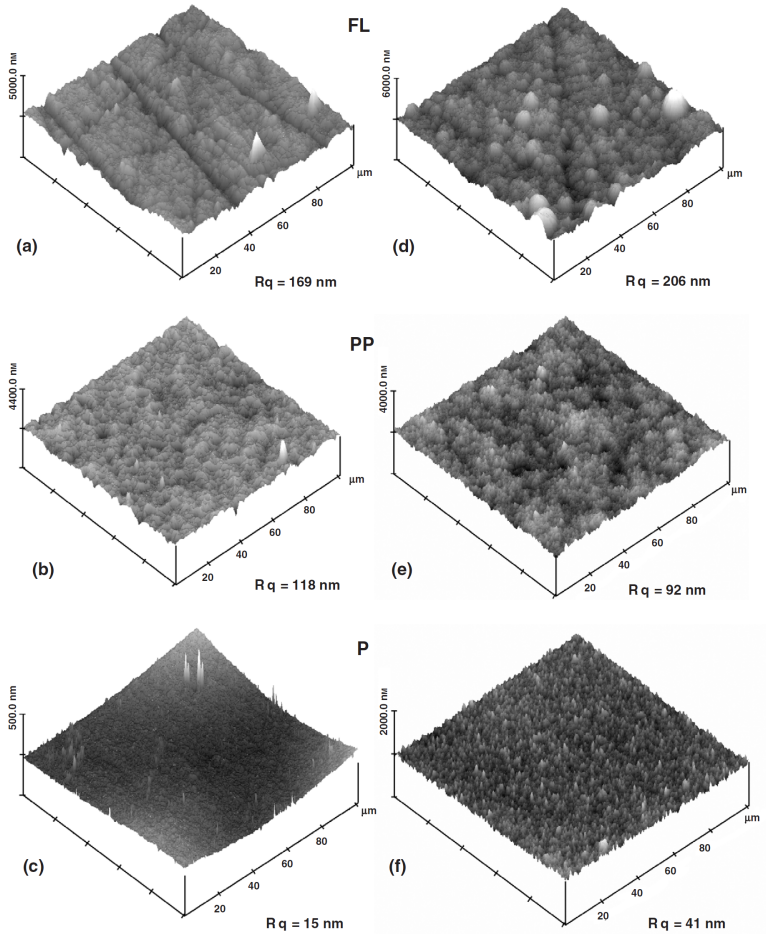

Figure 5.7: 3D AFM images of uncoated (left column) and NCD coated (right column) substrates. FL – flat lapped substrate; PP – pre-polished; P – polished.

Also noticeable (Fig. 5.8 (d)) is the crack pattern in lumps of material localized at the edge of the wear tracks, originated from the NCD wear debris smeared by the contact pressure and sliding interaction.

Representative friction evolution curves for each surface finishing condition are depicted in the plots of Fig. 5.9 (a)–(c). Regardless the analyzed sample, each friction coefficient (μ) curve is characterized by an intense narrow initial peak, originated from the mechanical interlocking of the film asperities. Following this main feature, a relatively short transition stage sets-in associated to the flattening of asperities, until the accommodation of the antagonist sur-

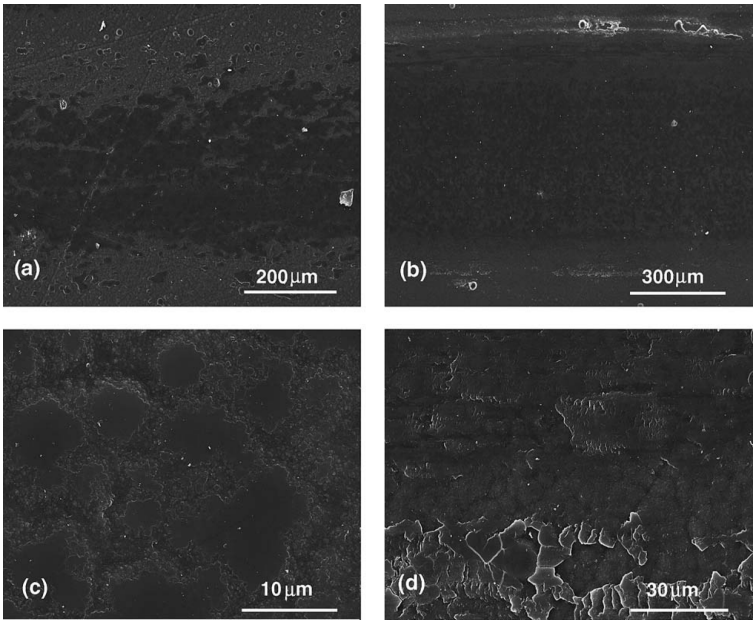

Figure 5.8: Aspect of the wear tracks for samples (a) FL and (b) PP under an applied load of 20 N and a sliding distance of 86 m; (c) detail of polished plateaus, originated from truncated NCD conglomerates; (d) lumps of cracked material at the edge of the wear track.

faces is reached. Finally, due to widespread polishing, the friction coefficient levels off, reaching extremely low values in the range of $0.02 - 0.03$. The friction behaviour of FL (Fig. 5.9 (a)) and PP (Fig. 5.9 (b)) samples is similar but the initial peak of the FL sample reaches a higher intensity due to its rougher surface.

On the contrary, the curve corresponding to the very smooth P sample reveals an enlarged friction peak (Fig. 5.9 (c)) from premature film detachment. In fact, the threshold load for this tribosystem is below 10 N, much lower than the more resistant FL (40 N) and PP ones (20 N), denoting poor adhesion. In the P system, the self-polishing transition regime is absent. Nonetheless, very small values for the friction coefficient are observed after the occurrence of delamination as a consequence of the tribological interaction between a smooth NCD film still present in the ball, sliding against a softer exposed Si_3N_4 flat substrate.
For the endurance tests (Fig. 5.9 (d)), the friction coefficient gradually increases with the sliding distance after remaining at its minimum for distances in the range of the regular tests. This

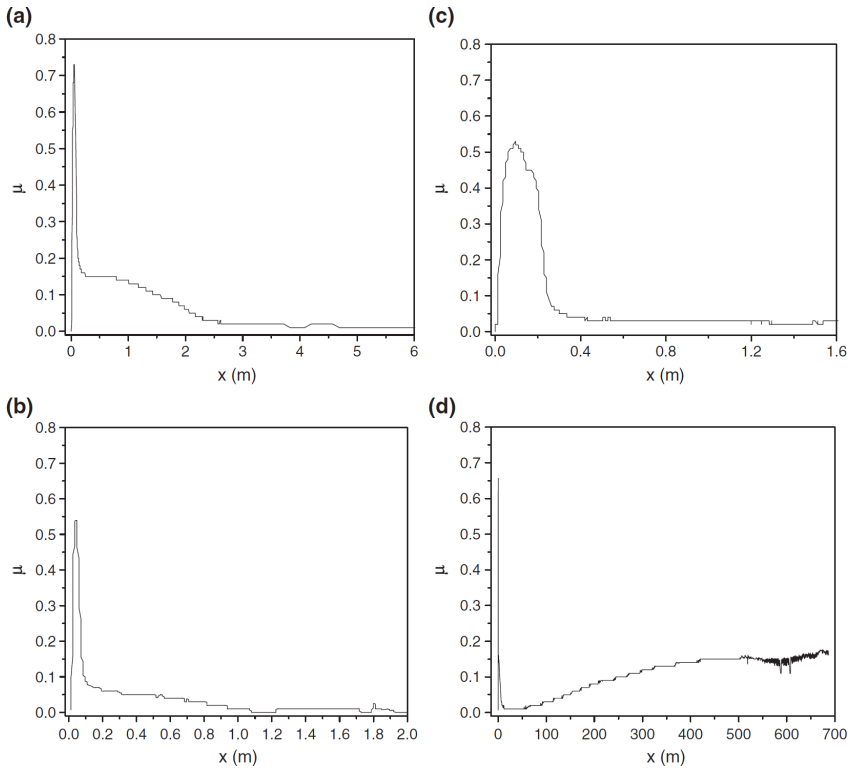

Figure 5.9: Typical friction curves obtained for the various surface conditions: (a) FL under an applied load of 20 N, (b) PP under 10 N, (c) P under 10 N and (d) 690 m endurance test under 10 N for a PP sample.

relates to a progressive surface degradation effect that is documented in Fig. 5.10 for the NCD coated balls, in which cracking is discernible and a chipping wear mechanism is revealed.

The general trend for the NCD friction behaviour is also characteristic of self-mated sliding systems of microcrystalline diamond coated Si_3N_4 ceramics [141]. However, a higher friction peak is obtained for NCD (~ 0.7) than for diamond (~ 0.25) for the same applied load (20 N). A possible explanation is related to the higher energy required for the truncating of NCD conglomerates when compared to the easier cleavage of micropyramidal sharp crystals, the reported main wear mechanism of diamond.

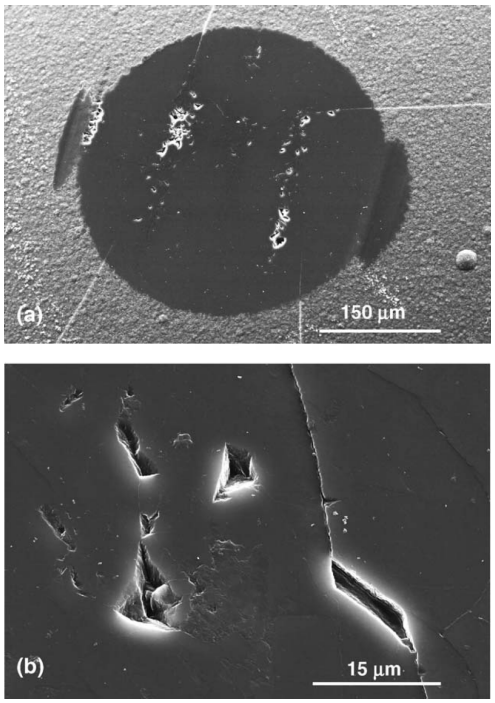

Figure 5.10: SEM micrographs taken from a ball specimen, depicting the surface degradation after the endurance tests at different magnifications. Crack features and the chipping wear mechanism are clearly evidenced.

The reported threshold load prior to delamination for the Si_3N_4 microcrystalline diamond coated tribosystem is 80 N, for a coating thickness close to that of the present work [141]. This value is twice the highest one obtained in the present work for the FL specimen, what denotes lower adhesion levels compared to the microcrystalline deposits. However, the same threshold of 40 N is found for self-mated tribosystems of NCD grown by MPCVD [150]. The wear performance of self-mated NCD films, in terms of the wear coefficient values for the ball specimens are in the order of 10^{-7} $mm^3N^{-1}m^{-1}$. These values point out to a mild wear regime. It is noteworthy that a very mild wear (5×10^{-8} $mm^3N^{-1}m^{-1}$) was measured for the endurance tests, which represent a more accurate assessment of this tribological parameter than the shorter ones. These results are similar to those obtained for self-mated microcrystalline diamond films and NCD grown by MPCVD on the same substrate material [141, 150].

5.3.4 Conclusions

NCD films were grown by HFCVD on Si_3N_4 ceramic substrates presenting surface roughness of 15 nm to 169 nm. NCD matches the starting surface during growth, mimicking its topography.

The friction behaviour of the NCD self-mated system is affected by the surface roughness, resulting in intense and ephemeral friction coefficient peaks up to 0.7. After an accommodation period also dependent on the surface roughness, very low μ values of $0.02 - 0.03$ are reached for dry sliding conditions. Self-polishing (micro-abrasion) is the predominant wear mechanism of the NCD films resulting in ultra-smooth surfaces. The lengthier tests indicate an increase of μ up to 0.15 due to some chipping of the worn NCD film on the ball.

The threshold load prior to delamination attained a value of 40 N, which denotes a good adhesion level. Wear coefficient values for the ball specimens are of the order of $\sim 10^{-7}$ $mm^3N^{-1}m^{-1}$, for the shorter tests, while the endurance tests result in very mild wear regimes (10^{-8} $mm^3N^{-1}m^{-1}$).

Acknowledgements

This work was supported by project NANODIAM (FCT/POCTI/CTM/59449/2004).

5.4 Enhanced performance of HFCVD nanocrystalline diamond self-mated tribosystems by plasma pretreatments on silicon nitride substrates [Publication VII]

C.S. Abreu, M.S. Amaral, F.J. Oliveira, A.J.S. Fernandes, J.R. Gomes, R.F. Silva

Diam. Relat. Mater., 15 (2006) 2024-2028

Abstract

Nanocrystalline diamond (NCD) coatings were grown by the hot-filament chemical vapour deposition (HFCVD) method on hydrogen plasma pretreated silicon nitride (Si_3N_4) substrates. The friction and wear behaviour of self-mated NCD films, submitted to unlubricated sliding and high applied loads (up to 90 N), was assessed using an oscillating ball-on-flat configuration in ambient atmosphere. The reciprocating tests revealed an initially high friction coefficient peak, associated to the starting surface roughness of NCD coatings ($R_q = 50$ nm). Subsequently, a steady-state regime with low friction coefficient values ($0.01 - 0.04$) sets in, related to a smoother ($R_q = 17$ nm) tribologically modified surface. A polishing wear mechanism governing the material loss was responsible for mild wear coefficients ($k \sim 10^{-7}$ mm^{3}N^{-1}m^{-1}). The hydrogen etching procedure notably increased the film adhesion with respect to untreated surfaces as demonstrated by the high threshold loads (60 N; 3.5 GPa) prior to film delamination.

Keywords: Nanocrystalline; Diamond film; Hot filament CVD; Tribology

5.4.1 Introduction

Diamond films grown by chemical vapour deposition (CVD) constitute materials of strategic importance in fields such as coatings for liquid pump seals and cutting tools [41], optical windows [58], surface acoustic wave (SAW) devices and conformal coatings for micromechanical systems (MEMS) [46, 62]. In addition, the exceptional chemical inertness and good biocompatibility of CVD diamond films, combined with an excellent wear resistance, foretell of future applications as tribomaterials in arthroplasty and other biomedical applications [151]. However, due to the polycrystalline nature of CVD diamond, the film surface is

usually too rough for immediate use of as-grown films, particularly in tribological components. One solution is polishing, which is, however, time-consuming, expensive and impractical in the case of complex geometries [94]. Another more interesting pathway consists in reducing the diamond grain size to the nanoscale level [24]. This is where very smooth nanocrystalline diamond (NCD) comes into play, with their inherent lower surface roughness while maintaining the exceptional physical properties of CVD diamond films.

Although tailoring the surface properties and structure of the films is crucial for any application, another mandatory requisite for high tribological performance is the adequate adhesion between the coating and the substrate. In that sense, because of their low thermal expansion coefficient mismatch relative to diamond and carburizing nature, silicon nitride (Si_3N_4) ceramics constitute a substrate material with high potential for the deposition of stress-free highly adherent NCD coatings [73]. Despite very promising results found in our previous studies regarding the tribological performance of self-mated NCD coated Si_3N_4 substrates [152], further optimisation of the adhesion levels is still needed in order to achieve higher threshold loads prior to film delamination under tribological stress.

The main motivation behind the present study is, therefore, to assess the effect of hydrogen plasma pretreatment prior to deposition on the adhesion levels of NCD coated Si_3N_4 ceramics subjected to sliding wear and, ultimately, on their tribological behaviour. Reciprocating sliding experiments were conducted using a self-mated configuration. Worn surfaces were analysed by scanning electron microscopy (SEM) and atomic force microscopy (AFM).

5.4.2 Experimental details

Flat square shaped Si_3N_4 samples ($10 \times 10 \times 3$ mm^3) were used as substrate material, whose processing can be found elsewhere [147]. Prior to NCD deposition, the flat ceramic substrates were submitted to the following surface finish conditions: flat lapping with 15 μm diamond slurry; hard cloth polishing with 15 μm diamond slurry; polishing to a specular finish with colloidal silica (0.25 μm). In order to activate the surface for better adhesion, the substrates were pretreated by hydrogen plasma for 30 min.

The deposition of NCD coatings was carried out in a hot-filament CVD (HFCVD) reactor

using a Ar-CH_4-H_2 gas mixture, where the Ar/H_2 and CH_4/H_2 ratios were fixed at 0.1 and 0.04, respectively. The values used for the deposition parameters were as follows: W filament temperature, 2300 °C; total gas flow, 50 ml min^{-1}; total pressure, 50 mbar; substrate temperature, 750 °C; deposition time, 12 h and 24 h. These conditions lead to a growth rate of 1.6 μmh^{-1} and a final crystallite size of about 28 nm estimated from X-ray low incident beam angle diffraction (LIBAD) measurements. A more in-depth description concerning the reactor setup can be found elsewhere [139]. For the counterface material, Si_3N_4 commercial balls (Kema Nord) having a diameter of 5 mm, were subjected, as received, to identical plasma pretreatment before NCD growth.

Self-mated unlubricated sliding tests were carried out in ambient atmosphere (ambient temperature, R.H. $50-60\%$). All tests were conducted with a reciprocating ball-on-flat tribometer, where the ball upper-specimen is pressed against an oscillating lower flat specimen at fixed applied loads varying in the range $10-90$ N. Considering a purely elastic contact model [10, p. 14–15] and a Young modulus for the Si_3N_4 substrate of 280 GPa [153], those values impose a mean Hertzian pressure in the range of about 1.9 to 4.0 GPa, respectively. The sliding experiments were performed at a constant frequency of 1 Hz, which translates to an average surface velocity of 9 mms^{-1} for a 6 mm stroke length. Total sliding distances were 86 m for the regular tests and 690 m for the endurance ones.
Friction coefficient values were determined from measurements of the lateral force from a load cell attached to the sample holder and a measure of the normal force. Wear rate assessment was done by determining the wear volume loss from SEM measurements of near-circular wear scars taken from the ball specimens [154]. SEM and AFM techniques were used to analyse the morphology of the as prepared and worn surfaces in order to identify the dominant wear modes and mechanisms, as well as to obtain surface roughness data and topographical information, respectively.

5.4.3 Results and Discussion

SEM micrographs and topographic AFM images of representative as-deposited NCD coated Si_3N_4 films (deposition time of 12 h) are shown in Fig. 5.11. The typical morphology of both plate and ball specimens can be observed on the side-by-side SEM micrograph of

Fig. 5.11 (a), where both exhibit the random nanometer-scale roughness characteristic of NCD. The spatial organisation of elemental structural units is characterised by clusters or collections of nano-sized diamond grains which appear to have grown outward in a randomised fashion from a single nucleation site. This distribution of clusters is represented on the AFM 3D scan of Fig. 5.11 (b), acquired using an intermittent contact "tapping mode" of a $100 \times 100\ \mu m^2$ region.

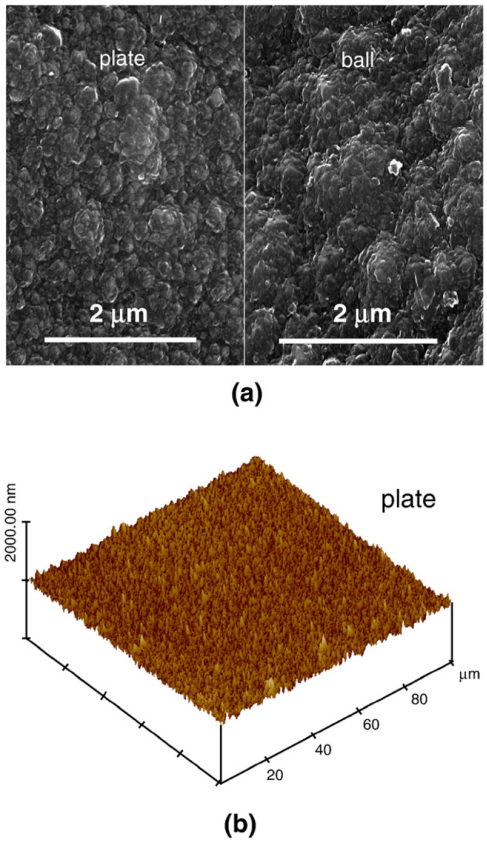

Figure 5.11: Representative SEM (a) and AFM (b) micrographs of the as-deposited NCD 12 h coated elements of the tribosystem.

The surface topography is characterised by closely spaced roughness irregularities, which could be classified as subroughness or physical relief according to the multi-level Archard's model [155]. Therefore, the surface is relatively smooth and exhibits a low r.m.s roughness (R_q) value of about 50 nm. As-grown 24 h deposited films were characterised by rougher surfaces with an R_q of about 115 nm.

NCD worn surfaces of flat and ball specimens (deposition time of 24 h) subjected to reciprocating self-mated sliding are shown in the SEM micrographs of Fig. 5.12 (a) and b, respectively. The elements of the tribosystems were subjected to an applied load of 60 N, which corresponds to a normal stress of about 3.5 GPa, and completed a sliding distance of 86 m. The flat specimen image (Fig. 5.12 (a)) shows a selected portion of the transition region corresponding to the border of the wear track.

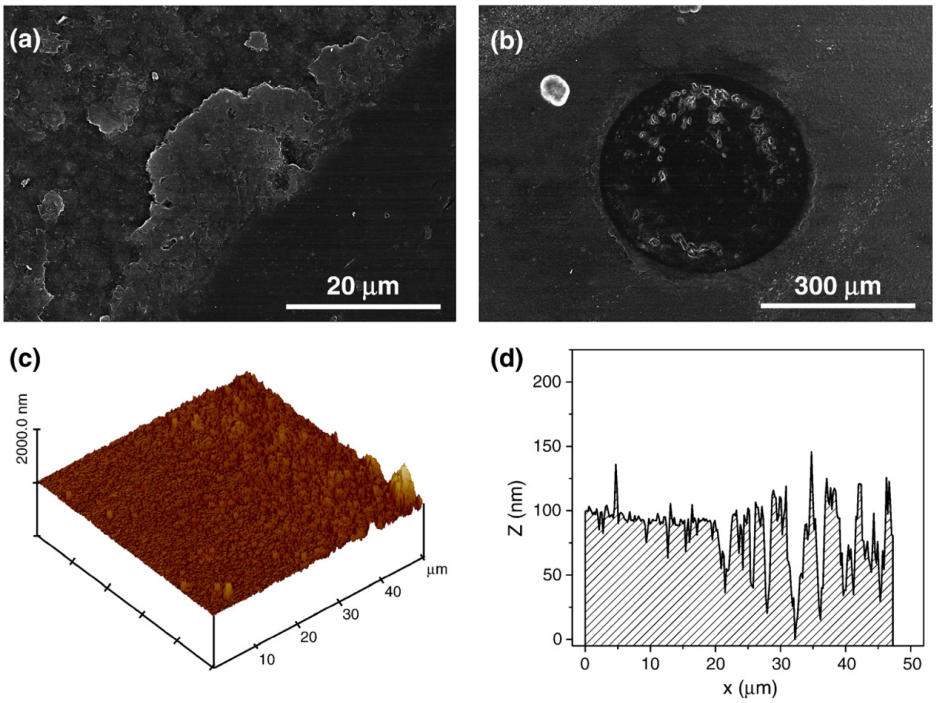

Figure 5.12: Morphologies of worn NCD 24 h coated plate (a) and ball (b). AFM 3D scan detail (c) and respective 2D profile (d) of the topographic transition between the worn track and the pristine region of the coating.

The polished NCD film (right lower side of the picture), leveled off by tribological interactions between protruding asperities [156], is sided by unworn diamond clusters (upper left side of the picture). Also visible at the transition region, there are smeared wear debris. The smooth morphology of the ablated clusters indicates a polishing wear mechanism. A similar polishing effect can be observed on the near-circular wear scar of the ball sample (Fig. 5.12 (b)). However, deep crevices are also observed, a possible evidence for brittle fracture. Such features

resulted from the intense tribological stress associated to high contact pressures combined with hard-on-hard dry sliding. Therefore, a mechanism of formation, propagation of fractures leads to the embrittlement of certain areas on the contact surface and possibly material loss by spallation. The circular areas inscribed on the balls were used to assess the wear rate of the NCD coatings. An average wear rate value for the balls (k_b) of 9.7×10^{-8} $mm^3N^{-1}m^{-1}$ was found for the 12 h deposited films. This denotes a mild wear regime for the self-mated unlubricated NCD coatings. This value was assessed from the lengthier endurance tests (690 m), which more accurately represents the wear rate since it corresponds to a "non-wear" stationary regime [135]. The highest wear rate, $k_b \sim 3.3 \times 10^{-7}$ $mm^3N^{-1}m^{-1}$, was determined for a 24 h film subjected to an applied load of 60 N and a sliding distance of 86 m. However, this value corresponds to a shorter length test and, therefore, is affected by a higher contribution from the "intensive wear" regime present at the initial running-in phase.
The AFM 3D scan in Fig. 5.12 (c) at the border of the wear track depicts the net variation on the topography from the unworn and polished regions, after 690 m of sliding distance. The respective R_q values acquired in 20×20 μm^2 scanned areas are 40 nm and 17 nm. The latter evidences the effectiveness of the polishing mechanism. A 2D profile perpendicular to the sliding direction is given in Fig. 5.12 (d) to stress the distinctive topography: extensive plateaus in the wear track region (left) and "hilly" configuration of the natural occurring NCD surface superimposed with adhered wear debris (right).

The friction behaviour of the CVD diamond films is governed by a combination of physical, chemical and mechanical interactions at their sliding interfaces. The amount of dissipated energy resulting from these friction interactions can be divided into two major contributions: a deformation component imparting from mechanical ploughing and a physical/chemical attraction or adhesion component. For rough microcrystalline CVD diamond films, a significant initial interlocking between asperities takes place, causing high friction levels at the beginning [135], in contrast to most engineering surfaces, where according to Coulomb's friction law the friction force is independent of the nature of the surface roughness. The threshold loads prior to film delamination under tribological stress were evaluated as 25 N (2.6 GPa) and 60 N (3.5 GPa), respectively for 12 h and 24 h of deposition time. Friction evolution curves at such threshold loads are depicted in Fig. 5.13 (a). An initial regime of high friction is noted, lasting

for a few cycles, but rapidly decays to very low steady-state friction coefficient values in the range $0.01 - 0.04$. This magnitude is the result of smooth passivated diamond surfaces [24, 46]. Therefore, after repeated traversals over the same contact zone and subsequent smoothing of the wear track region, friction notably drops off. For comparison purposes, in the same figure, a friction curve for an NCD/NCD experiment carried out with untreated surfaces is shown, also for an applied load at its threshold value (10 N) [152].

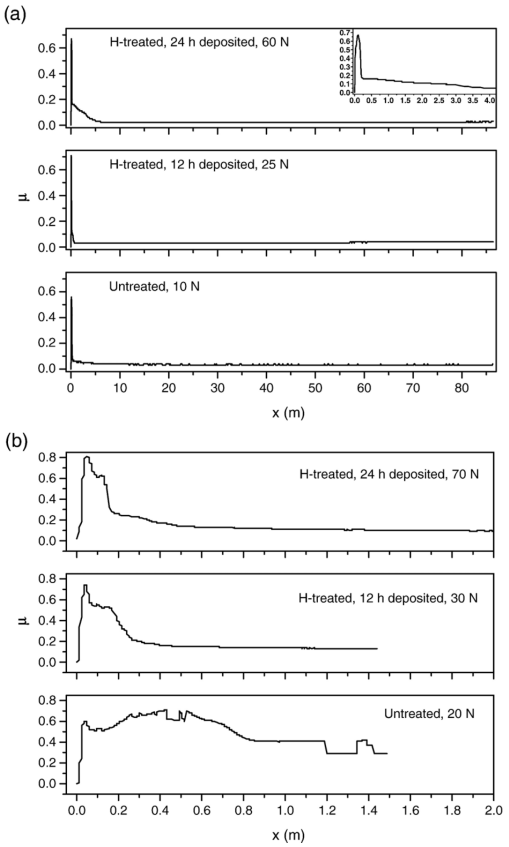

Figure 5.13: Friction coefficient evolution of self-mated experiments with NCD coated specimens subjected to: (a) threshold applied loads of 10 N, 25 N and 60 N respectively for the untreated, 12 h and 24 h coated specimens treated by hydrogen plasma (the inset gives a detail of the running-in stage of the 24 h film); (b) destructive running conditions above the threshold loads of the untreated samples (20 N), hydrogen treated 12 h (30 N) and 24 h coated (70 N) substrates.

Fig. 5.13 (b) reveals the characteristic signatures of the occurrence of early delaminations above the threshold loads for the two types of films on treated substrates. Also, a friction curve for the untreated system is given for an applied load above its threshold value. The initial friction peak in the experiments with treated substrates is substituted by a broader irregular one and the leveled value (~ 0.15) is worse than in the corresponding preserved sliding pairs (Fig. 5.13 (a)), being slightly higher than the reported one for a NCD-Si_3N_4 contact (~ 0.1) [24]. This difference may be due to the smoother NCD films ($R_q = 30$ nm) studied in the work of Erdemir et al. [24]. In the friction profile of the untreated substrates, premature film failure occurs followed by a high friction regime with a coefficient value near that of a Si_3N_4 homologous system. Direct comparison between the threshold loads of the untreated and hydrogen plasma treated substrates clearly enhances the sustained load under tribological action. This is likely the result of silicon nitride activation by an effective removal of the superficial silicon oxide layer, similar to what is observed in hydrogen plasma precleaning of silicon for electronic purposes [157].

5.4.4 Conclusions

Hydrogen plasma pretreatment of silicon nitride substrates has a beneficial effect on the delamination threshold loads under tribological stress of nanocrystalline diamond (NCD) coatings. However, the friction and wear behaviour is unchanged relatively to the untreated substrates when delamination does not occur. The hydrogen etching procedure increases the film adhesion with respect to untreated surfaces as demonstrated by the very high threshold loads (60 N; 3.5 GPa) prior to film delamination, evaluated in reciprocating ball-on-flat tests. The friction coefficient evolution is characterised by an intense initial peak, directly related to the starting surface roughness of NCD coatings ($R_q = 50$ nm). Subsequently, a steady-state regime with very low friction coefficient values ($0.01 - 0.04$) sets in, related to a very smooth ($R_q = 17$ nm) tribologically modified surface. A polishing wear mechanism governing the material loss, is responsible for mild wear coefficients ($k \sim 10^{-7}$ mm^{3}N^{-1}m^{-1}).

Acknowledgements

C.S. Abreu acknowledges PRODEP III funds for supporting his PhD work. M. Amaral acknowledges FCT for the grant SFRH/BD/9272/2002. Funding from the FCT project POCI/CTM/59449/2004–"NANODIAM" is gratefully acknowledged.

(B) WATER LUBRICATED TESTS

5.5 HFCVD nanocrystalline diamond coatings for tribo-applications in the presence of water [Publication VIII]

C.S. Abreu, M. Amaral, F.J. Oliveira, J.R. Gomes, R.F. Silva,

Accepted for publication in the international journal Diamond & Related Materials

Abstract

Nanocrystalline diamond (NCD) is increasingly popular as engineered surface coatings intended for tribo-mechanical applications. Sliding may occur in the presence of water, or aqueous solutions, for example in mechanical face seals, MEMS, or in preliminary testing bearing surfaces for biotribological applications. NCD coatings of 20 μm thickness were grown by the hot-filament chemical vapour deposition (HFCVD) method on Si_3N_4 ceramic substrates. The water lubricated NCD/NCD tribosystem was studied in an oscillating ball-on-flat tribometer. For all loading conditions up to the threshold load prior to film delamination (85 N), very low friction coefficient values ($\mu \sim 0.02$ to 0.05) combined with a high wear resistance (10^{-9} to 10^{-8} $mm^3N^{-1}m^{-1}$) were observed.

Keywords: Nanocrystalline diamond; Chemical vapour deposition (CVD); Tribology; Water lubrication

5.5.1 Introduction

Chemically vapour deposited (CVD) nanocrystalline diamond (NCD) is attracting considerable interest in functioning as an extremely hard and chemically inert material for use as protective coatings with conspicuous tribological performance [41, 46, 92, 158, 159]. Similarly to what is found for CVD polycrystalline diamond films [15], the friction behaviour of NCD is considerably affected by the environment in which sliding occurs. That being said, the evaluation of NCD friction properties and resistance to wear damage reveals itself of uttermost importance in many practical applications involving lubricated contact, frequently subjected to

high stress conditions or where stiction [160] is impairing on the good functioning of the tribosystem. In particular, sliding may occur in the presence of water, or aqueous solutions, for example in mechanical face seals [133], MEMS [60], or in preliminary testing bearing surfaces for biotribological applications [161]. To this date, tribological data concerning the sliding contact of water lubricated self-mated NCD coatings is very limited or nonexistent if involving high applied loads and, as a result, further comprehensive studies on the subject should be carried out.

To our best knowledge, a single publication [41] can be found addressing water lubricated systems involving NCD coatings, where a ball-on-disc geometry of contact was used for tribological evaluation. The sliding tests were performed with an applied normal load of 2 N, a sliding distance of 120 m and a linear speed of 0.1 ms^{-1}. Smooth ($R_a \sim 30$ nm) NCD coatings were tested against cemented carbide, two varieties of steel, titanium and aluminium alloy. They found that the initial friction coefficient was around 0.3 against cemented carbide and steel materials due to the ploughing component of friction. After a sliding distance of $5-10$ m, the friction decreased to a constant value in the leeway $0.06-0.08$ due to surface smoothening. Water lubrication further decreased the friction to very low values in the range $0.03-0.06$. They also estimated very low wear rates of the order of 10^{-10} $mm^3N^{-1}m^{-1}$ for the unlubricated NCD films.

The present authors have previously studied the tribological behaviour of unlubricated self-mated NCD coatings [152, 162]. Owing to their excellent thermal and chemical compatibility with diamond, substrates were made of silicon nitride (Si_3N_4) ceramics in order to achieve high levels of adhesion for the NCD films [73]. Results showed that the steady-state coefficient of friction displayed values in the range $0.01-0.04$, regardless of the applied load ($10-60$ N) and starting surface roughness. Calculated wear rates for the ball specimens showed a mild wear regime (10^{-7} $mm^3N^{-1}m^{-1}$).

In the present study, NCD coated Si_3N_4 films were deposited with a HFCVD apparatus and were tribologically characterised using a reciprocating ball-on-flat geometry. Applied normal loads ranged from 10 N to 90 N, in order to assess the maximum sustainable load for the water lubricated coatings submitted to tribological stress. Scanning electron microscopy (SEM) and atomic force microscopy (AFM) techniques were employed to study the morphology and

topography of worn films, as well as the prevailing friction and wear mechanisms. The friction behaviour is also compared to existing models of diamond friction.

5.5.2 Experimental Procedure

Dense Si_3N_4 ceramic substrates were produced using a processing route described elsewhere [147]. Flat samples with square geometry ($10 \times 10 \times 3$ mm^3) were diamond wheel ground (46 μm grit size), flat lapped in a metallic plate with 15 μm diamond slurry and finally polished in a soft cloth with 15 μm diamond paste. Commercial silicon nitride balls (5 mm diameter, Kema Nord) were employed as substrates for the counterbodies of the sliding experiments. In order to enhance film adhesion, all the Si_3N_4 ceramic substrates were submitted to a tetrafluoromethane (CF_4) plasma etching for 1 hour (Emitech, K 1050X). Afterwards, the substrates were immersed in an ultrasonically agitated bath of a 1 μm diamond powder suspension in n-hexane (1 g/100 ml), during 1 h, for diamond seeding and surface scratching purposes. The NCD deposition was carried out in a home-built hot-filament apparatus using a three gas mixture of $Ar/CH_4/H_2$ in volumic ratios of $Ar/H_2 = 0.1$ and $CH_4/H_2 = 0.04$. Deposition parameters were as follows: a tungsten filament temperature of 2300 °C, a total gas flow of 50 ml.min^{-1}, a total pressure of 50 mbar, and a substrate temperature of 750 °C. A deposition time of 22 hours lead to a film thickness of about 18 μm.

Self-mated tribotests were carried out using a ball-on-flat geometry contact with reciprocating motion in an adapted tribometer (Plint TE 67/R). The NCD coated balls and the square shaped flat specimens were mounted as the upper and the lower oscillating samples, respectively. The sliding contact region remained immersed in distilled water for the full 16 hours duration of the test (approx. 690 m of sliding distance). Other experimental parameters were the constant stroke length of 6 mm and 1 Hz frequency, corresponding to an average linear velocity of 9 mm.s^{-1}. Tested normal load values ranged from 10 to 90 N. These values impose a mean Hertzian pressure in the range of about 1.9 to 4.0 GPa, respectively [162]. The friction coefficient was acquired from the variation of the tangential force exerted on a load cell attached to the upper sample holder divided by the applied normal load.
The morphology and thickness of as-deposited and worn NCD films, as well as of wear debris, were studied by SEM (Hitachi S4100). The topographic features of the NCD coatings were also

characterized by tapping mode AFM measurements (Digital Instruments, IIIa). Moreover, the surface roughness parameter R_q (RMS) of pristine and damaged coatings was determined from AFM $50 \times 50\ \mu m^2$ scans.

The wear coefficient (k) of the ball specimens was estimated from Archard's law of wear considering the diameter (d) of near circular wear scars, the ball radius (r), the applied normal load (W) and sliding distance (x), as follow:

$$k = \frac{\pi d^4}{64 r W x} \tag{5.1}$$

Wear coefficient values were also estimated for the flat samples based on AFM bearing function for volume loss quantification data, described elsewhere [67].

5.5.3 Results and Discussion

The as-deposited NCD coating morphology and topography on a plate specimen is depicted in Figs. 5.14 (a) and (b), respectively. It shows a spatial organisation of micrometric clusters of nano-sized diamond grains which can be classified as subroughness or physical relief, according to the multi-level Archard's model [155]. Due to the roughening effect induced by the plasma chemical etching on the Si_3N_4 substrate, the NCD surface roughness is somewhat high, with a R_q value of about 315 nm, although localized roughness at the cluster level estimated from $2 \times 2\ \mu m^2$ AFM scans gives values around 65 nm.

The wear damaged surface of NCD coatings after testing at a load of 40 N is presented in Figs. 5.14 (c) and (d). Comparing to the as-deposited micro rough surfaces (Figs. 5.14 (a) and (b)) the worn surfaces are characterized by extensive smooth mesa-tops. The measured surface roughness attained a value of $R_q \sim 136$ nm, although a much lower figure of 15 nm was found in the mesa-tops regions alone, taken from $20 \times 20\ \mu m^2$ AFM scans. This morphology is the result of the truncation and leveling-off of salient clusters, followed by a self-polishing wear mechanism. In terms of ball specimens, the worn surfaces also exhibit a polished appearance without evidences of tribomechanically induced cracking (Fig. 5.14 (e)).

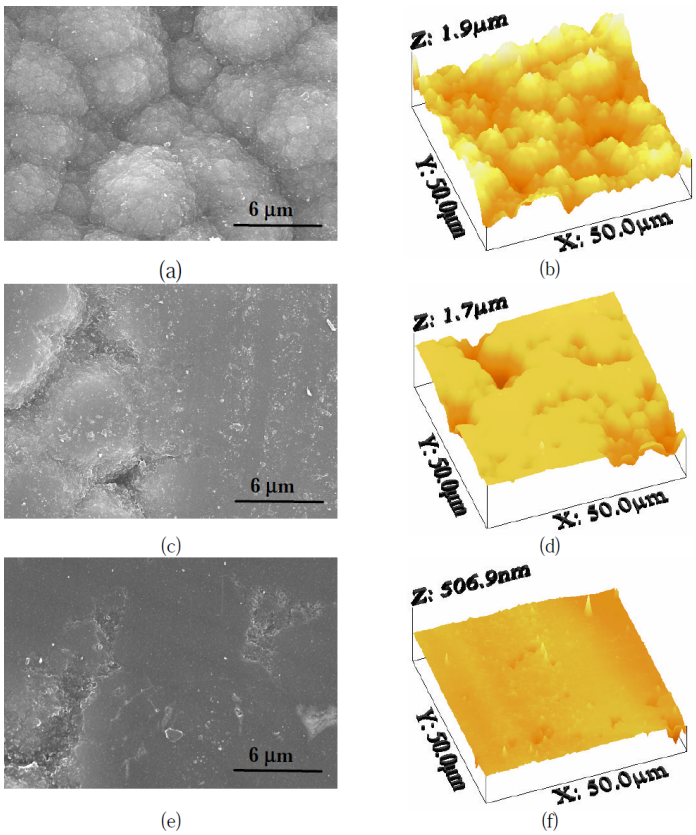

Figure 5.14: Morphology (SEM micrographs) and corresponding topography (AFM scans) of NCD coated specimens. As-deposited plates: (a) SEM and (b) AFM. Worn surfaces of plates under a load of 40 N: (c) SEM and (d) AFM. SEM micrographs of wear scars on the ball specimens tested at: (e) 40 N and (f) 85 N.

The determined threshold load before gross film detachment by delamination was 85 N. Under this stress condition, the worn surfaces became very smooth ($R_q \sim 22$ nm) in the vast majority of the wear track region of the plates (Figs. 5.15 (a) and (b)). However, lengthy cracks occur, both in the flat and ball (Fig. 5.14 (f)) specimens. Also, the onset of film delamination is visible on the ball (lower left mark at the border of the wear scar, in Fig. 5.14 (f)). This constitutes a further evidence of critical load condition in the present tribosystem. Comparing to the unlubricated performance of the NCD on NCD tribosystem, where film removal occurred above a threshold load of 60 N [162], the role of water contributed in reducing local contact stresses, therefore improving the load-supporting capability of the coating.

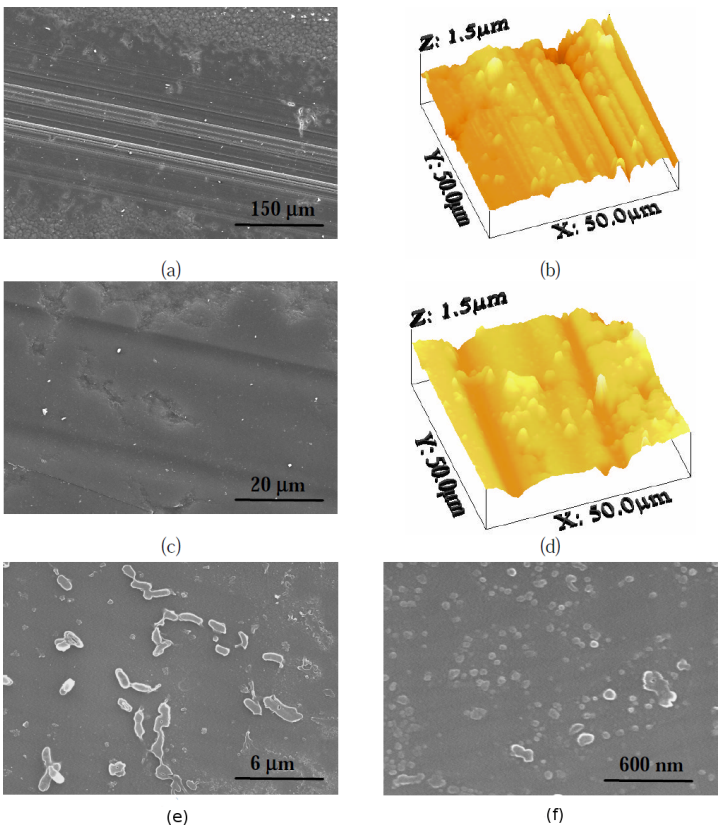

Figure 5.15: Worn surfaces of flat specimens under high loading conditions (85 N): (a) SEM and (b) AFM of ultra-polished regions, (c) SEM and (d) AFM denoting the presence of wear grooves on the wear tracks. SEM images of the morphology of the wear debris: (e) low magnification and (f) high magnification detail of the smallest particles.

Another feature observed using SEM and AFM analysis is the appearance of wear grooves oriented longitudinally in the flat specimen wear track, under high loading (Figs. 5.15 (c) and (d)). These marks are indicative of an abrasion wear process originated from three-body action of loose wear debris, whose size and morphology are depicted in Figs. 5.15 (e) and (f). These are constituted by two dimensional ranges: i) long blunted agglomerates (Fig. 5.15 (e)) originated from the initial truncation of NCD clusters, followed by smearing due to repeated traversals inside the contact interface; ii) nano-sized near-spherical debris (Fig. 5.15 (f)) resulting from wear removal of NCD nanocrystallites. A striking difference arises in relation to the dry sliding of self-mated NCD pairs, where grooves are absent and the worn surfaces appeared

very polished with the occurrence of deep crevices, for the highest loads [162]. The presence of grooves is due to the fact that water is not renewed during the test, therefore acting as a reservoir for the abrasive debris particles that cause the groove mechanism, contrarily to the dry experiments where the debris are expelled away from the contact region.

Fig. 5.16 shows representative friction coefficient curves at loads below the threshold load (Fig. 5.16 (a)) and above it (Fig. 5.16 (b)). The friction trace under a load of 60 N (Fig. 5.16 (a)) reveals an initial sharp peak of magnitude around 0.33 (regime I), associated to mechanical interlocking of protruding NCD clusters. A running-in phase (regime II) of accommodation between the opposing surfaces follows. This regime translates the blunting and leveling-off processes on the truncated clusters. Finally, a steady-state regime (regime III) sets-in with friction values of very low magnitude ($0.02 - 0.05$). A similar friction behaviour was observed for dry sliding experiments of NCD/NCD contacts, although the initial friction peaks attained two-fold values of 0.65 [162]. The reduction of the friction peak in the presence of water results from a less intense mechanical interaction between protruding NCD clusters, due to the lowering of local contact pressures. Moreover, water plays a second role in obtaining very low steady-state friction values, by passivation of the surface dangling bonds of diamond with hydrogen and hydroxyl ions [15]. In the present lubricated condition, when the experiments were conducted above the threshold load, extensive film delamination occurred. This phenomenon is depicted in the inset of Fig. 5.16 (b) and is translated by a second pronounced peak in the friction curve. Thereafter, a steady-state condition of sliding interaction between water-lubricated NCD/Si_3N_4 contact is reached, with a friction coefficient value of about 0.07.

The homologous contact of water lubricated NCD coatings denoted an excellent wear resistance, showing wear coefficient values in the range 10^{-9} to 10^{-8} $mm^3N^{-1}m^{-1}$ (Fig. 5.17), which correspond to mild to very mild wear regimes. The flat specimens exhibit one order of magnitude higher wear coefficient values than the ball counterparts. This difference is more accentuated for the highest loads, where mechanical cracking induced by fatigue becomes more important in relation to the self-polishing process that prevails at lower loads. Fatigue wear mode is characteristic of the intermittent loading on the flat specimen contrarily to what happens in the upper ball, thus explaining the lower wear coefficient values of the later. Another indi-

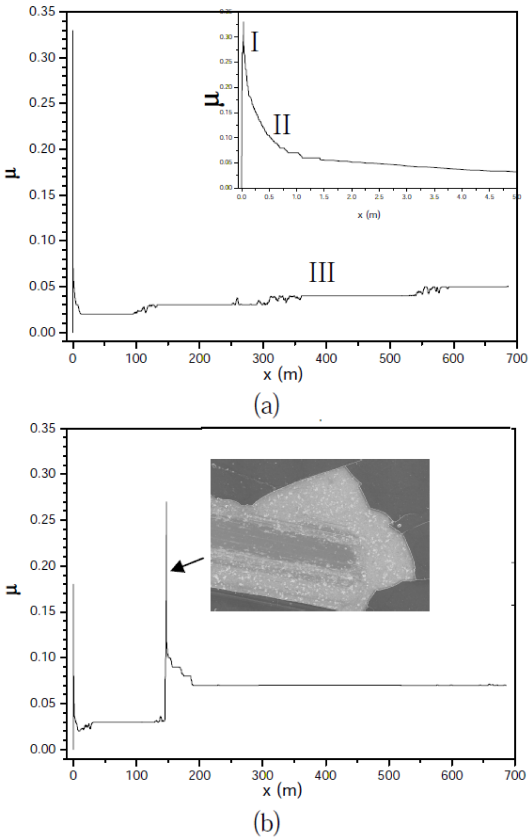

Figure 5.16: Friction curve evolution as a function of sliding distance under an applied load of 60 N (a) and 90 N (b). Details of the first 5 m of the tests are shown in the inset. Labels correspond to: I – initial friction peak; II – running-in period; III – steady-state regime. A SEM micrograph evidencing extensive film delamination is correlated to the second friction peak.

cation of this feature is the extensive delamination on the flat specimen at 90 N (Fig. 5.16 (b)), whereas the ball still preserves the NCD coating.

The results of the present NCD/NCD sliding pair in the presence of water can be compared with analogous systems involving diamond coatings. The authors of this work have also carried out a very similar study with microcrystalline CVD diamond films [163], that showed a steady-state sliding regime characterized by friction coefficient values in the range $0.04 - 0.05$ and a wear coefficient value of about 10^{-8} $mm^3N^{-1}m^{-1}$. Tribological data gathered from the present nanocrystalline CVD diamond coatings confirmed an improvement of the tribological

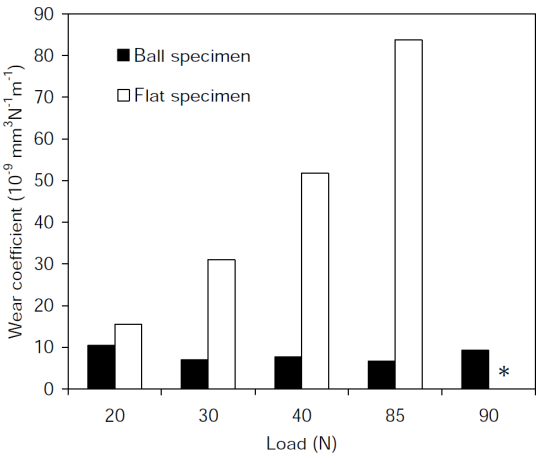

Figure 5.17: Wear coefficient values as a function of applied load for ball and flat specimens. *omitted value due to film delamination.

performance, namely in terms of wear resistance which exhibited a wear coefficient value one order of magnitude lower. As expected from the lower nominal surface roughness of the NCD films, the steady state friction regime is attained in a shorter sliding distance than for the microcrystalline CVD diamond tribopair. Nevertheless, the threshold load for film delamination is higher (160 N) in the case of microcrystalline diamond than for NCD (90 N), denoting the better adhesion level of the former coatings. Concerning the sliding of homologous surfaces of single crystal natural diamond in the presence of water, literature data [19] only refers to experiments at low normal loads ($0.5 - 1$ N) and low sliding speeds ($0.05 - 0.2$ mms^{-1}). The friction coefficient values lay in the range of $0.005 - 0.05$, although it must be pointed out that the testing conditions are not directly comparable to those of the present study. Another widely used tribological coating is DLC, however, to be best of our knowledge, there is no data on self-mated water lubricated systems for such carbon-based structures. For dissimilar pairs, like DLC/steel or DLC/tungsten carbide, it is reported that the DLC coating easily fails in the presence of water, even at low tribological loading [164, 165].

5.5.4 Conclusions

The wear behaviour of water-lubricated NCD/NCD self-mated pairs is characterized by a sequence of events: truncation, leveling-off of protruding NCD clusters and self-polishing, leading to very smooth worn surfaces. For high loading conditions (85 N), the abrasive action of debris particles results in wear grooves on the worn surface, as well as lengthy cracks start to arise. At 90 N, extensive delamination takes place in the flat specimen induced by intense fatigue wear mode.

For all loading conditions below the threshold load of 85 N, the friction behaviour shows an initial sharp peak ($\mu \sim 0.33$) related to the mechanical interlocking between salient NCD clusters, followed by a running-in regime that evolves into a very low friction regime ($\mu \sim 0.02$ to 0.05). This very low friction results from the key role of water in reducing local contact stresses and passivating the NCD surface.

Regarding the wear performance of the NCD/NCD tribopair, the wear coefficient values, varying in the leeway 10^{-9} to 10^{-8} $mm^3N^{-1}m^{-1}$, evidences a very mild to mild wear regime. The intermittent contact at the flat specimens leads to a one order of magnitude higher wear coefficient value than the ball counterparts, due to the surface fatigue contribution to the overall wear phenomenon.

Such excellent tribological behaviour envisages a great potential of applicability for NCD coatings in water-based lubricated sliding contacts such as found in face seals, MEMS for moving assemblies, and in the biotribology field.

Acknowledgements

C.S. Abreu acknowledges PRODEP III funds supporting his PhD work. The financial funding from the FCT Project POCI/CTM/59449/2004 is also gratefully acknowledged.

Chapter 6

Main conclusions and future work

The microcrystalline and nanocrystalline diamond coated silicon nitride coatings, deposited by microwave plasma-assisted and hot-filament CVD techniques, were characterized tribologically in open air and water lubricated conditions. Moreover, the load supporting capability under tribological stress of both diamond varieties was also ascertained.
The following main conclusions can be drawn based on the research conducted in this thesis:

- By using the microwave plasma-assisted CVD (MWPACVD) technique, high quality unstressed microcrystalline diamond (MCD) coatings exhibiting high levels of adhesion were deposited onto Si_3N_4 ceramic substrates, having spherical and flat geometries in order to be used in reciprocating ball-on-flat (BOF) tribo-experiments.

- SEM and AFM characterization of worn diamond films enabled to identify the prevailing wear mode of self-mated MCD coatings, under unlubricated sliding and the operating conditions of the present work, as abrasive. This mechanical wear type was driven by a self-polishing wear mechanism, achieved by the initial truncation and subsequent blunting of the diamond surface asperities in both counterparts.
  This predominant wear mechanism lead to very smooth surfaces, with AFM-based values for the surface roughness of approximately 8 nm (R_a) after sliding distances of $\sim$ 690 m (16 h tests).

- Surface damage by diamond grain pull-outs was observed for applied normal loads close to the threshold value, above which coating failure occurred by extensive delamination.

From the study involving different grain sized diamond crystallites, it was concluded that the lower grain sized MCD coatings (1.8 μm, 1 h deposition time) reached smoother surface finishings in result of the sliding wear, but tribologically failed at lower loads (> 35 N) than the larger grain sized (4.6 μm, 10 h deposition time) and thicker films that showed a threshold load of 105 N.

- Micro-Raman spectroscopic analysis revealed no detectable signs of surface graphitization or other non-diamond carbon phase, for the experimental conditions tested. On the other hand, spectra taken from worn MCD coatings revealed a diamond peak broadening effect and up-shift deviation from its characteristic position (1332 cm^{-1}), with increasing applied load and/or distance slid. This result from higher residual stress states and enhanced stress anisotropy imparted on the worn films by tribo-testing.
  The nature of the biaxial stress states was compressive and their intensity (≤ 1 GPa) was observed to be smaller for the thicker films (10 h deposition) for the whole range of applied loads ($40 - 105$ N), as a result of a better in-depth accommodation of the contact pressure during sliding contact.

- The friction behaviour of self-mated MCD coatings was characterized by three distinguishable regimes, in order: a short-life initial friction peak, arising from the mechanical interlocking between protruding diamond asperities on opposing surfaces; a "running in" regime corresponding to an accommodation phase between counterfaces and never spanning more than a few meters of distance slid; a steady-state regime characterized by very low friction coefficient values ($\mu_{st} \sim 0.03 - 0.04$), regardless of the diamond grain size, which persist through the end of the tribo-experiments.
  The magnitude of the initial peak shows strong dependence on the applied load and on the starting surface roughness of the coatings, reaching values as high as ~ 0.65 for the rougher coatings (10 h deposition time, $R_a \sim 400$ nm) under 55 N of normal load.

- Final specific wear rate values assessed from the imprinted wear scar on MCD-coated ball specimens, during tribo-testing in open air, were of the order of $10^{-8} - 10^{-7}$ $mm^3N^{-1}m^{-1}$, which denotes a very mild to mild wear regime. In the case of the flat specimens, estimates using a novel method based on AFM and OM measurements resulted in specific

wear rate values of the order of 10^{-7} $mm^3N^{-1}m^{-1}$, which are in perfect agreement with the balls' calculated specific wear rates.

▷ *In-situ* acoustic emission (AE) measurements of self-mated MCD tribo-pairs showed a correlation between the AE signal and the frictional response of sliding contacts. The features and evolution of the friction coefficient were showed to be in close agreement with the AE signal and events.

The feasibility of using AE data to monitor the different friction regimes of MCD tribosystems was, therefore, confirmed experimentally.

▷ Water lubricated self-mated MCD-coated Si_3N_4 ceramics were characterized by worn surfaces with a polished aspect after 16 h ($\sim$ 690 m) of sliding under moderate loads (up to 90 N), with the surface roughness exhibiting a five-fold reduction relative to virgin films, i.e. from R_q in the range $330-418$ nm to $\sim$ 74 nm. However, the worn surfaces also revealed the existence of some longitudinal abrasive grooves, oriented alongside the sliding direction.

From morphological and topographical data obtained by SEM and AFM techniques, the sequence of wear mechanisms taking place under water lubrication are essentially the same as those observed in open air, namely, in order: truncation of sharp diamond asperities, blunting of fractured asperities, abrasive grooving due to entrapped wear debris particles in the contact region, and a final steady-state wear regime linked to a prevailing self-polishing mechanism at the microscale by two-body and three-body abrasion.

▷ In the presence of water, the tribological assessment of MCD coatings resulted in very low friction coefficient values $(0.04-0.05)$ and specific wear rates of the order of 10^{-8} $mm^3N^{-1}m^{-1}$, despite the high applied loads.

The threshold load under tribological stress was evaluated at 160 N, above which coating failure occurred this time by progressive wear-through of the MCD films in the ball specimens, leading to the exposure of the ceramic substrate. An increase in density of abrasive wear grooves was also observed for the higher loads without, nonetheless, evidences of diamond grain pull-outs, like was the case in dry sliding. A high wear resistance ($k \sim 10^{-8}$ $mm^3N^{-1}m^{-1}$) was also sustained for loads up to the threshold limit,

which correspond to a very mild wear regime for water lubricated MCD-coated Si_3N_4 tribosystems.

- The tribological studies carried out in this thesis work show that MWPACVD microcrystalline diamond coated Si_3N_4 ceramics possess a great potential as ultra-hard tribological coatings for highly demanding applications, like in cutting tools, fluid handling, surgical instruments or where diamond-on-diamond tribosystems are required, as a result of the high wear resistance and very low friction response.

- Using a $Ar/H_2/CH_4$ three-gas mixture fed into a MWPACVD reactor, high quality nanocrystalline diamond (NCD) coatings deposited onto flat and ball-shaped Si_3N_4 substrates were successfully synthesized. The diamond grain size and film thickness were estimated to be about 12 nm and 4 μmh^{-1}, respectively, whereas typical surface roughness values (R_a) varied in the range $20-40$ nm.
  The tribological characterization of unlubricated self-mated NCD coatings using a reciprocating BOF configuration established a threshold load value of 35 N, prior to delamination by gross film detachment.

- The sliding friction behaviour of homologous pairs of MWPACVD-synthesized NCD coatings, without lubrication, was characterized by an initial ephemeral friction peak with magnitudes ranging from $0.13-0.44$, and showing an appreciable dependence on the starting surface roughness of the as-deposited coatings. This initial feature was attributed to the mechanical interlocking between opposing NCD surface asperities.
  A short running-in phase of accommodation between counterparts follows, rapidly changing into a steady-state regime that was characterized by very low friction coefficient values ($0.02-0.04$), irrespective of the starting surface roughness. This very low friction response under unlubricated conditions was attributed to the progressive worn down of the diamond nano-asperities, promoted by a self-polishing wear mechanism; thus leading to a decrease in importance of the mechanical/deformation component of friction, while the adhesional component remains unimportant in the overall friction phenomenon, as a result of the smooth passivated diamond surfaces in oxygen containing atmospheres.

- After sliding distances of ~ 690 m (16 h tests), the MWPACVD-based NCD coatings exhibited ultra-smooth surfaces with roughness values as low as 2 nm (rms). These highly polished surface finish were indicative of very low material loss rates taking place, which made the calculation of dimensional wear coefficient values for the flat specimens impractical using standard techniques, such as weight-loss or conventional profilometry.
  For the ball specimens, measurements of the lateral dimensions of the wear scars lead to low values in the range $1.0 - 1.4 \times 10^{-8}$ $mm^3N^{-1}m^{-1}$, which correspond to very mild wear regimes.

- NCD-coated Si_3N_4 films were grown successfully by the cost-effective and more versatile hot-filament CVD (HFCVD) technique, using three mechanical surface pretreatments for the ceramic substrates, i.e. flat-lapped (FL), pre-polished (PP) and polished (P). The NCD coatings matched approximately the starting surface roughness of the substrates ($R_q = 15 - 169$ nm), mimicking its topography.
  Tribo-testing using a self-mated BOF geometry in open air indicated a threshold value of 40 N and, therefore, good adhesion levels for the HFCVD-based smoother NCD coatings.

- The friction behaviour of HFCVD-based NCD coatings was characterized by very low steady-state friction coefficient values ($0.02 - 0.03$), regardless of the starting surface roughness of the samples, or in another words of the type of substrate surface pretreatment, and applied normal load up to the threshold value. In opposition, the accommodation period between antagonistic surfaces was found to be dependent on the intrinsic roughness of the as-deposited films.
  The lengthier (~ 690 m) tribo-experiments indicate an increase in friction ($\mu = 0.15$) in some of the smoother pretreated coatings (PP and P), as a result of the surface degradation originating from crack growth and chipping wear mechanism.

- The prevailing wear mode for dry sliding self-mated hot-filament NCD coatings was micro-abrasion, which results from a self-polishing wear mechanism. Specific wear rate values for the ball specimens were of the order of 10^{-8} $mm^3N^{-1}m^{-1}$, which indicates a very mild wear regime.

- ▷ Hydrogen plasma pretreatments of the Si_3N_4 substrates, prior to NCD growth by HFCVD, have showed a beneficial contribution in terms of film adhesion, resulting in a substantial increase (33%) in the threshold load (60 N, 3.5 GPa) under tribological stress, relatively to untreated coatings.

  The hydrogen etched films were also characterized by very low friction responses ($0.01-0.04$), as a result of the very smooth ($R_q = 17$ nm) tribologically modified surfaces and passivated dangling bonds. Moreover, the wear performance of these NCD coatings was also high, with an average specific wear rate of 9.7×10^{-8} $mm^3N^{-1}m^{-1}$.

- ▷ In presence of water, the wear behaviour of plasma-treated NCD/NCD self-mated pairs was characterized by the prevalence of similar wear modes and mechanisms as those happening in dry sliding. However, under high loading conditions the abrasive action of wear debris particles resulted in the production of wear grooves, as well as the initiation of lengthy cracks.

  For all loading conditions under the threshold load (85 N), the friction behaviour showed a similar trend to the one observed during dry sliding. In other words, the water was essentially responsible for reducing the local contact stresses - reflecting itself in a increased load supporting capability of the films - and for the passivation of NCD surfaces, whereby promoting a faster accommodation period.

- ▷ The wear performance of self-mated NCD films in the presence of water was characterized by even lower specific wear rates (10^{-9} $mm^3N^{-1}m^{-1}$), which denotes a very mild wear regime. One order of magnitude higher values were assessed for the flat specimens (using AFM's bearing function for volume loss quantification data) due to an intermittent contact effect, which produces a surface fatigue contribution to the overall wear phenomenon.

- ▷ The very good tribological performance demonstrated by plasma treated NCD-coated Si_3N_4 systems, envisage a great potential for these hard and highly adherent tribo-coatings in water-based lubricated sliding contacts such as found in mechanical face seals, moving assemblies or other torque generating devices for microelectromechanical systems (MEMS) and nanoelectromechanical systems (NEMS), as well as in biotribological applications like total arthroplasty.

The excellent tribological performance and enhanced adhesion demonstrated by the MCD- and NCD-coated Si_3N_4 films foretells a promising future in providing safe operation in demanding conditions and lines for future investigation will inevitably follow the route of increasing the complexity of tribo-testing, i.e. progressing from the ball-on-flat model tests to the simplified component tests, more closely related to the practical situation. Therefore, the higher degree of freedom intrinsic to say joint simulators will improve the validity of tribological data of NCD coatings for prosthetic applications, or by testing cutting tools made of MCD-coated Si_3N_4 systems during real cutting operations.

Another future line of investigation would consist on the micro-tribological evaluation of NCD-coated Si_3N_4 systems, using micro-tribometers to achieve the loading conditions particular to MEMS moving assemblies.

Bibliography

[1] M.I. Katsnelson. Graphene: carbon in two dimensions. *Materials Today*, 10(1–2):20–27, Jan-Feb 2007.

[2] C. Casiraghi, J. Robertson, and A.C. Ferrari. Diamond-like carbon for data and beer storage. *Materials Today*, 10(1–2):44–53, Jan-Feb 2007.

[3] O.A. Shenderova, Z. Hu, and D. Brenner. Carbon family at the nanoscale. In D.M. Gruen, O.A. Shenderova, and A.Y. Vul', editors, *Synthesis, Properties and Applications of Ultrananocrystalline Diamond*, volume 192 of *NATO Science Series*, pages 1–14, Dordrecht, The Netherlands, 2005. Springer.

[4] C.J.H. Wort and R.S. Balmer. Diamond as an electronic material. *Materials Today*, 11(1–2):22–28, Jan-Feb 2008.

[5] J.E. Field. *The Properties of Diamond*. Academic Press, London-New York-San Francisco, 1979.

[6] B.N.J Persson. *Sliding Friction, Physical Principles and Applications*. NanoScience and Technology Series. Springer-Verlag, Berlin Heidelberg, 1998.

[7] M. Sharif Uddin, K.H.W. Seah, X.P. Li, M. Rahman, and K. Liu. Effect of crystallographic orientation on wear of diamond tools for nano-scale ductile cutting of silicon. *Wear*, 257:751–759, 2004.

[8] F.P. Bowden and D. Tabor. *The Friction and Lubrication of Solids*. Oxford Classics Series, 2001.

[9] I.P. Hayward, I.L. Singer, and L.E. Seitzman. Effect of roughness on the friction of diamond on CVD diamond coatings. *Wear*, 157:215–227, 1992.

[10] I.M. Hutchings. *Tribology: Friction and Wear of Engineering Materials*. Metallurgy & Materials Science Series. Butterworth-Heinemann, UK, 2003.

[11] J.E. Field and C.S.J. Pickles. Strength, fracture and friction properties of diamond. *Diam. Relat. Mater.*, 5:625–634, 1996.

[12] B. Bhushan, V.V. Subramaniam, A. Malshe, B.K. Gupta, and J. Ruan. Tribological properties of polished diamond films. *J. Appl. Phys.*, 74(6):4174–4180, 1993.

[13] A. Erdemir, M. Halter, G.R. Fenske, A.R. Krauss, D.M. Gruen, S.M. Pimenov, and V.I. Konov. Durability and tribological performance of smooth diamond films produced by ar-c_{60} microwave plasmas and by laser polishing. *Surf. Coat. Tech.*, 94–95:537–542, 1997.

[14] B. Samuels and J. Wilks. The friction of diamond sliding on diamond. *J. Mater. Sci.*, 23:2846–2864, 1998.

[15] S.E. Grillo and J.E. Field. The friction of CVD diamond at high hertzian stresses: the effect of load, environment and sliding velocity. *J. Phys. D: Appl. Phys.*, 33:595–602, 2000.

[16] M. Casey and J. Wilks. The friction of diamond sliding on polished cube faces of diamond. *J. Phys. D: Appl. Phys.*, 6:1772–1781, 1973.

[17] Z. Feng and J.E. Field. The friction and wear of diamond sliding on diamond. *J. Phys. D: Appl. Phys.*, 25:A33–A37, 1992.

[18] S.E. Grillo and J.E. Field. High reduction of diamond friction by oxygen containing liquids. *Diam. Relat. Mater.*, 9:185–190, 2000.

[19] S.E. Grillo and J.E. Field. The friction of natural and CVD diamond. *Wear*, 254:945–949, 2003.

[20] K. Holmberg and A. Matthews. *Coatings Tribology, Properties, Techniques and applications in Surface Engineering*, chapter 1. Elsevier, 1994.

[21] C. Zuiker, A.R. Krauss, D.M.Gruen, X. Pan, J.C. Li, R. Csencsits, A. Erdemir, C. Bindal, and G. Fenske. Physical and tribological properties of diamond films grown in argon-carbon plasmas. *Thin Solid Films*, 270:154–159, 1995.

[22] K. Miyoshi. Surface design and engineering toward wear-resistant, self-lubricating diamond films and coatings. *NASA/TM-1999-208905*, pages 1–11, 1999.

[23] M.I. De Barros, L. Vandenbulcke, J. Fontaine, G. Farges, M. Vayer, and R. Erre. Tribological performance of diamond-coated Ti-6Al-4V alloy with respect to diamond characteristics. *Surf. Coat. Tech.*, 127:193–202, 2000.

[24] A. Erdemir, G.R. Fenske, A.R. Krauss, D.M. Gruen, T.McCauley, and R.T. Csencsits. Tribological properties of nanocrystalline diamond films. *Surf. Coat. Tech.*, 120–121:565–572, 1999.

[25] K. Miyoshi, M. Murakawa, S. Watanabe, S. Takeuchi, S. Miyake, and R.L.C. Wu. CVD diamond, DLC, and c-BN coatings for solid film lubrication. *Tribol. Lett.*, 5:123–129, 1998.

[26] K. Miyoshi and R.L.C. Wu. Measurements and diagnostics of diamond films and coatings. *Measurement*, 29:113–126, 2001.

[27] H.K. Tönshoff, A. Mohlfeld, C. Grey, and J. Winkler. Mechanical pretreatment for improved adhesion of diamond coatings. *Surf. Coat. Tech.*, 116–119:440–446, 1999.

[28] M. Schmitt, D. Paulmier, and T. Le Huu. Influence of diamond crystal orientation on their tribological behaviour under various environments. *Thin Solid Films*, 343–344:226–229, 1999.

[29] T. Xu, S. Yang, J. Lu, Q. Xue, J. Li, W. Guo, and Y. Sun. Characterization of nanocrystalline diamond films implanted with nitrogen ions. *Diam. Relat. Mater.*, 10:1441–1447, 2001.

[30] A. Sokołowska, J. Rudnicki, P. Niedzielski, A. Boczkowska, G. Bogusławski, T. Wierzchoń, and S. Mitura. TiN-NCD composite coating produced on the Ti6Al4V alloy for medical applications. *Surf. Coat. Tech.*, 200:87–89, 2005.

[31] Y. Tzeng. Very low friction for diamond sliding on diamond in water. *Appl. Phys. Lett.*, 63:3586–3588, 1993.

[32] M.N. Gardos. Tribological fundamentals of polycrystalline diamond films. *Surf. Coat. Tech.*, 113:183–200, 1999.

[33] K. Miyoshi. Friction and wear properties of as-deposited and carbon ion-implanted diamond films. *Mater. Sci. Eng. A*, 209:38–53, 1996.

[34] K. Miyoshi, M. Murakawa, S. Watanabe, S. Takeuchi, and R.L.C. Wu. Tribological characteristics and applications of superhard coatings: CVD diamond, DLC, and c-BN. *NASA/TM-1999-209189*, pages 1–6, 1999.

[35] C. Donnet and A. Erdemir. Solid lubricant coatings: recent developments and future trends. *Tribol. Lett.*, 17:389–397, 2004.

[36] S. Hogmark, S. Jacobson, and M. Larsson. Design and evaluation of tribological coatings. *Wear*, 246:20–33, 2000.

[37] A. Schade, S.M. Rosiwal, and R.F. Singer. Tribological behaviour of $\langle 100 \rangle$ and $\langle 111 \rangle$ fibre textured CVD diamond films under planar sliding contact. *Diam. Relat. Mater.*, 15:1682–1688, 2006.

[38] J. Gunnars and A. Alahelisten. Thermal stresses in diamond coatings and their influence on coating wear and failure. *Surf. Coat. Tech.*, 80:303–312, 1996.

[39] L. Vandenbulcke and M.I. De Barros. Deposition, structure, mechanical properties and tribological behavior of polycrystalline to smooth fine-grained diamond coatings. *Surf. Coat. Tech.*, 146–147:417–424, 2001.

[40] M. Perle, C. Bareiss, S.M. Rosiwal, and R.F. Singer. Generation and oxidation of wear debris in dry running tests of diamond coated SiC bearings. *Diam. Relat. Mater.*, 15:749–753, 2006.

[41] P. Hollman, O. Wanstrand, and S. Hogmark. Friction properties of smooth nanocrystalline diamond coatings. *Diam. Relat. Mater.*, 7:1471–1477, 1998.

[42] K.-H. Habig. Fundamentals of the tribological behaviour of diamond, diamond-like carbon and cubic boron nitride coatings. *Surf. Coat. Tech.*, 76-77:540–547, 1995.

[43] J. Qian, C. Pantea, J. Huang, T.W. Zerda, and Y. Zhao. Graphitization of diamond powders of different sizes at high pressure-high temperature. *Carbon*, 42:2691–2697, 2004.

[44] Yu. V. Butenko, V.L. Kuznetsov, A.L. Chuvilin, V.N. Kolomiichuk, S.V. Stankus, R.A. Khairulin, and B. Segall. Kinetics of the graphitization of dispersed diamonds at "low" temperatures. *J. Appl. Phy.*, 88(7):4380–4388, 2000.

[45] K. Miyoshi. Surface diagnostics in tribology technology and advanced coatings development. *NASA/TM-1999-208527*, pages 1–8, 1999.

[46] D.M. Gruen. Nanocrystalline diamond films. *Annu. Rev. Mater. Sci.*, 29:211–259, 1999.

[47] C. Met, L. Vandenbulcke, and M.C. Sainte Catherine. Friction and wear characteristics of various prosthetic materials sliding against smooth diamond-coated titanium alloy. *Wear*, 255:1022–1029, 2003.

[48] S. Affatato, M.Frigo, and A. Toni. An *in vitro* investigation of diamond-like carbon as a femoral head coating. *J. Biomed. Mater. Res. Part B: (Appl. Biomater.)*, 53:221–226, 2000.

[49] S.C. Scholes, A. Unsworth, R.M. Hall, and R. Scott. The effects of material combination and lubricant on the friction of total hip prostheses. *Wear*, 241:209–213, 2000.

[50] S.M. Pimenov, A.A. Smolin, E.D. Obraztsova, V.I. Konov, U. Bögli, A. Blatter, M. Maillat, A. Leijala, J. Burger, H.E. Hintermann, and E.N. Loubnin. Tribological behaviour of smooth diamond films. *Surf. Coat. Tech.*, 76–77:572–578, 1995.

[51] V. Ralchenko, A. Saveliev, S. Voronina, A. Dementjev, K. Maslakov, M. Slaerno, A. Podesta, and P. Milani. Nanodiamond seeding for nucleation and growth of CVD diamond films. In D.M. Gruen, O.A. Shenderova, and A.Y. Vul', editors, *Synthesis, Properties and Applications of Ultrananocrystalline Diamond*, volume 192 of *NATO Science Series*, pages 109–124, Dordrecht, The Netherlands, 2005. Springer.

[52] K. Mallika and R. Komanduri. Low pressure microwave plasma assisted chemical vapor deposition (MPCVD) of diamond coatings on silicon nitride cutting tools. *Thin Solid Films*, 396:145–165, 2001.

[53] A. Erdemir. Design criteria for superlubricity in carbon films and related microstructures. *Tribol. Int.*, 37:577–583, 2004.

[54] B. Bhushan. Chemical, mechanical and tribological characterization of ultra-thin and hard amorphous carbon coatings as thin as 3.5 nm: recent developments. *Diam. Relat. Mater.*, 8:1985–2015, 1999.

[55] P.J. Kelly, R.D. Arnell, M.D. Hudson, A.E.J. Wilson, and G. Jones. Enhanced mechanical seal performance through CVD diamond films. *Vacuum*, 61:61–74, 2001.

[56] B. Bhushan. Micro/nanotribology and materials characterization studies using scanning probe microscopy. In Bharat Bushan, editor, *Nanotribology and Nanomechanics: An Introduction*, chapter 8. Springer-Verlag, Berlin Heidelberg, 2005.

[57] E. Gnecco, R. Bennewitz, O. Pfeiffer, A. Socoliuc, and E. Meyer. Friction and wear on the atomic scale. In Bharat Bushan, editor, *Nanotribology and Nanomechanics: An Introduction*, chapter 10. Springer-Verlag, Berlin Heidelberg, 2005.

[58] T.P. Mollart and K.L. Lewis. The infrared optical properties of CVD diamond at elevated temperatures. *Phys. Stat. Sol. (a)*, 186:309–318, 2001.

[59] J.L. Davidson and W.P. Kang. Applying CVD diamond and particulate nanodiamond. In D.M. Gruen, O.A. Shenderova, and A.Y. Vul', editors, *Synthesis, Properties and Applications of Ultrananocrystalline Diamond*, volume 192 of *NATO Science Series*, pages 357–372, Dordrecht, The Netherlands, 2005. Springer.

[60] M. Dipalo, J. Kusterer, K. Janischowsky, and E. Kohn. N-type doped nano-diamond in a first MEMS application. *Phys. Stat. Sol. (a)*, 203:3036–3041, 2006.

[61] T. Çağin, J. Che, M.N. Gardos, A. Fijany, and W.A. Goddard III. Simulation and experiments on friction and wear of diamond: a material for MEMS and NEMS application. *Nanotechn.*, 10:278–284, 1999.

[62] A.R. Krauss, O. Auciello, D.M. Gruen, A. Jayatissa, A. Sumant, J. Tucek, D.C. Mancini, N. Moldovan, A. Erdemir, D. Ersoy, M.N. Gardos, H.G. Busmann, E.M. Meyer, and M.Q. Ding. Ultrananocrystalline diamond thin films for MEMS and moving mechanical assembly devices. *Diam. Relat. Mater.*, 10:1952–1961, 2001.

[63] F. Deuerler, N. Woehrl, and V. Buck. Characterisation of nanostructured diamond coatings on various hardmetal surfaces. *Int. J. Refract. Met. & Hard Mat.*, 24:392–398, 2006.

[64] C. Manfredotti, A. Lo Guidice, C. Ricciardi, C. Paolini, E. Massa, F. Fizzoti, and E. Vittone. CVD diamond microdosimeters. *Nucl. Inst. Meth. Phys. Res. Sect. A*, 458:360–364, 2001.

[65] A.R. Mahon, J.H. MacDonald, A. Mainwood, and R.J. Ott. Characterisation of CVD diamond as a detector of DNA. *Diam. Relat. Mater.*, 8:1748–1752, 1999.

[66] M. Adamschik, M. Hinz, C. Maier, P. Schmid, H. Seliger, E.P. Hofer, and E. Kohn. Diamond micro system for bio-chemistry. *Diam. Relat. Mater.*, 10:722–730, 2001.

[67] M. Amaral, C.S. Abreu, F.J. Oliveira, J.R. Gomes, and R.F. Silva. Biotribological performance of NCD coated Si_3N_4-bioglass composites. *Diam. Relat. Mater.*, 16:790–795, 2007.

[68] M. Amaral, C.S. Abreu, F.J. Oliveira, J.R. Gomes, and R.F. Silva. Tribological characterization of NCD in physiological fluids. *Diam. Relat. Mater.*, 17:848–852, 2008.

[69] S. Danyluk, M. McNallan, and D.S. Park. Friction and wear of silicon nitride exposed to moisture at high temperatures. In S. Jahanmir, editor, *Friction and wear of ceramics*, chapter 4. Marcel Dekker Inc., New York, USA, 1994.

[70] S. Jahanmir. Advanced ceramics in tribological applications. In S. Jahanmir, editor, *Friction and wear of ceramics*, chapter 1. Marcel Dekker Inc., New York, USA, 1994.

[71] S.F. Wayne and S.T. Buljan. Microstructure and wear resistance of silicon nitride composites. In S. Jahanmir, editor, *Friction and wear of ceramics*, chapter 11. Marcel Dekker Inc., New York, USA, 1994.

[72] L.M.M. Stals, M. Nesladek, and C. Quaeyhaegens. Current industrial practice. Critical issues in hard PVD and PA-CVD coatings. *Surf. Coat. Tech.*, 91:230–239, 1997.

[73] M. Belmonte, A.J.S. Fernandes, F.M. Costa, F.J. Oliveira, and R.F. Silva. Adhesion behaviour assessment on diamond coated silicon nitride by acoustic emission. *Diam. Relat. Mater.*, 12:733–737, 2003.

[74] F. Bénédic, F. Mohasseb, P. Bruno, F. Silva, G. Lombardi, K. Hassouni, and A. Gicquel. Synthesis of nanocrystalline diamond films in $Ar/H_2/CH_4$ microwave discharges. In D.M. Gruen, O.A. Shenderova, and A.Y. Vul', editors, *Synthesis, Properties and Applications of Ultrananocrystalline Diamond*, volume 192 of *NATO Science Series*, pages 79–92, Dordrecht, The Netherlands, 2005. Springer.

[75] F. Mohasseb, K. Hassouni, F. Bénédic, G. Lombardi, and A. Gicquel. Modelling of $Ar/H_2/CH_4$ microwave discharges used for nanocrystalline diamond growth. In D.M. Gruen, O.A. Shenderova, and A.Y. Vul', editors, *Synthesis, Properties and Applications of Ultrananocrystalline Diamond*, volume 192 of *NATO Science Series*, pages 93–108, Dordrecht, The Netherlands, 2005. Springer.

[76] A.C. Ferrari and J. Robertson. Origin of the 1150-cm^{-1} Raman mode in nanocrystalline diamond. *Phys. Rev. B*, 63:121405(R)–4, 2001.

[77] T. Wang, H.W. Xin, Z.M. Zhang, Y.B. Dai, and H.S. Shen. The fabrication of nanocrystalline diamond films using hot filament CVD. *Diam. Relat. Mater.*, 13:6–13, 2004.

[78] K.-H. Zum Gahr. *Microstructure and wear of materials*. Number 10 in Tribology Series. Elsevier Science Publishers, Amsterdam, The Netherlands, 1987.

[79] M.N. Gardos and S.A. Gabelich. Atmospheric effects of friction, friction noise and wear with silicon and diamond. part I. test methodology. *Tribol. Lett.*, 6:79–86, 1999.

[80] J.H. Dumbleton. *Tribology of natural and artificial joints*. Number 3 in Tribology Series. Elsevier Scientific Publishing Company, Amsterdam, The Netherlands, 1981.

[81] R. Bennewitz. Friction force microscopy. *Materials Today*, 8(5):42–48, May 2005.

[82] D. Klaffke. Fretting wear of ceramics. *Tribology Int.*, 22:89–101, 1989.

[83] A. Skopp and D. Klaffke. Aspects of tribological testing of diamond coatings. *Surf. Coat. Tech.*, 98:1027–1037, 1998.

[84] S. Chandrasekar, T.N. Farris, and B. Bhushan. Ceramics for magnetic recording applications. In S. Jahanmir, editor, *Friction and wear of ceramics*, chapter 16. Marcel Dekker Inc., New York, USA, 1994.

[85] T.F.J. Quinn. *Physical analysis for tribology*. Cambridge University Press, UK, 2005.

[86] J.H. Hafner. Probes in scanning microscopies. In Bharat Bushan, editor, *Nanotribology and Nanomechanics: An Introduction*, chapter 3. Springer-Verlag, Berlin Heidelberg, 2005.

[87] F.J. Giessibl. AFM's path to atomic resolution. *Materials Today*, 8(5):32–41, May 2005.

[88] S. Morita, F. J. Giessibl, Y. Sugawara, H. Hosoi, K. Mukasa, A. Sasahara, and H. Onishi. Noncontact atomic force microscopy and its related topics. In Bharat Bushan, editor, *Nanotribology and Nanomechanics: An Introduction*, chapter 4. Springer-Verlag, Berlin Heidelberg, 2005.

[89] A. Schirmeisen, B. Anczykowski, and H. Fuchs. Dynamic force microscopy. In Bharat Bushan, editor, *Nanotribology and Nanomechanics: An Introduction*, chapter 8. Springer-Verlag, Berlin Heidelberg, 2005.

[90] G.W. Stachowiak and A.W. Batchelor. *Engineering Tribology*. Butterworth-Heinemann, 2 edition, 2001.

[91] Y. Fu, B. Yan, N.L. Loh, C.Q. Sun, and P. Hing. Characterization and tribological evaluation of MW-PACVD diamond coatings deposited on pure titanium. *Mater. Sci. Eng. A*, 282:38–48, 2000.

[92] A. Olszyna and J. Smolik. Nanocrystalline diamond-like carbon coatings produced on the Si_3N_4-TiC composites intended for the edges of cutting tools. *Thin Solid Films*, 459:224–227, 2004.

[93] N. Anderson, A. Hartschuh, and L. Novotny. Near-field Raman microscopy. *Materials Today*, 8(5):50–54, May 2005.

[94] L.C. Nistor, J. Van Landuyt, V.G. Ralchenko, E.D. Obraztsova, and A.A. Smolin. Nanocrystalline diamond films: transmission electron microscopy and Raman spectroscopy characterization. *Diam. Relat. Mater.*, 6:159–168, 1997.

[95] H. Windischmann and K.J. Gray. Stress measurement of CVD diamond films. *Diam. Relat. Mater.*, 4:837–842, 1995.

[96] D.S. Knight and W.B. White. Characterization of diamond films by raman spectroscopy. *J. Mater. Res.*, 4:385–393, 1989.

[97] H. Herchen, M.A. Cappeli, M.I. Landstrass, M.A. Plano, and M.D. Moyer. First-order Raman scattering in homoepitaxial chemical vapor deposited diamond at elevated temperatures. *Thin Solid Films*, 212:206–215, 1992.

[98] H. Richter, Z.P. Wang, and L. Ley. The one phonon Raman spectrum in microcrystalline silicon. *Solid State Commun.*, 39:625–629, 1981.

[99] J.W. Ager III and M.D. Drory. Quantitative measurements of residual biaxial stress by Raman spectroscopy in diamond grown on a Ti alloy by chemical vapor deposition. *Phys. Rev. B*, 48:2601–2607, 1993.

[100] S. Lingard and K.K. Ng. An investigation of acoustic emission in sliding friction and wear of metals. *Wear*, 130:367–379, 1989.

[101] C.L. Jiaa and D.A. Dornfeld. Experimental studies of sliding friction and wear via acoustic emission signal analysis. *Wear*, 139:403–424, 1990.

[102] A. Morhain and D. Mba. Bearing defect diagnosis and acoustic emission. *Proc. Inst. Mech. Eng, Part J: J. Eng. Tribol.*, 217:257–272, 2003.

[103] T. Yoshioka and T. Fujiwara. A new acoustic emission source locating system for the study of rolling contact fatigue. *Wear*, 81:183–186, 1982.

[104] T. Skåre and F. Krantz. Wear and frictional behaviour of high strength steel in stamping monitored by acoustic emission technique. *Wear*, 255:1471–1479, 2003.

[105] X. Li. A brief review: acoustic emission method for tool wear monitoring during turning. *Int. J. Machine Tools & Manufacture*, 42:157–165, 2002.

[106] K.-H. Cha, S.-C. Lee, D.-K. Han, S.-M. Lee, and D.-E. Kim. Experimental investigation of AE and friction signals related to the durability of head/disk interface. *Tribol. Int.*, 32:399–405, 1999.

[107] K. Matsuoka, K. Taniguchi, and M. Nakakita. In-situ wear monitoring of slider and disk using acoustic emission. *J. Trib.*, 123:175–180, 2001.

[108] T. Hisakado and T. Warashina. Relationship between friction and wear properties and acoustic emission characteristics: iron pin on hardened bearing steel disk. *Wear*, 216:1–7, 1998.

[109] E.N. Diei. *Investigation of the milling process using acoustic emission signal analysis.* PhD thesis, Department of Mechanical Engineering, University of California, Berkeley, CA, 1985.

[110] J. Miettinen and V. Siekkinen. Acoustic emission in monitoring sliding contact behaviour. *Wear*, 181–183:897–900, 1995.

[111] J. Hanchi and B.E. Klamecki. Acoustic emission monitoring of the wear process. *Wear*, 145:1–27, 1991.

[112] S.A. Catledge and Y.K. Vohra. Mechanical properties and quality od diamond films synthesized on Ti-6Al-4V alloy using the microwave plasmas of CH_4/H_2 and CO/H_2 systems. *J. Appl. Phys.*, 83:198–204, 1998.

[113] N.G. Ferreira, E. Abramof, N.F. Leite, E.J. Corat, and V.J. Trava-Airoldi. Analysis of residual stress in diamond films by X-ray diffraction and micro-Raman spectroscopy. *J. Appl. Phys.*, 91(4):2466–2472, 2002.

[114] G.A. Jones. On the tribological behaviour of mechanical seal face materials in dry line contact, part II. Bulk ceramics, diamond and diamond-like carbon films. *Wear*, 256:433–455, 2004.

[115] M. Belmonte, V.A. Silva, A.J.S. Fernandes, F. Costa, and R. Silva. Surface pretreatments of silicon nitride for CVD diamond deposition. *J. Am. Ceram. Soc.*, 86(5):749–754, 2003.

[116] M.R. Soares, M. Belmonte, and R.F. Silva. Low incident angle and classical X-ray diffraction analysis of residual stresses in diamond coated Si_3N_4. *J. Appl. Phys.*, 94:5633–5638, 2003.

[117] P.D. Warren. Determining the fracture toughness of brittle materials by hertzian indentation. *J. Euro. Ceram. Soc.*, 15:385–394, 1995.

[118] M. Mermoux, B. Marcus, L. Abello, N. Rosman, and G. Lucazeau. In situ Raman monitoring of the growth of CVD diamond films. *J. Raman Spectrosc.*, 34:505–514, 2003.

[119] E. Zeiler, D. Klaffke, K. Hiltner, T. Grögler, S.M. Rosiwal, and R.F. Singer. Tribological performance of mechanically lapped chemical vapor deposited diamond coatings. *Surf. Coat. Tech.*, 116–119:599–608, 1999.

[120] S. Hogmark, P. Hollman, A. Alahelisten, and P. Hedenqvist. Direct current bias applied to hot flame diamond deposition produces smooth low friction coatings. *Wear*, 200:225–232, 1996.

[121] E. Uhlmann, U. Lachmund, and M. Brucher. Wear behavior of HFCVD-diamond coated carbide and ceramic tools. *Surf. Coat. Tech.*, 131:395–399, 2000.

[122] U. Bogli, A. Blatter, S.M. Pimenov, E.D. Obraztsova, A.A. Smolin, M. Maillat, A. Leijala, J. Burger, H.E. Hintermann, and E.N. Loubnin. Tribological properties of smooth polycrystalline diamond films. *Diam. Relat. Mater.*, 4:1009–1019, 1995.

[123] P. Hollman, H. Bjorkman, A. Alahelisten, and S. Hogmark. Diamond coatings applied to mechanical face seals. *Surf. Coat. Tech.*, 105:169–174, 1998.

[124] R. Gahlin, A. Alahelisten, and S. Jacobson. The effects of compressive stresses on the abrasion of diamond coatings. *Wear*, 196:226–233, 1996.

[125] M. G. Donato, G. Faggio, M. Marinelli, G. Messina, E. Milani, A. Paoletti, S. Santangelo, A. Tucciarone, and G. Verona Rinati. High quality CVD diamond: a Raman scattering and photoluminescence study. *Eur. Phys. J. B*, 20:133–139, 2001.

[126] M.I. De Barros, L. Vandenbulcke, and J.J. Bléchet. Influence of diamond characteristics on the tribological behaviour of metals against diamond-coated Ti-6Al-4V alloy. *Wear*, 249:68–78, 2001.

[127] Maria Isabel de Barros. *Procédés de dépôt de revêtements de diamant sur substrats métallurgiques, caractérisations et propriétés tribologiques.* PhD thesis, Université D'Orléans, 2000.

[128] J.W. Ager III. Residual stress in diamond and amorphous carbon films. *Mater. Res. Soc. Symp. Proc*, 383:143–152, 1995.

[129] K.J. Gray, J.M. Olson, and H. Windischmann. Measurement of stress in CVD diamond films. *Mater. Res. Soc. Symp. Proc*, 383:135–142, 1995.

[130] T. Grögler, A. Franz, D. Klaffke, S. M. Rosiwal, and R.F. Singer. Tribological optimization of CVD diamond coated Ti-6Al-4V. *Diam. Relat. Mater.*, 7:1342–1347, 1998.

[131] Z.M. Zhang, H.S. Shen, F.H. Sun, X.C. He, and Y.Z. Wan. Fabrication and application of chemical vapor deposition diamond-coated drawing dies. *Diam. Relat. Mater.*, 10:33–38, 2001.

[132] H. Yoshikawa and A. Nishiyama. CVD diamond coated insert for machining high silicon aluminum alloys. *Diam. Relat. Mater.*, 8:1527–1530, 1999.

[133] M.A. Tomé, A.J.S. Fernandes, F.J. Oliveira, R.F. Silva, and J.M. Carrapichano. High performance sealing with CVD diamond self-mated rings. *Diam. Relat. Mater.*, 14:617–621, 2005.

[134] Y. Enomoto, S. Miyake, and S. Yazu. Friction and wear of synthetic diamond with and without n+ implantation and CVD diamond coating in air, water and methanol. *Tribol. Lett.*, 2:241–246, 1996.

[135] C.S. Abreu, F.J. Oliveira, M. Belmonte, A.J.S. Fernandes, J.R. Gomes, and R.F. Silva. Self-mated CVD diamond coated silicon nitride films: tribological behaviour under high loads. *Tribol. Lett.*, 21:141–151, 2006.

[136] P. Kapsa and Y. Enomoto. Sliding damage on hot-pressed and sintered silicon nitride caused by a diamond tip under controlled humidity. *Wear*, 127:65–83, 1988.

[137] J. Lee, B. Hong, R. Messier, and R.W. Collins. Nucleation and bulk film growth kinetics of nanocrystalline diamond prepared by microwave plasma-enhanced chemical vapor deposition on silicon substrates. *Appl. Phys. Lett.*, 69:1716, 1996.

[138] D.M. Bhusari, J.R. Yang, T.Y. Wang, K.H. Chen, S.T. Lin, and L.C. Chen. Effects of substrate pretreatment and methane fraction on the optical transparency of nanocrystalline diamond thin films. *J. Mater. Res.*, 13:1769–1773, 1998.

[139] M. Amaral, F.J. Oliveira M. Belmonte, A.J.S. Fernandes, F.M. Costa, and R.F. Silva. Hot-filament chemical vapour deposition of nanodiamond on silicon nitride substrates. *Diam. Relat. Mater.*, 13:643–647, 2004.

[140] M. Amaral, F. Mohasseb, F.J. Oliveira, F. Bénédic, R.F. Silva, and A. Gicquel. Nanocrystalline diamond coating of silicon nitride ceramics by microwave plasma-assisted CVD. *Thin Solid Films*, 482:232–236, 2005.

[141] C.S. Abreu, F.J. Oliveira, M. Belmonte, A.J.S. Fernandes, R.F. Silva, and J.R. Gomes. Grain size effect on self-mated CVD diamond dry tribosystems. *Wear*, 259:771–778, 2005.

[142] P. Bruno, F. Bénédic, A. Tallaire, F. Silva, F.J. Oliveira, M. Amaral, A.J.S. Fernandes, G. Cicala, and R.F. Silva. Deposition of nanocrystalline diamond films on silicon nitride ceramic substrates using pulsed microwave discharges in $Ar/H_2/CH_4$ gas mixture. *Diam. Relat. Mater.*, 14:432–436, 2005.

[143] G. Cicala, P. Bruno, F. Bénédic, F. Silva, K. Hassouni, and G.S. Senesi. Nucleation, growth and characterization of nanocrystalline diamond films. *Diam. Relat. Mater.*, 14:421–425, 2005.

[144] R. Pfeiffer, H. Kuzmany, P. Knoll, S. Bokova, N. Salk, and B. Günther. Evidence for *trans*-polyacetylene in nano-crystalline diamond films. *Diam. Relat. Mater.*, 12:268–271, 2003.

[145] P. Bruno, F. Bénédic, F. Mohasseb, F. Silva, and K. Hassouni. Effects of substrate temperature on nanocrystalline diamond growth: an in-situ optical study using pyrometric interferometry. *Thin Solid Films*, 482:50–55, 2005.

[146] J.E. Gerbi, J. Birrel, M. Sardela, and J.A. Carlisle. Macrotexture and growth chemistry in ultrananocrystalline diamond thin films. *Thin Solid Films*, 473:41–48, 2005.

[147] M. Amaral, F.J. Oliveira, M. Belmonte, A.J.S. Fernandes, F.M. Costa, and R.F. Silva. Tailored Si_3N_4 ceramic substrates for CVD diamond coating. *Surf. Eng.*, 19(6):410–416, 2003.

[148] H.D. Espinosa, B. Peng, B.C. Prorok, N. Moldovan, O. Auciello, J.A. Carlisle, D.M. Gruen, and D.C. Mancini. Fracture strength of ultrananocrystalline diamond thin films - identification of weibull parameters. *J. Appl. Phys.*, 94(9):6076, 2003.

[149] R. Pfeiffer, H. Kuzmany, N. Salk, and B. Günther. Evidence for *trans*-polyacetylene in nanocrystalline diamond films from H-D isotropic substitution experiments. *Appl. Phys. Lett.*, 82:4149, 2003.

[150] C.S. Abreu, M.S. Amaral, F.J. Oliveira, A. Tallaire, F. Bénédic, O. Syll, G. Cicala, J.R. Gomes, and R.F. Silva. Tribological testing of self-mated nanocrystalline diamond coatings on Si_3N_4 ceramics. *Surf. Coat. Tech.*, 200:6235–6239, 2006.

[151] M.D. Fries and Y.K. Vohra. Properties of nanocrystalline diamond thin films grown by MPCVD for biomedical implant purposes. *Diam. Relat. Mater.*, 13:1740–1743, 2004.

[152] C.S. Abreu, M. Amaral, A.J.S. Fernandes, F.J. Oliveira, R.F. Silva, and J.R. Gomes. Friction and wear performance of HFCVD nanocrystalline diamond coated silicon nitride ceramics. *Diam. Relat. Mater.*, 15:739–744, 2006.

[153] J.M. Carrapichano, A. Tallaire, F.J. Oliveira, and R.F. Silva. Complete densification of Si_3N_4-SiC ceramic matrix composites (CMC's) by a pressureless sintering route. *Mater. Sci. Forum*, 455–456:225–229, 2004.

[154] E.P. Whitenton and P.J. Blau. A comparison of methods for determining wear volumes and surface parameters of sperically tipped sliders. *Wear*, 124:291–309, 1988.

[155] N.K. Myshkin, A. Ya. Grigoriev, S.A. Chizhik, K.Y. Choi, and M.I. Petrokovets. Surface roughness and texture analysis in microscale. *Wear*, 254:1001–1009, 2003.

[156] A. Erdemir, C. Bindal, G.R. Fenske, C. Zuiker, A.R. Krauss, and D.M. Gruen. Friction and wear properties of smooth diamond films grown in fullerene + argon plasmas. *Diam. Relat. Mater.*, 5:923–931, 1996.

[157] Y.-B. Park and S.-W. Rhee. Effect of hydrogen plasma precleaning on the removal of interfacial amorphous layer in the chemical vapor deposition of microcrystalline silicon films on silicon oxide surface. *Appl. Phys. Lett.*, 68:2219, 1996.

[158] S.-P. Honga, H. Yoshikawa, K. Wazumi, and Y. Koga. Synthesis and tribological characteristics of nanocrystalline diamond film using CH_4/H_2 microwave plasmas. *Diam. Relat. Mater.*, 11:877–881, 2002.

[159] N.A. Feoktistov, V.G. Golubev, S.A. Grudinkin, A.V. Nashchekin, T.S. Perova, and A.Ya. Vul'. Nanodiamond injection into the gas-phase during CVD diamond film growth. In D.M. Gruen, O.A. Shenderova, and A.Y. Vul', editors, *Synthesis, Properties and Applications of Ultrananocrystalline Diamond*, volume 192 of *NATO Science Series*, pages 145–156, Dordrecht, The Netherlands, 2005. Springer.

[160] Y.X. Zhuang and A. Menon. On the stiction of MEMS materials. *Tribol. Lett.*, 19:111–117, 2005.

[161] A. Choubey, B. Basu, and R. Balasubramaniam. Tribological behaviour of ti-based alloys in simulated body fluid solution at fretting contacts. *Mater. Sci. Eng. A*, 379:234–239, 2004.

[162] C.S. Abreu, M. Amaral, F.J. Oliveira, A.J.S. Fernandes, J.R. Gomes, and R.F. Silva. Enhanced performance of HFCVD nanocrystalline diamond sefl-mated tribosystems by plasma pretreatments on silicon nitride substrates. *Diam. Relat. Mater.*, 15:2024–2028, 2006.

[163] C.S. Abreu, E. Salgueiredo, F.J. Oliveira, A.J.S. Fernandes, R.F. Silva, and J.R. Gomes. CVD diamond water lubricated tribosystems for high load planar sliding. *Wear*, 265:1023–1028, 2008.

[164] J. Sallard, D. Mercs, M. Jarrat, D.G. Teer, and P.H. Shipway. A study of the tribological behaviour of three carbon-based coatings, tested in air, water and oil environments at high loads. *Surf. Coat. Tech.*, 177-178:545–551, 2004.

[165] X. Wu, M. Suzuki, T. Ohana, and A. Tanaka. Characteristics and tribological properties in water of Si-DLC coatings. *Diam. Relat. Mater.*, 17:7–12, 2008.